ISBS
Institut für Straßenwesen
T U B r a u n s c h w e i g

Technische Universität Braunschweig

Noor Ahmad

Crack detection in asphalt pavements by means of Ground Penetrating Radar (GPR)

2016

Heft 30 • Braunschweig 2016 • ISBN 978-3-932164-30-9

Von der Fakultät Architektur, Bauingenieurwesen und Umweltwissenschaften
der Technischen Universität Carolo-Wilhelmina zu Braunschweig
zur Erlangung des Grades eines Doktor-Ingenieurs (Dr.-Ing.)
genehmigte Dissertation.

Eingereicht am:	22 Oktober 2015
Disputation am:	21 Juni 2016

Berichterstatter:	Professor Dipl.-Ing. Dr.techn. Michael P. Wistuba
	Professor Dr Andreas Hördt

Vorwort

Dr.-Ing. Noor Ahmad, geb. 1978 in Pakistan, Bauingenieur der Balochistan University of Engineering and Technology (Diplomstudium) und der Technischen Universität München (Aufbaustudium M.Sc. in Transportation Systems), war von 2010 bis 2013 im Rahmen eines DAAD-Stipendiums als Doktorand am Institut für Straßenwesen der TU Braunschweig tätig.

Das Thema dieser Arbeit ist der messtechnischen Zustandserfassung von Asphaltstraßen mit Hilfe von Bodenradar gewidmet. Die Zustandskontrolle und die Erhaltungsplanung von Straßen basiert auf Informationen zum jeweils aktuellen strukturellen Zustand und auf einer Vorhersage der zu erwartenden Zustandsentwicklung. Die Zustandserfassung erfolgt heute optisch und messtechnisch auf mehrfache Weise. Zu den aussagekräftigen messtechnischen Methoden zählen zerstörende Verfahren. Dabei werden Probestücke, meist Bohrkerne, aus der Straße entnommen und an diesen mechanische Kennwerte bestimmt, die aus zeitraffenden statischen und zyklischen Laborprüfungen gewonnen werden. Die Nachteile solcher zerstörender Verfahren sind der versuchstechnisch große Aufwand, dass die Probe, die an einem Punkt oder an wenigen Punkten innerhalb der vergleichsweise riesigen Straßenfläche entnommen wurde, nicht a priori repräsentativ ist, und dass die Straße durch die Probenahme selbst geschädigt wird.

Eine mögliche Alternative sind nichtzerstörende Messverfahren. Dabei wird mittels Schall- oder Wellenphysik auf den strukturellen Zustand der Straße geschlossen. Beispiele sind fotooptische Methoden zur Rissaufnahme, das Fallgewichtsdeflektometer zur Ermittlung der Tragfähigkeit, die Thermografie zur Ermittlung von Inhomogenitäten in der Temperaturverteilung, oder das elektromagnetische Wellenverfahren ‚Bodenradar' zur Erfassung des Straßenaufbaus. Von Vorteil ist, dass solche nichtzerstörende Messverfahren darauf ausgelegt sind, nicht ausschließlich punktuelle, sondern auch flächendeckende Informationen zum Straßenzustand zu generieren, die vorzugsweise während der Überfahrt bei Fahrgeschwindigkeiten bis 80 km/h gewonnen werden. Die Anwendung des Bodenradars für die Straßenzustandserfassung ist bezüglich der Bestimmung von Schichtdicken und der Lagebestimmung von Stahleinlagen in Betondecken rund 30 Jahre alt und gilt als erprobt. Vergleichsweise neu ist die Anwendung des Bodenradars zur Detektion von Fehlstellen, und insbesondere von Rissen in Asphaltstraßen.

Das Prinzip von Bodenradar basiert auf elektromagnetischen Radarwellen, die sich in einem Medium ausbreiten und an benachbarten andersgearteten Medien abgelenkt werden, sodass das Zeitdiagramm der reflektierten Wellenanteile, das sog. Radargramm, ein Bild der unterschiedlichen Medien ergibt. Die Technik funktioniert grundsätzlich in vielerlei Medien, so auch in ungebundenen Schichten, Asphalt und Beton. Die „Andersartigkeit" von zwei Medien wird durch die Dielektrizitätskonstante beschrieben, welche für Luft bei 1, für Asphalte zwischen 4 und 10 liegt, für tonige Böden bei 25 bis 40 und für Wasser bei

80. Aufgrund dieser großen Unterschiede in den Dielektrizitätskonstanten ist eine Rissdetektion in Asphaltstraßen grundsätzlich denkbar, insbesondere wenn der Riss mit Wasser und/oder Schmutz gefüllt ist. Dabei werden die vom Sender emittierten elektromagnetischen Radarwellen über den zu untersuchenden Rissbereich hinwegbewegt, abgelenkt und vom Empfänger detektiert und schließlich die Beschreibung von Rissbreite und –tiefe angestrebt.

In Konferenzbeiträgen und bei internationalen Fachausstellungen wurde mehrfach von der erfolgreichen Anwendung des Bodenradars zur zielsicheren flächendeckenden Detektion von Rissen in Straßen und Flugbetriebsflächen berichtet. Es fehlten aber die notwendigen Detailinformationen zur Nachvollziehbarkeit. Es fehlte der wissenschaftliche Beweis. Aus diesem Grund wurde die vorliegende Promotion initiiert, deren Ziel es war, mit Hilfe von systematischen Untersuchungen die Forschungsfrage zu klären, ob und wenn ja unter welchen Bedingungen das Bodenradar als Routinemessverfahren zur Rissdetektion in Asphaltstraßen geeignet ist bzw. dazu weiterentwickelt werden kann. Insbesondere wurde untersucht, wie folgende Einflussfaktoren die Qualität der Rissdetektion beeinflussen: (1.) die Wahl der Hardware und die Einstellung der systembedingten Messparameter des Bodenradars, (2.) die Eigenschaften des Messobjektes, wie die Materialeigenschaften der Straße, die Temperatur, die Rissbreite und –tiefe sowie eine eventuelle Rissfüllung durch Wasser oder Schmutz, und (3.) die Wahl der Auswertesoftware und den Möglichkeiten zur Aufbereitung und Analyse der Messdaten.

Die Arbeit von Dr.-Ing. Ahmad im Rahmen seiner Promotion bestand im Wesentlichen aus drei Teilen: Der erste Teil war gewidmet einer umfassenden Recherche und Dokumentation unterschiedlicher Systeme für Bodenradarmessungen sowie einer Marktanalyse. Diese Arbeiten mündeten in der Spezifikation jenes Messsystems, welches durch das ISBS beschafft wurde und ab Sommer 2011 zur Verfügung stand. Im zweiten Teil führte Herr Ahmad umfangreiche Test- und Messreihen zur Rissdetektion im Labor und auf der Straße durch. Der dritte Teil war schließlich der Aufbereitung und Interpretation der Messdaten gewidmet und der Beantwortung der Forschungsfrage.

Als wichtige Teilergebnisse der Arbeit können für das hier eingesetzte Bodenradar-System und die gewählte Messmethodik festgehalten werden: (1.) Eine Erfassung von Netzrissen war nicht möglich. (2.) Weil Einzelrisse in Straßen überwiegend vertikal zur Oberfläche verlaufen, ist die Detektion mittels einfacher Antennen mit vertikalem oder schrägem Messwinkel nicht zielsicher möglich. Die Verwendung einer Dipolantenne bzw. mehrerer Antennen gleichzeitig verbessert die Erfassung. (3.) Einzelrisse konnten mittels der bodengekoppelten Dipol-Antenne mit mindestens 2 mm Messabstand, im Frequenzbereich von 2 GHz und mit Hilfe der in der Arbeit beschriebenen Auswertemethode „time delay technique“ detektiert werden. (4.) In den Radargrammen zeigten sich deutliche Unterschiede zwischen breiten und schmalen, sowie kurzen und langen Vertikalrissen. (5.) Eine Verfüllung des Risses mit Schmutz und/oder Wasser war für die Erkennung vorteilhaft, weil sich die Dielektrizitätskonstanten von Füllstoffen deutlich von jenen für

Asphalt unterscheiden. (6.) Die Qualität der Rissdetektion ist abhängig von der Messtemperatur. Es wird empfohlen, Messungen nicht unter 15 °C durchzuführen. (7.) Es wurden Risse mit Abmessungen im Millimeterbereich, mindestens 2 mm breit und 5 mm tief, nur zufällig detektiert. Eine zielsichere Rissdetektion war erst ab Rissgeometrien im Zentimeterbereich möglich, sodass auf der Grundlage dieser Arbeit der Einsatz dieses Systems und dieser Messmethodik für die routinemäßige Zustandserfassung nicht empfohlen wird.

Die vorliegende Arbeit wurde von Herrn Dr.-Ing. Noor Ahmad im Frühjahr 2016 an der Fakultät für Architektur, Bauingenieurwesen und Umweltwissenschaften der TU Braunschweig zur Promotion eingereicht und als Promotionsschrift angenommen.

Braunschweig, im Dezember 2016

Michael P. Wistuba

Abstract

This research investigates the possibilities of using Ground Penetrating Radar (GPR) as crack investigation tool for asphalt pavements. The investigation includes crack detection and crack analysis. The crack investigation comprises crack depth and width measurement. Although GPR is being used as a pavement characterisation tool, its use as a crack detection tool has not been verified and systematically documented. In this regard, some parameters affecting GPR use were selected from literature and were verified. These parameters include GPR system attributes, material properties, crack characteristics and data processing techniques. To investigate the GPR hardware related characteristics, six up to date systems were used in laboratory and in field. The selected systems included 250 MHz to 3 GHz frequency antennas with impulse and continuous electromagnetic wave generation techniques. Artificial as well as natural cracks were investigated by the GPR systems to bring forward the optimum system requirements for crack analysis. To investigate the asphalt and crack filling material characteristics, different asphalt mix specimens were prepared from various laboratories in Germany. A range of different width and depth cracks were designed in the asphalt specimens to be tested for crack analysis. Air, sand, bitumen and water were used as crack filling materials to investigate their influence on GPR outcomes. The effect of temperature on material properties was also investigated. Moreover, the relation between crack and electromagnetic wave propagation path was investigated regarding crack detection survey.

The selected software related parameters were based on known techniques used for data processing such as wave processing and image processing. This also included investigations on 2-D and 3-D data processing techniques and f-k filtering and electromagnetic wave velocity analysis. The outcomes of this study were verified in laboratory and on pavements. The pavement survey results were verified by taking core samples. Investigations made in this research may broaden the use of GPR for crack detection in asphalt pavements.

Acknowledgements

I would like to express my greatest gratitude and appreciation to my supervisor Professor Dipl.-Ing. Dr.techn. Michael P. Wistuba and to my co-supervisor Professor Dr.-Ing. Holger Lorenzl (Fachhochschule, Lübeck) respectively, for their valuable guidance, support, and assistance throughout the length of my research work. Without their encouragement and guidance, its completion would not have been possible. Special thanks to Professor Dr. Andreas Hördt (Institut für Geophysik und extraterrestrische Physik, TU Braunschweig) for his valuable guidance.

Sincere thanks to Institut für Straßenwesen TU Braunschweig (ISBS) team for their co-operation and help in conduction of this research. Also thanks for all the fun we have had in the last four years.

I would also like to show appreciation to the financial support of the German Academic Exchange Service (DAAD).

Special thanks go to my parents; I can feel how difficult this whole time was for them in my absence. Lots of love to my wife and children, who stood with me in all the difficult times. I dedicate this thesis to my wife Rehmat and my sweet children Javeria, Hafsa and Talha.

M.Sc. (TUM) Noor AHMAD

Soltau, 20th November, 2016

Contents

1 Introduction

1.1 Background information

For the crack detection and evaluation in asphalt pavements, the technique choice is limited. This is because the current pavement evaluation techniques i.e. destructive and non-destructive techniques have their own functional boundaries. The destructive technique is based on evaluation of pavement samples collected from selected pavements locations and evaluated in the laboratory. However, the decision of pavement sample's size and extraction location is based on visual assessment. Thus in case of hidden damages such as bottom-up cracking, the selection of sample extraction site on pavement will be difficult. Moreover, the destruction technique is disturbed sampling and therefore, crack dimensions measured in samples may differ from reality. Therefore, the use of destructive technique for cracks detection and evaluation in road pavements are limited (Ahmad et al., 2011). Moreover, destructive evaluation technique is expensive, time-consuming and requires traffic disruption (Al-Qadi et al., 2005b).

On the other hand, the non-destructive pavement evaluation techniques are based on video survey, pavement deflection assessment (e.g. Falling Weight Deflectometer), thermography and electromagnetism. These non-destructive techniques may overcome the limitations of destructive technique such as no disturbed sampling but, still they are not optimum for crack detection and evaluation in pavements. This is because of the limits associated with their working principles and phenomenon. For example, video or image survey requires pavement surface to be clean and free from foreign materials. Moreover, video survey is limited to detection of visible cracks on pavement surface i.e. no detection of top-down cracking. In addition to, the crack evaluation (depth, severity) with video survey is not possible due to its inability of penetrating into pavement. Similarly, the pavement deflection techniques are not suitable for crack detection due to their working phenomenon. The thermography on the other hand, is dependent on the emission of infrared radiations from the pavement which is subjected to suitable weather conditions. Thus the use of this technique is limited. In addition, thermography technique has limited penetration depth and hence cannot be used for overlaid layers analysis (Maser, 2003). Thus the choice of technique for crack detection in asphalt pavement is limited to electromagnetic (EM) technology. The EM technology is capable for penetrating into materials and thus evaluation of material's properties is possible (Maser, 2003).

The principle of electromagnetic technology is based on sending EM wave pulses into a material (pavement) and then collection of reflected EM waves (Daniels, 1996). The direct EM waves (coming through the material) are also collected in some surveys such as Core-hole or Cross-hole survey (Annan, 2004). Based on information from EM waves coming back from material, material's properties such as presence of foreign materials (targets) or abnormalities (cracks) and their location/position is analyzed. The equipment based on electromagnetic technology is called RADAR.

"RADAR" is an acronym for **RA**dio **D**etection **A**nd **R**anging (Lahouar, 2003). The history of radar dates back to the first reported experiments conducted by Hülsmeyer, a German scientist in 1904 (Lahouar, 2003; Daniels, 2007). Hülsmeyer's device (German patent No. 165546) was designed for traffic monitoring in water ways. The use of RADAR for probing hidden objects was started by two German scientists Leimbach and Löwy in 1910 (Daniels, 2004). However, the use of RADAR for pavement evaluation started in the late 1970s (Morey, 1998).

The radar specific for probing earth is known as "Ground Penetrating Radar" abbreviated as GPR. In literature, GPR has also been named as Ground Probing Radar, Georadar, Sub-Surface Radar or Surface Penetrating Radar (Daniels, 2007). However, in this research, GPR will be used to refer the aforementioned equipment.

The first GPR company "Geophysical Survey Systems, Inc." (GSSI) was established in 1970 and the first GPR available for sale was in 1974 (Saarenketo, 2006; Morey, 1998). GPR due to its ability of penetrating into materials could evaluate the overlaid pavement layers and thus its use started in pavement industry (Maser, 2003). To date, GPR has been used as a pavement characterizing tool from the last 35 years (Diamanti et al., 2012; Al-Qadi et al., 2010; Saarenketo, 2006; Al-Qadi et al., 2005b; Hugenschmidt et al.,1998). The first vehicle mounted survey for pavements characterization was conducted by Federal Highway Administration (FHWA) in 1985 (Morey, 1998). In the mid and late 1990s, GPR has been successfully used by highway agencies as a pavement characterizing tool for pavement layer thickness measurements, voids detection, layer delamination, depth to steel bars, etc. Less satisfactory results are reported for voids detections whereas unsatisfactory results for asphalt stripping (Morey, 1998; Saarenketo, 2006). Recently GPR is being used to evaluate pavement properties like layer thickness, HMA density and moisture content to detect many pavement distresses like potholes, spalling (Al-Qadi et al., 2010). Although GPR has been used for hidden pavement distresses evaluation such as layer delamination, its use as a crack detection tool in asphalt pavements has not been sufficiently documented (Manuel et al., 2010).

Additionally, as explained before, the GPR can penetrate through a vast range of materials including cement concrete, asphalt mixtures, clay, silt, sand, etc. (Saarenketo, 2006; Annan, 2009). This ability of GPR is important for the crack detection as EM waves must pass through the crack including crack fill. The crack fill can be any material including host material (bitumen, used as asphalt binder) or foreign material including air, clay, sand, water, organic materials or their mixtures. Thus GPR fulfils the basic criteria to be used as crack detection equipment in asphalt pavements.

1.2 Objective

The scope of this thesis is to investigate the GPR capabilities for crack detection in asphalt pavements. For this reason, some parameters influencing GPR capabilities as a crack detection tool were selected. The selection of parameters was based on the available resources during conduction of this research. The selected parameters investigated in this research were:

- GPR characteristics such as its antenna type, frequency and transmitter type,
- Temperature of the asphalt pavement,
- asphalt mixture and crack filling material properties,
- crack properties such as its geometry and position in pavement structure,
- effect of data processing techniques on GPR outcomes such as image and wave data processing algorithms,
- effect of surveying techniques (2-D and 3-D survey) and,
- effect of GPR antenna directivity and crack direction during survey,

The tests were carried out in laboratory as well as on site. For the laboratory tests, asphalt specimens were designed based on the standard asphalt pavement specifications. For the onsite investigation, asphalt pavements with varying layer thickness, asphalt mixture, layers composition and crack types were selected. Together with above listed parameters, the GPR ability regarding cracking cause investigations was also verified.
In this thesis, the GPR equipment "Aladdin" was primary used for field and laboratory tests. Limitations of this study are:

1) Material properties related to EM properties were not investigated rather; standard values were used wherever needed, for example dielectric constant of asphalt. This might affect some results such as exact pavement layers thickness, etc.
2) Software effects were not completely investigated. Few data types could not be processed by specific software due to software use limitations.
3) To verify GPR abilities for crack cause investigations such as support loss, it was not possible to take undisturbed samples beneath asphalt pavements. Therefore, GPR tests were repeated to increase the confidence level and remove this shortcoming.

1.3 Thesis structure

The thesis is organized as follows:
Chapter 1 provides an overview of the problem statement, the methodology and the objectives of this research work. The shortcomings of existing crack investigation methods in context of current demands are described. The reason for selecting GPR as a crack investigation tool is highlighted. The selected parameters in regard of crack investigation are fixed and some limitations are mentioned in advance.
Chapter 2 represents state-of-the-art on use of GPR for crack investigation. The GPR working principles are explained with examples. The types of EM waves, their generation and back reflection phenomenon are explained. The related terminologies such as wave length frequency and bandwidth of EM waves are explained. The material properties, GPR hardware with block diagram and survey types are explained. Moreover, the material electrical property i.e. dielectric constant is explained together with methods to calculate it. The GPR data standard and advance processing techniques are highlighted. In the end, an overview of past literature is presented in this chapter, focusing on the research carried out

for crack investigation through GPR including difficulties and limitations faced by various scientists.

Chapter 3 discusses the research approach and the test setup. It is focused on the methodology carried out for the investigation of selected parameters. The tests setup for control environment (laboratory) to the pavement sections selected for tests is presented. The ingredients and physical characteristics of asphalt specimens are presented. The information regarding damages on selected sites is highlighted with figures. In addition the software used for data processing are described briefly.

Chapter 4 presents the outcomes of laboratory and field testing. The investigations are presented in the context of crack detection parameters i.e. GPR characteristics, effect of temperature, material properties and surveying techniques.

Chapter 5 draws the GPR abilities exploration regarding crack cause investigation. Different cracks on selected asphalt pavement sections were tested to investigate their sources. The tests conducted in the regard on asphalt pavements were validated by coring.

Chapter 6 draws the conclusions of the research work, GPR potential applications, possibilities and limitations as a crack investigation tool.

2 State-of-the-art

2.1 Introduction

The aim of this section is to make reader able to understand and conduct GPR survey, by understating electromagnetic (EM) waves, material properties, GPR hardware and process the GPR data. Therefore, the working phenomenon of GPR is explained together with the EM wave's properties. The material electrical and magnetic properties related to EM wave propagation are described. As in most cases material electrical and magnetic properties are unknown, methods to find these material properties are provided. The asphalt pavement and its damages related to cracking are explained. The choice of optimum GPR system is no doubt, technical and is the first step towards successful surveying. A good decision can be made if the GPR user has knowledge of GPR components, their functioning, limitations and processing techniques. For this reason, GPR hardware is explained according to their optimisation for various functions. Types of surveying and their suitability for applications are provided. The processing of GPR data from various techniques is highlighted to enhance GPR outcomes. In the end, a review on past literature is provided to identify the deficiencies for using GPR as a crack investigation tool.

2.2 GPR principles

The GPR working phenomenon is based on the analysis of the back reflected EM waves due to change in material properties, in which it propagates (Annan, 2009). The material properties include its electrical and magnetic properties. The propagation of EM waves, their transmission (partial/full) and reflection in the materials is governed by the electrical and magnetic properties of the materials. This is because the EM waves, as the name suggest, are formed by coupling electric and magnetic parts (Figure 2.1). Therefore, the electric and magnetic waves either from another EM wave generation source or from materials influence the EM wave generated by the GPR. Thus the electrical and magnetic properties of material (under observation) must be considered when conducting GPR survey (Annan, 2009; Daniels, 2004).

On the other hand, the influences by the material's electric and magnetic properties are responsible for the EM wave back reflection. The EM wave is reflected back wholly or partially whenever it encounters change in material electromagnetic properties of the medium (Davis et al., 1989; Boll et al., 1996; Morey, 1998; Saarenketo, 2006). The reflection extents of EM waves not only depend on the change in material properties but also on the size, shape and distance of the foreign object in the medium (Al-Qadi et al., 2010). In case of gradual material properties change, e.g. increase in water content of soil with depth, the reflection of EM wave is also gradual.

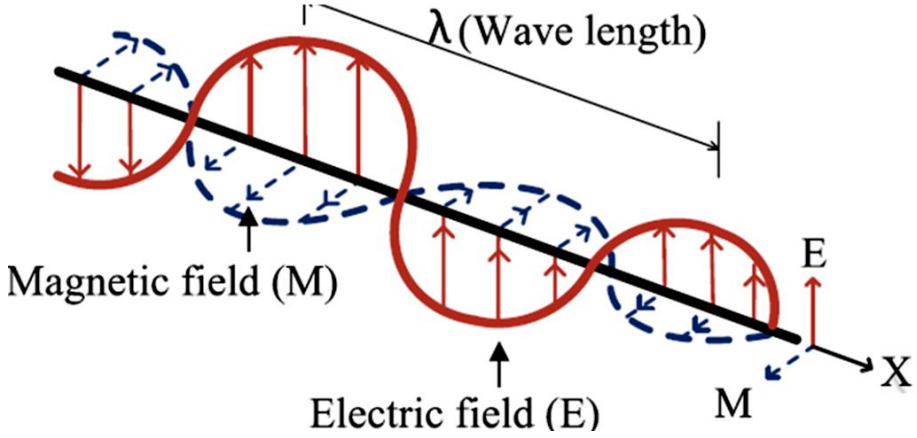

Figure 2.1. The EM wave components and attributes (Ghazanfari et al., 2012)

The GPR is effective for analysis of non-conducting materials (insulators) called dielectrics such as glass, wood, paper, etc. (Annan, 2009; Cassidy, 2009a). The GPR effectiveness in dielectric materials is due to their electronic and molecular structure (Cassidy, 2009a; Annan, 2004). In an ideal dielectric material, the free movement of electrons is not possible. The specific electronic and molecular structure of materials result in three electrical and magnetic properties which includes, magnetic permeability (μ), electrical conductivity (σ) and the electrical permittivity (ε) (Cassidy, 2009a; Saarenketo, 2006). The electric and magnetic properties of materials may vary depending on their influencing factors (Annan, 2009).

The magnetic permeability (μ) of a material is its ability to store energy in its magnetic field due to its magnetic nature (Cassidy, 2009a). Most dielectric materials (dry sand, clay, etc.) do not exhibit magnetic permeability and therefore, in case of pavement survey with GPR, magnetic permeability is not taken into account (Jaselskis et al., 2003).

The electrical conductivity (σ) (Siemens per meter (S/m)) describes the response of materials under free charge movement in presence of an electric field (Annan, 2009). In conductive materials such as wet clay, moist sand, metals, the total energy of EM waves reflects back, making material analysis difficult for GPR. However, a conductive material can be well detected by the GPR in a dielectric medium. In general, most materials or earth are mixture of dielectric and conductive materials. This results in energy dissipation of EM wave in materials which limits probing depth of GPR (Annan, 2009).

The electric permittivity (ε) (farads per meter (F/m)) is the ability of a material to resist an electric field by its polarisation (Cassidy, 2009a). The polarisation means orientation of material's atomic or molecular charges respond to the electric field. The electric permittivity is explained by modified Maxwell's equation as (Annan, 2009),

$$\overline{D} = \tilde{\varepsilon}\,\overline{E} \qquad 2\text{-}1$$

Where,

$\overline{D}$ = Electric displacement vector (coulomb per meter square - C/m^2)

$\tilde{\varepsilon}$ = Dielectric Permittivity (tensor) (Farads per meter - F/m)

$\overline{E}$ = Electric field strength vector (V/m)

In Equation 2-1, the electric displacement vector represents the influence of electric field on a material related to the presence of free and bound electric charges on atomic or molecular level. In case of electric field, the induced polarisation results in orientation of charges according to the electric field i.e. positive dipoles to negative pole of electric field and vice versa. Higher the ability of material to polarise in presence of electric field, more will be its electric permittivity and thus less possibility to be analysed by GPR (Equation 2-1).

Usually in GPR surveys, the relative electric permittivity (ε_r) of materials is considered. The relative electric permittivity is the ratio of material dielectric permittivity (ε) and vacuum dielectric permittivity (ε_0) (ε_0 = 8.85 x 10 exp (-12) F/m) (Annan, 2009), i.e.

$$\varepsilon_r = k = {}^{\varepsilon}/_{\varepsilon_0} \ [-] \qquad 2\text{-}2$$

The relative electric permittivity is often expressed relative dielectric permittivity (ε_r) or dielectric constant (k) (Annan, 2009). In this research, the term dielectric constant denoted by (k) will be used further to address the relative electric permittivity or dielectric constant material property. The dielectric constant is of utmost importance in GPR surveys. Therefore, dielectric constant is further discussed in Section 2.2.3.

2.2.1 GPR basic components

To perform the basic operations of GPR survey i.e. generation of EM waves, their induction in the ground, receiving of back reflected EM waves, their analysis and display of results is carried out by four main parts of a GPR system. The GPR system comprises of four basic components i.e. transmitter, receiver, control unit and the display unit, shown in Figure 2.2 (Saarenketo, 1998). The transmitter and receiver can be separate or jointed in a single box called the GPR antenna. The transmitter generates EM waves of specific properties from other forms of energy such as electricity (Harari, 1996; Daniels, 2004; Koppenjan, 2009). The transmitter then induces the EM waves into the ground. Generally two main types of EM waves are generated by the transmitter i.e. Continuous Waves (CW) and pulsed waves (Lahouar, 2003). Based on the EM waves generated, called the modulation technique, GPR systems are divided into two main types i.e. CW and Impulse GPR systems. In case of impulse radar systems, the EM waves are in form of pulses (nanoseconds duration) and the transmitter switches on and off repeatedly (Daniels, 1996). In case of CW GPR systems, as the name suggests, CW is a never ending EM wave and the transmitter/receiver functions continuously.

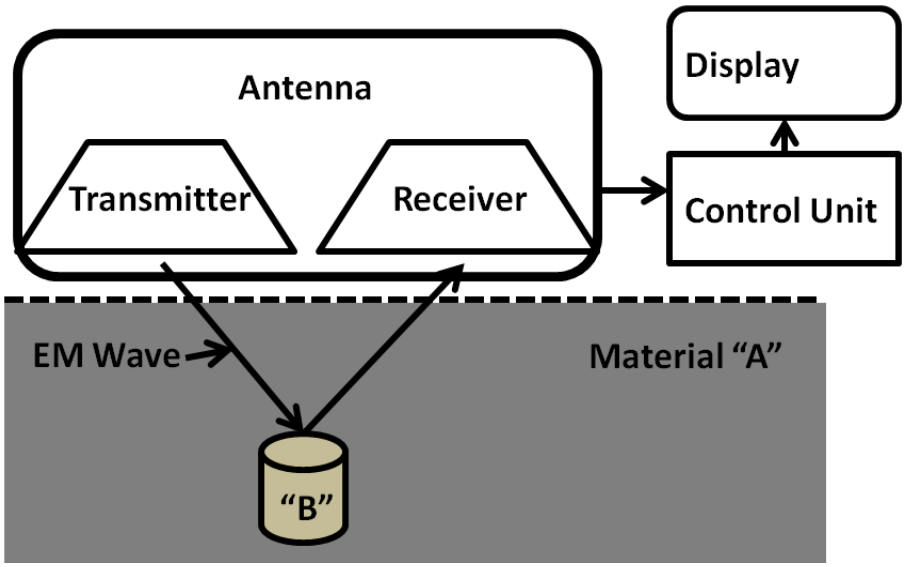

Figure 2.2. The basic four components of GPR system (Daniels, 2004)

The receiver starts collecting the back reflected EM waves also within a specified time. The receiver amplifies the signals (if required), changes their form e.g. energy waves to signals and forwards the information to the control unit (Davis et al., 1989; Harari, 1996). The data is then processed (initially) by the control unit. As in impulse GPR systems, it is required to shutdown the transmitter during reception of reflected EM waves and the receiver during induction of EM waves, control unit makes sure that the requirement is fulfilled. The time lapse between transmitter blinking is called time-window (Annan, 2009; Daniels, 2004). In case of Impulse GPR system, consecutively functioning of transmitter and receiver and their synchronization is important to ensure the accuracy of travel time calculation of backscattered EM waves and avoid recording noise or clutter (Koppenjan, 2009). The control unit also performs the initial processing of received data before they are displayed. The results are shown in the display unit. The real-time results display helps control the survey direction and take necessary on spot actions. For the detailed processing of survey data, sophisticated software can be used which may be however, time consuming. The use of sophisticated software helps achieve survey objectives, ranging from the verification of changes in the medium to the presence of foreign material in the medium ref.

2.2.2 EM wave reflection

The sinusoidal EM wave carries energy which is measured by its sinusoidal peaks (negative and positive) called amplitudes. The EM wave from laboratory survey is shown in Figure 2.3(a). After striking with the interface, the energy of EM wave (partially/fully) reflects back which is received by the receiver (Loizos et al., 2010; Morey, 1998). To calculate the amount of back reflected energy, materials properties at the interface must be considered. It is therefore, material properties can also be analysed by studying the EM wave's amplitude before and after reflection in any material or at the interface (AI-Qadi et al., 2005a). The pavement dielectric constant measurement by amplitude measurement is given Equation 2-3.

The Figure 2.3(a) shows received EM wave amplitude from medium composed of air, asphalt and sand. The interface of air-asphalt resulted in the first amplitude in Figure 2.3(a), (dark line) whereas; the second peak is result of asphalt-dry sand. The second dark line indicating asphalt-sand is finishing earlier right hand side because of no sand support on the right side of specimen. When considering negative or positive peaks to differentiate among materials, the choice of peaks depends upon material, type, antenna configuration and user's experience (Yelf, et al., 2006). In this research, the first positive peaks were considered.

The energy of EM wave dissipates with increase in penetration depth (Figure 2.3(a)). This is due to the fact that most dielectric materials are not perfect non-conductors (dielectric constant = 1) and thus losses in EM wave's energy occur (Annan, 2004; Daniels, 2007). The decreased energy results in lower amplitudes of reflected EM waves and thus lower resolution of GPR outcomes called GPR-grams (Figure 2.3(b)). The GPR probing depth reaches its maximum when no EM wave energy reflects back.

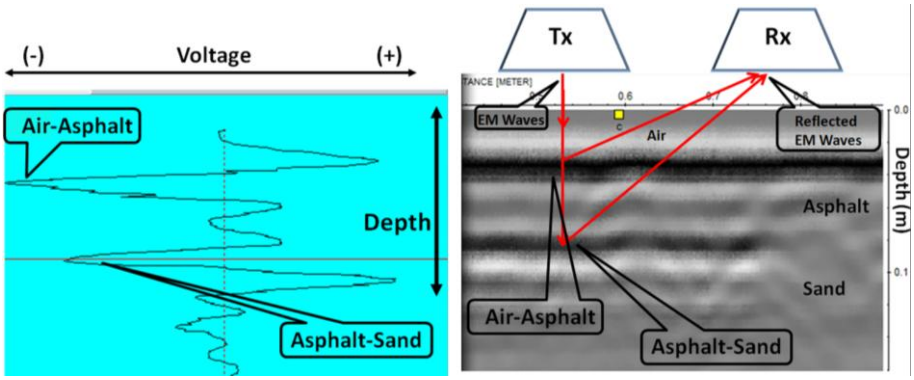

Figure 2.3. The formation of GPR-gram by reflected EM waves, (a) reflected EM wave with different amplitude levels (b) GPR-gram of an asphalt specimen over a sand layer (Software: ReflexW)

The formation of GPR-gram is based on stacking on EM reflected waves according to their arrival time (Morey, 1998; Daniels, 2004). The EM wave shown in Figure 2.3(a) together with many other reflected waves is converted to form GPR-gram in Figure 2.3(b). In Figure 2.3(b) the GPR-gram is from Aladdin GPR system. The "Tx" and "Rx" are the transmitter and receiver of GPR system, respectively.

2.2.3 Asphalt pavements and their dielectric constant calculation

Although there are many types of cracks in asphalt pavements, there are two main types of cracks based on their propagation direction. The two categories of cracks are top-down and bottom-up cracks. The top-down cracks as shown in Figure 2.4 start from pavement surface and travel towards bottom. The bottom-up cracks on the other hand, start from the bottom of pavement and propagate towards pavement surface. The top-down cracks are visible at the surface whereas the bottom-up cracks are not visible until they reach pavement surface (MS-4, 1989). Therefore, the bottom-up cracks are hard to detect by classical pavement analysis techniques.

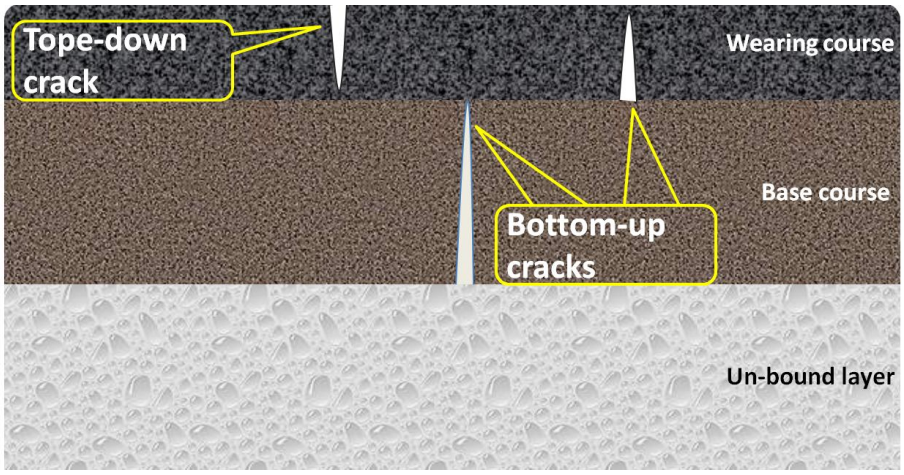

Figure 2.4. Transversal cross-section of asphalt pavement showing top-down and bottom-up cracks (after:(MS-4, 1989)**)**

The cracks may damage the asphalt pavement as they allow intrusion of foreign materials such as water or de-icing agents and decrease its bearing capacity by uneven distribution of loads to underlying layers (MS-4, 1989). The cracks also allow water penetration into pavement structure thereby reducing bond between bitumen and aggregates which may result in pavement damages such as lowering the bearing capacity of pavement, ravelling, pot-holes, stripping, etc. (Papagiannakis et al., 2008). The cracks in asphalt pavements must therefore be timely detected and cured to prevent asphalt pavement damages.

The layer thickness anomaly and support loss are one of the main causes of asphalt pavement cracking. The support settlement can be in form of asphalt layers delimitation or sub-grade settlement, subjecting asphalt layers to extreme stress and ultimately cracking. For the cracks detection or crack source investigation in asphalt pavements with the help of GPR, it is important to understand the asphalt pavement material composition thereby deciding for optimum EM waves and the survey type for investigations.

The asphalt concrete is a mixture of air, bitumen, aggregates and filler. The characteristics of asphalt pavements depend upon its ingredients (bitumen and aggregates) and their reaction with each other (Papagiannakis et al., 2008). The, dielectric constant of asphalt pavements therefore depends upon the chemical changes within the asphalt mix and the volumetric fraction of its ingredients. In this asphalt mix, aggregates are non-polar materials whereas bitumen (the binder in the mix) is a polar material (Saarenketo, 2006). The bitumen's ingredients form a colloidal system in which the "asphaltenes" are the polar molecules dispersed in low polar fluid called "maltenes" (Papagiannakis et al., 2008; Braun, 1991). Therefore, the asphalt concrete dielectric constant is vulnerable to temperature variations i.e. decreased at high temperatures and vice versa (Saarenketo, 2006).

To calculate the dielectric value of asphalt pavement, there are several methods in use. These dielectric constant calculation methods have different accuracy levels and are based on applications of different techniques. The dielectric constant calculation methods include

common midpoint (CMP), energy calculation of reflected wave's amplitudes, comparing GPR outcomes to the real values and finally investigating dielectric constant in laboratory under control environments. Although in this research work the last two methods were used to find out asphalt specimens and pavement dielectric constant, a short overview of all four methods to calculate dielectric constant of asphalt is provided in the following sections.
The CMP method to find the dielectric constant of material is carried out with bi-static GPR system i.e. a GPR system with detached transmitter and receiver units. The technique is based on finding the travel time of striking and reflection of transmitted EM wave to a known position object (Figure 2.5). The position of transmitter and receiver is changed gradually such that the striking object is always in the middle of the two. The change in position and recording more EM wave travel time readings helps enhance the data accuracy. The EM wave travel time is then converted to EM wave propagation velocity which ultimately gives dielectric constant of the material by Equation 2-5 (Cassidy, 2009a; Liu et al., 2006).

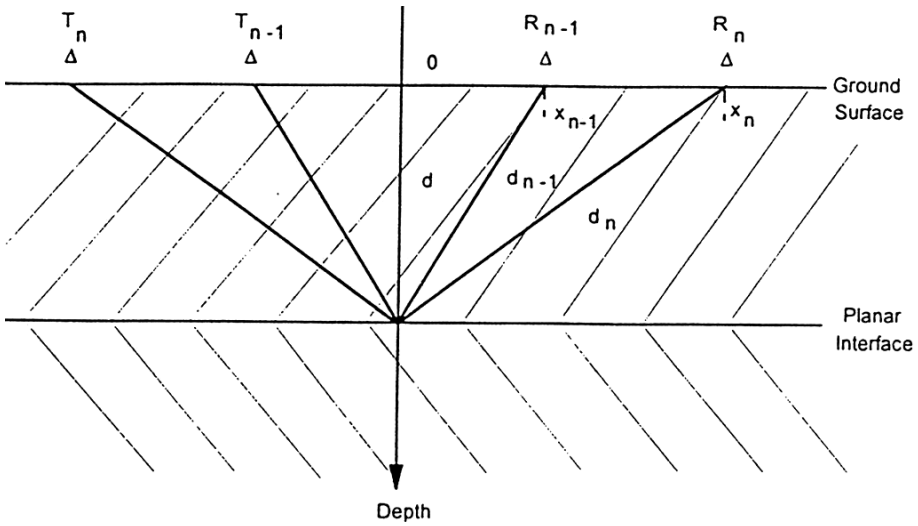

Figure 2.5. Common Midpoint (CMP) survey (Daniels, 2007)

The dielectric constant calculation from comparing reflected EM amplitudes is by recording reflected EM waves from a metal plate (placed on pavement's surface) and without metal plate. In the later case the reflected EM waves coming from asphalt pavement are recorded. The amplitudes of both waves are then compared to calculate pavement dielectric constant (Leng et al., 2011). For this method of dielectric calculation of asphalt pavement, Horn-antennas, a type of antennas hanging in the air, are used as shown in Figure 2.6.

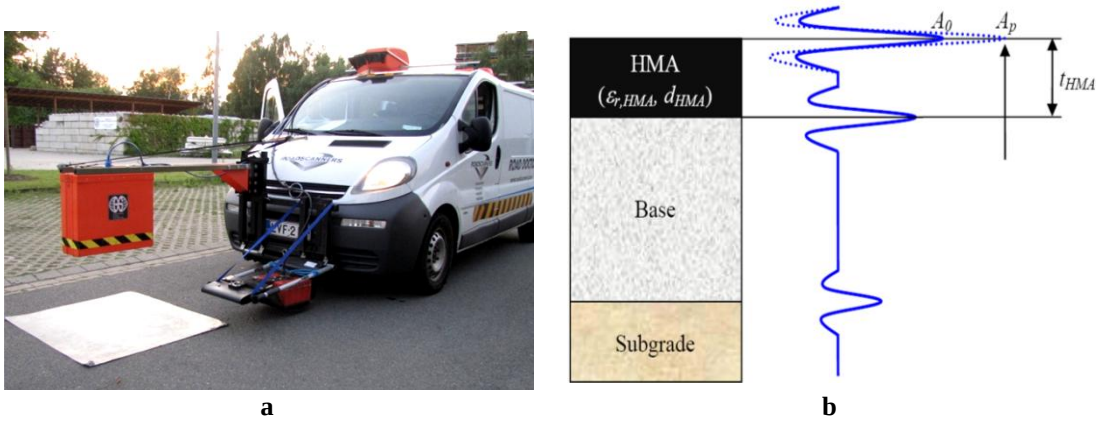

Figure 2.6. In situ pavement dielectric value calculation, (a) measuring EM wave amplitude (Roadscanners, Finland), (b) the EM wave's amplitudes comparison (Al-Qadi et al., 2010)

In Figure 2.6, "HMA" is used as an abbreviation for Hot Mix Asphalt and $k_{(HMA)}$ is the dielectric constant of HMA. The "d" is HMA's thickness (m) and "t" is the two way travel time (nanoseconds) of EM wave. The "A_p" is the first amplitude peak of EM wave reflected from metal plate placed on pavement surface whereas "A_o" is the first amplitude peak of EM wave reflected from air-asphalt pavement interface. The metal plate is used to calculate EM wave amplitude energy as metals do not absorb EM wave energy and thus all the energy is reflected back (Loizos et al., 2010). The difference between A_o and A_p (measured in volts) as shown in Figure 2.6, gives the amount of energy passed through the pavement surface (Al-Qadi et al., 2010). The dielectric constant of pavement is then calculated (based on the amount of energy absorbed by the pavement) from the Equation 2-3, (Al-Qadi et al., 2010; Saarenketo, 2009; Wimsatt et al., 1998;).

$$k_{(HMA)} = \left[\frac{1 + A_o/A_p}{1 - A_o/A_p}\right]^2 \qquad 2\text{-}3$$

Where,

$k_{(HMA)}$ is the dielectric constant of HMA

A_o is the amplitude of the pavement surface reflection.

A_p is the amplitude of the GPR wave reflection obtained over a copper plate placed on the surface of the pavement

Due to the assumptions made in this method i.e. homogeneous layer and the equal distribution of EM wave energy, the dielectric constant of HMA may differ from the real values (AI-Qadi et al., 2005a). This is due to the fact that HMA is seldom a homogeneous layer due to mixing of foreign material such as de-icing agents, tyres residue, clay, dust, sand etc. Moreover, the dielectric constant of underlying layers depends upon the dielectric constant value of all layers above it, if calculated by Equation 2-3. Thus error in the dielectric constant estimation of top layers can result in incorrect dielectric constants of layers beneath it (Al-Qadi et al., 2005b).

The dielectric constant of pavement can also be calculated by comparing real values to that of measured by the GPR, either before or after the survey. The thickness/distance of the pavement is then fixed (Equation 2-6) and different values are tried for the dielectric

constant. For this purpose software such as ReflexW can be used (as was used also in this research), which allow changing data input parameters such as EM wave propagation velocity. The pavement layer thickness in this research work was measured by taking core samples from the pavement structures (Figure 2.14) whereas for specimens, it was directly measured. This method of dielectric calculation has its limitations such as asphalt pavement was regarded as composed of homogeneous layers and thus the dielectric constant calculated was a mean value.

The dielectric constant of asphalt was also calculated in the laboratory to compare those calculated by pavement coring. For this reason, sophisticated equipments capable of recording EM wave's characteristics such as its amplitude, energy and travel time were used. The test setup is shown in Figure 3.13 and Figure 3.14. The tests were conducted in isolated environment to reduce possible interfere from unwanted EM waves. The asphalt dielectric constant outcomes are described in Section 3.4.2. compared to other previously discussed three methods for the calculation of asphalt dielectric constant calculation, this method is more accurate but is also time consuming and costly.

It must be noted that the measured dielectric constant of asphalt pavement from a specific section may not be applicable to other sections. This is because the same asphalt pavement's properties changes with time and location due to intrusion of foreign materials (from surface or bottom of pavement) such as moisture, air and HMA density variation (Jaselskis et al., 2003). On the other hand, the dielectric constants of different pavement sections composed of same HMA may also vary due to environmental factors, traffic variation, etc. (Van Wijk et al., 2007; Loizos et al., 2007).

The dielectric constant of materials due to its nature is influenced by temperature and the frequency of propagating EM wave (Saarenketo, 2009; Daniels, 2004; Jaselskis et al., 2003). At high temperature, the dipolar orientation in material is increased thereby decreasing the material dielectric constant (Cassidy, 2009a). The dielectric constant of asphalt increases on rise in temperature (Jaselskis et al., 2003) however, the difference from -5 to +45 ^{o}C is 7.3 to 20% of the original value (Evans et al., 2008).

The dielectric constant of materials changes at higher frequencies usually in THz (terahertz) range (Daniels, 2004). The dielectric constant of asphalt below 12 GHz, has no significant change in values, however, the physical and chemical properties of asphalt must be considered (Chang et al., 2011; Jaselskis et al., 2003). As in this research work, all GPR systems used were below 3 GHz, the influence of frequency on material properties was ignored. Furthermore, the asphalt specimens were tested to verify the effect of frequency on dielectric constant in controlled environment and the results showed dielectric constant below 3 GHz remains constant (Section 3.4.2).

In case of soil, special care must be taken for moisture content variation. The changes in volumetric water content (k=81 (Table 2-1)) are the biggest dielectric value fluctuation factors in most materials (Davis et al., 1989; Morey, 1998).

However, in case of asphalt pavements the dielectric constant changes with time and asphalt pavement use. With passage of time, either mixing of new materials in form of

pavement rehabilitation or altering of asphalt properties (asphalt aging) are responsible for the change in dielectric constant value. With continuous use of asphalt pavement, its physical properties such as void ratio, density, etc. changes thereby affecting dielectric constant values. Therefore, before each GPR survey, the asphalt pavement ingredients, their mixing ratio, its age and intrusion of foreign material must be considered when calculating pavement dielectric constant. Thus same asphalt pavement layer or asphalt pavement in general may have different dielectric constant values when measured in different times. The situation can be challenging when asphalt pavement properties (dielectric constant) change in short distances however, such accurate values of dielectric constant may not be needed for many GPR outcomes. For example, the crack detection is possible with estimated dielectric constant values. However for increased accuracy such as pavement's layers thickness calculation (in millimetres), the change in asphalt properties with time or due to mixing of foreign materials in asphalt pavement must be considered each time before survey.

The prior information about host or target's dielectric constant helps estimate the amount of reflections from an interface, thus ultimately defining the efficiency of GPR in target detection. The material's dielectric constant information also helps estimate the propagation velocity of EM wave in the material (travel time) which is needed for depth estimations (Equation 2-6) (Saarenketo, 2006). The dielectric constant values of some common material are given in Table 2-1.

Table 2-1. Dielectric constant values of some common materials (Saarenketo, 2006).

Materials	Dielectric value [-]
Air	1
Water	81
Clay	25-40
Silt	16-30
Sand	4-6
Asphalt	4-8
Asphalt (slag)	8-15
Asphalt pavement new and dry (average)	5
Asphalt pavement old and wet (average)	7-8

2.2.4 Probing depth calculation

For the analysis of target's location, either the travel time of EM wave from transmitter to the object and back from object to receiver (in nanoseconds) must be known or the propagation velocity of EM wave in the material. Sometime trial and error method is used to calculate the targets depth (Ahmad et al., 2011). For the calculation of travel time, a medium composed of two different materials is shown in Figure 2.7. The "T1" is the travel time of EM wave from transmitter to interface 1. The "T2" is time taken by the partially reflected EM wave from interface to the GPR receiver. Meanwhile, the EM wave strikes with interface 2 in T1+T3 time. The time taken by EM wave reflected from interface 2 is T4+T2. For the targets locations calculation, the travel time of EM wave is taken single sided e.g. (T1+T2) / 2.

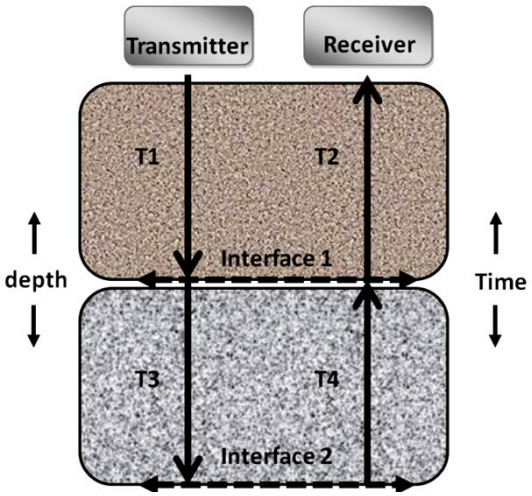

Figure 2.7. Object location by travel time calculation of EM waves

Also if the calculation of EM wave propagation velocity is possible, an absolute measurement of depth or thickness can be made (Daniels, 2007). To calculate the travel time of EM waves in any material, the propagation velocity of EM is needed. The propagation velocity of EM waves in any medium is governed by medium's electrical properties i.e. dielectric constant and the magnetic permeability (Saarenketo, 2009). As discussed before, the magnetic permeability of materials is ignored thus leaving behind the dielectric constant.

For the calculation of EM wave velocity in any material, the velocity of EM wave in free space (vacuum) is considered. The EM wave propagation velocity in vacuum is given by Equation 2-4 (Daniels, 2004),

$$C_0 = \frac{1}{\sqrt{\mu_0 \varepsilon_0}} \text{ (m/s)} \qquad 2\text{-}4$$

Where,

C_0 is the propagation velocity of EM waves in the free space ($3\ 10^8$ m/s)

μ_0 is the absolute magnetic permeability of the free space ($4\pi\ 10^{-7}$ H/m) and,

ε_0 is the absolute electric permittivity of the free space ($8.8541\ 10^{-12}$ F/m)

From Equation 2-4, it can be concluded that the velocity of EM wave is inversely proportional to the electrical properties of any material. By knowing the EM wave velocity in free space and the electrical properties of material under observation, the velocity of EM wave is calculated by Equation 2-5 (Daniels, 2004; Huisman et al., 2003),

$$C = \frac{C_0}{\sqrt{\mu_r k}} \text{ (m/s)} \qquad 2\text{-}5$$

Where,

C_0 is velocity of light in free space ($3 \cdot 10^8$ m/s)

C is velocity of propagation of EM waves in any material (m/s)

μ_r is relative magnetic permeability of material under observation and,

k is dielectric constant of the material

Knowing the propagation velocity of EM wave, the depth of target is calculated by the Equation 2-6 (Daniels, 2004; Saarenketo, 2006):

$$S = \frac{C_0 \left(\frac{m}{ns}\right) t(ns)}{2\sqrt{k}} \quad (m) \qquad 2\text{-}6$$

Where,

S distance of the object from the transmitter/receiver (meters)

C_0 propagation velocity of EM wave in free space (3×10^8 m/s ≈ 0.29979 m /ns)

t travel time of EM waves from transmitter to object and then back to the receiver (nanoseconds "ns")

k is the dielectric constant of the material

Further details about EM wave properties, GPR systems, material properties, the surveying methods and the processing techniques are explained in the Sections below.

2.3 EM waves characteristics

The EM waves are of many types for example radio waves, light waves, mobile waves, etc. Each type of EM waves is different from other type of waves based on its properties. These properties are important regarding optimum EM wave selection for material analysis is first step towards successful GPR survey. In the following sections, some EM wave's properties and related terminologies are given to provide a brief knowledge about EM waves.

2.3.1 Wavelength

The wavelength can be defined as the distance between the two peaks (positive or negative) of the same phase of an EM wave in the direction of propagation, in consecutive cycles (Figure 2.1) (Daniels, 2004). The wavelength is one of the key factors describing EM wave attributes i.e. describing extent of material investigation by EM waves and the depth of EM wave penetration in the material (Annan, 2009). The probing depth decreases with decrease in EM wavelength (Saarenketo, 2006). The wavelength "λ" (m) can also be related to other EM waves properties such as the velocity "v" (m/s) and frequency f (Hertz) by Equation 2-7 (Daniels, 2004),

$$v = \lambda f \qquad 2\text{-}7$$

Where,

v is the EM wave velocity in material (m / s)

λ is the wave length of EM wave (m), and

f is the frequency of EM wave (Hertz (cycles/second))

From Equation 2-7, if we keep velocity of EM wave constant, the wave length and frequency are inversely related to each other.

2.3.2 Frequency

The frequency is the number of repetitions of cycles in unit time. Its unit is hertz "Hz". The frequency of GPR systems is usually expressed by its central frequency "fc" which is the

arithmetic mean of the "lower cut-off frequency" and "upper cut-off frequency" of the EM wave spectrum, generated by the transmitter (Figure 2.8) (Daniels, 2007; Annan, 2009). The term central frequency is used because GPR transmitter usually generates a pulse of wide range of frequencies (Bristow, 2009). A frequency spectrum of Aladdin GPR system, taken on standard asphalt pavement is shown in Figure 2.8. The spectrum starts from ≈ 0.2 GHz and goes up to ≈ 4.2 GHz. The central frequency of the system is taken as 2 GHz.
The relationship of EM wave frequency to its wavelength is given by Equation 2-7. The central frequency "f_c" (Hertz) of a GPR system can be related to its bandwidth "B" (Hertz) by ratio "R" (Annan, 2009). The relationship between "f_c" and "B" is given by Equation 2-8,

$$R = {}^{B}/_{f_c} \qquad 2\text{-}8$$

Where,

R Ratio of bandwidth to central frequency

B Bandwidth (Hz)

f_c Central frequency (Hz)

The EM wave pulses are characterised based on the ratio of bandwidth to central frequency. The greater the bandwidth is more will be the resolution and penetration depth of system. For example, ultra wideband ($R \geq 1$) GPR systems are preferred over narrow wide band systems (Annan, 2004).
The central frequency is one of the most important characteristics for GPR systems (Annan, 2004). It defines GPR important characterises like resolution of test results and the penetration ability of EM wave in the material. The penetration ability of EM wave in any material is inversely proportional to its frequency i.e. the probing depth of EM wave decreases with increase in its frequency (Annan, 2009). Therefore, selection of EM wave frequency for required penetration depth and outcomes resolution is crucial (Skolnik, 1981).

2.3.3 Bandwidth

Bandwidth can be defined as the specific range of frequencies (upper and lower frequencies) over which performance of an antenna confirms some defined standards (Balanis, 1997). In a bandwidth, the electromagnetic wave generated by an antenna continuously changes its magnitude of frequency in lower – upper – lower frequency form. From this complete frequency range, a selected part (criteria differ for each GPR equipments) is called as antenna bandwidth. The remaining frequencies below certain antenna power level (in dB) may not be useful (Daniels, 2007). The bandwidth is measured in "hertz". Most of the antennas in market are distinguished on basis of their bandwidth as it defines the ability of a GPR system to handle a frequency range i.e. send and receive EM signals in a medium (Annan, 2004).

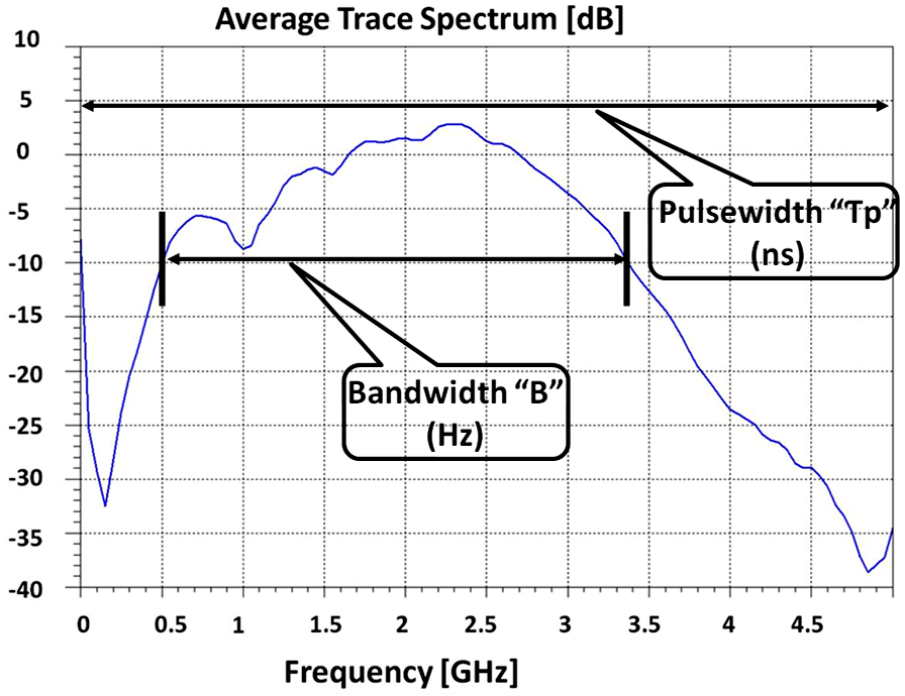

Figure 2.8. The average trace spectrum of Aladdin antenna (survey on asphalt pavement) showing central frequency (GHz) and power (dB) (Software: GRED)

Bandwidth for impulse and continuous wave radars is different. This is because of the technique used for EM wave generation in both systems (pulse and continuous waves). For impulse radars, bandwidth "B" is defined by Equation 2-9 (Annan, 2004; Koppenjan, 2009):

$$B = {}^{1}/_{\tau_p}\,(\text{Hertz})(\text{for impulse radars}) \qquad 2\text{-}9$$

Where "τ_p" is the pulse width of the transmitted EM wave. The pulse width can be described as the time taken for a single EM wave (sinusoidal) to be generated followed by sleep time of transmitter and then again EM wave generation. On the other hand, the bandwidth for continuous wave (CW) radars systems is different as they continuously transmit EM waves. In case of CW radars, it's the difference in start frequency "f_{min}" to the maximum frequency peak "f_{max}".

$$B = (f_{max} - f_{min})(\text{Hz})(\text{for CW radars}) \qquad 2\text{-}10$$

2.4 GPR hardware system

The GPR system hardware beside its basic four components, may include additional units such as Global Positioning System (GPR), distance calibration wheels, noise reduction units, etc. (Saarenketo, 2006; Morey, 1998). Some of these components of GPR system are shown in Figure 2.9. The system shown in Figure 2.9 has antenna system with separated transmitter and receiver i.e. bi-static GPR system. The GPR systems based on the position of transmitter and receiver in antenna can be divided into mono-static and bi-static systems (Lahouar, 2003; Koppenjan, 2009). The mono-static radars are those which use a single

antenna for transmitting and receiving the EM waves. On the other hand, bi-static antennas use separate hardware for the EM wave's transmission and back reception (Annan, 2004).

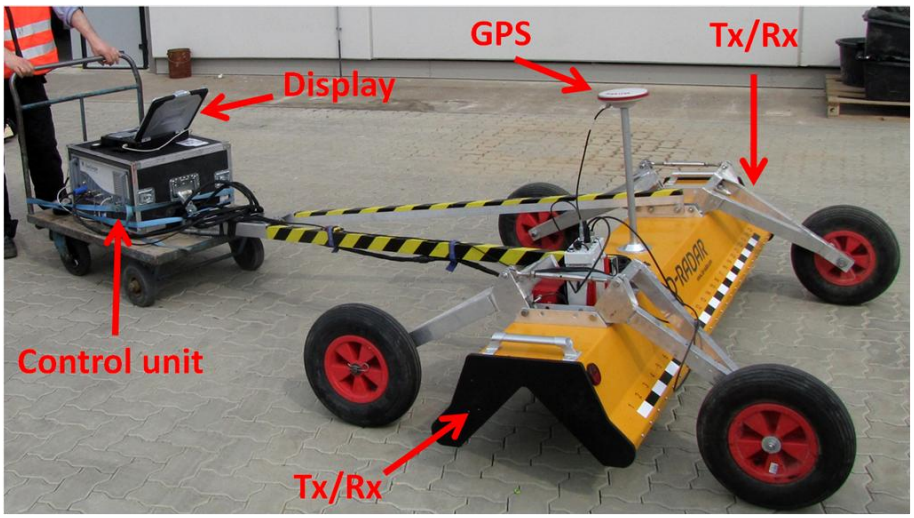

Figure 2.9. The components of GPR system (3D-Radar, Norway)

The above mentioned parts of GPR with respect to their functioning are illustrated in the block/ schematic diagram in Figure 2.10. In this schematic diagram (Figure 2.10) connection between various parts of GPR system is shown such as the sampling head, generator. The schematic diagram describes the GPR processes in a glance for example, where the EM waves are generated and how they are initially processed before display.

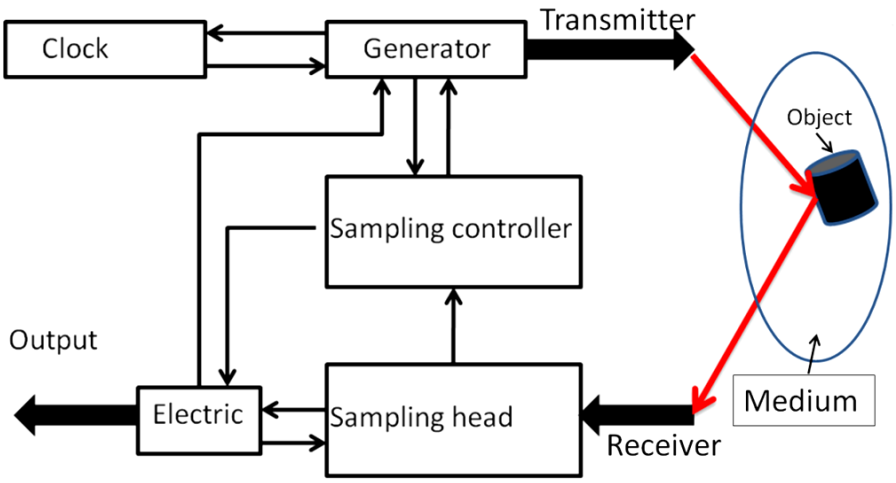

Figure 2.10. Schematic diagram showing the basic working phenomenon of GPR (Daniels, 2007)

It must be noted that the clock in the block diagram (Figure 2.10) is attached to GPR generator as well as to receiver. This is because the time plays a vital role to synchronize the GPR parts for optimum functioning. The GPR transmitter and receiver are explained in the Section 2.4.1 and 2.4.2 respectively.

2.4.1 GPR transmitter

The GPR transmitter characteristics are negotiations among the conflicting needs of good signal reliability over a wide bandwidth, transmitter gain, and portability (Davis et al., 1989). In most cases of GPR measurements, the medium is inhomogeneous dielectric and hence the properties of transmitters are governed by material under study. For example, in case of wide bandwidth transmitters, the possibility of noise recording is more due to reflections from fine details. The total bandwidth is not always useful as a defined bandwidth limit is received back by receiver. For example, the bandwidth shown in Figure 2.8 for Aladdin GPR system, is useful "-10 dB" range for Aladdin (GPR), although each GPR system may have its own defined useful bandwidth range limits.

Typical parameters of GPR transmitter efficiency are gain, radiation pattern, beam width, and polarization (Daniels, 2009). A basic transmitter emits EM waves as emitted by an isotropic transmitter (Figure 2.11(a)).i.e. constant transmitting power and equal radiation in all directions (Koppenjan, 2009). However, if the radiated power is redistributed and directed in single direction in form of beam, then this results in increase of the power density (Skolnik, 1981). This effect is called antenna gain, a term widely used to mention GPR antenna attributes. The antenna gain is expressed in decibel "dB" (10 log10). In case of comparison with isotropic antenna, the units are "dBi" and dipole "dBd". The isotropic transmitter is shown in Figure 2.11(a).

Another type of transmitter mostly used in modern GPR hardware is dipole transmitter. The dipole transmitter radiation pattern is different from isotropic transmitter i.e. the EM waves strength is not equally distributed (Balanis, 1997). This helps efficient use of transmitter power. The radiation patterns of dipole transmitters are shown in Figure 2.11(b).

The reported advantage of dipole over isotropic transmitter gives the possibility for promising investigations of shallow and deeper objects with single frequency (Daniels, 2009). The radiation and gain pattern of a dipole transmitter is shown in Figure 2.11(c). The power gain of a dipole transmitter on its radius on azimuth plane (Figure 2.11(b)) is unity. The radiation pattern is however different on "x", "y" and "z" plane (Figure 2.11(c)). Every effort is made to make transmitter 100 % efficient, i.e. no losses of energy. However, the dream comes not true due to losses during EM wave propagation in medium (Section 2). Transmitter efficiency can be described as the ratio of its power available for radiation to the total power applied at transmitter terminals (Daniels, 2007). There are many kinds of losses responsible for decreasing transmitter efficiency. The losses are summed up in Equation 2-11 below (Daniels, 2004),

$$Lp = Le + Lm + Lt1 + Lt2 + Ls + La + Lsc \qquad 2\text{-}11$$

Where,

Lp	Total path loss
Le	transmitter efficiency loss in dB
Lm	transmitter mismatch losses in dB
Lt1	transmission loss from air to material in dB
Lt2	retransmission loss from material to air in dB

Ls	transmitter spreading losses in dB
La	loss due to material in dB
Lsc	target scattering loss in dB

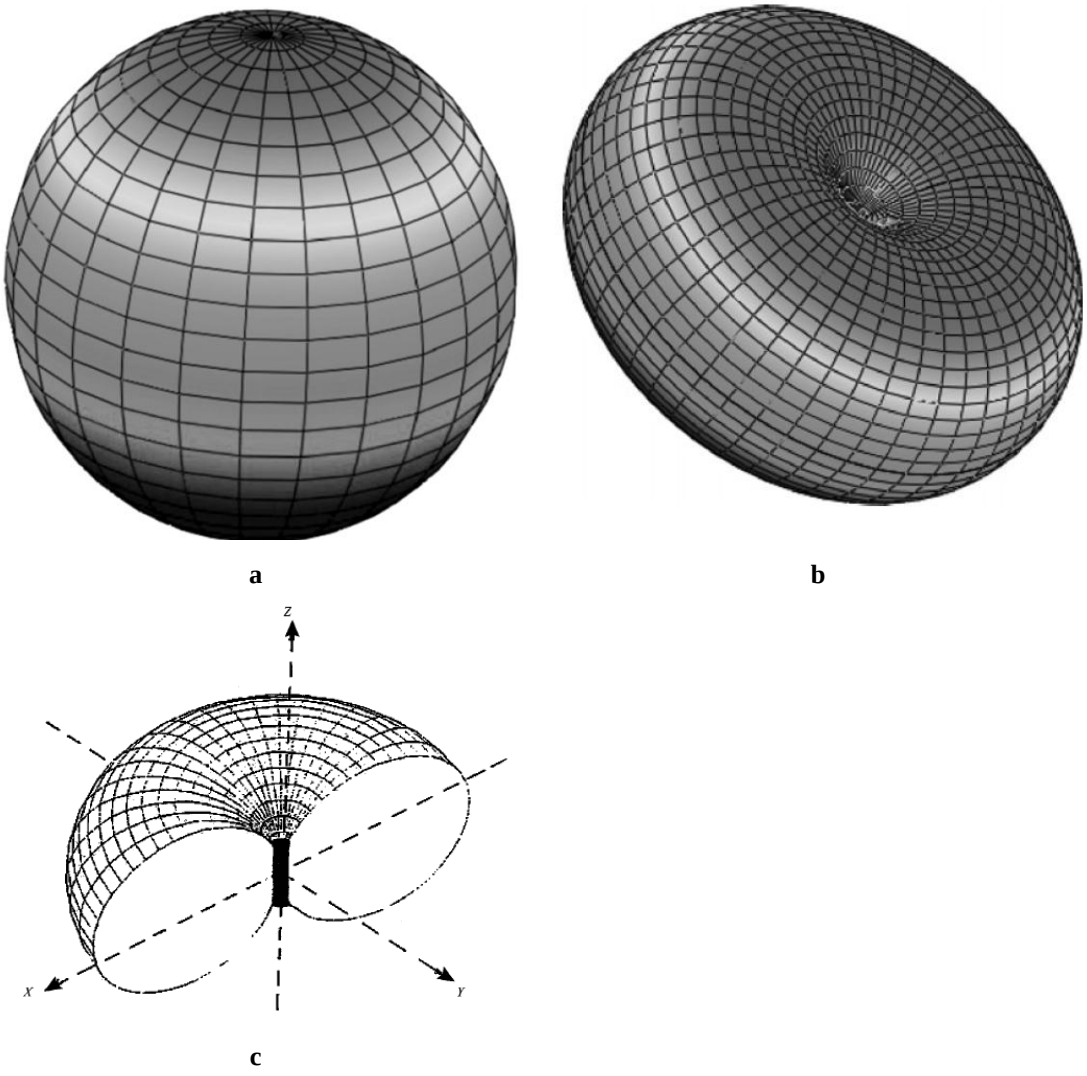

Figure 2.11 The radiation patterns of GPR transmitters, (a) isotropic transmitter, (b) dipole transmitter and, (c) cross-section of a dipole transmitter (Daniels, 2009)

Based on EM waves generated, the GPR systems can be divided into two main types i.e. CW and pulse systems. Due to the different type of EM waves, both systems look apparently different. This is because CW radar systems, due to continuous functioning of transmitter and receiver, are bi-static systems (Figure 2.9) whereas the pulse systems are mono-static systems (Figure 3.2). The systems are explained in the sections below.

2.4.1.1 Continuous Wave (CW) radar

The CW radar is the GPR system which transmits a high frequency EM wave continuously and also receive back reflected waves continuously. In radar history, the CW radars were developed first. This was due to the simple design mechanism of radar which involved separate transmitter and receivers. The two main problems associated with CW radars are to prevent the direct reception of EM waves from transmitter to receiver (antenna shielding), and analysis of reflected EM waves in time domain. The antenna shielding due to modern day sophisticated materials is solved successfully. However, the later problem is due to the data analysis in frequency domain or object detection by Doppler-frequency shift (Skolnik, 1981). The initial radar systems developed were not useful to be used as GPR. This was due to the inability of Doppler-frequency shift analysis in detecting multiple objects, as nowadays carried out in most GPR surveys. This shortcoming was removed by altering CW technology to Frequency-Modulated Continuous Wave (FM-CW) (Koppenjan, 2009).

The difference between CW and FM-CW is that the later is with alternating EM wave characteristics (Section 2.3) either in wave length or amplitude. The EM wave properties (frequency) repeat themselves after specific time and thus reflected wave can be compared to that of incident wave. Thus the presence of objects, its size and depth analysis is possible by comparing the amplitudes of transmitted and received signals (Leckebusch, 2011; Koppenjan, 2009). The wave comparison of FM-CW systems is shown in Figure 2.12. In Figure 2.12, f_1 is the lowest frequency and f_2 is the highest frequency of generated EM wave. At any given time "T", the received EM wave is compared to that of transmitted wave. The difference in frequency of received wave at time "T" is Δf. The Δf or the lag in amplitude peaks of transmitted and received wave is transmitted into travel time. By knowing the propagation velocity of EM wave in the material, the depth or distance of object is calculated.

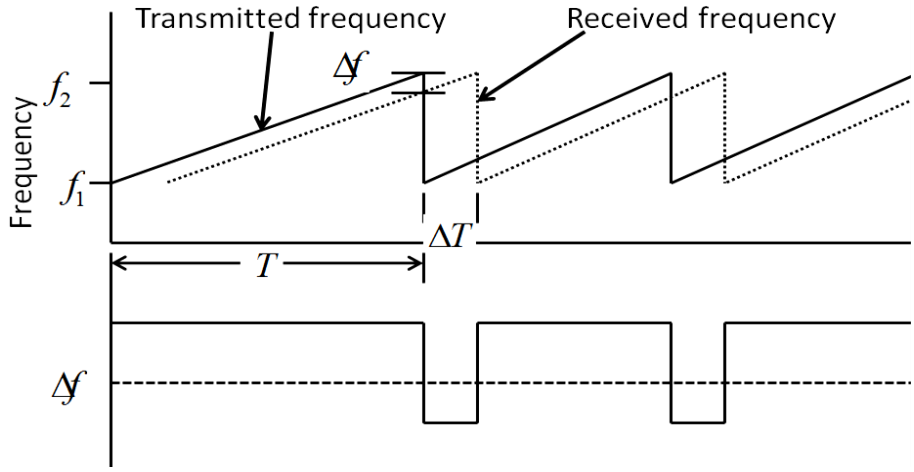

Figure 2.12. The operating mechanism of FM-CW radar (Daniels, 2004)

2.4.1.2 Impulse radar

The impulse radars, as the name suggests, have transmitters which generates pulses of EM wave. The time interval between the pulses generation is fixed (in nanoseconds) and therefore, the impulse radar acquires data in time domain (Annan, 2009). The time between two pulse generations is called the pulse repetition time (PRT) or time-window and the number of pulses transmitted in one second is called the pulse repetition frequency (PRF). The time taken for each pulse to be transmitted is called the pulse width (PW) or pulse duration. The PRT is based on the knowledge of EM wave propagation velocity and the required probing depth. The performance of GPR system (the total dynamic range (TDR)) which is the measure of its ability to receive least reflected signal, is influenced by PRF. This is because the receiver shutdowns and does not wait for far signals.
Due to mono-static nature of impulse GPR systems, the systems are handy and economical. The other benefits include, smaller sized control units (compare to FM-CW systems), smaller data size and most important economical prices. Therefore, most modern GPR systems available in the market are impulse radar systems (Koppenjan, 2009; Cassidy, 2009b). In this research, all GPR systems used were impulse radar systems except the GeoScope system (Section 3.2.4).

2.4.2 GPR receiver/antenna

The receiver in GPR systems can be of many types depending on survey type, EM wave type, environmental issues such as amount of noise and the material properties. In the following paragraphs, the details of receiver according to GPR survey types are provided.

2.4.2.1 Ground-Coupled Antennas (GCA)

The GCAs are nearly in contact with the ground surface as shown in Figure 2.13 (Saarenketo, 2009). The GCAs are deployed for better EM wave penetration into the ground and thus resulting in better resolution (Al-Qadi et al., 2010; Saarenketo, 2009; Morey, 1998). Therefore, GCAs are used for fine details investigation in pavement surveys such as cracks, reinforcements, cables, etc. (Saarenketo, 2009). Nonetheless, ground-coupled antennas can also be used for pavement layers thickness measurements and layers delamination (Ahmad et al., 2011). The precaution in using GCA is that their EM wave properties e.g. central frequency, bandwidth, etc. can be affected by ground materials especially by conductive materials (Conyers, 2004).

2.4.2.2 Air-coupled antennas

The air-coupled antennas are suspended above the surface (150 to 500 mm) with varying height (Morey, 1998). Mostly horn antennas are used as air-coupled antennas due to their better reception power (Al-Qadi et al., 2010; Lahouar, 2003). The Air-coupled antennas are mostly used when surveying area is large and high surveying speed is required. In such surveys, the pavement is investigated for e.g. pavement settlement analysis, layer's thickness measurement, etc. The most frequent use of air-coupled antenna in pavements is

for layers thickness measurement although pavement density investigation, in-situ dielectric constant measurements also have been reported (Al-Qadi et al., 2010). The air-coupled antenna is shown in Figure 2.13. Depending on survey objectives, with the air-coupled antennas GPR survey can be carried out at nearly highway speed (Hugenschmidt et al., 1998) (Figure 2.13).

Figure 2.13. The GPR survey types including air-coupled antennas suspended in air and a ground-coupled antenna, both attached to vehicle

The drawback of air-coupled antenna survey is the low depth of penetration into the pavement structure since part of the EM energy, sent by the antenna, is reflected back by the pavement surface (Lahouar, 2003).

2.5 GPR surveying

For optimum GPR surveying, selection of GPR system plays a vital role. Based on the discussions in previous sections, a range of parameters such as bandwidth, adequate signal to noise/clutter ratio (SNR, SCR), antenna frequency, transmitter polarization, receiver strength, etc. must be considered when system selection is required (Yelf, et al., 2006). On the other hand, the survey objectives (details to be investigated in this thesis later on) must be taken into account. Some requirements for GPR survey include efficient induction of EM energy into the ground, adequate energy of EM waves to bring enough information from reflected objects (Daniels, 2004; Daniels, 1996).
Furthermore, prior knowledge about target properties leads to better survey and data analysis. The material properties can also be examined on site as is shown in Figure 2.14. To examine the layers thickness and visual inspection of materials, core samples of ≈ 5 cm in diameter can be enough. However, for the calculation of pavement dielectric constant, core samples of ≈ 15 cm in diameter are required. The system shown in Figure 2.14 shows an equipped mobile GPR system with the capability of onsite coring in real time. This not only saves time but the GPR surveys can also be monitored and guided in real time. The

material properties are investigated again before survey as the material properties changes with time.

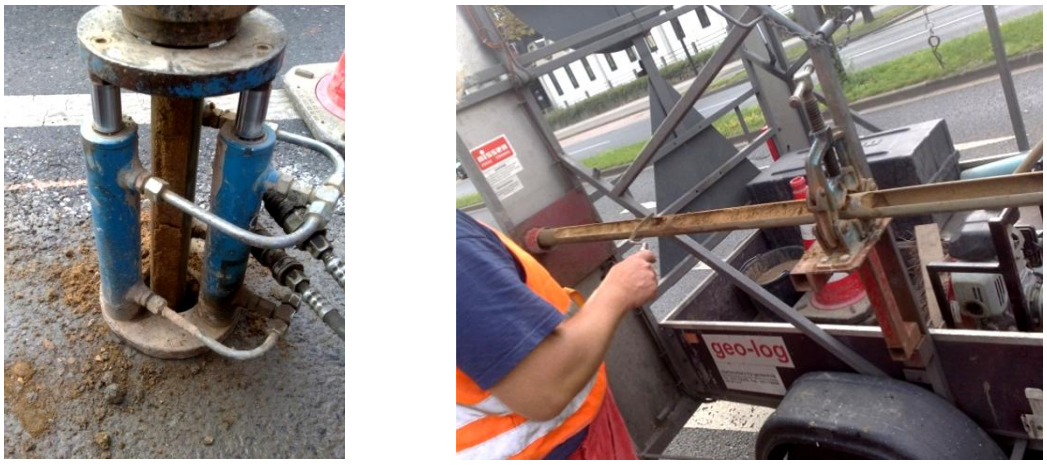

a b

Figure 2.14. Onsite coring for GPR outcomes validation, (a), coring in progress and, (b) material properties and layers thickness analysis (geo-log Inc. Germany)

Moreover, the GPR survey extremely depends upon users experience (Annan, 2009). This is because the user defines the survey direction by inspecting the onsite data during surveys. Therefore, understanding GPR hardware and GPR-grams is required to conduct the GPR survey.

In GPR surveys, the purpose is to collect data by moving the GPR antenna. The data can thus be collected by holding GPR in hand, attached to vehicle, in cored holes or by aircraft (Olhoeft, 1999). The data collection is performed by scanning the material which depends on survey objectives (target properties) and therefore multiple scans may be required. In case of 3-D survey, scans in perpendicular-horizontal direction are required.

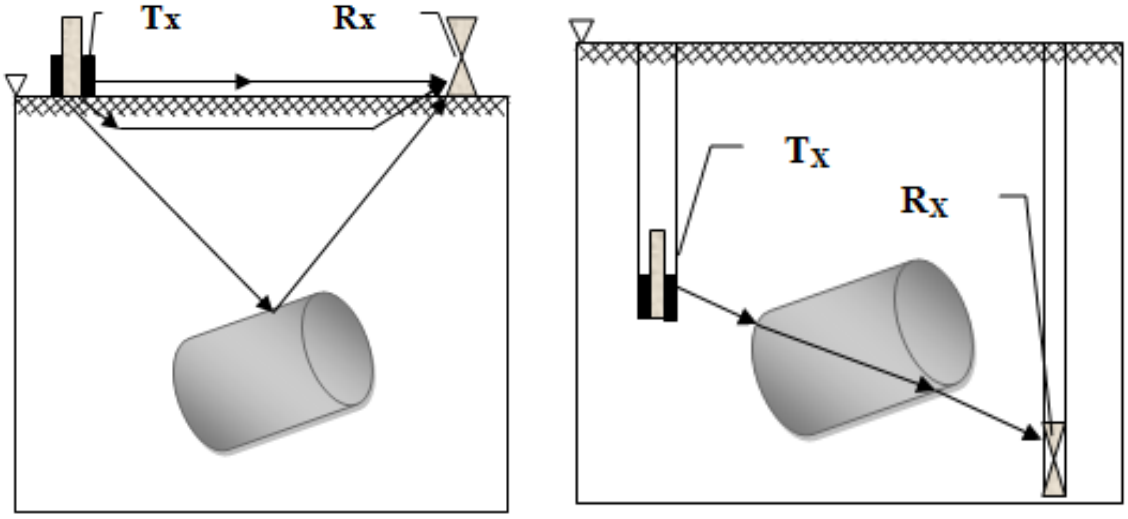

a b

Figure 2.15. The GPR surveying methods, (a) Reflection survey, and (b) Refraction survey

On the basis of EM waves received, GPR surveys are divided into reflection and refraction surveys as shown in Figure 2.15 (Annan, 2009; Daniels, 1996). The reflection survey principle is shown in Figure 2.15(a). The EM waves transmitted by the transmitter are reflected due to obstruction (object) and the reflected EM waves are collected on the ground surface. The reflection survey method is widely used in most of the GPR surveys (Liu et al., 2006). This is due to the simplicity of survey e.g. no core-holes required (as required in refraction survey) and possibility of mono-static antenna usage.
On the other hand, refraction survey is conducted by bi-static GPR systems. The refraction survey is shown in Figure 2.15(b). In this kind of GPR survey, the medium is packed between transmitter and receiver placed in core-holes, opposite to each other. The refraction survey is used where air-clutter has to be avoided such as surveying in rock tunnels (Daniels, 2004). As refraction survey was not carried out in this study it will not be discussed anymore.

2.5.1 GPR limitations

There are some limitations associated with GPR hardware use. To increase the survey accuracy, it is recommended to avoid using GPR in those areas where its abilities are the lowest such as Blind zone, Fresnel zone, etc. Therefore, a short description of these limitations is provided below.

2.5.1.1 Blind zone

The Blind zone or sometimes also referred to as the dark zone which is nearest to GPR system where it cannot detect the same object which is normally detected by the same system when placed far from the system (Daniels, 2007). This zone starts from transmitter and goes deeper into medium. The blind zone length depends on the properties of EM waves such as its wavelength (Daniels, 2004). As the wavelength of a GPR decreases, the blind zone of GPR system decreases. As a thumb rule, the blind zone is taken as 1/3 wavelength of the EM wave (Annan, 2004). The signals recorded within the blind zone of a GPR may thus not represent the ground truth and thus must be confirmed with different EM wave frequencies (Pearce et al., 2002).

2.5.1.2 Fresnel zone

The Fresnel zone can be defined as the distance within which transmitted and received EM waves interact with each other and result in miscalculations like weak or strong reflected EM waves (Daniels, 2004; Pearce et al., 2002). The shape or pattern of Fresnel zone of a GPR system depends on its antenna radiation pattern (Pearce et al., 2002). Beside GPR antenna characteristics, the Fresnel zone of GPR system depends on EM wave attributes and system properties (Bristow et al., 2003). The EM wave propagation and energy attributes contribute influencing Fresnel zone whereas, the target influences it by its characteristics like geometry and distance from the antenna. The medium geometry, in case of asphalt specimens or on pavement corners/sides, care must be taken to avoid investigations in Fresnel zone.

2.5.2 EM waves survey angles

When EM wave propagates thorough more than two materials, Snell's law is applied. The Snell's law defines the change in direction of wave where the velocity of EM wave in the mediums at the interface is not the same. This phenomenon is applicable for the determination of critical angle in radar surveys, if necessary. However, in most GPR surveys because of the dielectric nature of materials, Snell's law takes the simplest form (Annan, 2004) i.e.

$$\frac{\sin\theta_1}{V_1} = \frac{\sin\theta_2}{V_2} \qquad 2\text{-}12$$

Where,

θ_1 and θ_2 = EM wave propagation angles to the vertical axis in medium 1 and 2

V1 and V2 = EM wave velocity in medium 1 and 2 respectively (m/s).

Also in GPR surveys the distance are shorter and thus even considering EM wave refraction or reflection angels may not result in vast differences. The calculation of many reflection and refraction angles in the medium may not be possible due to unknown parameters such as point of reflection. To show how complex the angle calculation can be in GPR surveys some possible reflection and refraction angles by the EM wave in a two layered medium are shown in Figure 2.16. In this figure, the 12 cm antenna total width is taken for "Aladdin" system antenna (the GPR system mostly used in this research). However, the exact location of transmitter and receiver in the antenna were known. It can be seen in Figure 2.16 that transmitted and reflected EM waves make θ1 and θ2 angles respectively according to medium change. It is difficult to calculate the angle value in case of each scan, EM wave angle is ignored. The ε_{r1} and ε_{r2} are the relative dielectric permittivities of asphalt pavement layers.

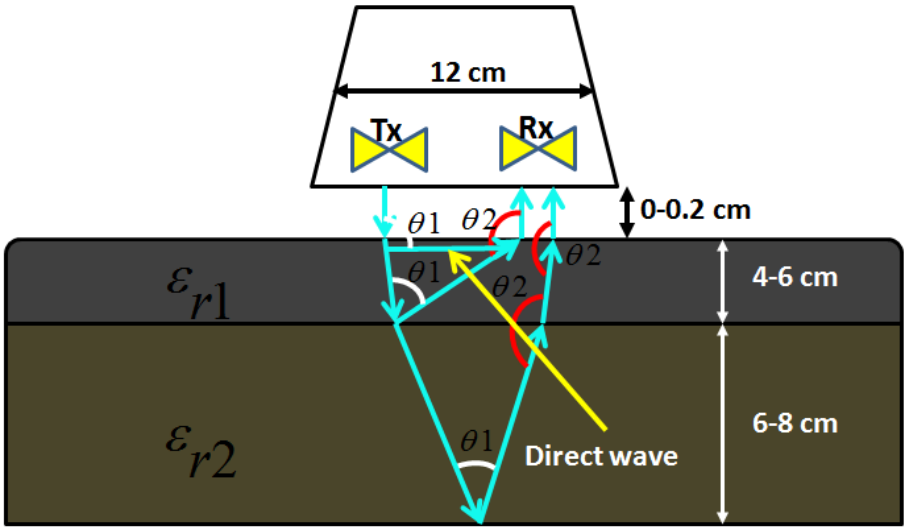

Figure 2.16. The EM wave reflection and refraction angles in the medium

The GPR reflection or refraction angles may be considered in surveys where the GPR systems are bi-static and the EM wave travelled distance is known (Annan, 2004). The examples of surveys conducted by bi-static systems are common midpoint "CMP", common-offset and core-hole surveys. In these surveys the objective is to find out material properties by keeping EM wave propagation distances. In routine GPR surveys with mono-static systems (also with most bi-static systems such as GeoScope) the refraction or reflection angles of EM wave in the materials is ignored.

2.5.3 The GPR data

The GPR antenna collects data by gathering a series of traces at discrete points along the travel direction. The depth is presented by stacking of reflected EM waves according to their arrival time (Morey, 1998). The EM waves in material starts being affected by the object's energy even when it is away from the object. The influence of object on incident EM wave is shown in Figure 2.17(a). The EM wave starts being affected when it is at point -2 on x-axis. The amplitude of EM is shifting upward when GPR is moving on x-axis, towards +2. The amplitude is on its maximum elevation when GPR is directly above the object, at position 0. The phenomenon is reversing when GPR is moving away from the object.

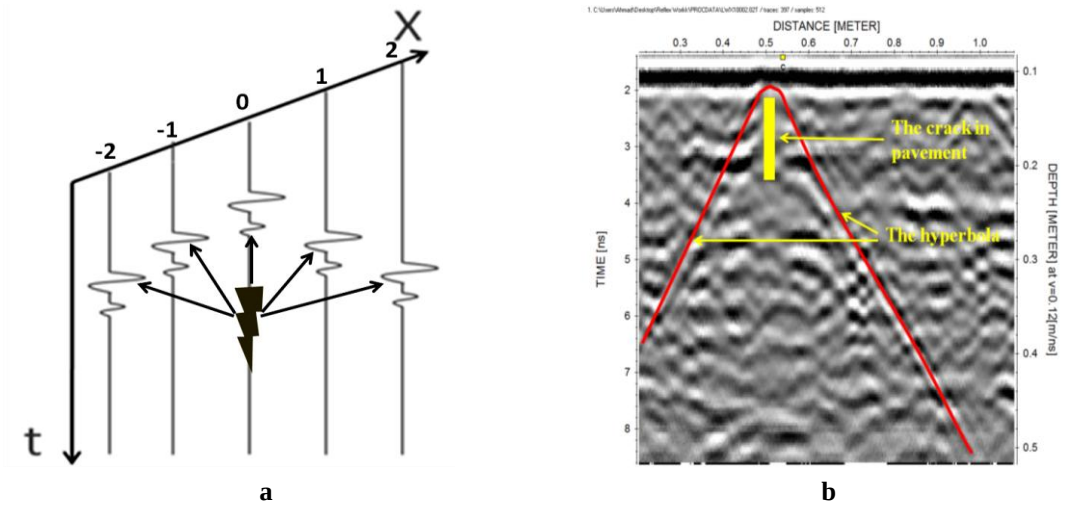

Figure 2.17. The data collection by GPR, (a), reflected EM wave's (A-scans) position in GPR-gram due to a crack, (b) a 2-D GPR-gram showing a hyperbola due to a crack in asphalt pavement

Each EM wave on x-axis shown in Figure 2.17(a), is called single pulse. These pulses unite to form a one dimensional A-scan which provides EM wave reflection related to its propagation velocity on y-axis (Daniels, 2007).

Many A-scans combined side by side form a profile of the subsurface. This combined file is called two dimensional or 2-D. It is called 2-D because it contains two dimensional data set b(x, t) where x is the horizontal distance (x-axis) and t is the EM wave travel time (y-axis) (Daniels, 2007). A 2-D survey result, called GPR-gram is shown in Figure 2.17(b). The disturbed scans as shown in Figure 2.17(a) form a hyperbola, in 2-D GPR-gram as is presented in Figure 2.17(b). Therefore, any object, responsible for EM wave reflection is

seen as a hyperbola when appears in a 2-D scan. The 2-D GPR-gram is informative and object location can be marked with increased accuracy.

For the three dimensional or 3-D scans, many 2-D GPR-grams are combined to form a 3-D GPR-gram (Figure 2.18(a)). The 2-D GPR-grams are stacked side by side with the help of suitable software. The additional axis in 3-D is the width of scan area (x, y, t) (Figure 2.18(b).). The missing information between two 2-D scans is interpolated wherever required.

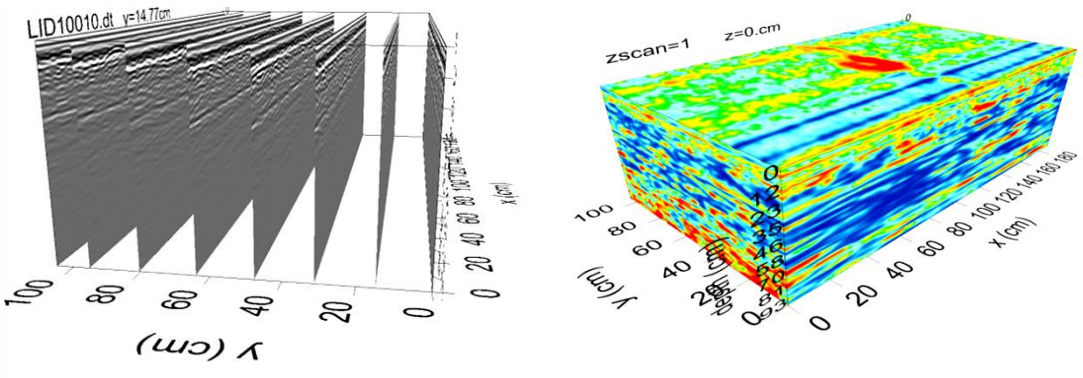

a **b**

Figure 2.18. The 2-D and 3-D GPR-grams, (a) stacking of 2-D GPR-grams and, (b) 3-D GPR-gram (Software: GPR-SLICE)

The quality of 3-D scans can be improved in two ways. Firstly by improving the quality of individual 2-D scan by decreasing the pulse repetition time (PRT). This is called increasing sampling rate which helps taking information on short intervals and thus less interpolation between two scans (shown in Figure 2.17(a)) is needed (Annan, 2009). By this way more 2-D data is collected and error chances in 3-D survey decreases. Secondly the quality of data is enhanced by collecting data with more number of samples per scan. The number of samples per scan is the stocking of data in GPR-grams on y-axis (depth). This means that information is collected on decreased depth intervals and thus 2-D GPR-gram contains more and clear information. The samples per scan in GPR surveys are in the form of "$f(2)^x$", where x ranges normally from 6 to 13 in most GPR systems i.e. 64, 128, 256, 512, 1024, 2048, 4096, etc.

2.6 Data processing

The raw data collected from GPR survey is not readable before it is processed. Usually, depending on the required investigation, the data analysis takes more time then surveying. The data processing depends on personal opinion, experience and the nature of survey/data (Cassidy, 2009b). The primary objective of data processing is to remove clutter/noise and clear the information required (Annan, 2009). The data processing is divided into standard processing and advanced processing. The standard processing is required for extracting basic information such as layers in pavements. The standard data processing steps include dewow, time-zero correction, band-pass filtering, gain control and topographic correction.

Nevertheless, for the investigation of fine details advanced processing is carried out. The advanced data processing techniques include migration, time into depth conversion and f-k filtering. Hence more processing and data interpretation is required in case of asphalt pavements then of homogeneous materials. The precaution about data processing is that before processing the data, it must be ensured that there is required information within the data. Extreme processing may damage the data and can lead to misconceptions (Cassidy, 2009b). The selected data processing steps applied on GPR data in this study are discussed below.

2.6.1 Dewow filtering

The term "wow" in GPR survey means receiver saturation by recording early arrived signals i.e. the direct EM waves (Annan, 2009). The "dewow" is then the removal of the initial EM wave's component/bias in the frequency band (Figure 2.8) (Cassidy, 2009b). This is done with passing the received signal from a high-loss temporal filter (Annan, 2004). The process is shown in Figure 2.19. The raw recorded GPR signal in Figure 2.19 is out of phase due to which it is low amplitude (energy). The processed signal on the other hand, brings all signals in accordance with the traces and hence the information is visible. The practical situation is shown in Figure 2.20(a) where received raw data is not at all readable.

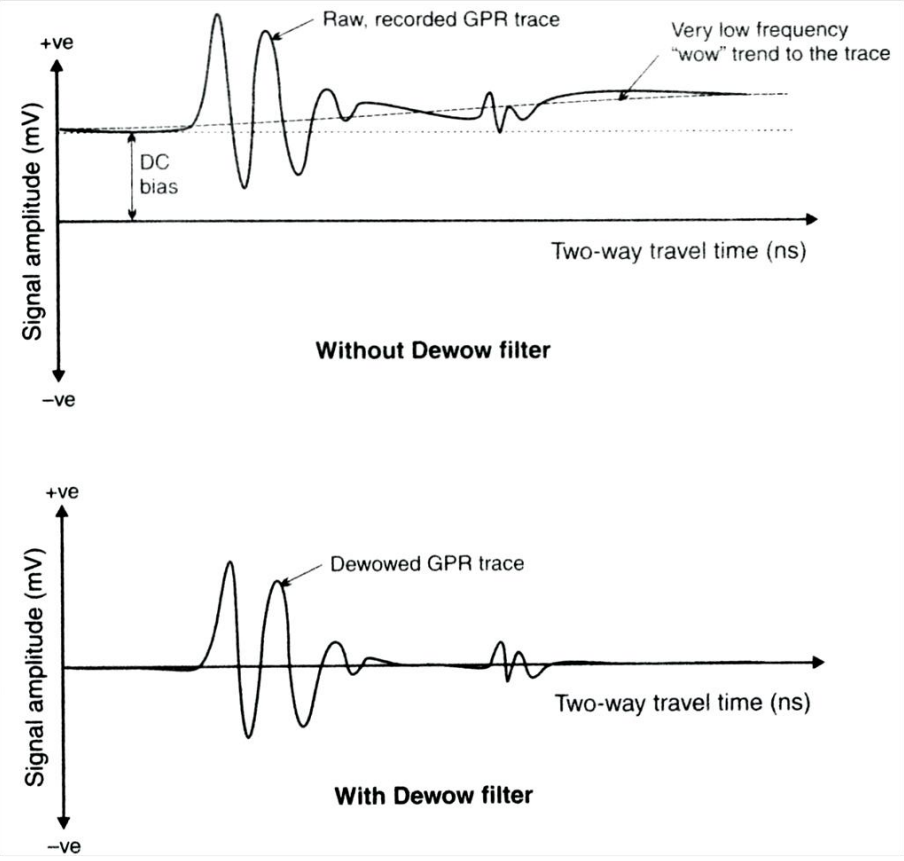

Figure 2.19. Dewow processing of radar data, (top) raw signal, (bottom) signal after dewow filtering (Cassidy, 2009b)

The data from MALA GPR system is shown in Figure 2.20(a) (top) which is not readable before dewowing process. However, the information can be seen in the outcomes followed by data processing with ReflexW software (Figure 2.20(a) (bottom)).

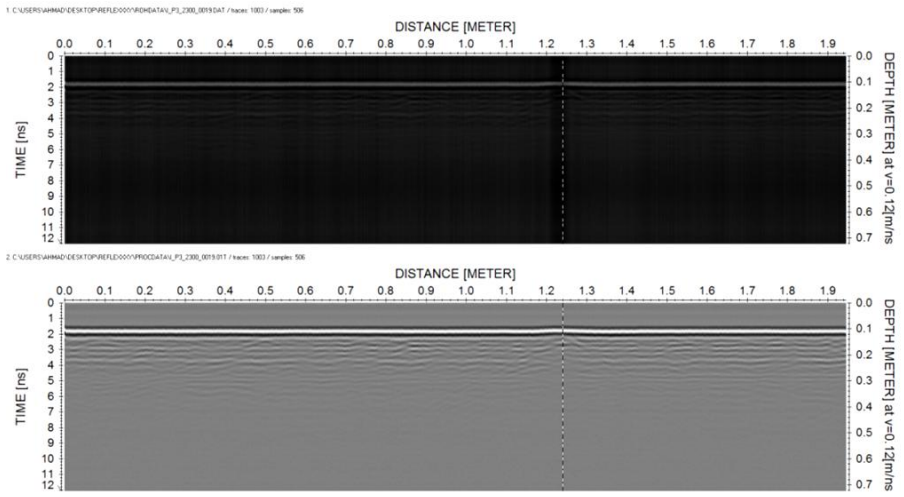

Figure 2.20. GPR raw data before (top) and after dewow filter (bottom) (MALA HF, 2300 MHz, Software: ReflexW)

2.6.2 Background removal

Background removal is the process of subtracting average of all traces (scans) from the GPR data (Annan, 2009). The process is useful for removing unwanted signals (noise) removal and compensating for the antenna ringing (Cassidy, 2009b). The constant noise or clutter level, for example in data is deducted. In Figure 2.21, for example the surface reflections are masking GPR-gram information. After processing, the week hyperbolas are made visible.

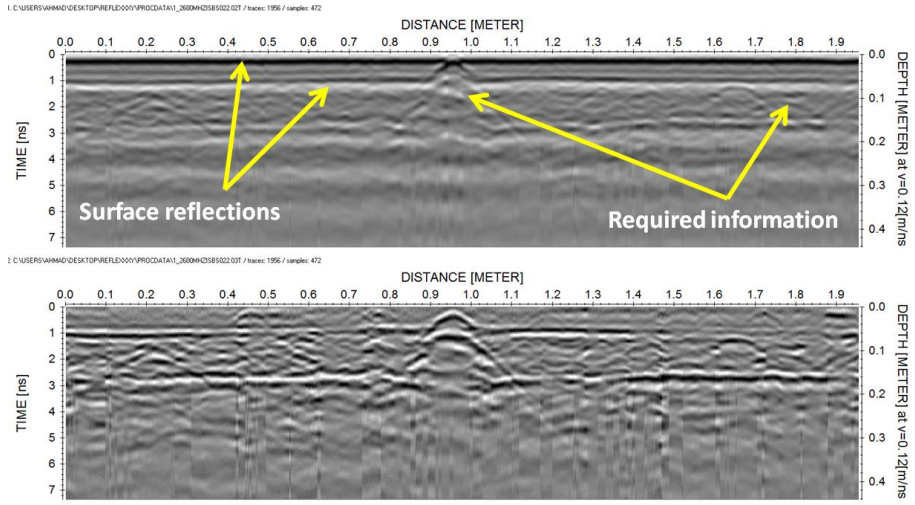

Figure 2.21. GPR data before and after background removal, (top) before background removal, (bottom) after background removal processing (System: SIR-20, 2600 MHz, Software: ReflexW)

2.6.3 Time zero correction

The first arrived EM wave effects the position of ground interface in GPR data (Cassidy, 2009b). The height of antenna above surface also plays a vital role in dislocating pavement surface in GPR data. The surface level shown in raw data may not be the real surface of medium. Therefore, the surface of pavement is brought to zero level first to calculate the exact depth of any object inside pavement or layer's thickness. This phenomenon is called correcting time zero in GPR data (Yelf, et al., 2006). For the calculation of true time zero, there is no definite method in literature. The negative or positive amplitude is taken for this processing. In this research, the first positive amplitude was taken as zero level.

In Figure 2.22 the GPR data collected over asphalt pavement is shown. The surface reflection can be easily marked as the material seen above surface is air i.e. different from the material which begins beneath surface (Figure 2.22(top)). The removal of air or finding true time zero is accomplished by closely marking the surface and recording the depth on y-axis. The trace is then subtracted from the data and surface on zero level is shown in Figure 2.22(bottom). The red circles in Figure 2.22 are shown the shift of zero depth. For further study, the research carried out by Richard Yelf and Daniel Yelf in 2006 can be a good source to start.

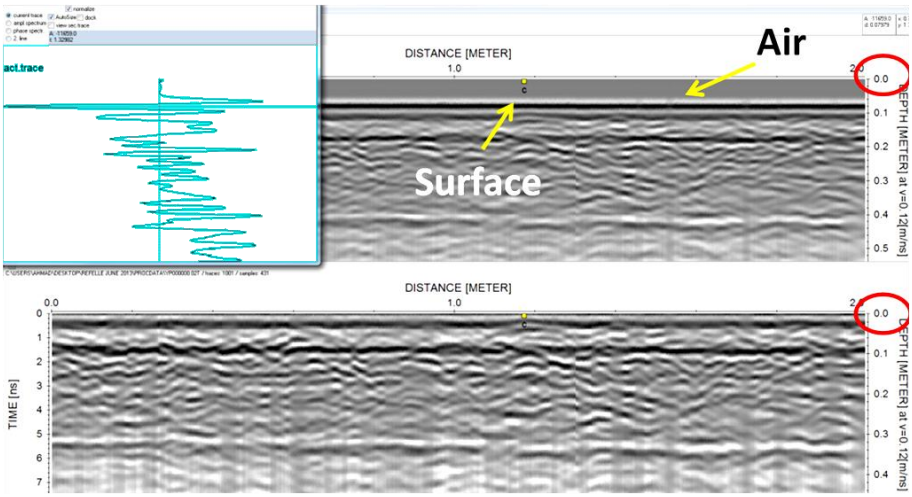

Figure 2.22. The GPR data time zero correction, (top) data without correction and (bottom) data after time zero correction (Aladdin, 2000 MHz, Software: ReflexW)

2.6.4 Time gain

The energy of reflected GPR signal decreases with increase in depth, as is shown in Figure 2.3. The time-dependent gain processing compensates for the radar signals loss due to propagation in dielectric materials. The signal loss in energy is shown graphically in Figure 2.23(a) where the data have only first two peaks. Now the data is multiplied by a factor (Figure 2.23(b)), to reveal the information coming from deep down. The multiplication factor depends upon information required, probing depth and GPR antenna type (Annan, 2009). After multiplication of the data by a gain factor, the objects from deep down are also revealed (Figure 2.23(c)).

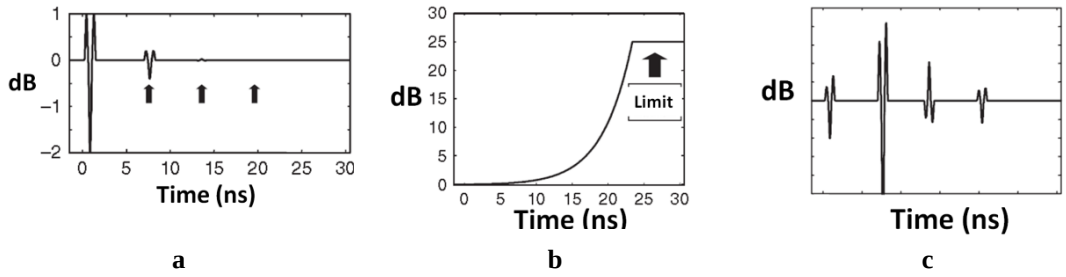

Figure 2.23. Gain increase by data processing, (a) original EM wave, (b) a sample time gain function, (c) the resultant EM wave signal (Annan, 2009)

The data collected over an asphalt pavement by Aladdin GPR system (2 GHz) is shown in Figure 2.24(top). In this GPR-gram, the pavement surface and interfaces are hardly seen. After multiplying with a gain factor, the GPR-gram in Figure 2.24(bottom) revealed the surface and interfaces in pavement.

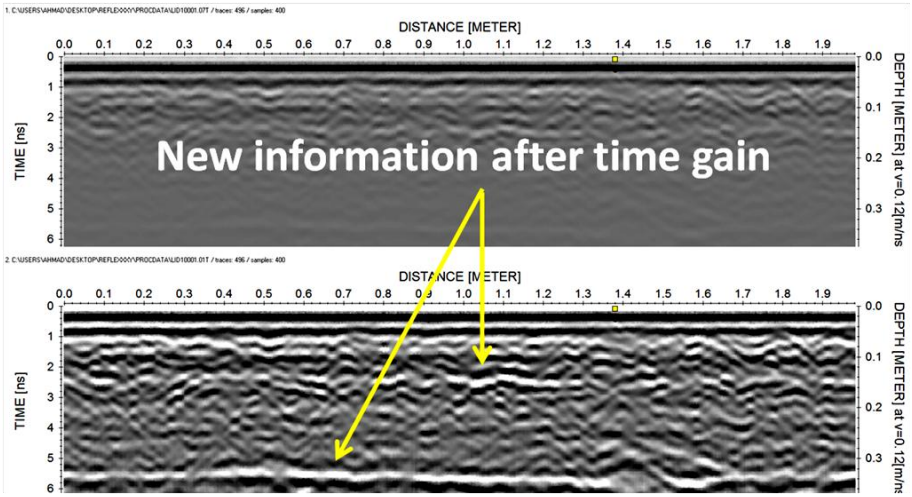

Figure 2.24. GPR data before and after gain processing (SIR-20, 2600 MHz, software: ReflexW)

2.6.5 Data migration

To convert GPR-gram hyperbolas back into objects shape, data migration technique is used. The data migration is spatial deconvolution of data i.e. it converts the energy of hyperbola's back into the objects shape (Annan, 2009). The data migration helps compensate for the effect of ground materials on antenna radiation pattern and the disturbance by nearby objects. In data migration technique, disturbance (in data) is reduced by selecting lower and upper energy ranges. This is done by choosing smallest required hyperbola and bigger, in the GPR-gram. The energy of selected hyperbolas is then converted back to the objects shape. There are different kinds of data migration techniques e.g. f - k (Stolt), Kirchhoff migration technique, etc. The selection of suitable migration technique is based on data type, hyperbola velocity and the energy reflected by the target (Annan, 2004). In this research, f - k migration process is selected for data processing.

The requirement for the f - k migration is the velocity of EM wave when striking the object which is calculated by measuring the hyperbola intensity in ReflexW software. The process of data migration is shown Figure 2.25. The EM wave propagation velocity, for example in Figure 2.25(a) is adopted for the specific hyperbola as an input in data migration techniques.

A survey data collected by Aladdin GPR system is shown in Figure 2.25. In Figure 2.25(a) the velocity adoption by measuring the hyperbola intensity is shown. By this technique a range of velocity (in meter per nanoseconds) can be defined within which certain hyperbolas only related to cracks can be filtered and displayed. The suitable velocity ranges (two pairs) are in negative and positive values depending on being left or right side of EM-wave (Section 4.5.2). In Figure 2.25(b), the same data is filtered with f-k technique. The top GPR-gram is only initially processed. It can be noted in the result provided in Figure 2.25(b) bottom that not only crack has been highlighted but also the noise is removed successfully.

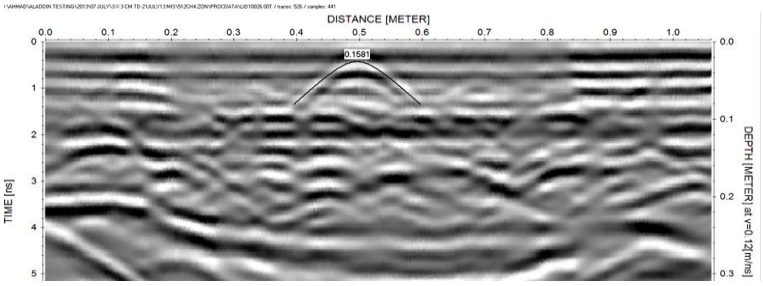

a

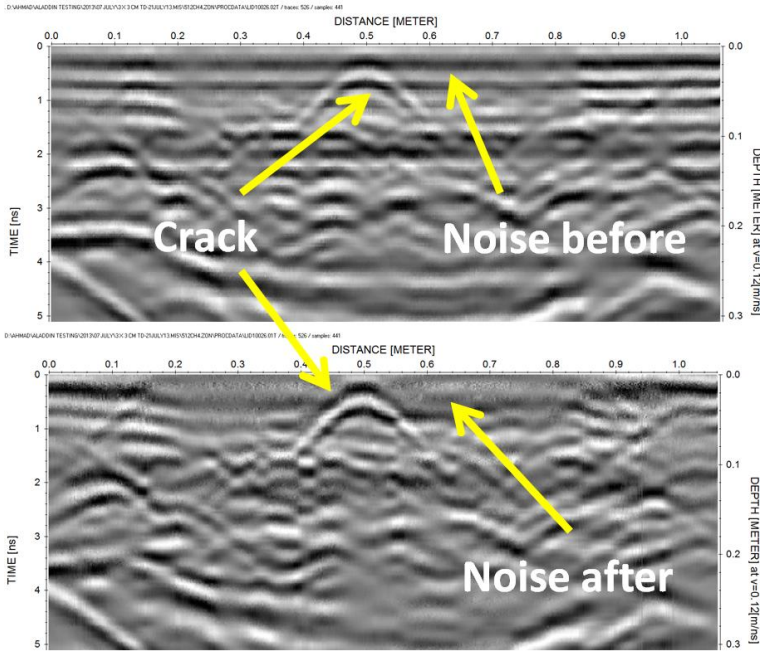

b

Figure 2.25. The application of f-k filter, (a) calculating the velocity of EM wave in ReflexW software (b) the GPR data before (top) and after (bottom) f-k filter application, (system: Aladdin, 2000 MHz, software: ReflexW, Specimen BA 3x3 cm^2 crack)

2.7 Literature review

The first use of GPR was for civil engineering structures (also on pavements) by Ulriksen (1982). The manuscript by Ulriksen not only provided a general understanding of GPR and its usage but also focused on GPR abilities for pavement characterisation such as chemicals content and moisture content variation measurements. The pavement conditions were initially modelled by Ulriksen and then the pavement conditions outcomes by GPR were compared. The promising outcomes of Ulriksen to use GPR instead of classical pavement characterisation methods attracted attention of many scientists. However, the questions like factors effecting pavement dielectric values and the relation of dielectric constant to pavement damages was unclear. Due to variation in pavement dielectric constant throughout pavement life time made it difficult to compare the results of pavement condition outcomes. This shortcoming in pavement assessment by GPR was investigated by a number of scientists such as the research carried out by Jaselskis et al. (2003).

The research work by Jaselskis et al. (2003) comprised of tests conducted on asphalt specimens from sand and aggregate filler with different binder percentage. Moreover, the density of asphalt specimens was also taken into account. The results concluded that the dielectric constant of asphalt has negligible influence of frequency below 12 GHz. Also the dielectric constant of asphalt increases with increase in asphalt density. The impact of temperature and moisture however, was not significant on asphalt dielectric constant. The slight changes in asphalt dielectric constant with increase in temperature were related to evaporation of moisture from samples. However, the moisture content of asphalt samples before and after tests was not recorded.

The research conducted by Evans et al. (2008) investigated the influence of temperature and moisture on core samples of pavement in use. The samples from pavements in use were brought in the laboratory and the tests were conducted in controlled environment. The conclusion of outcomes was that from a change in temperature of -5 to +45 degrees, the dielectric permittivity of pavement changes about 7.3 to 20% of original value. The effect of temperature changes on dielectric constant are provided in Figure 2.26. On the other hand, the effect of moisture content brought a change of about 16% in dielectric permittivity (from dry to soak in water) (Evans et al., 2008). Although the influence of some factors on pavement dielectric constant was proved by Evans et al., some information is missing in that research. For example, the asphalt type, its age, its properties such as void ratio, density etc. Without knowing the properties of asphalt, the amount of influence by temperature and moisture on asphalt cannot be verified.

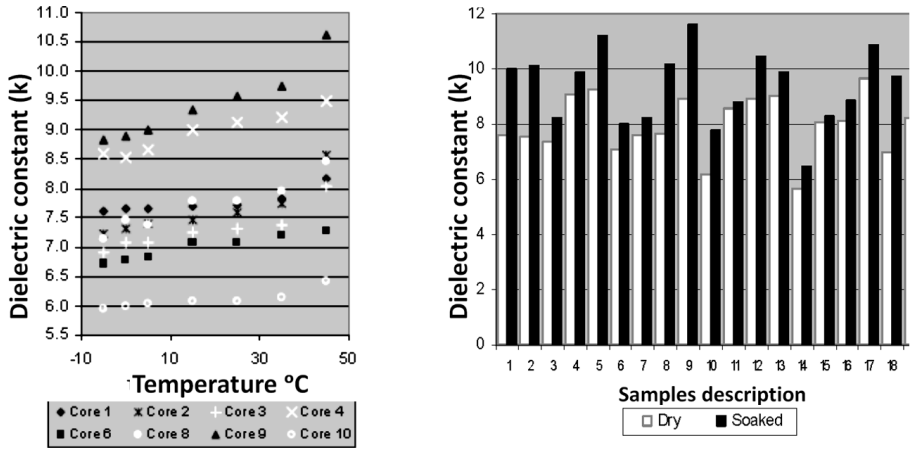

Figure 2.26. The influencing factors on asphalt pavement dielectric constant, (left) effect of temperature, (right) effect of moisture (Evans et al., 2008)

The research conducted by Loizos et al. (2010) investigated the effect of asphalt aging on its dielectric constant. They investigated the thickness of foamed asphalt treated layers by air-coupled GPR system with a frequency of 1 GHz. The onsite measurements were taken on foam asphalt stabilised base in four stages i.e. one day old (a), two days old (b), pavement with binder course (asphalt concrete) (c) and finally the total pavement with asphalt concrete surface course (d). The dielectric constant of each stage is shown in Figure 2.27. It can be seen that the dielectric constant of asphalt can change even within 24 hours, although the reasons for the difference were not investigated.

The pavement dielectric constant was investigated again after the application of base course and finally after wearing course. The change in pavement dielectric constant almost remains the same at c and d stages. The reason of outcomes was not clear as pavement moisture content and density values were not provided. Also information about the time lapse between "c" and "d" stages of GPR surveys is missing.

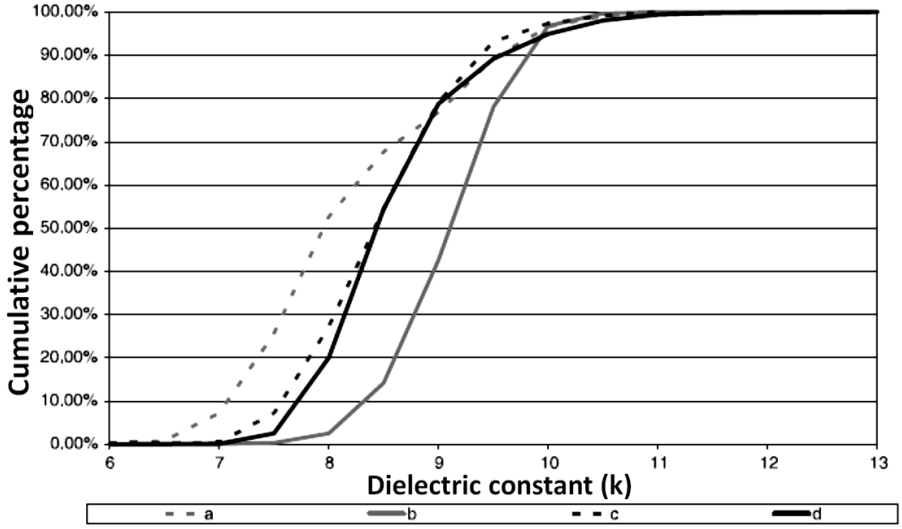

Figure 2.27. Variation in dielectric values of stabilized base layer with time (Loizos et al., 2010)

Where,

a = stabilised base layer after one day of construction
b = stabilised base layer after second day of construction
c = stabilised base layer + asphalt binder course
d = stabilised base layer + asphalt binder course + wearing course

The research work of Chang et al. (2011) investigated the relationship between asphalt void content, density and its dielectric permittivity (Chang et al., 2011). The outcomes are shown in Figure 2.28. The dielectric constant of laboratory prepared asphalt (AC-20) specimens was investigated at different void ratios. The specimens were prepared with 4, 5 and 6% binder content. The results confirmed that the pavement dielectric constant increases with decrease in void content. The increase in asphalt dielectric constant was also observed when the density of asphalt specimens was increased (Figure 2.28).

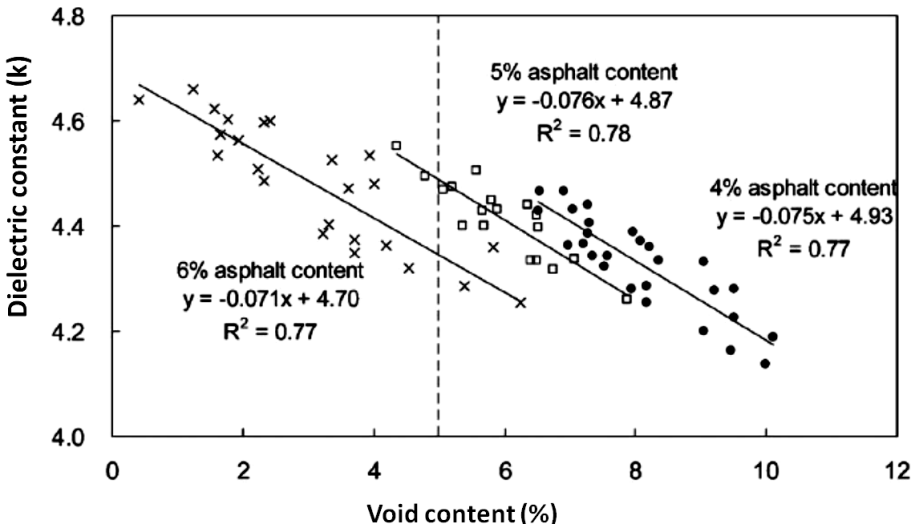

Figure 2.28. Variation in asphalt dielectric constant by change in asphalt voids content (Chang et al., 2011)

The research studies conducted by Saarenketo in 1998 investigated the relation between pavement dielectric constant to its damages such as cracking. This research which was conducted in different life time of pavement was focused on influence of pavement bound and un-bound layers properties such as compaction, moisture content variation and aging on pavement electromagnetic properties. The research work provides a good overview on GPR abilities, relation of EM wave scattering and the change in pavement properties. The example of such a relationship between pavement electromagnetic properties and literally condition is shown in Figure 2.29. The increase in dielectric constant value is related to asphalt pavement cracking.

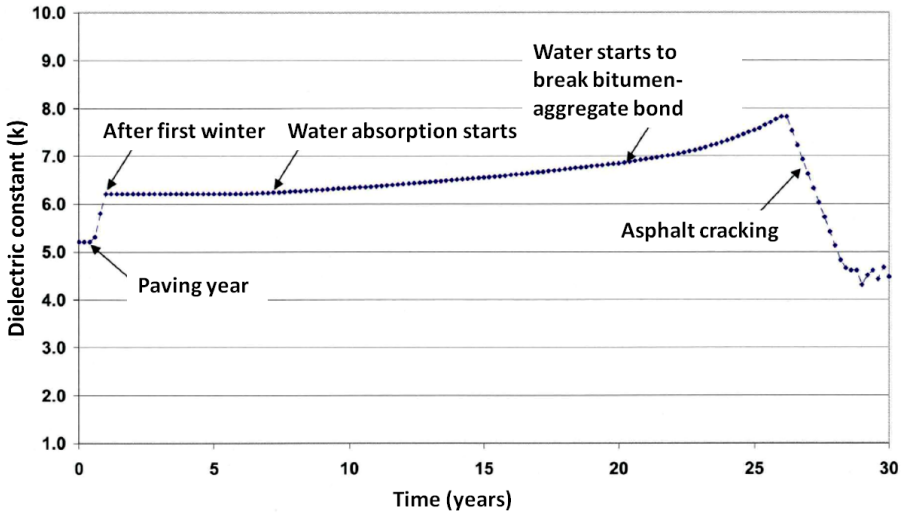

Figure 2.29. The relationship of change in pavement dielectric constant to that of pavement conditions (Saarenketo, 1998)

Investigation on the relation of dielectric constant to that of asphalt pavement damages was carried by Hugenschmidt (2009). The research conducted by Hugenschmidt was on network level in Finland, Greece and Switzerland. The investigations were carried out on pavements composed of same asphalt specification. The investigations resulted that the dielectric constants of pavements differ widely. Although there is no clear information regarding difference in pavement individual layers composition and the difference in design standards of each country, the research correlates pavements properties investigation with its electrical properties. The factors influencing dielectric constant parameters such as asphalt binder type, aggregate type, moisture content, temperature during survey, etc. are not provided in the document.

GPR has been used by numerous scientists for crack detection in various materials. Toshioka et al. (1995) investigated cracks in rock slopes with SIR 10 (GSSI) GPR system with centre frequencies of 100, 300, 500, and 900 MHz. Despite working with systems having central frequency below 1 GHz, the ≈ 60% of the total cracks were detected. However, the same width cracks (1-2 mm) in dry condition were not detected compared to the cracks full with water. Despite the test results, the use of GPR for crack detection started and importance of crack fill was highlighted.

Molinda et al. (1996) conducted tests to detect cracks in roof of underground mines. As the system used was 500 MHz central frequency, the resolution of GPR-grams was reduced. It is therefore hard for the reader to detect cracks. Although scientists claim to detect cracks, the information regarding crack width is not provided. The achievement in the tests was to be able to detect a layer delamination of 1.27 cm in the mine rock roof.

Cracks in buildings were investigated by continuous monitoring in the research work of Orlando et al. (2009). The monitoring was spread over a year span. This research work considered crack geometry influence on crack detection with respect to transmitted pulse direction. The cracks were surveyed from some fixed angles with a bi-static GPR system.

The research outcomes concluded that for same crack detected by same EM pulse, the detection probabilities can be different. This is because crack geometry can be different from different angles, but crack geometry plays a vital role.

The repaired cracks (sealed with bitumen) were investigated on motorways in Switzerland by Hugenschmidt et al. (1998) with help of GPR. For the data collection, 2.5 GHz (GSSI Model H4205) and 900 MHz (GSSI Model 3101D) GPR systems were used. The objective of the survey was to analyse sealed off cracks once they were detected by GPR together with other pavement damages such as layer separation and voids in pavement. Despite using 2.5 GHz antenna, the cracks could not be detected by the GPR however; the other pavement damages could be successfully detected. Although the crack detection was not successful in this research work, the importance of crack fill was highlighted for crack detection.

Forest et al. (2004) used a special device "The Non Destructive Crack Depth (NDCD)" for the crack detection in pavements. The device with frequency range of 700 MHz to 2.5 GHz was designed by Utsi electronics for Transport Research Laboratory (TRL), UK. The radar scans were taken at every 10mm distance. The NDCD was used to detect 34 cracks in dry condition and 5 again but filled with water. Core samples were taken from these cracked sections at the end of GPR survey, and results were compared with GPR outcomes. The accuracy of NDCD vs. real data is shown in Figure 2.30.

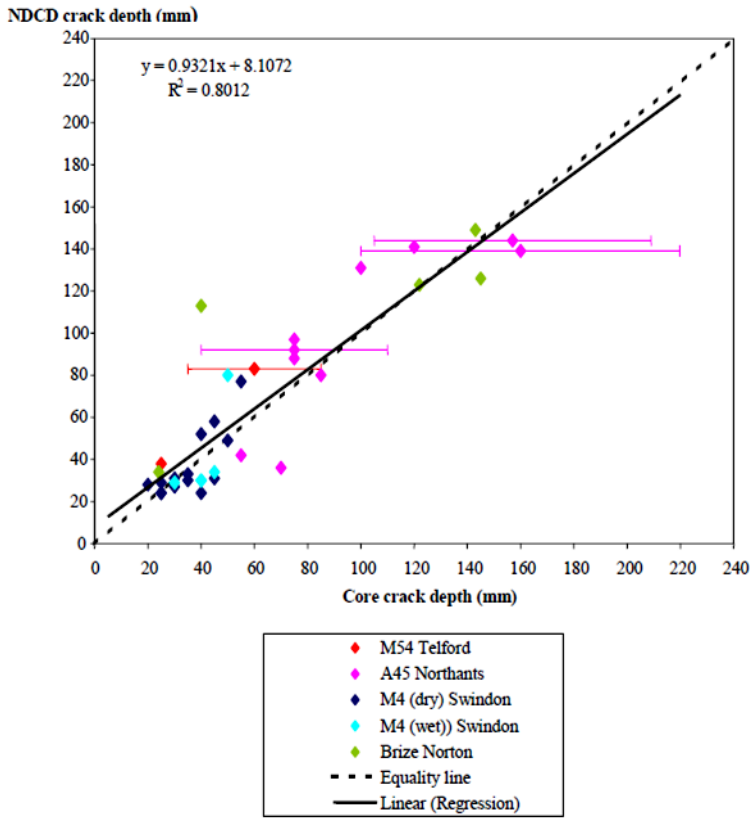

Figure 2.30. Accuracy of cracks depth measured with NDCD to core samples (Forest et al., 2004)

Although the outcomes shown in Figure 2.30 are promising, the difference between dry and water filled cracks is minimal. Missing information in the survey is on cracks width, crack fill material of dry and wet cracks, asphalt mix type and temperature during survey. The survey also considered the depth of cracks only.

Ranalli et al. (2007) carried out research on transverse and longitudinal pavement crack investigation by EM wave energy absorption. A 1600 MHz array GPR system was used for the survey. The research was based on comparison of induced EM signals energy absorption by un-cracked (undamaged) and cracked pavements. The survey also included heavy and light traffic data. Their relation to pavement damage and to EM wave energy absorption was not investigated. The crack detection accuracy was not discussed. Missing information is on crack fill material, pavement design mix properties, temperature, age, etc.

The investigations by Utsi et al. (2008) on reflective cracks were carried out to detect hidden cracks in composite pavements (asphalt layer laid on top of cement concrete pavement). The reflective cracking is a kind of bottom-up cracking which is caused by joints in the underlying cement concrete layers. A special device called "Crack detection Head (CDH)" was used to investigate the cracks. The system comprised two ground-coupled antennas (CDH) with operating frequency of 1.5 GHz, working simultaneously. The survey considered crack-GPR angle on crack detection. The EM scans were recorded for every 1 cm interval.

Although the joints resulting in reflective cracking were detected successfully, information on width of joints and fill material is missing. On the other hand, the detection of joints is easy, as steel bars are used in joints, which are a strong EM wave reflector. Other information regarding GPR survey such as temperature during survey and asphalt type is also missing.

Al-Qadi et al. (2009) investigated reflective cracking in composite pavements with the help of visual and video techniques in addition to GPR. The GPR system comprised one air-coupled antenna with 1.0 GHz central frequency and one ground-coupled antenna with 1.5 GHz central frequency. Even though GPR detected most of the reflective cracks, assistant from other techniques was included. The GPR could successfully differentiate between joints filled with HMA or cement concrete. The GPR outcomes were later confirmed by pavement coring, pre-construction pavement maps and the maintenance record of transport department. Despite detecting cracks with the information on its fill material, the author recommended further research as the efficiency of air-coupled and ground-coupled antenna for crack detection could not verified. On the other hand, most cracks in pavement were identified due to strong reflections from steel bars present in cement concrete joints. Furthermore, the survey parameters such as number of scans per length, asphalt type, temperature, and crack width are not provided.

Recent work on crack detection was carried out by Diamanti et al. (2012). The survey was intended to investigate cracking in composite and asphalt pavements. The investigations made by Diamanti et al. were unique in the sense that the GPR responses from cracks were first modelled, using different crack and EM wave properties. For the GPR survey, two different ground-coupled systems were used. The cart based GPR system shown in Figure

2.31(a) was equipped with two antennas having a central frequency of 250 and 1000 MHz respectively. The vehicle attached GPR system shown in Figure 2.31(b) was equipped with three antennas hanging left and right of wheel path of the system whereas one in the middle. Each antenna at wheel path was a 1000 MHz central frequency antenna whereas the central one being 250 MHz. The data with cart system was at walking speed whereas survey with vehicle attached GPR was at highway speed (ranging from 60 to 100 km/h).

a **b**

Figure 2.31. The GPR systems used for crack detection, (a) two channel cart system and, (b) the vehicle attached GPR system (Diamanti et al., 2012)

The crack modelling included crack related parameters such as the dielectric value or the electrical conductivity (Siemens per meter (S/m)) of materials, crack width, crack height or depth, crack types (bottom-up, top down and complex geometry), crack fill material properties, the transmitted antenna properties (shielded, dipoles) and the processing parameters (de-wow and gain limits).

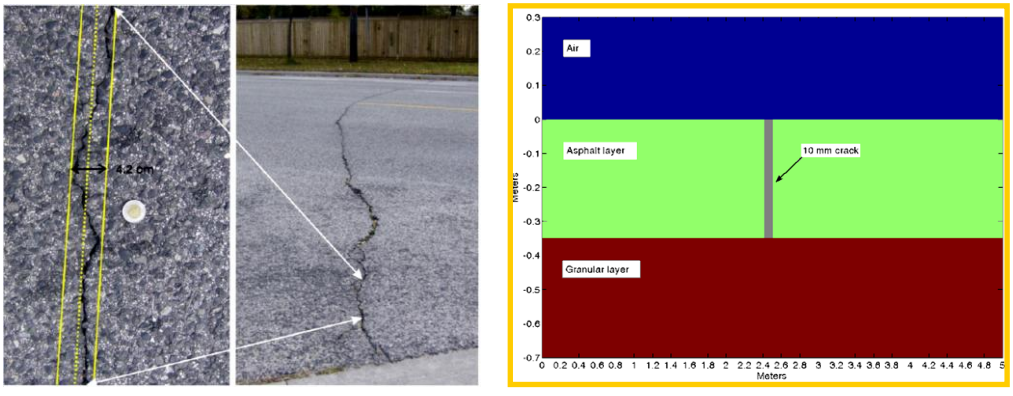

a **b**

Figure 2.32. The crack investigation by Diamanti et al., (2012) (a) the crack dimensions and (b) the crack model

However, many of these properties were not considered during field survey such as dielectric constant of crack and crack fill, transmitted pulse properties (pulse width, voltage/energy, and directivity). The details of survey are shown in Figure 2.32. The cracks

attributes are shown in Figure 2.32(a). The cracks are tapered and not straight. The width of crack is ≈ 2-5 mm with crack fill as air. The modelled asphalt pavement crack is shown in Figure 2.32(b).

In first phase of the survey, the cracks in asphalt pavement were detected by GPR system attached to vehicle. The samples were collected with 250 MHz antenna and 1000 MHz antenna with EM pulse induction rate of 0.05 and 0.03 m intervals respectively. The outcomes were then verified with the cart system shown in Figure 2.31(a), the pulse induction rate was 0.01 m. Crack reflection response was more from 250 MHz antenna, compared to 1000 MHz antenna which is surprising, as a uniform width crack is supposed to be well detected by higher frequency antenna. Same outcomes were observed in the modelled crack reflections. The results are shown in Figure 2.33. It must be however noted that the GPR-gram in Figure 2.33(a) is showing a total pavement depth of 2.8 m whereas the GPR-gram of 1000 MHz (Figure 2.33(b)) is showing a depth of 0.9 m.

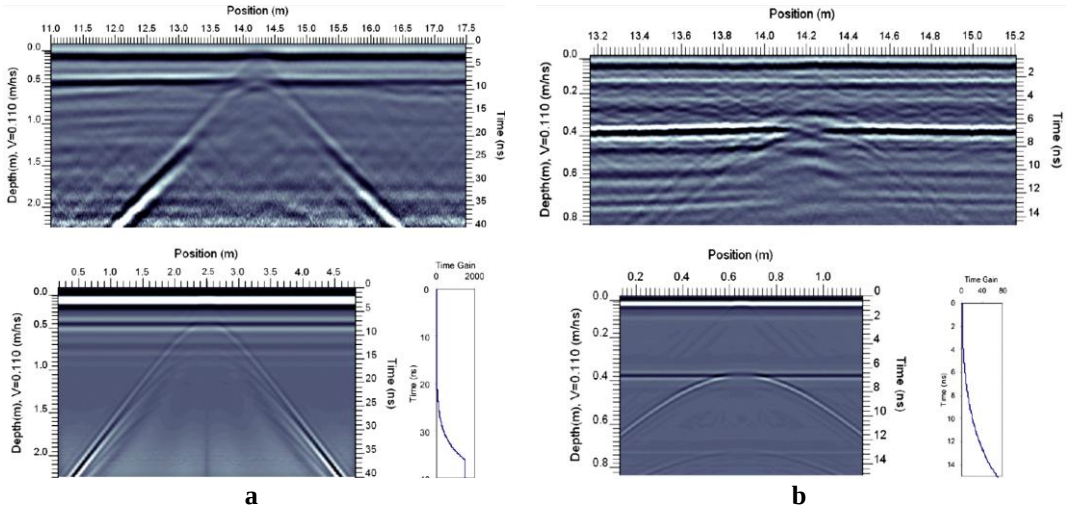

Figure 2.33. The crack detection outcomes together with modelled reflections at the bottom, (top) the result of 250 MHz antenna and, (bottom) the result of 1000 MHz antenna (Diamanti et al., 2012)

It can be seen in Figure 2.33(a) that the 250 MHz crack detection hyperbola is stronger than of 1000 MHz GPR-gram for the same crack (Figure 2.33(b)). The same effect can be seen from the modelled GPR-grams. The reason for the stronger reflections by 250 MHz antenna was explained by the reflections from aggregates at the pavement base. The survey results were also not confirmed by pavement coring which creates areas of uncertainty in survey outcomes.

The causes of cracks on composite pavements have been investigated by Chen et al. (2007). The objective of the survey was to investigate the reason for longitudinal cracks in direction of travel before applying any maintenance technique. The cracks in pavement despite full depth repair were continuously propagating in pavement structure. The cracks in the pavement are shown in Figure 2.34.

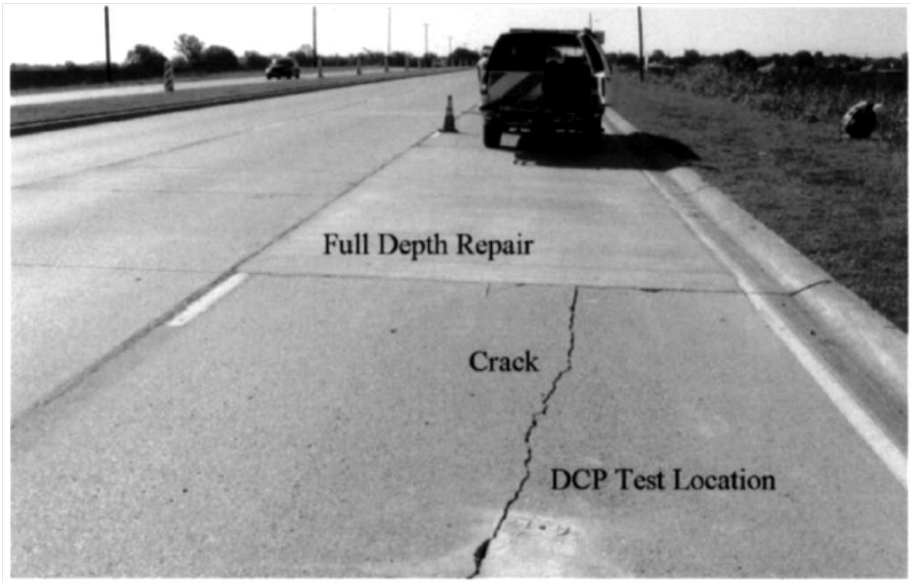

Figure 2.34. The survey site showing crack and the repaired area (Chen et al., 2007)

The survey results revealed that the cracks in pavement were not due to pavement material failure or volumetric expansions of concrete but were due to poor base support. However, no GPR-gram is presented in the survey findings.

The accuracy of GPR for pavement layers anomaly was carried out by Al-Qadi et al. (2005a). The used GPR systems were air-coupled antennas with 1000 MHz central frequency and a ground-coupled antenna with 1500 MHz central frequency. The pavements investigated were flexible pavements together with composite and cement concrete pavements divided into categories according to their age. The survey conducted on flexible pavements was at a rate of scans per 0.3 m. The data was processed with unique software developed by the author. The dielectric constant of each layer was calculated individually by Equation 2-3. The outcomes of the research are provided in Figure 2.35.

Figure 2.35. Effect of pavement age vs. accuracy of GPR for measuring layer's anomaly (surf = surface course) (Al-Qadi et al., 2005a)

As shown in Figure 2.35, the researchers found influence of pavement age on the measurement of pavement's layers thickness measurement. The minimum error in layers thickness measurement with GPR was 4.4% for 0 to 5 year old pavement which increased to 5.8% error for the pavements older than 20 years with surface course older than 10 years. The reason for the influence of pavement age was however, not further investigated.
As far as the asphalt pavement age is concerned, its density increases and voids ratio decreases with age (Papagiannakis et al., 2008). Therefore the dielectric constant of aged asphalt increases (Figure 2.28). Thus it can be predicted that old pavements layers must be clearly detectable by GPR, which however is not observed in these outcomes.
The GPR was applied specifically on asphalt pavements to verify its abilities for investigating layers thickness anomaly by Al-Qadi et al. (2005b). In this research, copper plates were placed under each pavement layer during construction. This helps identify each layer with great accuracy due to strong reflections from the copper plates. By this mean, the error in layers thickness measurement for three HMA pavement layers was reduced to 2.9%. One of the survey outcomes is shown in Figure 2.36.

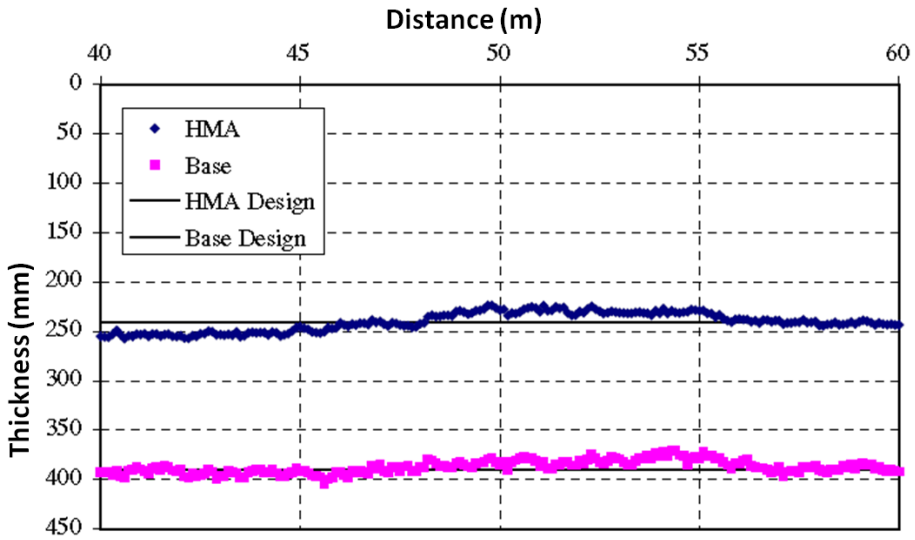

Figure 2.36. Support loss and layer anomaly investigation by GPR (AL-Qadi et al., 2005b)

It can be seen in Figure 2.36 that the HMA layer together with base of the asphalt pavement differs from their design values. Thus it is possible that the damages were due to the uneven base and HMA layers. Thus in future such investigations can be carried out before applying maintenance techniques. Information on temperature, GPR system and the processing techniques are not provided.

2.8 Summary and background of this thesis

GPR is a non-destructive probing technique which can provide underground information in high resolution (Hugenschmidt et al., 1998; Harari, 1996; Davis et al., 1989). The GPR survey benefits include continuous data collection (no interpolation), better resolution compared to other geophysical subsurface investigation methods, dynamic/fast speed surveying thus no or less hurdle to traffic flow (Daniels, 2007; AI-Qadi et al., 2005a;

Olhoeft, 1999; Hugenschmidt et al., 1998). The additional ability of GPR is to provide 3D images of sub-surface elements and different hidden layers (Van Wijk et al., 2007). In pavement investigations the ability of GPR for continuous profiling adds extra preference over other non-destructive techniques (Daniels, 2007). Thus no lane closures needed ultimately avoiding highway traffic and some surveys are even carried at highway speed (Van Wijk et al., 2007; Hugenschmidt et al., 1998). However, if GPR is used for investigation of fine details with high accuracy, the surveys are mostly slow and conducted at walking speed (Van Wijk et al., 2007). Core samples are required in GPR surveys, but the number of core samples is reduced compared to classical methods of pavement characterisation (Al-Qadi et al., 2005b).

However, the advantages of GPR are governed by some factors such as optimum GPR system selection, properties of EM wave, material properties information and the influence of environmental factors. The material and environmental factors changes with time and thus therefore, must be controlled before/after each survey (Ahmad et al., 2011). Furthermore, the asphalt properties changes with time such as its void content, density, etc. In addition, the intrusion of foreign material like water, clay, salt or chemicals may change the GPR measuring outcomes. Moisture barriers within the layer and collecting data shortly after significant rain can also complicate the analysis.

The antenna bandwidth increases GPR system resolution (lateral or angular) by which it can differentiate among two closely spaced objects (Olhoeft, 1999; Koppenjan, 2009; Daniels, 2007). Increased bandwidth helps to increase the resolution due to presence of a large EM wave spectrum which can record from very fine to major details of the medium (Annan, 2004). High resolution of GPR in pavement surveys is important where fine voids, cracks, etc. are closely spaced. Other factors influencing GPR resolution are the EM wave energy losses, distance of objects from the system, and the antenna beam type (Perez-Gracia et al., 2008).

The GPR detects, but does not identify the changes in material itself (Annan, 2004). The GPR data interpretation is subjective and depends upon user's experience (Lahouar, 2003; Annan, 2004). The difficulties in GPR data analysis and interpretation are one of the reasons for hesitation of many Transportation authorities to use GPR as an official pavement evaluation tool (Al-Qadi et al., 2005a).

The crack fill material, on the other hand, mostly remains the same i.e. air or clay, etc. (Ahmad et al., 2011). However, the contrast between asphalt and crack fill increases in old pavements. Thus the detection of cracks must get easier in old pavements compared to new pavements. This could be helpful as cracks mostly appear in old pavements.

For crack detection with GPR, the contrast between pavement and crack fill is important (Ahmad et al., 2012). This contrast between asphalt and crack fill is dependent on temperature, crack fill type, asphalt mix type and aggregate type, which will be further investigated in this research work.

The literature review explores the work carried out on investigating and understanding the GPR abilities used as a pavement characterization tool. By reviewing the past literature it is

revealed that crack investigation by GPR particularly in asphalt pavements has never been carried out systematically in field and in laboratory at the same time. Furthermore, GPR has never been tested in controlled environment for cack investigation to explore its abilities. The important factor which influences GPR abilities as a crack investigation tool is the angle of EM wave propagation and crack geometry. It can be concluded so far that,

1) although a lot of work has been done on GPR abilities to be use as a reliable characterization tool in asphalt pavements such as layer thickness determination, objects (dowel bars) detection, its use for crack investigation and crack cause detection is still in focus of pavement research
2) the parameters effecting GPR abilities for crack investigation have rarely been discussed in the literature
3) although there is some research regarding crack detection in asphalt pavements by GPR reported in literature, the results have not been verified in controlled environment through laboratory testing
4) the chemical and physical properties of asphalt changes with time due to aging effect and therefore, whenever asphalt pavements are investigated, its chemical and physical properties such as density, void ratio, etc. must be documented and presented together with GPR outcomes
5) the influence of processing techniques together with surveying methods (2-D and 3-D) on GPR outcomes are not reported in the literature
6) the angle between crack and GPR antenna is important regarding GPR surveys, which is not documented in literature

.

3 Test program

3.1 Introduction

In this section, a description of the GPR systems and software used in this thesis is provided, as well as information on the prepared asphalt specimens and selected pavement sections. The difference between the different GPR systems is highlighted together with their abilities. The software programs related to data processing are described which include selected and compulsory software. The compulsory software are the one which either are integrated into the GPR system or are software options for specific data processing only. The need for the specific specimens is highlighted together with cracking types simulated in the specimens. The physical and material properties of asphalt specimens as well as of selected pavement sections such as aggregate, binder type, density, void ratio and particle size distribution (gradation curve) are documented. For the field testing, asphalt pavements of different highway categories were considered. The selection of asphalt pavements was based on asphalt mix types, cracking characteristics and allowance for testing. In the end, specifically the functioning of the mainly used GPR system Aladdin, IDS is described.

3.2 The GPR systems used

A variety of GPR systems were studied in this research. They were selected based on their central frequency, pulse transmitting technique and antenna configuration. The shift from one GPR system to other was based on limitations of previous one and the requirements for further investigations. All systems used were ground-coupled antennas, otherwise stated elsewhere. The GPR systems selected were, (a) Groundvue 3 (Utsi Electronics), (b) GeoScope (3d-radar) (21 channel array), (c) SIR-20 (GSSI), (d) MALA High frequency (HF), (e), Detector DUO (f) Aladdin (IDS). A description of their basic principles is provided below.

3.2.1 Groundvue 3

This system is a 3 GHz central frequency system, designed and manufactured by Utsi Electronics, UK. The GPR system is shown in Figure 3.1(a) whereas the crack detection head (CDH) is shown in Figure 3.1(b). The CDH was not a standalone system but was attached to Groundvue 3 system as an extra channel. The data obtained by CDH were stored in controller of Groundvue 3 system.

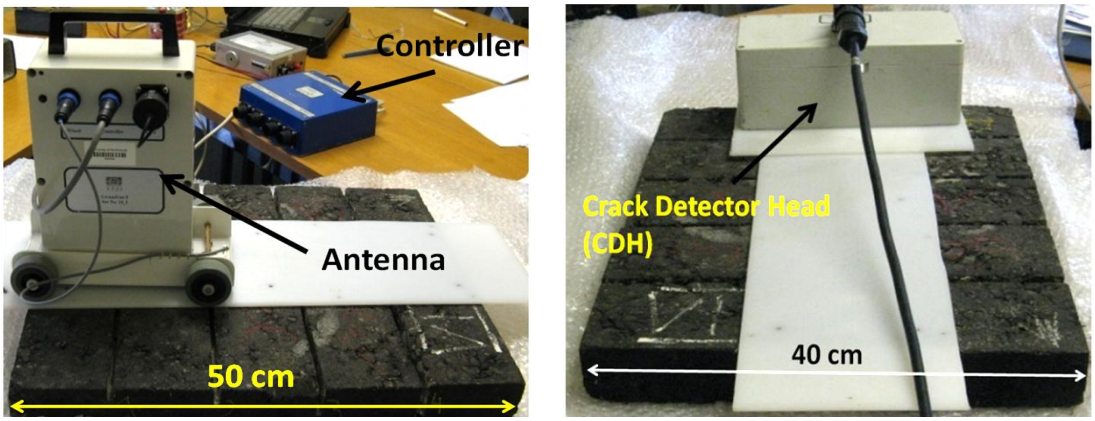

a b

Figure 3.1. The Groundvue-3 GPR system, (a) main antenna being tested on cracked asphalt specimen and, (b) the crack detector head (CDH) is being used for crack detection (Utsi Electronics, UK)

Central frequency of CDH was 1.5 GHz. For crack investigations, asphalt specimens were taken to Utsi Electronics laboratory, United Kingdom and were tested there. For the processing of data obtained from Groundvue 3 and CDH, ReflexW software was used. Only 2-D surveys on asphalt specimens were carried out with this system.

3.2.2 SIR-20

SIR-20 systems are manufactured by Geophysical Survey Systems (GSSI), Inc. United States. The SIR-20 GPR system used in this thesis was a multichannel system equipped with two antennas (Figure 3.2a). The antennas were of 1500 and 2600 MHz central frequency. Output data from the system was in RADAN format, a typical coding system for GSSI systems.

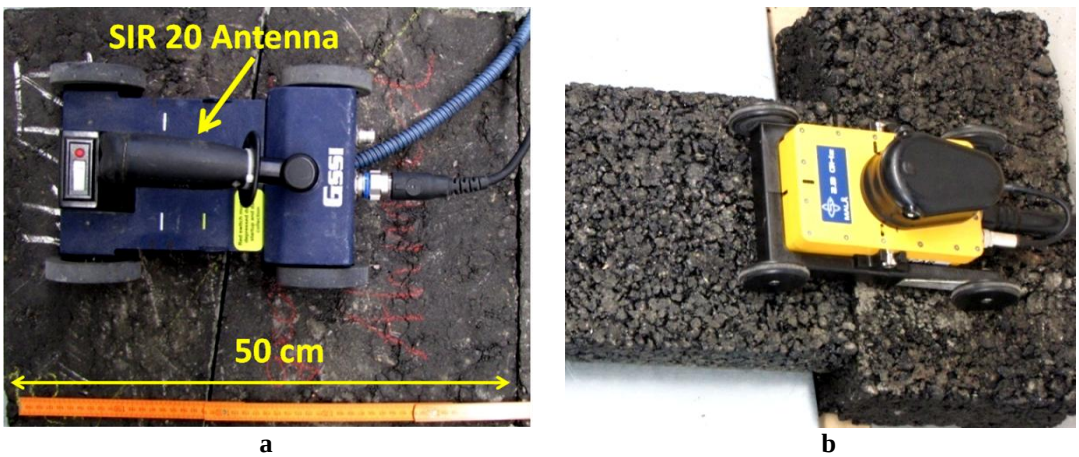

a b

Figure 3.2. GPR systems used for crack investigations, (a) SIR-20 GPR system and, (b) MALA HF GPR system (GSSI, USA and MALA, Sweden)

The ReflexW software was used for data analysis. Advantage of SIR-20 system was the availability of two antennas with wide range frequencies. This helped in investigating effects of different frequencies for crack detection. The system was used for testing

laboratory specimens as well as field pavements. The outcomes of this system were carried out in 2-D format only.

3.2.3 MALA HF (High Frequency)

The used MALA HF was a multichannel system with two antennas of 1600 and 2300 MHz frequency. The system was used together with SIR-20 system on same asphalt specimens and field pavements. The system is shown in Figure 3.2(b). The benefit of this system was that it had also two different frequency antennas which were useful to investigate the effect of frequency on crack detection. The data output format was called RAMAC, which could be also analysed by ReflexW software. Only 2-D surveys were carried by this system. The technical information regarding system is available in Table 3-1.

3.2.4 GeoScope Array system (3d-radar, Norway)

The used GeoScope system was a 3-D survey capable GPR system. The system was selected due to its unique system properties such as EM wave transmission technique i.e. continuous wave (CW-FM), its frequency (3.0 GHz), array antenna and its bandwidth of 100 to 3000 MHz. The system array antenna had 21 pairs of Rx-Tx channels. The width of array antenna was 2.5 m. The system is shown in Figure 3.3(a). The GPR outcomes could be analysed from viewing the pavement longitudinally, horizontally and vertically. The data obtained was processed by the integrated system software only. Due to the antenna size, system was used only in field on asphalt pavements. The details of system can be found in Table 3-1.

a **b**

Figure 3.3. The GPR systems, (a) the GeoScope system and, (b) Detector DUO system with cart (3D-RADAR and IDS, respectively)

3.2.5 Detector DUO (IDS)

The used Detector DUO system was selected to investigate crack causes on one of the asphalt pavement sections. This GPR system had two antennas of 250 and 700 MHz frequency. The data was collected simultaneously with both antennas by moving the system in cart. The output data was in “dt” format, analysed by ReflexW software. Only 2-D survey was carried out with this system. The system is shown in Figure 3.3(b). Technical details are provided in Table 3-1.

3.2.6 Aladdin (IDS)

The "Aladdin" GPR system was intensively used in this research. The system is made by Ingegneria Dei Sistemi (IDS), Italy. The system is capable of 2-D as well 3-D survey. The 2-D surveys can be carried out either by moving the antenna with a designed stick or in a cart (Figure 3.4(a)). For 3-D survey, a plastic gridded mat called "Pad Survey Guide" (PSG) is provided to guide antenna on equal distance and parallel paths (Figure 3.4(b)). The PSG can be laid on ground and survey is carried out by moving antenna in single directions. The system output data is in "dt" format and can be analysed with software GRED-3D, ReflexW and GPR-SLICE. The software "K2 Fastwave" is the integrated software used for initial processing of the data in real time.

a **b**

Figure 3.4. The Aladdin GPR system, (a) survey with cart and, (b) the 3-D survey on PSG

The system allows surveying with more than one transmitter at a time. Therefore, object can be surveyed from different angles with a single survey pass. This also makes it possible to conduct 3-D survey with single passes. The position of transmitter and receiver in Aladdin antenna is shown in Figure 4.25. The technical details of system are provided in Table 3-1.

Table 3-1: Details of GPR systems used in this research

Name	Central frequency (MHz)	Antenna type	Software used for data analysis	Survey type
Groundvue-3	3000	Pulse-frequency	ReflexW	2-D
SIR-20	1500 & 2600	Pulse-frequency	ReflexW	2-D
MALA (HF)	1600 & 2300	Pulse-frequency	ReflexW	2-D
GeoScope	3000	Step-frequency, Array	3dr-Examinar	3-D
Detector DUO	250 & 700	Pulse-frequency	3D-GRED, ReflexW	2D
Aladdin	2000	Pulse-frequency, dipole	3D-GRED, ReflexW, GPR-SLICE	2D & 3D

3.3 Software

The software selection in this research was based on two categories, i.e. wave analysis technique and image analysis. The first is used to analyse the received EM wave by processing the EM wave properties. GPR-Slice is the only image based software used. The software selection excludes the system integrated software, such as 3dr-Examinar which was the only option to process the data obtained from 3D-RADAR system. The second integrated software was "GRED-3D" which comes with Aladdin GPR system. However, the data from Aladdin system could also be analysed by other software such as ReflexW or GPR-Slice.

3.3.1 3dr-Examinar

The 3dr-Examinar software is the integrated software in GeoScope system. The software used in this research was a limited version and hence, able to perform standard actions only. Nonetheless, the data was processed to investigate cracks in pavements. The standard processing options available in the software were background removal, antenna calibration, edge filter, range gain, smoothening filter and stolt migration. The advanced processing functions included Inverse Fast Fourier Transform (IFFT) and de-convolution techniques. The extent of these processing steps was automatic and hence the data was standard processed. The software user interface is shown in Figure 3.5.

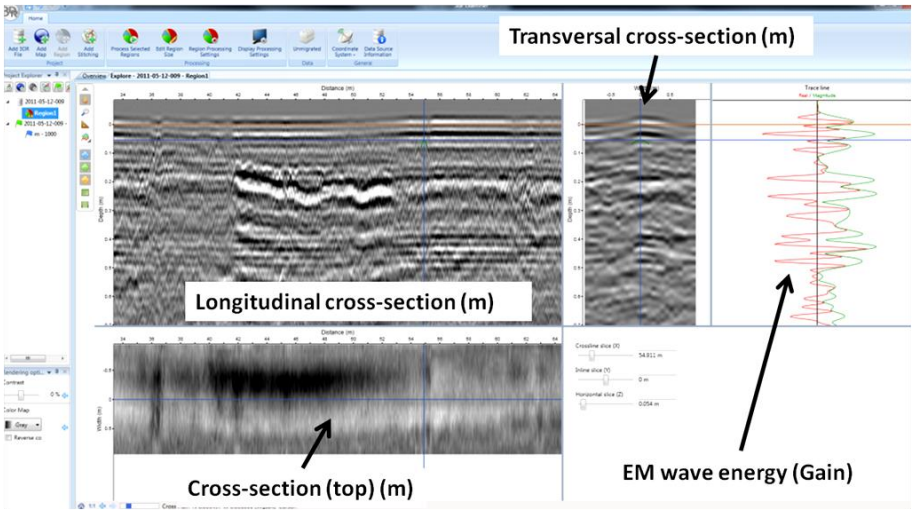

Figure 3.5. The 3dr-Examinar software used for data processing of GeoScope GPR (3D-RADAR, Norway)

The processed data could be viewed from three angles i.e. vertical cross-section, longitudinal cross-section and top cross-section. The gain curve of received and processed EM could be viewed on the right side of window (Figure 3.5). It must be noted that data obtained only from GeoScope system was processed by the 3dr-Examinar.

3.3.2 GRED-3D

The GRED-3D software is the standard software used for Aladdin data analysis. This software can analyse 2-D and 3-D data. However, the processing manoeuvre is limited as

the extent of processing degree cannot be changed. Data processing is less time consuming and many major details in the data can be analysed quickly. The processed areas (surveyed by GPR) can be rotated, cut and viewed from many angles, which is the advantage of this software. The shortcoming of software is no control on outcomes axis format and values which are fixed to standard. Therefore, the axis in outcomes from GRED-3D software may not be clearly visible and logical to results.

3.3.3 ReflexW

ReflexW software offers good flexibility in software functions. It can be used to analyse the data obtained from all GPR systems used in this research except GeoScope system. The flexibility of processing includes user defined processing steps and their extent. The software version available, was however not able to handle 3-D data. The uniqueness of software is to save processing steps and their extents which could afterwards be applied to data from other systems. Further information can be found under: http://www.sandmeier-geo.de/.

3.3.4 GPR-SLICE

The GPR-SLICE is capable of 2-D as well as 3-D data analysis. The software initially processes the EM wave and builds a GPR-gram before starting image processing techniques. The execution of further processing steps are based on appearance of resultant images.

As the word "slice" in software name suggests, it produces slices of data in image format. The 3-D results of survey are sliced which gives a better view of objects in medium. The uniqueness of the software includes its flexibility for processing steps (user defined), their intensity, application level and (the most important) possibility of processing selected data within GPR-grams. The software can (like GRED-3D) rotate, cut and view the processed areas from many angels. More information regarding software features can be obtained from website: http://www.gpr-survey.com/.

3.4 Laboratory study

3.4.1 Asphalt specimens preparation

Asphalt specimens of varying sizes were prepared in laboratory with different asphalt mixtures. The objective was to investigate the effect of asphalt mix type on crack investigation by GPR. The asphalt specimens were prepared in two laboratories, Pavement Engineering laboratory, Brandenburgische Technische Universität Cottbus and in Institut für Straßenwesen (ISBS) at Technische Universität Braunschweig. Seven asphalt specimens labelled as AD, AE, AF, AG, AH, AI and AJ were prepared in Cottbus. The other specimens were prepared in Braunschweig. All GPR tests on specimens were conducted in ISBS except specimen "AH" which was also tested in Utsi laboratories, United Kingdom. The details about laboratory specimens are provided in sections below. The asphalt specimens were unique in asphalt mix and aggregate types to investigate material effect on crack detection ability of GPR. The choice of asphalt mix types was

based on design standards for pavement construction in Germany. The design procedure of specimens in the laboratory was according to the specifications "TP Asphalt-StB" (Asphalt-StB-33, 2010) of the German Road Research Association (FGSV). The abbreviations "DS", "B S" and "T S" used in this research work indicate Surface-course, Binder-course and Base-course respectively regarding specimen's type according to asphalt mix design. The categorisation of asphalt specimens was according to their geometry and dimensions which includes three groups "A", "B" and "C". The details of specimens are provided in the next sections.

a. Asphalt specimens of type A

The asphalt specimens type "A" were the specimens ranging from 20 cm breadth to 50 cm in size. The specimens were further subdivided from "AA" to "AJ" on the basis of asphalt mix type, layers configuration and cracks attributes. The specimens AA, AB and AC were 32 x 20 x 7.5 cm^3 in size whereas the specimens "AD" to "AJ" were 50 x 40 cm^2 in size with varying height.

- Asphalt specimen type AA

The specimen "AA" was a base course sample prepared with asphalt mix type AC 32 T S. The specimen was 7.5 cm thick. A straight and 4 mm wide crack was engraved into the specimen by saw cut. The specimen is shown in Figure 3.6. The details are given in Table 3-2.

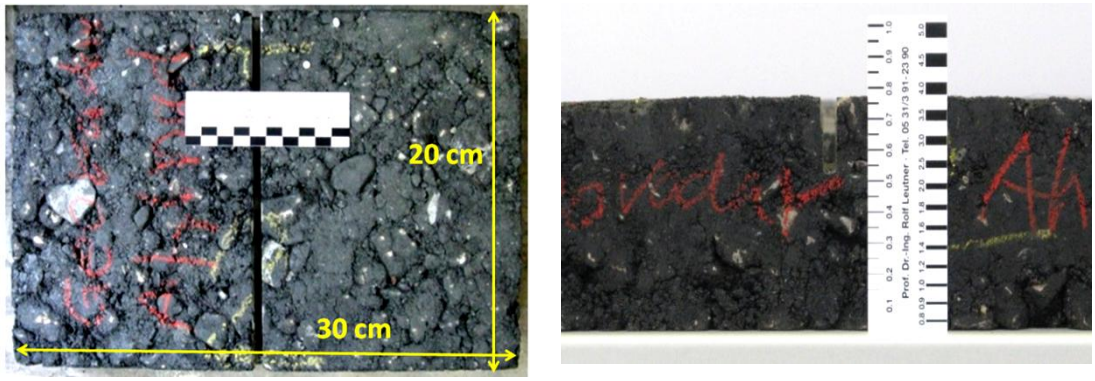

a **b**

Figure 3.6. Laboratory specimen AA (a) top view, (b) cross-section view

Table 3-2: Properties of asphalt specimen AA

Properties	Remarks
Aggregate type and size	Diabase, 0-32 mm
Bitumen type	Non modified Bitumen (50-70 penetration)
Layer type	Prepared as a Base-course
Degree of compaction	Compacted in the laboratory up to 99.8 %
Void content	NA
Crack width	4 mm
Crack depth	25 mm

- Asphalt specimen type AB

The specimen "AB" was a "porous asphalt" (PA) specimen with a thickness of 7.5 cm composed of PA 11 S asphalt mix. The sample was prepared to investigate the asphalt mix type (void content) effect on GPR outcomes. Due to smaller size of the specimen resulting in side reflections effecting GPR investigations, the specimen was replaced by the specimen "AE", of larger size. Properties of the specimen are provided in Table 3-3.

Table 3-3: Properties of asphalt specimen AB

Properties	Remarks
Aggregate type and size	Diabase, 0-11 mm
Bitumen type and percentage	25/55-55 A (5.3-6.5 %)
Layer type	Prepared as a wearing course
Degree of compaction	≈ 97% (ref to lab specimen)
Void content	≥ 24.0
Crack width	No crack
Crack depth	NA

This specimen had no crack. The specimen is shown in Figure 3.7. The aim of using such characteristic specimen was to see the effect of porous asphalt (PA) on analysis of sample characterisation by GPR.

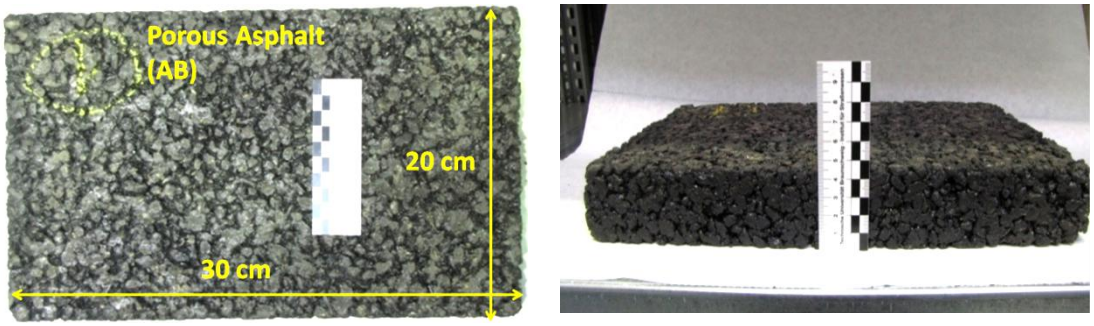

a b

Figure 3.7. Laboratory specimen AB, (a) top view, (b) front view

- Asphalt specimen type AC

The asphalt specimen AC was a dual-layered specimen. The upper layer was "Stone Mastic Asphalt" (SMA 11 S) having a thickness of 3 cm while the second layer was composed of asphalt mix "AC 16 B S" with 6 cm thickness. Properties of the top and bottom layers are provided in Table 3-4.

Table 3-4: Properties of asphalt specimen "AC"

Properties specimen AC	Wearing-course	Base-course
Aggregate type and size	Diabase, 0-11 mm	Diabase, 0-16 mm
Bitumen type and percentage	25/55-55 A (≥7.5%)	25/55-55 A (4.5-6.5%)
Layer type	Wearing course	Base course
Degree of compaction	≈ 97% (ref to lab specimen)	≈ 97 (ref to lab specimen)
Void content	≤ 3.5	≤ 6.0

Properties specimen AC	Wearing-course	Base-course
Crack width	No crack	No crack
Crack depth	NA	NA

The use of two layered asphalt specimen was to investigate the ability of GPR for differentiating layer boundaries. The specimen is shown in Figure 3.8.

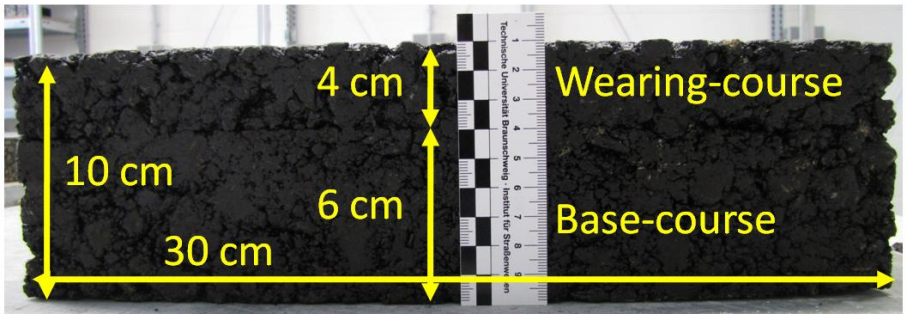

Figure 3.8. The dual layered asphalt specimen AC

- Asphalt specimen type AD

Sample AD was made of AC 22 T S. The sample dimensions were 50 x 40 x 9 cm^3. This specimen was prepared as a binder course. Properties of the specimen are provided in Table 3-5.

Table 3-5: Properties of asphalt specimen "AD" (AC22 T S)

Properties specimen AD	Remarks
Aggregate type and size	Limestone, 0-22 mm
Bitumen type and percentage	50/70 (4.0%)
Layer type	Prepared as a base course
Degree of compaction	≈ 98% (ref to lab specimen)
Void content	6.2%
Bulk density	2.307 g/cm^3
Crack width	No crack
Crack depth	NA

- Asphalt specimen type AE

Sample AE was made of porous asphalt (PA). The sample dimensions were 50 x 40 x 6 cm^3. Properties of the specimen are provided in Table 3-6.

Table 3-6: Properties of asphalt specimen "AE" (PA 8)

Properties specimen AE	Remarks
Aggregate type and size	Crushed Moraine, 0-8 mm
Bitumen type and percentage	40/100-65 (6.5%)
Layer type	Prepared as a wearing course
Degree of compaction	≈ 99%
Void content	24.8%
Bulk density	1.789 g/cm^3

Properties specimen AE	Remarks
Crack width	No crack
Crack depth	NA

- Asphalt specimen type AF

Sample AF was made of SMA 11 S (EOS). The "EOS" is an acronym used for "Electronic Oven Slag" which is a by-product from steel industry. The use of slag in asphalt pavements is possible (as the test sites "C" and "D") and thus was decided to be included in material effect investigations on GPR outcomes. The dimensions of specimen "AF" were 50 x 40 x 6 cm^3. Properties are provided in the Table 3-7.

Table 3-7: Properties of asphalt specimen "AF" (SMA 11 S (EOS))

Properties	Remarks
Aggregate type, size and percent	EOS (8/11mm) = 50 %, Gabbro (<8 mm)
Bitumen type and percentage	25/55-55A (6.8%)
Layer type	Wearing course
Degree of compaction	≈ 99%
Void content	2-3%
Crack width	NA
Crack depth	NA

- Asphalt specimen type AG

Sample AG was made of SMA 11 S (DS). The sample dimensions were 50 x 40 x 6 cm^3. Sample was prepared to test binder content and air void percentage. Properties are provided in Table 3-8.

Table 3-8: Properties of asphalt specimen "AG" (SMA 11 S)

Properties	Remarks
Aggregate type and size	Crushed Moraine, 0-11 mm
Bitumen type and percent	25/55-55A (old = PmB 45A) (Olexobit 45) (7.2%)
Layer type	Wearing course
Degree of compaction	≈ 99%
Void content	2.6%
Bulk density	1.308 g/cm^3
Crack width	NA
Crack depth	NA

The specimen AD, AE, AF and AG are shown in Figure 3.9.

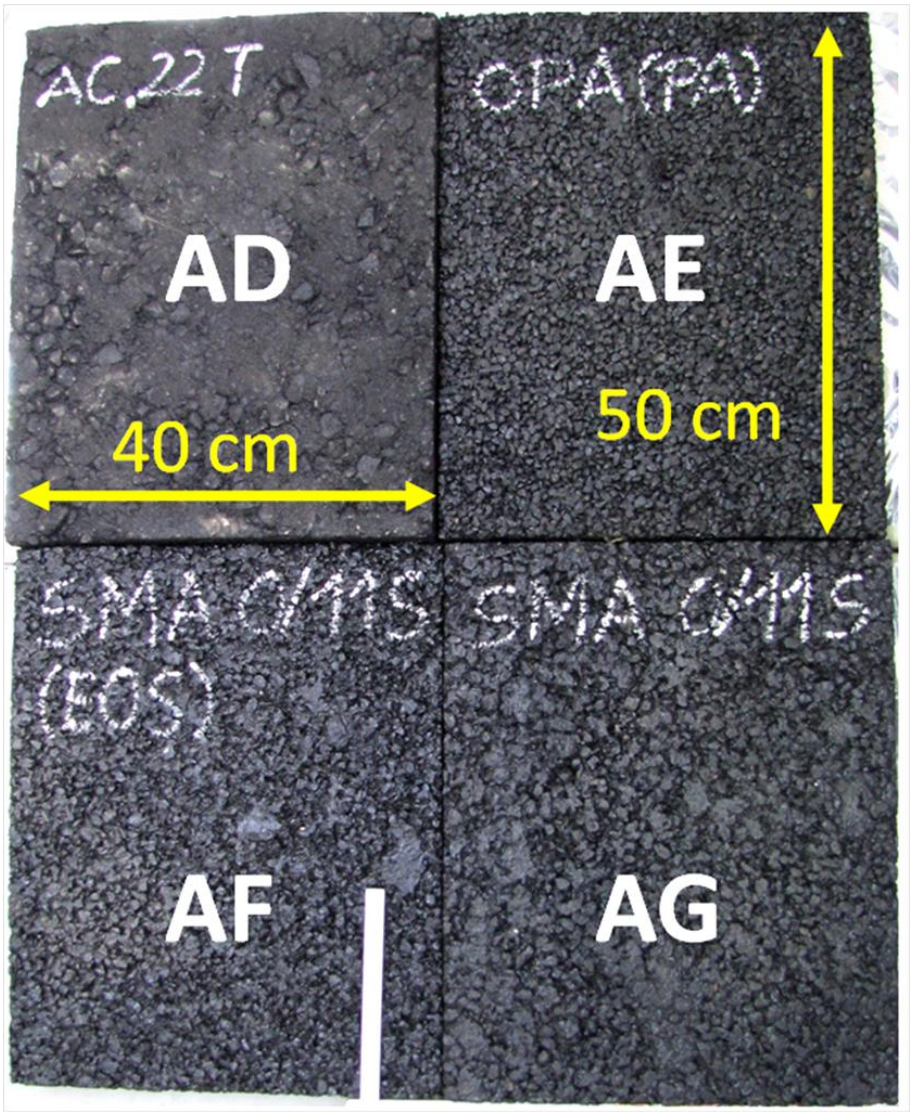

Figure 3.9. Asphalt specimens AG (top left), AF (down left), AE (top right) and AD (down right)

- Asphalt specimen type AH, AI and AJ

For the specimens "AH", "AI" and "AJ", the asphalt mix AC 32 BS was taken from a commercial asphalt mixing plant. The asphalt mix was then sent to Cottbus for specimen preparation. The asphalt specimen size was 50 x 40 x 6 cm^3. The cracks were engraved in finished specimens AI and AH in ISBS laboratory. The properties of specimens are given in Table 3-9 whereas the specimens are shown in Figure 3.10.

Table 3-9: Properties of asphalt specimen AH, AI and AJ

Properties of the specimens	Remarks
Aggregate type and size	Lime stones, 0-32 mm
Bitumen type and percentage	70/100 (3.9%)
Layer type	Base course
Degree of compaction	≥ 97 (ref to lab specimen)
Void content	5.7
Crack width	4 mm
Crack depth	Varying
No of cracks in AH	4 (Straight) (refer to Figure 3.10 please)
No of cracks in AI	1 (diagonal) 3.5 cm deep
No of cracks in AJ	None

The crack width in specimens AH and AI was 7 mm but the crack depth was varied. The specimen AI (Figure 3.10(c)) had a diagonal crack which was 1 cm deep. The diagonal crack pretended to portray irregular cracks in asphalt pavements. The specimen "AH" (Figure 3.10(a)) had four cracks; which were 4, 3, 2 and 1 cm deep respectively. The specimen AJ was left intact to be used as reference specimen wherever needed. Investigations were intended to study the effect of crack depth on GPR outcomes. Also plan was to investigate if different crack depths can be distinguished in GPR-grams.

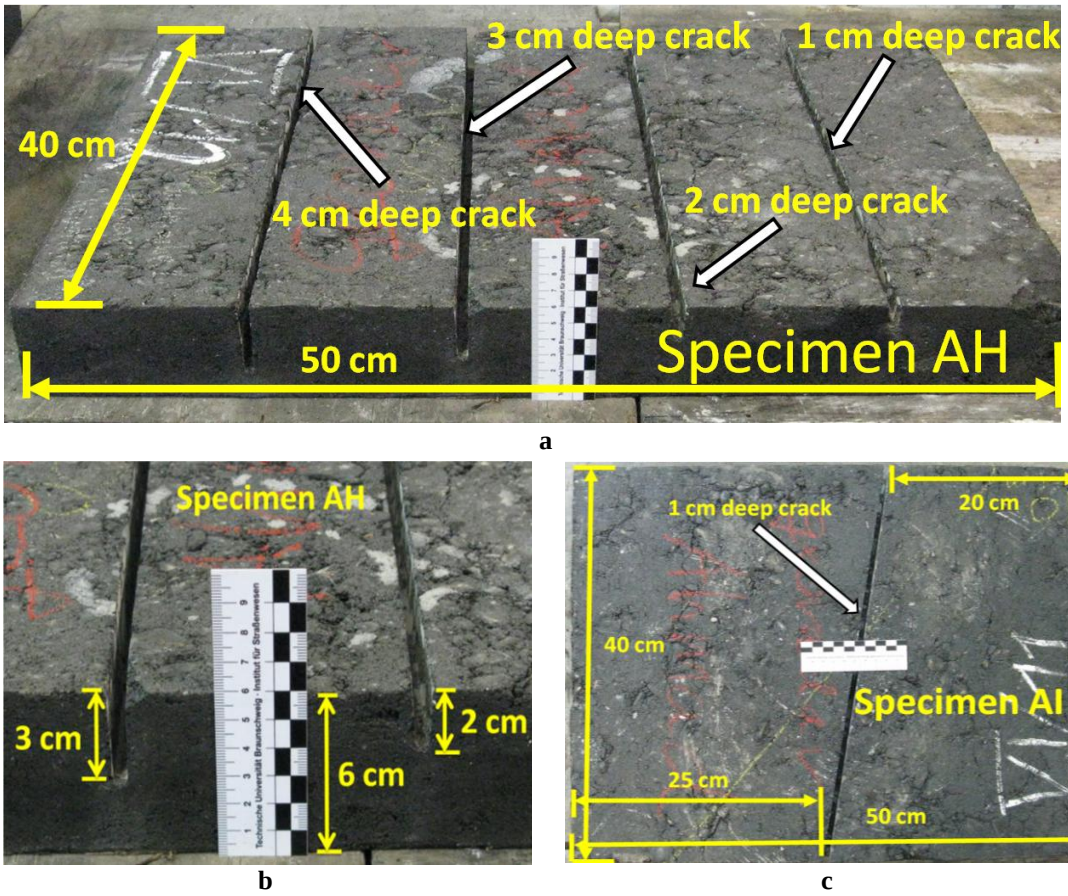

Figure 3.10. Specimens AH and AI, (a) specimen AH with four cuts, (b) the close-up of specimen AH cuts showing different cut depths, and (c) the specimen AI having diagonal cut

b. Asphalt specimens of type B

The size of specimens "B" were larger compared to specimens "A". The specimens were of size 70 X 50 cm^2 with a varying thickness. All asphalt specimens were prepared in ISBS laboratory. The details of the specimens are provided in the following sections.

- Asphalt specimen BA

The asphalt specimens "BA" were three in number. The specimens were composed of "SMA 11 BS" asphalt mix. The thickness of specimen was 6 cm. One of the specimens had two cracks of 5 mm width which were dividing the specimen in three equal parts. The depth of the first crack was 15 mm whereas of the second crack was 25 mm respectively. Another specimen was used for the effect of crack geometry on GPR-grams. For this purpose, a single crack middle of the specimen was engraved with different dimensions (Section 4.2.1). The details of the specimen are provided in the Table 3-10.

Table 3-10: Properties of asphalt specimen BA

Properties of specimen BA	Remarks
Aggregate type and size	Lime stones, 0-11 mm
Bitumen type and percentage	70/100 (3.9 %)
Layer type	Base course
Degree of compaction	≥ 97 (ref to lab specimen)
Void content	5.7
No of cracks	2 (each 5 mm wide)
Crack1 (depth)	15 mm
Crack 2 (depth)	25 mm

- Asphalt specimen BB

The asphalt specimen "BB" was dual-layered. The wearing course (top layer) was composed of Mastic Asphalt (Gussasphalt) "MA 11 S" with a thickness of 7 cm. The bottom layer was composed of "SMA 16 BS" with a thickness of 10 cm. Both specimens were prepared individually but later were glued with emulsion. The Mastic Asphalt specimen was cut thoroughly into two pieces. The cut pieces of specimens were placed on emulsified SMA 16 specimen to make them stick together. The prepared dual-layered specimen was placed in oven at a temperature of 80 °C for 10 hours. The specimen is shown in Figure 3.11.

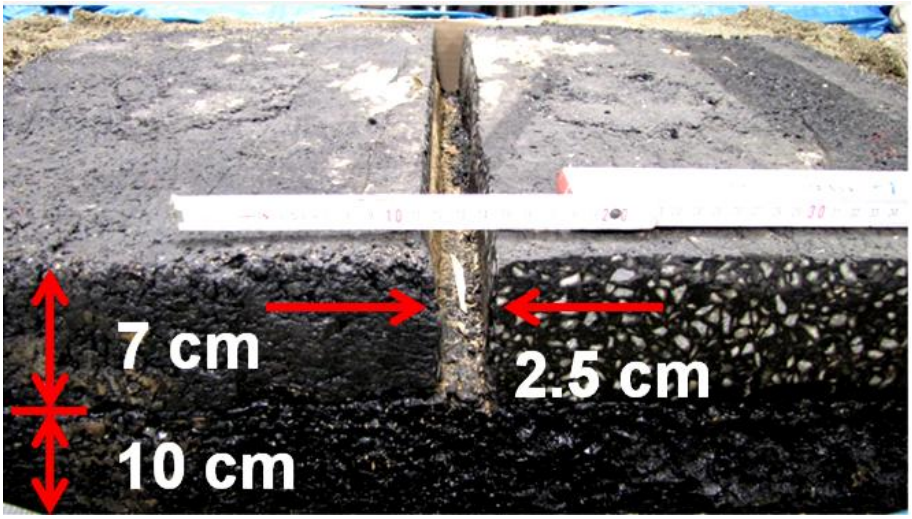

Figure 3.11: The multi-layered specimen with crack dimensions

The width of crack / joint in finished specimen was 2.5 cm whereas its depth was 7 cm. The specimen was used for the investigations of crack type and crack fill material. The details of the specimen's layers are provided in Table 3-11.

Table 3-11: Properties of asphalt specimen "BB" wearing-course (Mastic Asphalt) and base-course AC 0/16 BS

Properties of specimen BB	Wearing-course	Base-course
Material used	Kieselsplitt, 0-11 mm	Diabase, 0-11 mm
Bitumen type and percentage	45/100-65 (≥7.5%)	25/55-55A (4.5%)
Layer type	Prepared as a wearing course	Prepared as wearing course
Degree of compaction	≈ 98% (ref to lab specimen)	≈ 97 (ref to lab specimen)
Void content	≥1.5%	≤ 4.0%
Crack width	2.5 cm	Not applicable
Crack depth	7 cm	Not applicable

- Asphalt specimen BC

Two specimens "BC", 3 cm thick were of wearing course material i.e. asphalt mix type "AC 8 DS". These specimens were prepared to be used in investigation of bottom-up and top-down cracking in asphalt specimens.

c. Asphalt specimens of type C

The specimen "C" was of a base course material. The sample was cut from a road section. The road was composed of "AC 22 BS" asphalt mix. The thickness of specimen was 6 cm. Properties are given in Table 3-12.

Table 3-12: Properties of asphalt specimen C

Property	Remarks
Material used	Lime stones (0-22)
Bitumen type and percentage	25/55-55 A (4.2%)
Layer type	Base course
Degree of compaction	≥ 97 (ref to lab specimen)
Void content	5.7
No of cracks	None

The specimen is shown in Figure 3.12. The cut section from used pavement helped compare results from fresh asphalt to that of aged asphalt when detecting cracks with GPR.

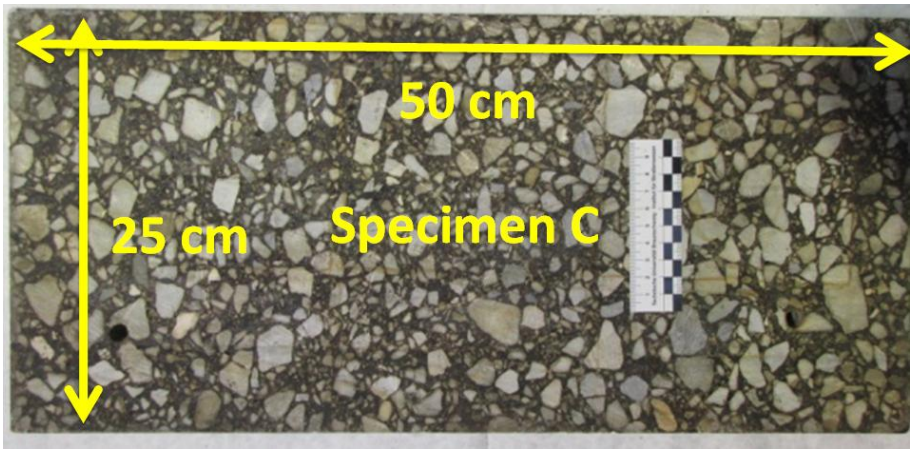

Figure 3.12. Asphalt specimen "C", a cut section of asphalt pavement

3.4.2 Asphalt EM properties

For the GPR tests conducted during this research work, dielectric constant values were calculated from trial and error method explained in Section 2.2.3. However, to validate whether or not the values calculated were in acceptable range, dielectric constants were also investigated in the laboratory of Institut für Hochfrequenztechnik, TU Braunschweig. For this purpose, the specimens AD, AE, AF and AG were investigated. The specimens were tested with a bi-static radar system with a frequency of 0.8 to 6 GHz but 2 to 3 GHz range was considered for testings. The tests were conducted in an isolated chamber to avoid influence of noise. The test temperature was 20° C. The test setup is shown in Figure 3.13(a).

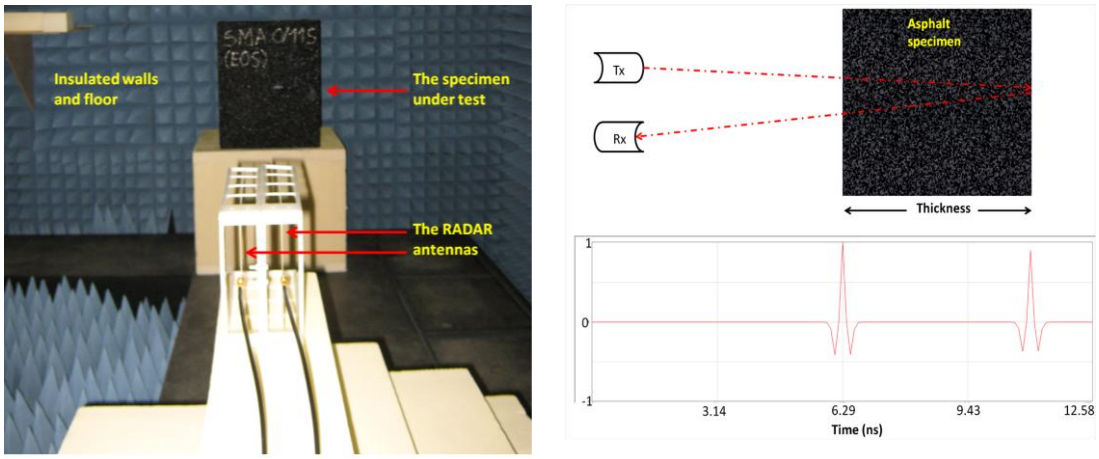

a **b**

Figure 3.13. The measurement of asphalt EM properties, (a) test setup in insulated chamber, (b) the calculation phenomenon (demo) (specimen "AG", Software: GPRSim)

The dielectric constant was calculated by measuring the time difference between specimen surface reflected EM waves and from its end. The test was repeated by moving radar closer to the specimen. With the help of known specimen thickness and arrival time difference, the dielectric constant of specimen was calculated using Equation 2-5. The test setup is shown in Figure 3.13(a) whereas an example is shown in Figure 3.13(b) to explain testing phenomenon. The average dielectric constants "k1"measured from this setup for specimens AD, AE, AF and AG were 6.64, 4.13, 8.09 and 5.93 respectively.

From dielectric constant values, it can be observed that porous asphalt specimen AE has the lowest dielectric constant value. This is because porous asphalt mixture has more air voids compared to other mixtures. On the other hand the specimen AF has the highest value of dielectric constant. This is because in the specimen AF, slag (EOS) was used as aggregate which is a by-product from steel industry. The steel has higher dielectric constant as thus specimen AF also has the higher value. As for as difference in Specimen AG and AD dielectric constant is concerned, the specimen AD has more aggregate percentage and less bitumen.

Figure 3.14. Test setup used to investigate dielectric constant k2

Although the asphalt dielectric constants measured from this setup were in the same range as obtained from trial and error method, it was decided to conduct further tests where there is no influence of air as air contains noise. For that purpose, specimens AD, AE, AF and AG were tested inside the radar machine by placing them in a structure shown in Figure 3.14. The samples sizes were 8.5 x 4.0 x 1.0 cm^3 and it was ensured to leave no gap between mould and specimen by gluing the gaps, if any, with bitumen. The EM waves were made penetrate through one end of the specimen and collected on the other end. The asphalt dielectric constant values were calculated in the frequency range of 2.35 GHz to 3.0 GHz. The dielectric values of asphalt are provided in Figure 3.15.

It can be seen in the results shown in Figure 3.15 that the values of dielectric constant (k2) are in the same order of magnitude as were in previous tests however, their magnitude is different. The average values of dielectric constant for Specimen AF, AD, AG and AE are 10.024, 5.818, 5.416 and 3.887 respectively. To compare the values obtained from both tests, the outcomes are presented in Table 3-13.

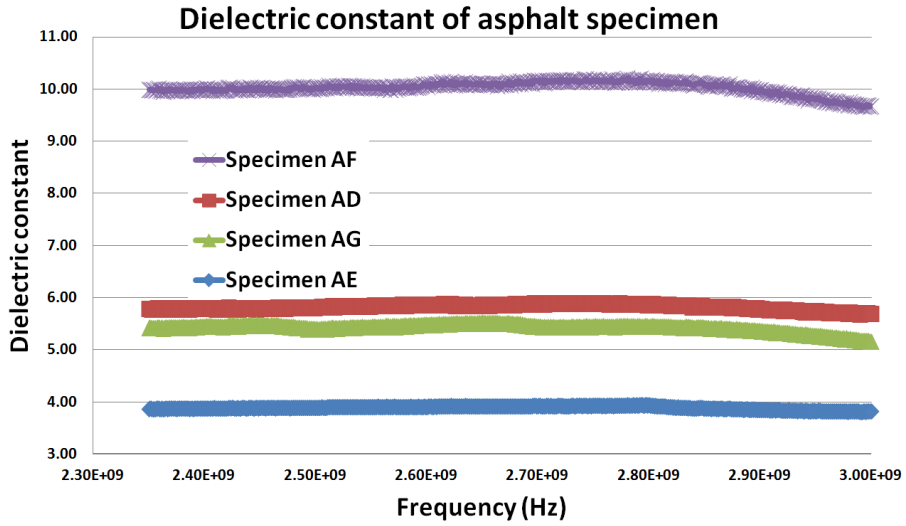

Figure 3.15. The dielectric constant values of asphalt specimens AD to AF

It can be seen in Table 3-13 that the dielectric constant values obtained from test 2 are 12.4, 6.05 and 8.77 percent lower for specimen AD, AE and AG respectively compared to the values obtained from previous tests. This may show some interference from open air noise, e.g. telecommunication and wireless signals, noise from machine itself, etc. The exact cause however, has to be investigated. On the other hand, the dielectric constant value of Specimen AF increased in test 2 contrary to other outcomes. The reason for increase in the dielectric constant value of specimen AF is unknown and therefore further testing is recommended. The dielectric constant of asphalt from trial and error method used in all the outcomes of this research was though validated to be within the range.

Table 3-13: Dielectric values of selected asphalt specimens

Specimens	Dielectric value (k1)	Dielectric value (k2)	k2 vs. k1 (percentage)
AD	6.64	5.818	87.5
AE	4.13	3.887	93.95
AF	8.09	10.024	123.86
AG	5.93	5.416	91.23

3.5 Test sites description

For field testing, real asphalt pavements under traffic were investigated. The test sites had visible cracks with unknown geometry and the reason for cracking was not known. Core samples from surveyed sections were analysed in ISBS laboratory. Material characteristics and pavement layer's properties were studied and documented. A description of the test sites is provided in following sections.

3.5.1 Site "A" (Beethovenstraße)

This test site is located near ISBS laboratory at Beethovenstraße Braunschweig. The reason for choosing the site was the appearance of different crack types on a single site. The

location of site and cracks are described in Figure 3.16. One crack was transversal named as Crack "α" whereas other one named Crack "β" was longitudinal joint (sealed).

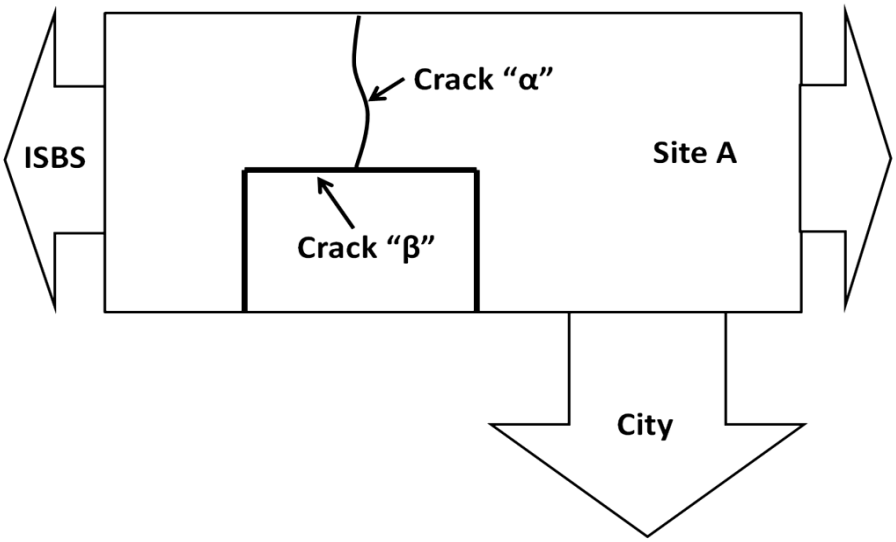

Figure 3.16. Test site A, Beethovenstraße Braunschweig

The cracks "α" and "β" (site A), were naked eye visible cracks/joints where crack "α" was filled with sand, clay, etc. and crack "β" was filled with bitumen. Width of crack "α" was about 10 mm (Figure 3.17(a)) and that of crack "β" was 20 mm (Figure 3.17(b)). The crack "α" had enough width to let water penetrate into sub-layers. Thus, it was selected as a severe crack type. The deflection test results also showed that this crack runs through the whole pavement structure. Crack "β" was a joint between two different pavement sections having different layer properties which were later confirmed by pavement cores. As "β" was a joint, it was assumed that it runs through the pavement structure till un-bound layers.

a

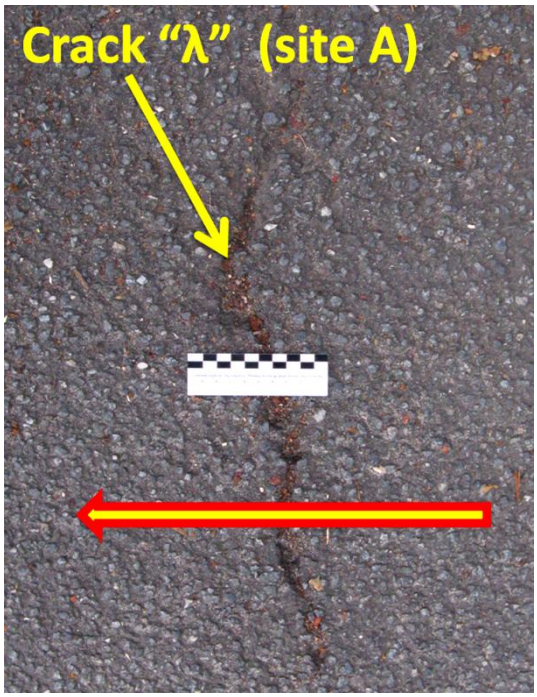

b

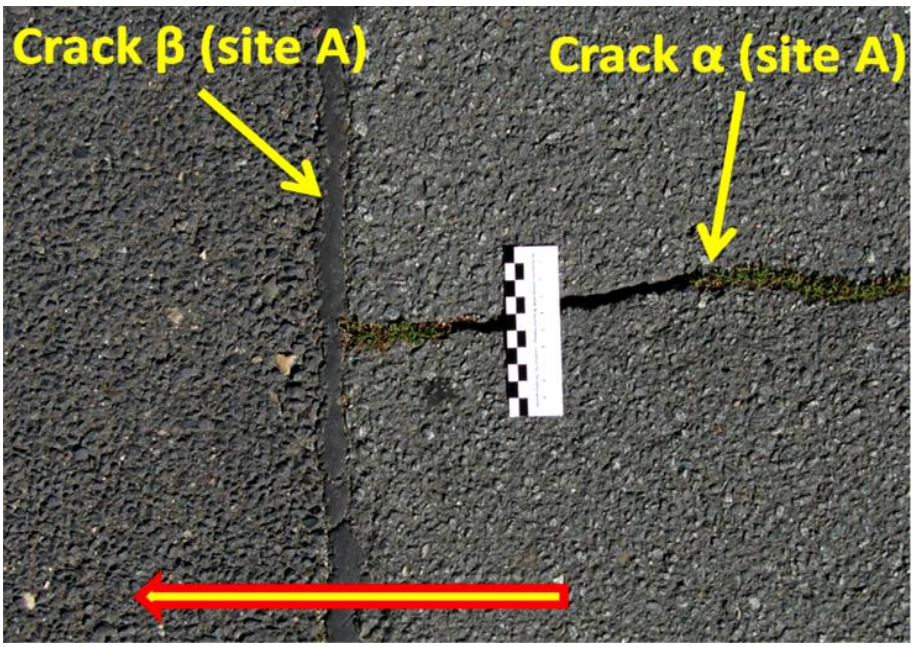

c

Figure 3.17. The cracks in asphalt pavement at Sites A and B (a) crack "α" Section A, (b) crack "λ" Section B and (c) crack "β" Section A (red arrow showing direction of survey)

3.5.2 Site "B" (Bültenweg)

This site is located at Bültenweg 4, Braunschweig. The reason for choosing this site was a transverse pavement failure crack "λ" which could be visually identified. The crack is shown in Figure 3.17(b). The tempered crack was starting from pavement edge and stopping in the pavement centre. The average width of crack was about 4 mm. The fill material in the crack was clay, de-icing agents, tire fines and plants. As the crack was not throughout pavement width, it was assumed that it was not separating the pavement super-structure.

3.5.3 Site "C" (Holzweg)

The name of Site C is "Holzweg", an asphalt pavement located in Cremlingen (Figure 3.18). It is a village road mostly used by agricultural vehicles. The use of slag was also one of the factors why this pavement was selected for testing. A 60 m pavement section was selected for GPR testing, as is shown in Figure 3.18. The cracks were marked and mapped. The survey path and direction was fixed to be investigated in future by the GPR systems. Thus each time the survey was carried out on same position.

Figure 3.18. The view of test site "C" where red arrow in map and yellow arrow on pavement indicates the direction of survey

In the first 42 m section of the test site C, there were eight cracks with varying width and depth. The location and dimensions of cracks are shown in Figure 3.19(a). The red arrow (Figure 3.19(a)) is indicating the direction of survey.

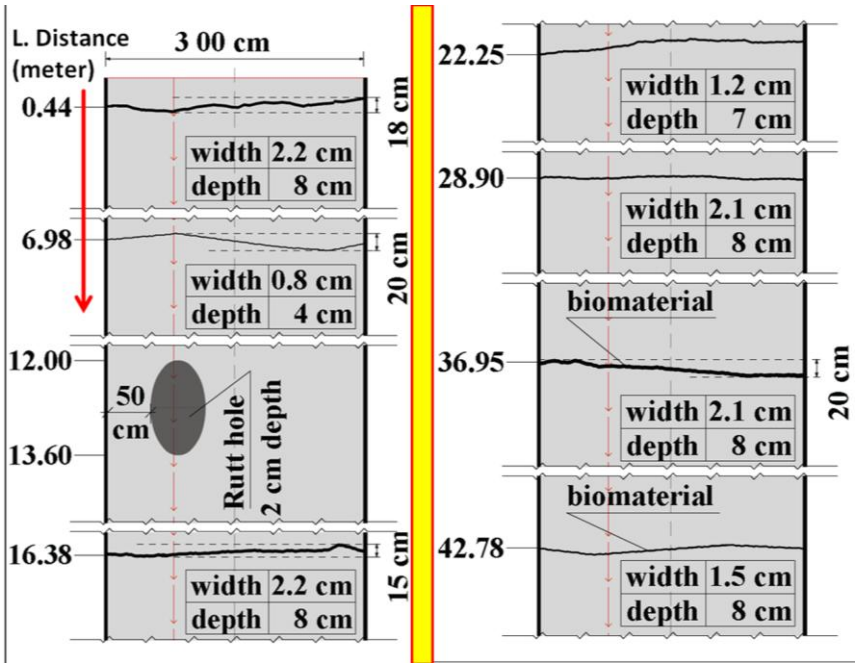

a

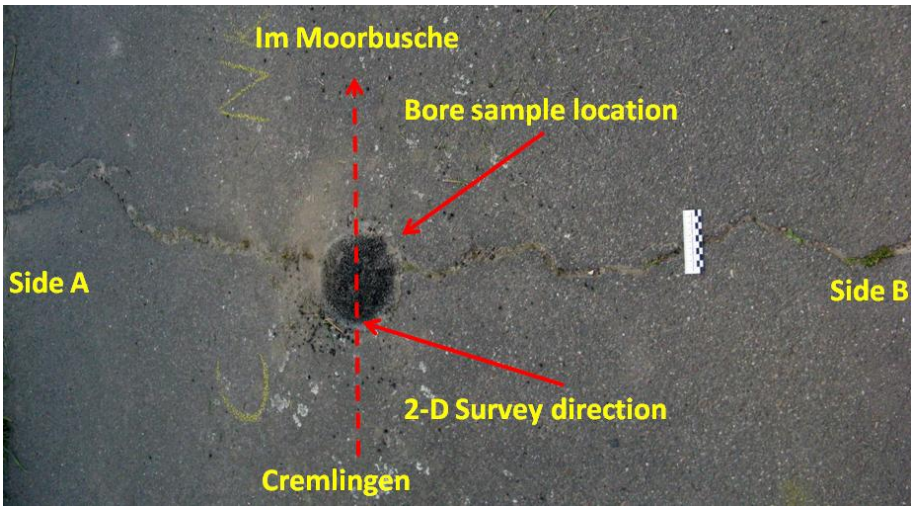

b

Figure 3.19. The cracks on Section C, (a) location and dimensions of cracks (red arrow indicating direction of survey) and, (b) the crack and core location on 46 m of Section C

On 46 meter station (Figure 3.19(b)), there was a transverse crack with varying width. The average width was 1.4 cm. The pavement surface was also showing some signs of settlement.

On 55.60, 56.35 meter station, there were more cracks. The crack 1, 2 and 3 (Figure 3.20(a)) were 2 cm, 2.5 cm and 2 mm wide respectively. The cracks are shown in Figure 3.20(a) and (b). Apparently there was some settlement (≈ 1 cm) on pavement surface. The settlement was along Crack 3.

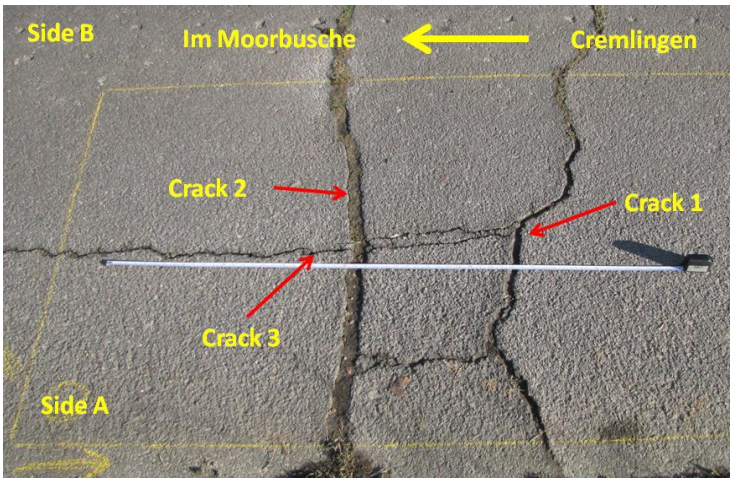

a

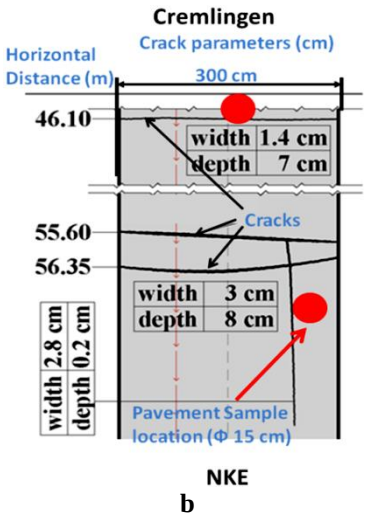

b

Figure 3.20. A view of test tracks (a) crack at 55 m location and (b) crack details of Holzweg with red circles indicating core sample location

Based on destructive sampling at 46 meter from pavement start point, the thickness of pavement asphalt layers was determined to 2 cm wearing course and 6 cm asphalt base course. The base course was 8 cm thick on 56 meter station.

The slag material was used together with crushed gravel aggregate in binder-course (Figure 3.21). Due to iron slag, the dielectric constant of binder-course was higher than for normal asphalt pavement layers.

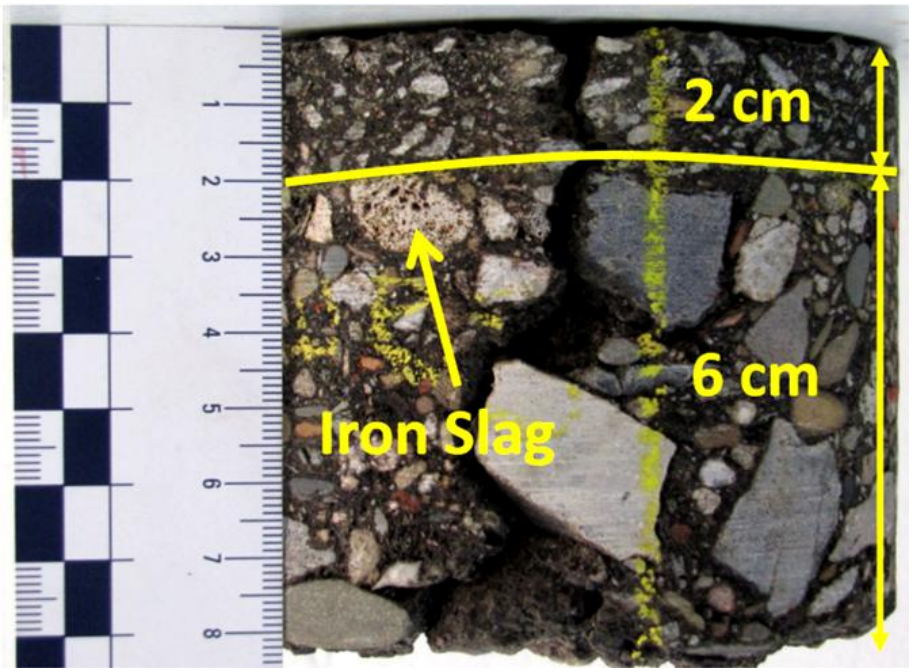

Figure 3.21. Holzweg layer's profile and crack geometry (traces of slag are marked)

The estimated dielectric constant values of asphalt and crack filling materials are given in Table 2-1. Further details of cracks are provided in Table 3-14.

Table 3-14: Crack properties of site C (Holzweg)

No	Distance (m)	Width summer (cm)	Width winter (cm)	Crack depth (cm)	Crack fill
1	0.44	2.50	2.54	8	Grave, sand, clay
2	6.91	0.40	0.52	5	Sand, clay
3	16.29	2.00	2.20	8	Gravel, clay, organic material
4	22.35	1.00	1.20	8	Sand, clay
5	29.89	1.50	2.10	7	Sand, clay
6	36.82	2.10	2.40	8	Gravel, sand, clay, organic material
7	42.62	1.20	1.50	8	Sand, clay
8	45.96	1.00	1.40	7	Sand, clay
9	55.13	1.8	2.08	10	Sand-clay
10	56.26	3.2	3.45	10	Sand-clay-organic material

3.5.4 Site "D" (Gutswiese)

The site "D", pavement section called "Gutswiese" was reconstructed in May 1999 and new wearing course was provided in April 2002. There was only one crack in the pavement

selected for testing which was 30 m away from section junction with main road. The crack width was decreasing when moving away from pavement side D (Figure 3.22(a) and (b)). The detailed survey plan of GPR survey is provided in Figure 3.22(a).
The rectangular areas marked in red (Figure 3.22(a)) are 3D survey areas. The numbers 1 to 3 show the route for 2D survey. For 2D survey, a 22 meter section was selected. The crack was in the mid of this 22 meter section. The dark dots show the location of core samples. The material and asphalt mix details of Holzweg and Gutswiese are provided in Table 3-15.

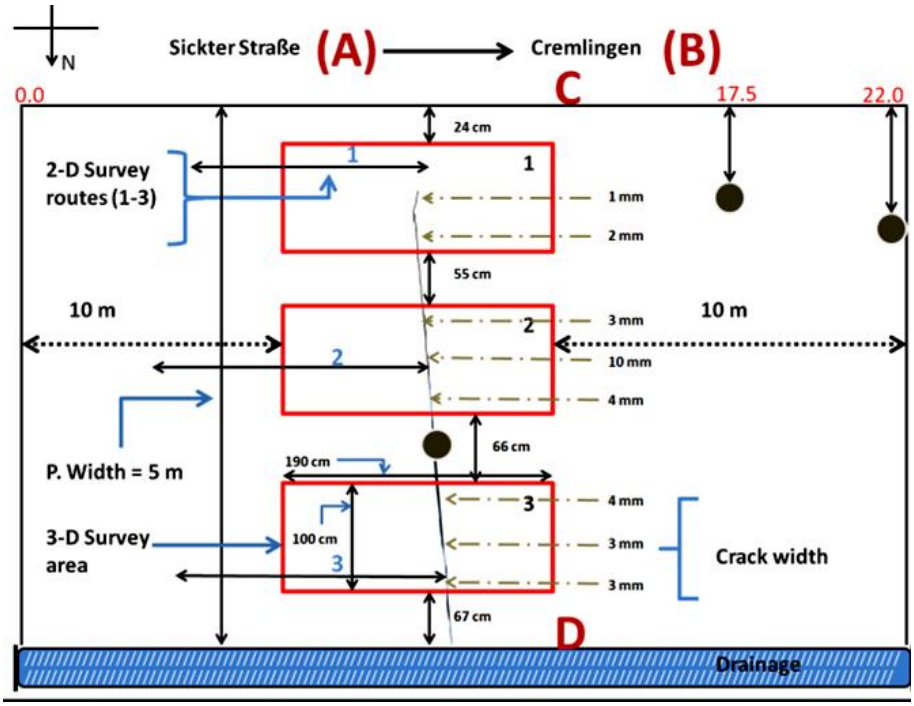

a

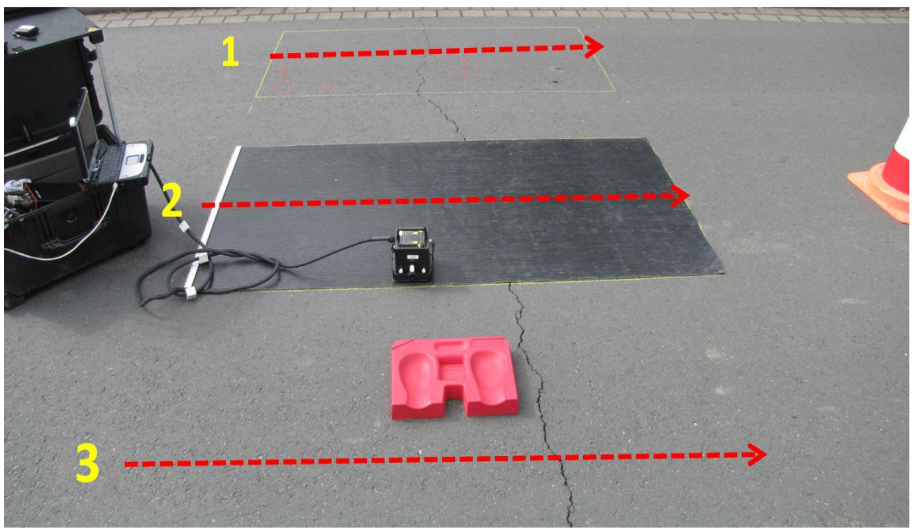

b

Figure 3.22. Test site D "Gutswiese", (a) survey plan with the black dots indicating core samples location, (b) the 2-D and 3-D survey locations

Table 3-15: Asphalt mix properties of Site C (Holzweg) and Site D (Gutswiese)

	Site C (Holzweg)			Site D (Gutswiese)		
	Wearing course	Base course		Wearing course	Base course	
Thickness (cm)	2	6*	8**	4	6***	8****
Dielectric constant (ε_r)	3.5	5		4	6	
Bulk density (g/cm^3)	2.521	2.497		2.656	2.517	
Softening point (°C)	67.7	83.6**		63.4	79.4	
	68.1	84.0**		64.3	81.4	
Binder content (%)	6.09	3.63		4.66	4.78	
Aggregate (type & percentage)	Gabbro	B. F. Slag (3.33 %), Gabbro, limestone.		Basalt	B. F. Slag (29. 45 %), Gabbro, limestone	

*On 46 m location at Site C (Holzweg)

**On 55 m location at Site C (Holzweg)

***In pavement centre at Site D (Gutswiese)

****On 22m at Site D (Gutswiese)

3.6 Aladdin survey procedure

The component parts of Aladdin system must be connected correctly and data-logger must be switched on. Before starting the survey, the survey type must be selected, as configuration of programme is needed for 2-D and 3-D survey. For moving GPR on smooth surfaces, a stick is provided which can be attached to the system. The stick cable must be attached to the system wheel for distance calibration. In case of surveying with cart, the cable must be connected to the cart wheel. When surveying with stick, marker points can be placed in GPR data on required locations whereas in case of survey with cart, this is not possible. The system has Wi-Fi option thus making it possible to avoid direct connection of data-logger and display (computer).

3.6.1 2-D survey

For 2-D survey, from configuration menu, Aladdin antenna configuration, sampling rate, acquired time and horizontal step distance must be configured. The sampling rate is the sample resolution of data. Increasing sapling rate increases data resolution and vice versa. The horizontal is the distance in meter between two parallel horizontal scans. After selecting the required vales, radar configuration is saved with specific name for future use. The precaution is that wheel calibration is needed each time when antenna configuration is changed. The final step is to calibrate the EM wave energy transmitted by the antenna on the material to be surveyed. The antenna calibration is automatic and manual as well.

3.6.2 3-D survey

The "Pad Survey Guide" (PSG) (Section 3.2.6) is used to facilitate 3-D survey with Aladdin. Therefore, PSG survey mood must be selected from options menu. 3-D survey is done on a mat with grids on regular distances. Precaution for 3-D survey is that dual antenna system must be on to facilitate longitudinal (survey direction) and transversal

direction of survey. Thus with a single pass, both files are collected which are needed for 3-D survey. The rest of the procedure is same as for 2-D survey.

3.7 Summary

In this section, the GPR systems selected for crack investigation are explained together with their manufacturer information and data collection techniques. The systems are explained with figures and most important the shape of their antenna is shown. This helps understand the data collection methods followed by specific GPR system. The explanation of software helps to understand the application of specific processing steps limited to some acquired data. The reason for selecting multiple processing techniques is explained with the limitations associated to the software. The asphalt specimens were explained according to their labelling. The difference and need for design of asphalt specimens and the tests associated with these specimens are explained. The wide range of asphalt specimens will help bring forward the impact of material type on crack investigation by GPR. The selected test sections are explained with labelled figures showing ranges of crack types. The crack fill is also considered and explained with figures. In the end, the survey procedure by Aladdin equipment is provided. The 2-D and 3-D survey is explained briefly for understanding the test results and their repeatability in future.
The overview of all the specimens used in this research is provided in Table 3-16.

Table 3-16: Asphalt specimen properties

Type	Asphalt mix type	Void Content (%)	Bitumen		Dimensions [mm]	Crack (cut)
			Type	Content %		
AA	AC 32 TS	≥ 4	50/70	4.0- 6.0	320 x 200 x 75	1
AB	PA 11 S	≥ 24	25/55-55 A	5.3-6.5	320 x 200 x 75	None
AC	SMA 11 S	≤ 6.0	25/55-55 A	≥7.5	320 x 200 x 30	None
	AC 16 BS	≥ 6.5	25/55-55 A	4.5-6.5	320 x 200 x 60	None
AD	AC 22 TS	6.2	50/70	4.0	500 x 400 x 90	None
AE	PA 11	24.8	40/100-65	6.5	500 x 400 x 60	None
AF	SMA 11 S (EOS)	2.3	25/55-55A	6.8	500 x 400 x 60	None
AG	SMA 11 S	2.6	25/55-55A	7.2	500 x 400 x 60	None
AH	AC 32 BS	5.7	70/100	3.9	500 x 400 x 60	4
AI	AC 32 BS	5.7	70/100	3.9	500 x 400 x 60	1
AJ	AC 32 BS	5.7	70/100	3.9	500 x 400 x 60	None
BA	SMA 11 S	5.7	70/100	3.9	700 x 500 x 60	2 and 1
BB	SMA 11 S	≥1.5	45/100-65	≥7.5	700 x 500 x 70	1
	SMA 16 BS	≤ 4.0	25/55-55A	4.5	700 x 500 x 100	None
BC	AC 8 DS	3.5	25/55-55A	5	700 x 500 x 30	None
C	AC 22 BS	5.7	25/55-55 A	4.2	520 x 240 x 60	None

4 Crack evaluation through GPR

4.1 Introduction

In this chapter, abilities of GPR as crack evaluation tool in asphalt pavements are verified. The verification comprises crack detection ability and crack geometry measurements. The tests were conducted in laboratory on asphalt specimens and on asphalt pavements in field. The outcomes are verified by comparing laboratory-field outcomes and taking core samples from asphalt pavements.
Furthermore, the processing of raw data obtained from GPR is studied as processing steps, sequence of processing steps and the extent of processing governs GPR outcomes. Therefore, multiple software programs are used for data processing to investigate effect of processing techniques on crack evaluation ability of the GPR. In addition to, state of the art GPR hardware and software techniques (other than classical techniques) will be investigated regarding their effect on GPR abilities for crack evaluation. The aim is to identify technique of efficient accuracy and also user friendly and time saving.

4.2 Effects of crack type and material properties

The investigations carried out to verify effect of crack geometry, crack position and crack fill on crack investigation is explained. During on site testing, the cracks were investigated together with their crack fill material. The crack type was investigated with pavement coring and the crack fill material was collected in air tight containers, later examined in the ISBS laboratory. Due to limited flexibility of investigation on pavement testing, the asphalt specimens were tested in controlled environment regarding crack geometry, crack position and crack fill. The combination of crack fill materials together with different asphalt mixtures is used to verify material difference effect on crack investigation. The effect of temperature was verified on pavement sections and asphalt pavements in laboratory. The effects of above discussed parameters were confirmed by testing on pavements and then repeating the same parameters in control environment on asphalt specimens. The outcomes were discussed and explained with GPR-grams.

4.2.1 Crack geometry

For the investigation of crack geometry a crack in the centre of the specimen “BA” was engraved. The effect of crack geometry on the crack detection by GPR was tested in two phases. In the first phase, the crack’s width was kept constant whereas the depth was varied and in the second phase, the crack width was variable whereas depth was constant. These cracks were then investigated with the GPR by keeping hardware and software attributes constant throughout the investigation period. This includes the same GPR equipment (Aladdin) and same software use (ReflexW). The data was collected by antenna configuration of 512 samples per scan, 8 ns time window and 0.00202 m pulse transmission distance. For 3-D data processing, GRED-3D software was used. The processing steps in

ReflexW software were dewow, background removal, static/zero correction and y-gain. The test setup is shown in Figure 4.1.

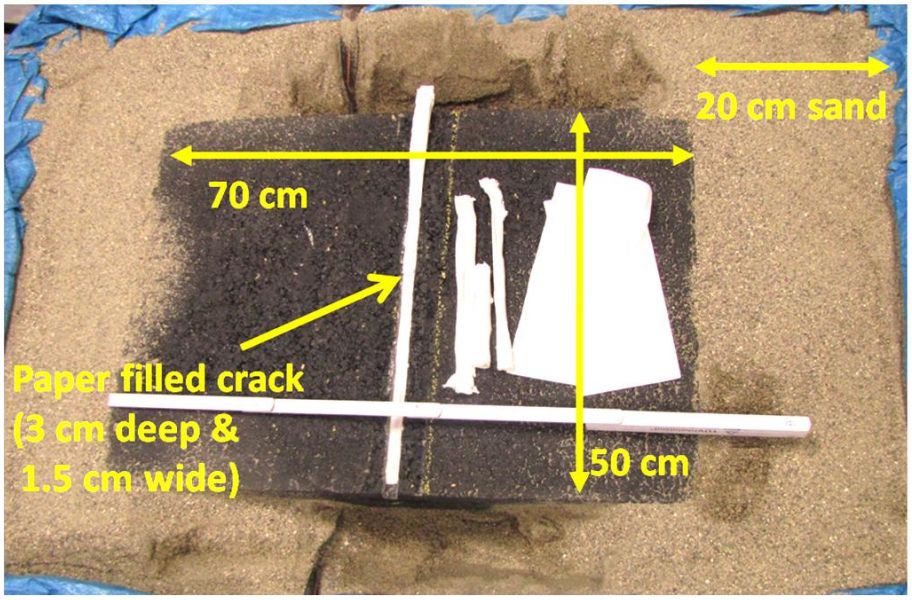

Figure 4.1. The test setup for investigating the crack geometry effect on GPR survey (specimen "BA" crack sealing with dry paper)

The asphalt specimen BA was placed on 4 cm thick sand layer. The specimen was surrounded by 20 cm sand in the direction of survey whereas 10 cm sand on specimen sides. The crack was sealed with dry paper to simulate air as fill material. The specimen was placed in a sand-box designed for prevention of side reflection (Fresnel Zone, Section 2.5.1.2) during data collection. The Aladdin PSG was placed on top of the specimen during testing. The 512 samples per scan was kept for all testing phases. The specimen cracks were investigated as top-down crack only. Test outcomes are provided in the following sections according to test phases, described above.

4.2.1.1 The effect of crack depth

The specimen "BA" with 1 x 1 cm^2 crack was investigated to verify the crack depth influence on GPR outcomes. The crack depth was extended from 1 to 2 and 3 cm. The data was collected in 2-D as well as in 3-D format. The outcomes of 1 x 1 cm^2 crack detection are shown in Table 4-1.

In the first row of Table 4-1, the 2-D crack detection result is presented. The crack survey was performed in the centre of the specimen. The GPR data was processed using ReflexW software. The detected crack is encircled with yellow in the GPR-gram. The intersection of sand and asphalt specimen is also clear. However, the bottom of specimen is unclear due to less material properties contrast. The crack is nonetheless, easily be seen in the GPR-gram by marking the specimen's surface.

In the 3-D survey of the same crack (Table 4-1-2nd row), the crack is clearer compared to 2-D survey outcomes. Also the specimen boundary (marked in red) is distinguishable from

surrounded sand. The 3-D survey outcomes were therefore promising regarding accuracy and confidence level for crack detection. To investigate further the effect of crack depth, survey was carried out on 2 and 3 cm deep cracks, with fixed width of 1 cm.

Table 4-1: Detection of 1 x 1 cm^2 crack with 2-D and 3-D survey (specimen BA)

Depiction	Outcomes
2-D crack detection	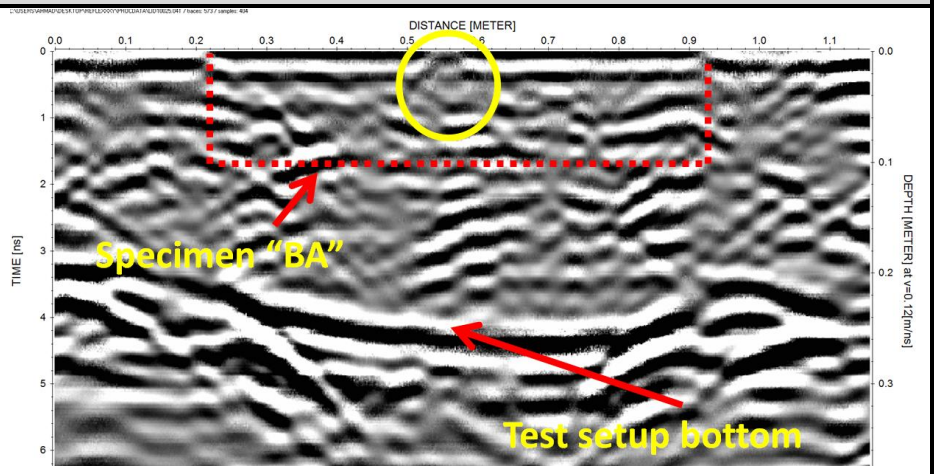
3-D scan cross-section at depth = 0.540 cm	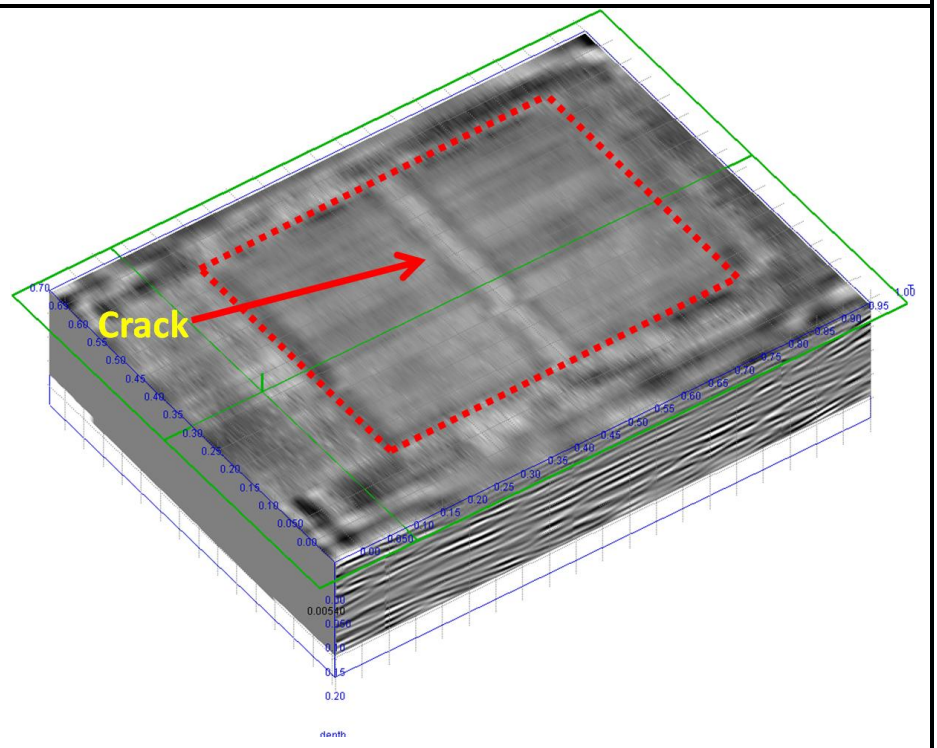

After promising results of 1 x 1 cm^2 crack detection, GPR surveys were carried out for 2 and 3 cm deep cracks. The 2-D survey results (including the results shown in Table 4-1) are shown in Table 4-2. The survey data was processed with ReflexW software keeping processing parameters same for each survey. It can be observed in the outcomes shown in (Table 4-2) that the hyperbola of 1 cm deep crack differs from 2 and 3 cm deep crack. The hyperbola of 1 cm deep crack shown in first column (Table 4-2) is broken at the top and has right wing missing. Its left wing span is shorter than 2 and cm crack's hyperbola. On

the other hand the 2 cm deep crack's hyperbola had both left and right wings with solid top. The 3 cm deep crack's hyperbola was clearer among all and had wings down deep in the GPR-gram.

To investigate affect of crack depth on crack's hyperbola, hyperbola's dip (Table 4-2) in GPR-gram is measured. The 1 cm deep crack's hyperbola was 2.2 cm, 2 cm deep crack was 2.0 and 3 cm deep crack was 4 cm deep in the GPR-gram.

Table 4-2. The relation of increase in crack depth and increase in its hyperbola intensity (1 cm wide crack specimen BA)

Crack dimensions	Crack hyperbola
1 cm deep crack	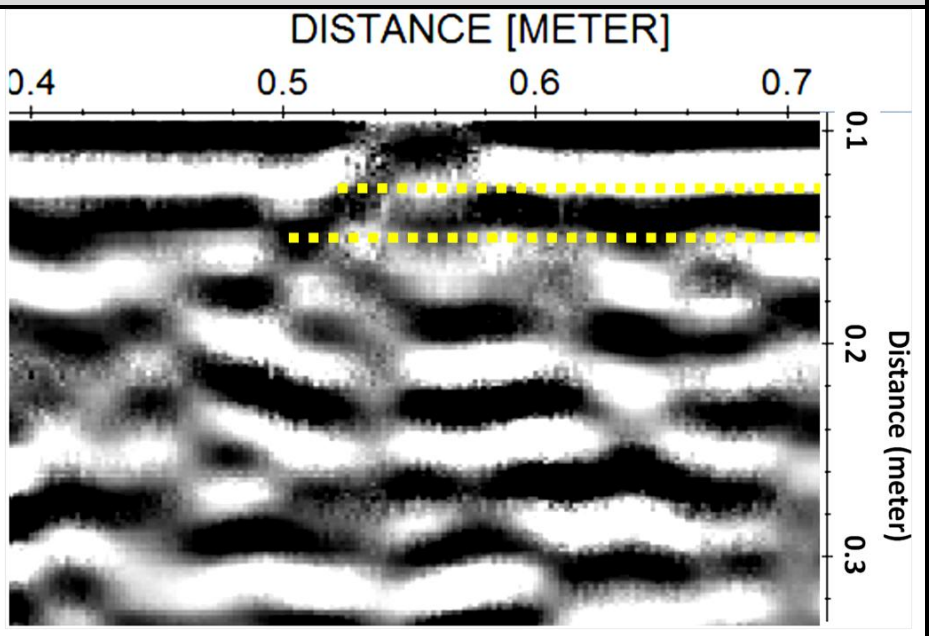
2 cm deep crack	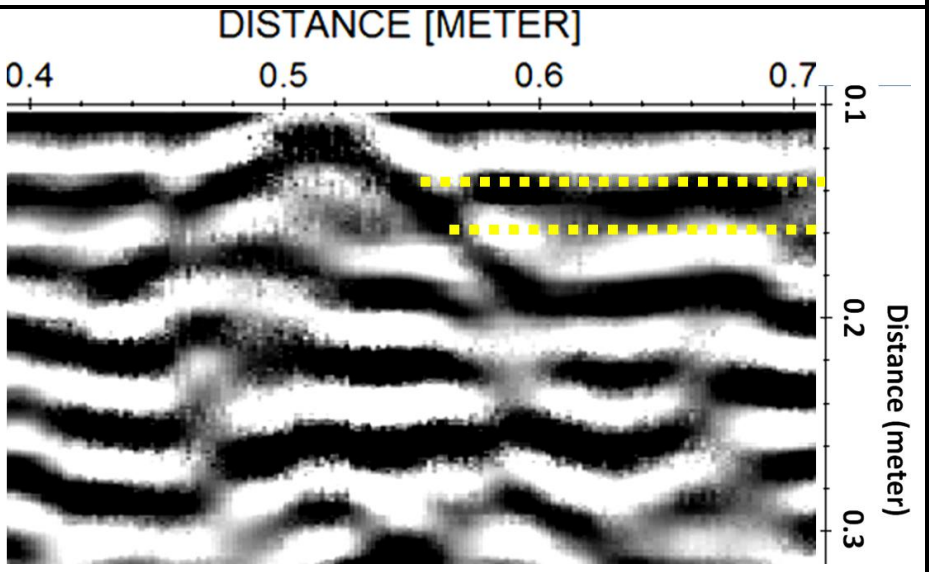

Crack dimensions	Crack hyperbola
3 cm deep crack	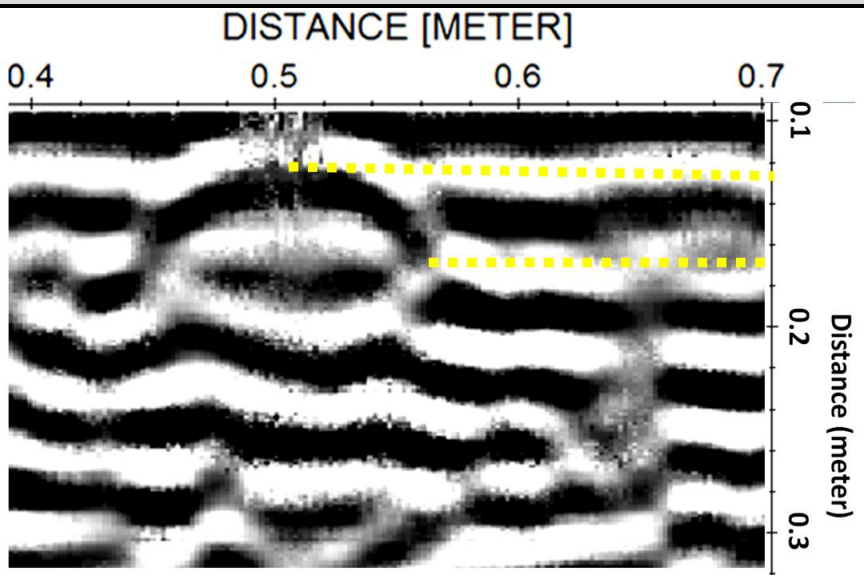

The results of Table 4-2 are plotted in Figure 4.2. The results reveal that accuracy of crack depth measurement is greater for 2 cm cracks. The error in measuring cracks depths of 1 and 3 cm can be visual limitations and scattering of EM respectively. It is though recommended to collect more data by changing crack depth and GPR frequencies before developing a relationship between crack depth and GPR outcomes.

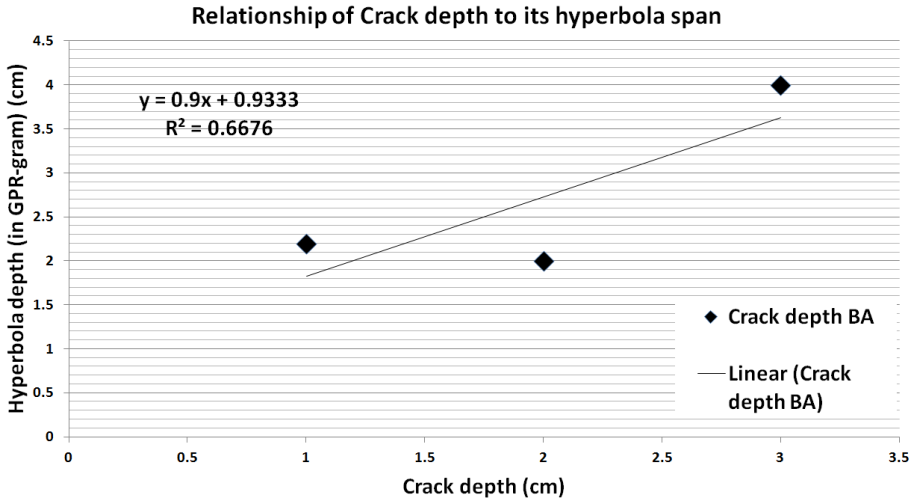

Figure 4.2. The accuracy of crack depth measurement on specimen "BA"

For 3-D survey, the test setup shown in Figure 4.1 was used. The crack in Specimen BA was initially 1 cm wide and 1 cm deep. The crack depth was then increased to 2 and 3 cm keeping crack width constant to 1 cm. 3-D GPR survey was carried out for 1, 2 and 3 cm deep crack. The 3-D GPR-grams were sliced and analysed at depths of 0.54, 1.3, 2.02 and 3.0 cm depths. The test setup together with GPR-gram cross-section locations are shown in Figure 4.3.

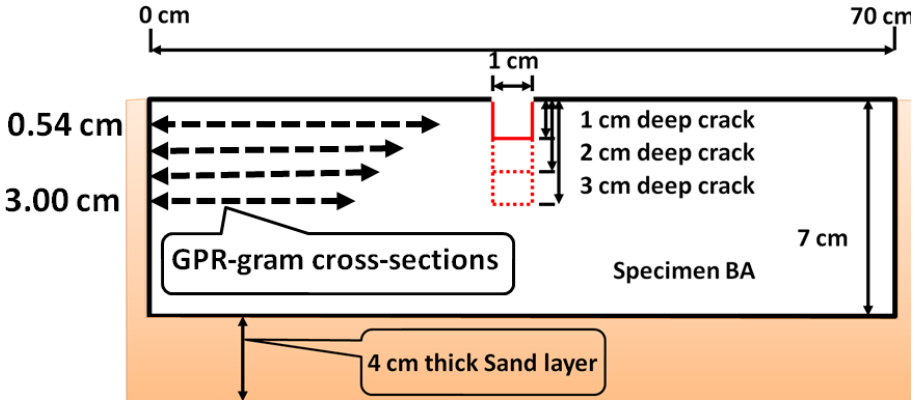

Figure 4.3. Test setup for investigation of crack depth influence on GPR-grams (specimen BA)

The processed data by GRED-3D are presented in Table 4-3. In GPR outcomes, not only crack was detected but also the boundaries of specimen were successfully differentiated from its surrounding. The GPR outcomes in first row shows specimen surface which is slightly brighter than its surrounding (sand). The specimen is darker in the GPR-grams shown in second and third row of Table 4-3 whereas the surrounding colour intensity remains same as in first row (Table 4-3). The 3-D result of 1 x 1 cm^2 crack shown in first column is same as shown in Table 4-1. The 3-D GPR-grams are taken at a cross-sectional depth of 0.54, 1.3, 2.02, 3.0 cm respectively. It can be observed in the outcomes presented in Table 4-3 that the crack detection quality is increased in case of increased crack depth. The crack detection quality of 1 x 1 cm^2 in GPR-grams decreases with increasing depth. It can also be observed that 1 x 1 cm^2 crack is not visible in GPR-gram taken at a depth of 3.0 cm.

In case of 2 cm deep crack, its intensity in GPR-grams is more compared to 1 cm deep crack starting from 0.54 to 3.0 cm cross-sections. The 2 cm deep crack boundaries have more contrast especially at 1.3 and 2 cm cross-section than 1 cm deep crack. Also at 3.0 cm depth, the intensity of 3 cm deep crack is higher than 2 cm deep crack. Although the 1 cm and 2 cm deep crack are seen at 2 and 3 cm depth due to EM wave reflections. However, it can be concluded that GPR has the ability to differentiate among different crack depths although the exact crack depth measurement by the GPR may be difficult. Also the crack detection quality in 3-D compared to 2-D is higher.

Table 4-3: Effect of crack depth increase on 3-D survey (1 cm wide crack)

Cross-section	1 cm deep crack	2 cm deep crack	3 cm deep crack
0.54 cm	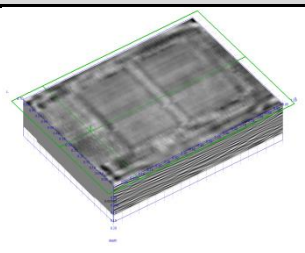	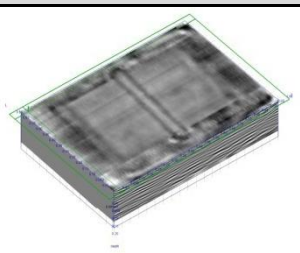	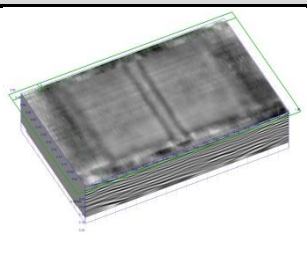
1.3cm	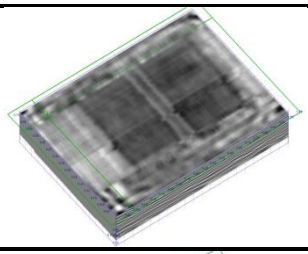	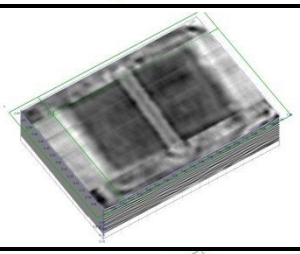	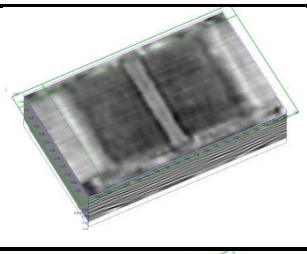
2.02 cm	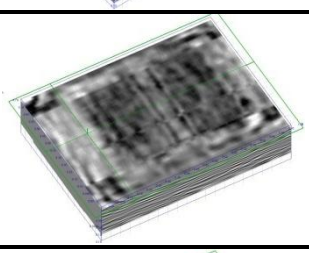	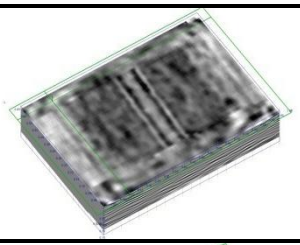	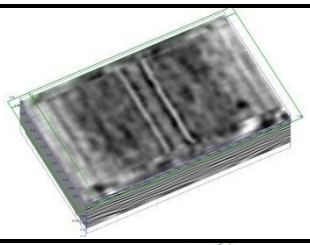
3.0 cm	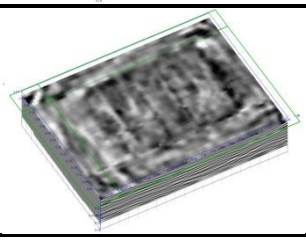	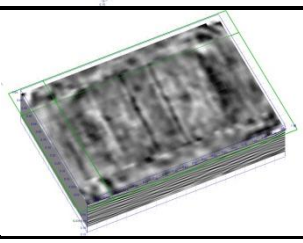	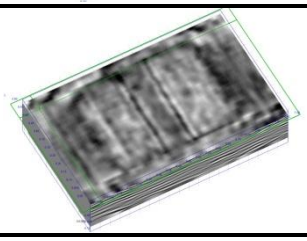

4.2.1.2 The effect of crack width

To find out the effect of crack width on the outcomes, 1, 2 and 3 cm wide cracks were investigated in specimen BA by keeping crack depth constant at 3 cm. The crack was initially 1 cm wide which was increased to 2 and then 3 cm. The investigations were carried out by Aladdin GPR system. The 2-D GPR results are provided in Table 4-4. It can be observed from the survey results (Table 4-4) that the wings of hyperbola are increasing with increase in crack width. The span of 1 cm wide crack, red arrow was taken as standard and was placed on hyperbolas of 2 and 3 cm wide crack. The difference of hyperbolas span is obvious in when 2 and 3 cm cracks hyperbolas are compared to that of 1 cm wide crack. Although scaled roughly, the 2 and 3 cm wide cracks can be successfully differentiated from 1 cm wide crack based on their relative hyperbola's wing span in the GPR-gram.
The hyperbola's wings were measured on horizontal axis. The span of 1, 2 and 3 cm wide crack's hyperbolas were 10, 17, and 18 cm respectively. The scaling of hyperbolas and the measurements are shown in Table 4-4. Compared to crack depth investigations, the crack width affect analysis results were promising. This is because 1 cm wide crack had roughly 10 cm wide hyperbola wing span in GPR-grams except for 3 cm wide crack. Despite

promising results, a definite relationship of crack width to its relative hyperbola wing span is difficult to set at this stage.

Table 4-4: Comparison of 3 cm deep crack's hyperbolas with a width of 1, 2 and 3 cm

1 cm wide crack	2 cm wide crack	3 cm wide crack
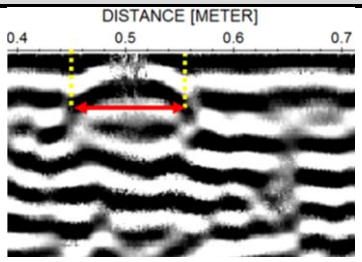	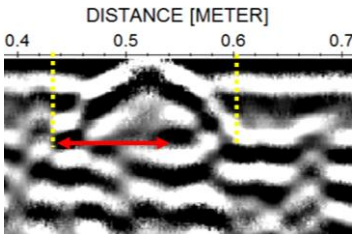	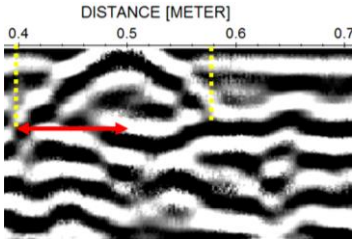

The outcomes resented in Table 4-4 were plotted and are shown in Figure 4.4. It can be seen that the crack width measurement ability of GPR is almost equally erroneous for 1 and 2 cm wide cracks whereas for the 3 cm crack width, the error is higher. This reason for this is that related hyperbolas of cracks need to be read with higher accuracy which in this case i.e. visual reading was not possible. Although the crack width and their relative hyperbola length (wing span) are not directly proportional, a relationship among these two can be formed. It is however recommended to collect more data by changing crack widths and GPR frequencies before developing a final relationship among crack depth to its relative hyperbola width in GPR-grams.

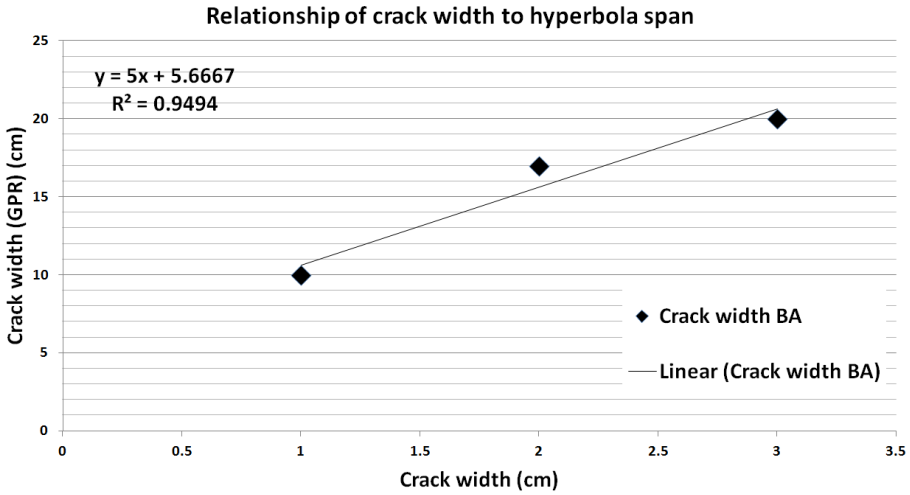

Figure 4.4. Relationship of crack width to hyperbola span/width (Specimen BA)

The same cracks of specimen BA i.e. 1, 2 and 3 cm wide were investigated by 3-D surveying. The results are provided in Table 4-5. The effect of crack width on GPR outcomes is clearer in 3-D outcomes compare to 2-D survey results. The promising 3-D survey outcomes were able to differentiate among different width cracks at crack start and then its end. The difference among 1, 2 and 3 cm crack intensity can be observed in Table

4-5 (first row) at a cross-sectional depth of 0.54. The 1 cm wide crack can hardly be seen where as 3 cm wide crack has a brighter crack structure in GPR-gram. The brightness is also gradual i.e. low for 1 cm wide crack and maximum for 3 cm wide crack. The GPR-grams at a cross-sectional depth of 2.02 cm were confusing. It was hard to differentiate among different width cracks. Nonetheless, the GPR-grams at a cross-sectional depth of 3.0 cm (Table 4-5 (third row)) were promising. The span of crack's hyperbolas was different for different width crack. The GPR-grams at 3.0 cm cross-sections were taken and stacked for 1, 2 and 3 cm crack. The results are presented in Table 4-6.

Table 4-5: Crack width effect of a 3 cm deep crack on 3-D GPR-grams (specimen BA)

Cross-sectional depth	1 cm wide crack	2 cm wide crack	3 cm wide crack
0.54 cm	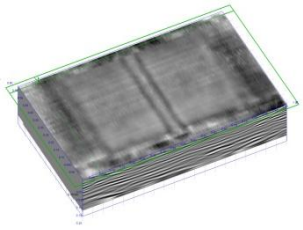	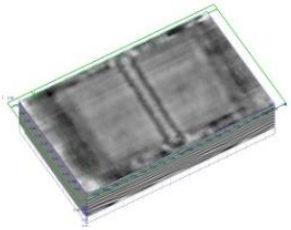	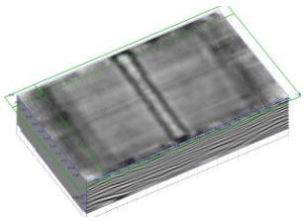
2.02 cm	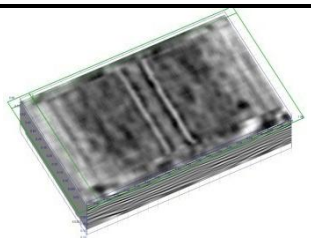	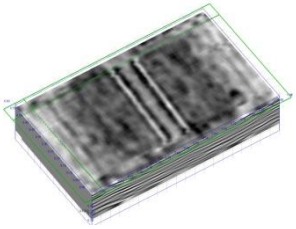	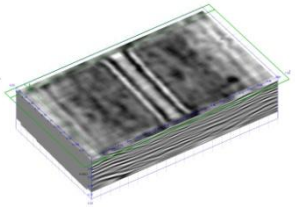
3.0 cm	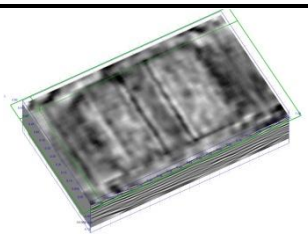	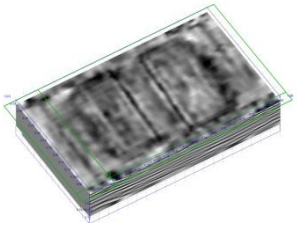	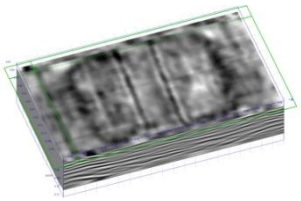

For the comparison of crack, the span of 1 cm wide crack (Table 4-5 (third row-first column) was taken as reference (yellow arrow) and was placed on other two cracks. The change can be expressed in cm by reading the horizontal distance in the GPR-gram. The difference in cracks compared to 1 cm wide crack is highlighted in red lines. Although it is difficult to relate the hyperbola characteristics to that of crack width, it is interesting that wider cracks can be distinguished in the GPR data.

Table 4-6: Measuring crack width by 3-D GPR survey at cross-sectional depth = 3.0 cm

1 cm wide crack	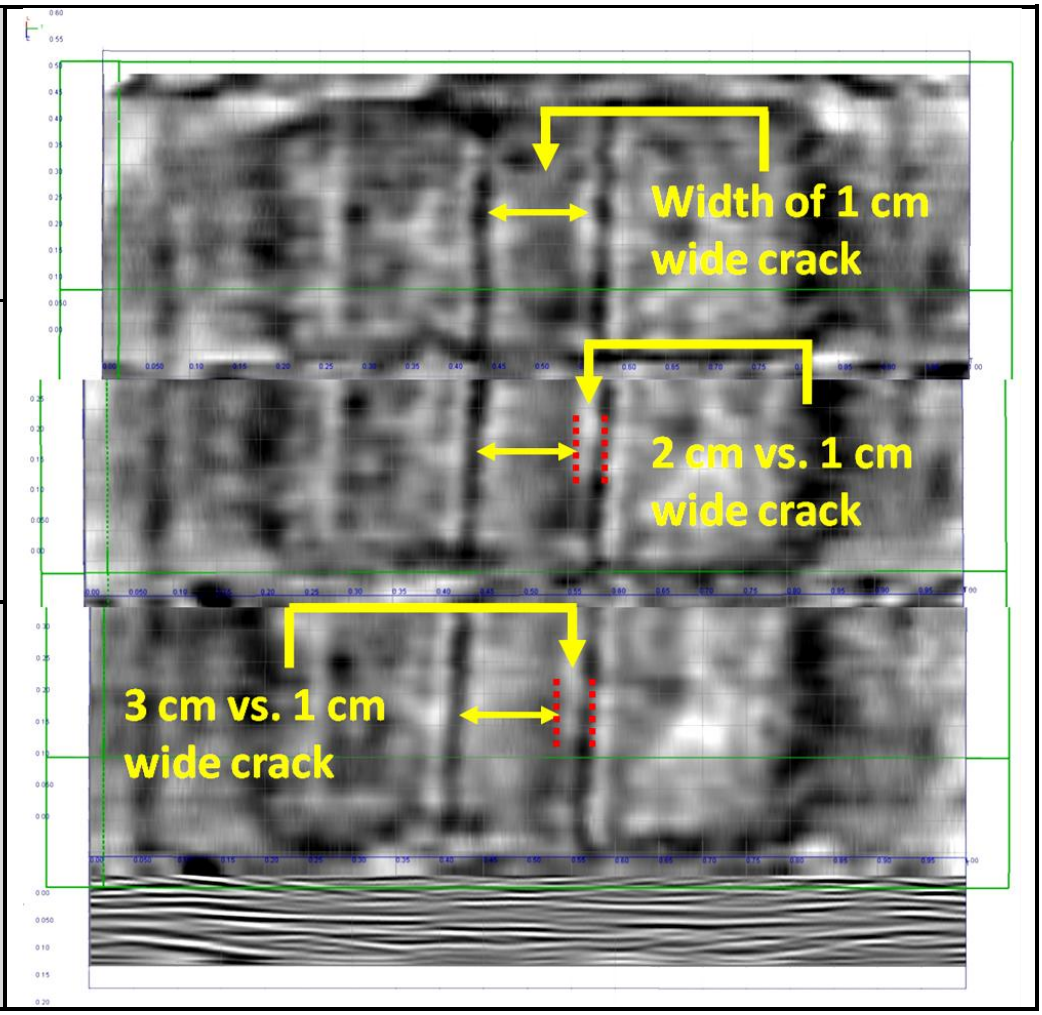
2 cm wide crack	
3 cm wide crack	

4.2.2 The effect of crack type (bottom-up cracking)

The cracks detected in Section 4.2.1 were top-down cracks. To investigate whether GPR is equally useful in case of bottom-up crack detection, bottom up cracks in asphalt specimens were analysed. The test setup for the bottom-up cracking was simulated in laboratory by inverting the specimens with cracks. The tests were conducted with Aladdin system only. The hardware and software configuration were kept constant for all the tests on each specimen, i.e. specimens "BA" and "BB". The field testing regarding bottom-up cracking was not conduced due to technical limitations. The test setup and outcomes are provided in the following sections.

- The specimens “BA”

The two “BA” specimens were tested for bottom-up crack detection. The cracks grooved were of different width and depth to find the crack detection limitations. The specimens were laid on a 12 cm thick sand layer, as shown in Figure 4.5. The sand layer was provided to damp the EM waves as otherwise scattering of waves was making it difficult to analyse the outcomes. The 2-D and later on 3-D survey was conducted on the same setup shown in Figure 4.5(bottom).

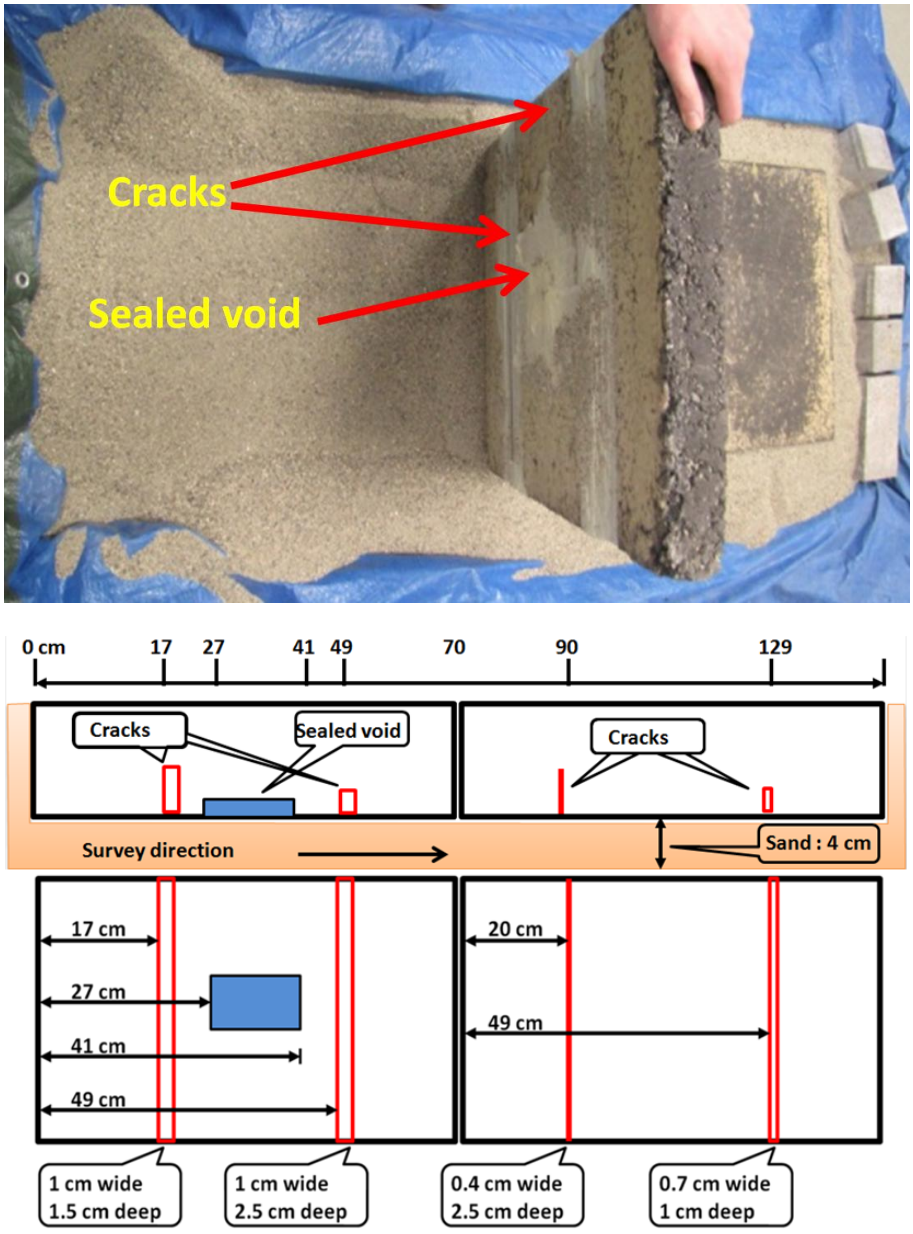

Figure 4.5. Bottom-up crack investigation, (top) two “BA” specimen with sealed cracks inverted on sand, (bottom) the test setup

The test outcomes are presented in Figure 4.6. The GPR could successfully detect the cracks in both specimens together with the rectangular void in the first specimen. In Figure 4.6(top), the GPR-gram is showing crack hyperbolas encircled in yellow and specimen

boundaries in red dashed line. The first two cracks shown in the GPR-gram in Figure 4.6(top) had a slight difference in hyperbola which is due to the crack geometry i.e. same width but different crack depths. The first crack with more crack volume has a stronger hyperbola compared to the second crack in the same specimen. Similarly, the third crack (second specimen) has a hardly seen weak hyperbola compared to the cracks in first specimen. This is because the third crack has lesser volume than first two cracks (first specimens). As the third crack with 0.4 x 2.5 cm^2 dimensions had a stronger hyperbola than the fourth crack with 0.7 x 1.5 cm^2 dimensions, it supports the argument that crack volume plays an important role in crack detection. For the further analysis for crack four, it was decided to analyse the data by f-k filtering technique. The results are shown in Figure 4.6(bottom).

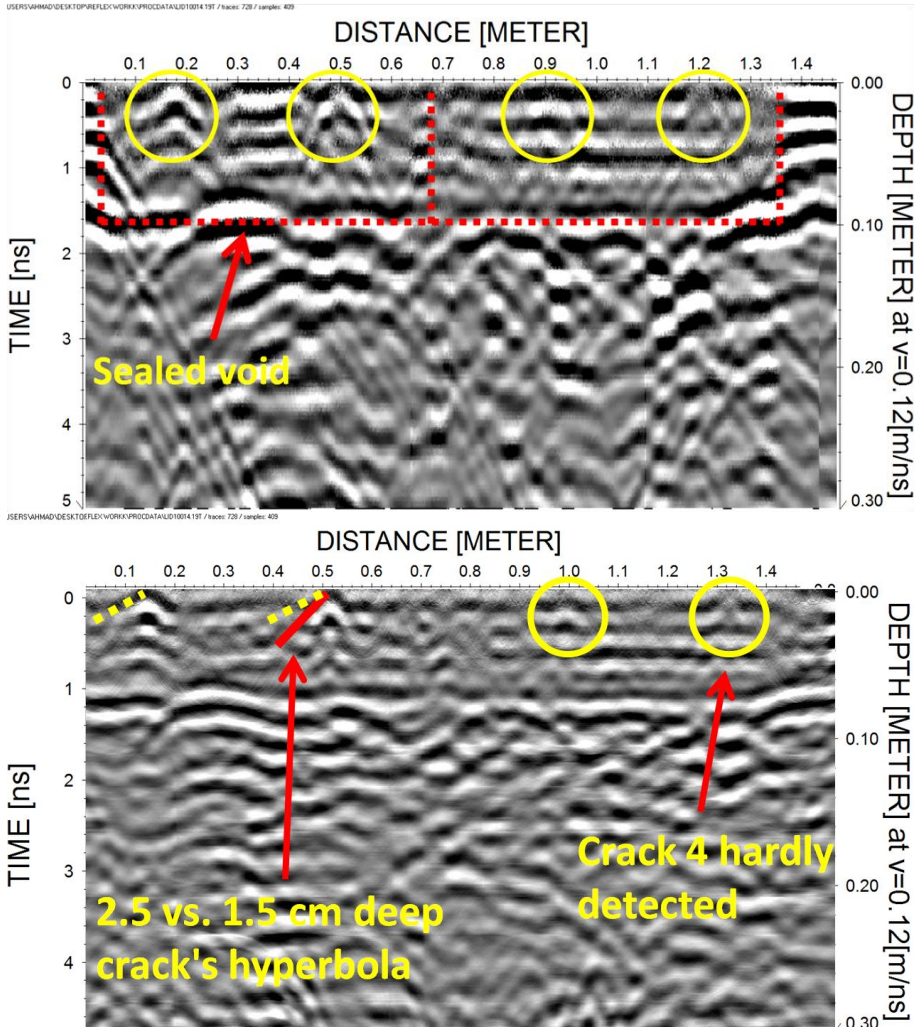

Figure 4.6. The 2-D outcomes of bottom-up crack investigations, (top) the 2-D results by standard processing, (bottom) the f-k filtering results

The f-k filtering of the same data helped concise the crack's hyperbolas and hence the cracks can be differentiated clearly. The first two cracks in specimen with 1 cm width but with 2.5 cm and 1.5 cm depth have stronger hyperbolas compared to the cracks in second specimen. The intensity of cracks hyperbolas can be measured by the spread of hyperbola

wings. In case of 2.5 cm deep crack (first specimen) the hyperbola wings are spreading with a wide angle compared to 1.5 cm deep crack (first specimen). The spread of first crack is marked by yellow line and is placed on second crack whose hyperbola is marked in red. The obvious difference in hyperbolas of two same width but different depth cracks confirms that crack geometry as a whole plays a vital role in crack detection.

The two cracks in the second specimen encircled in yellow, can also be differentiated in the GPR-grams based on their crack volume. The 2.5 cm deep crack hyperbola is concentrated at the crack bottom whereas the hyperbola of 1 cm deep crack is hardly seen. Also the first crack (second specimen) with 0.4 x 2.5 cm^2 dimensions have more volume than 0.7 x 1 cm^2 crack and therefore, the crack detection quality of first crack (second specimen) is improved.

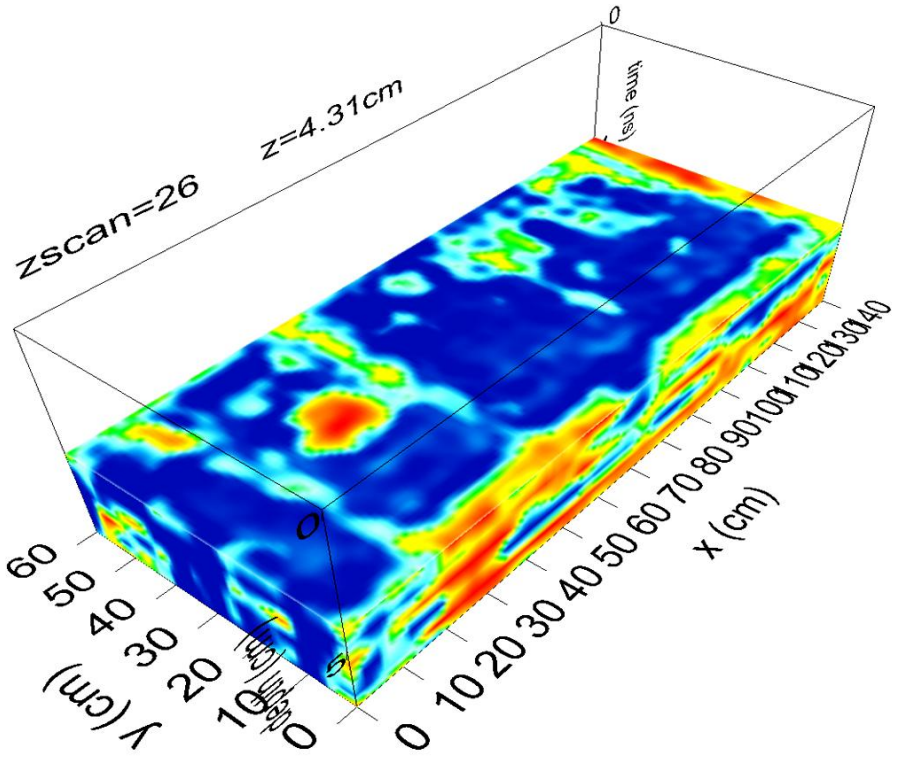

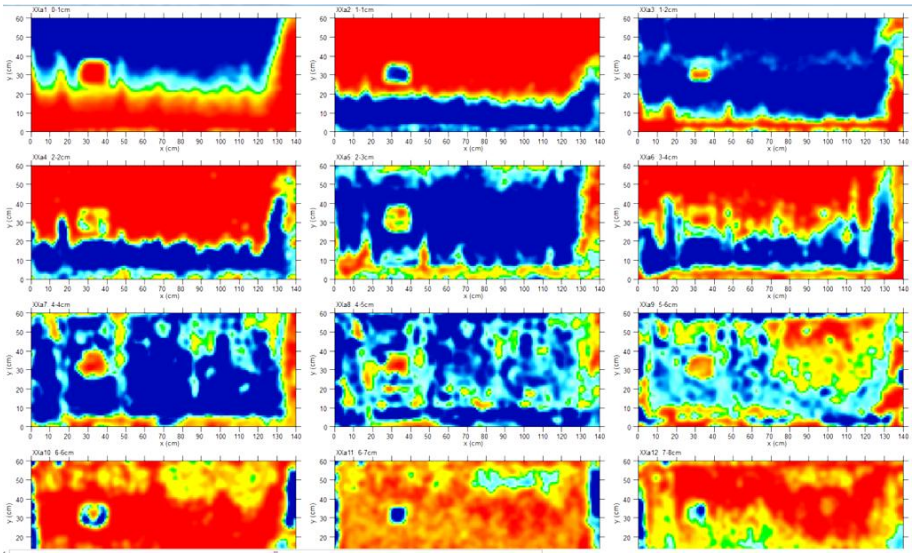

Figure 4.7. The 3-D results of bottom-up crack investigation: Software: GPR-SLICE, (a) the 3-D GPR results (b) the slices from 3-D cube

For the processing of 3-D collected data, the GPR-SLICE and GRED-3D software were used. The 3-D results helped slice the 3-D GPR-gram and investigate if crack hyperbolas have a relation to crack location and its geometry. The results are presented in Figure 4.7. The 3-D cube in Figure 4.7(top) is showing cross-section at 4.3 cm depth where three cracks are visible together with the void in first specimen. The 3-D results of survey were sliced and each slice was observed with respect to its depth. The slices are shown in Figure 4.7(bottom). It can be seen that the cracks are not visible at top of specimens so that they are starting to appear at a depth of 2-3 cm (5th slide). In the 6th slide, the fourth crack (second crack in second specimen) appears at a depth of 3-4 cm. All the cracks can be well seen in the 7th slide. As the dielectric constant was estimated, the depth of crack location is approximated. Extraordinary (Figure 4.7(bottom)) is the void detection which can be seen in the first slide (at surface) whereas the cracks are not detected. The cracks start to appear in the third slide at a depth of 1 to 2 cm. The third crack is detected in slide 6 at a depth of 3 to 4 cm. The fourth crack was however, not detected. Moreover, all the cracks vanish in slide number 9 at a depth of 5 to 6 cm. The approximation of depth was a limitation of software.

To enhance data authenticity, the same data was processed with GRED-3D software. Therefore, the outcomes x and y-axis are not clear. The results are presented in Figure 4.8. The processing with GRED-3D software helped locate crack 1 and 2 at a depth of 2.5 cm and finally crack 3 and 4 at a depth of 3.5 cm. The unclear was the equal intensity of crack 3 and 4 in the GPR-gram at depth of 3.5 cm, despite having different crack depth. This was not however the case when 3-D results were processed with GPR-SLICE software. In Figure 4.7(bottom) the slice number 7 shows crack 1 and 2 whereas crack 3 with a less intensity. The crack 4 cannot be seen anymore contrary to results of GRED-3D.

For the further investigation regarding bottom-up cracking, it was decided to go for a thicker specimen with increased crack volume compared to specimens BA. Furthermore, presence of many cracks in GPR-gram was making it complicated for processing. Therefore, specimen BB with a single crack was considered for further testing.

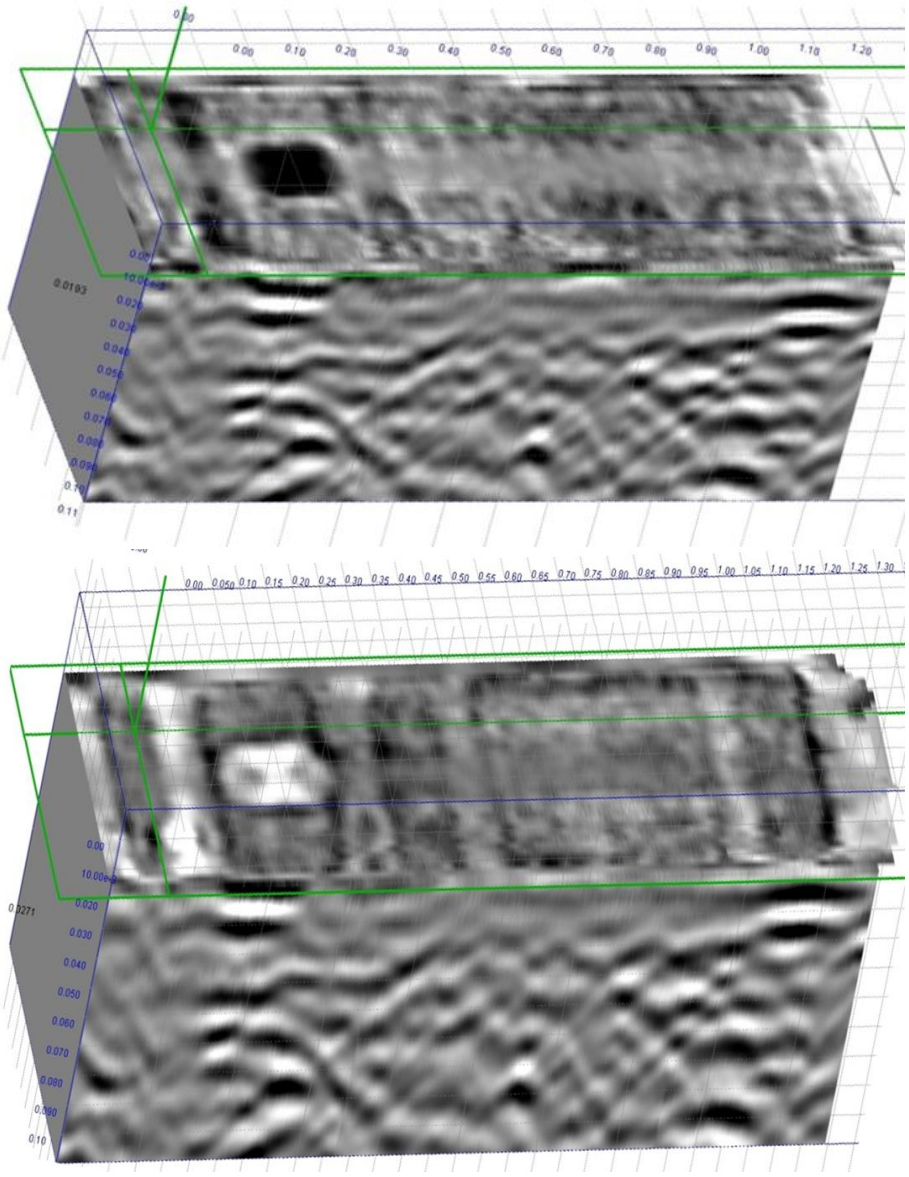

Figure 4.8. The 3-D results of bottom-up crack investigation: Software: GRED-3D, (a) cross-section at 2.5 cm depth (b) cross-section at 3.5 cm depth

- The specimen “BB”

The specimen “BB” was inverted on a 4 cm thick layer to simulate bottom-up cracking. The crack was sealed with dry paper to prevent the intrusion of sand in the crack. The 2-D

and 3-D survey types were carried out on this specimen. The antenna configuration was set to 8 ns time window, 512 samples per scan and a 0.00202 m pulse transmission distance. The test outcomes are provided below.

The 2-D survey data was processed with software GRED-3D. The bottom-up cracks was successfully detected in the GPR-gram. The result is shown in Table 4-7 (first row). This time not only the crack hyperbola was clear, compared to past investigations but with little processing efforts the crack dimensions could also be detected. The crack's location in the GPR-gram is marked together with the geometry of specimen in Table 4-7.

For the first time in bottom-up crack investigations, the crack hyperbola is not at the specimen's surface. The hyperbola is starting from the crack's end. Also the hyperbola's wings are ending at the bottom of the specimens (or the start of crack). Thus it was verified that GPR can not only detect bottom-up crack but also its location in the asphalt structure.

Due to data processing limitations in GRED-3D, same data (LID100025) was processed with ReflexW software. The processed outcome is shown in second row of Table 4-7.

The processed data by ReflexW software Table 4-7 (second row) was promising. Not only the crack in the GPR-gram was detected with high quality but borders of the specimen "BB" were also successfully detected. In the next stage, 3-D survey was carried out to investigate deeper GPR abilities for detecting bottom-up cracking.

The 3-D data was processed by GRED-3D software. The crack was again detected successfully in 3-D data. The results are provided in Table 4-8. The crack dimensions were this time detected with more accuracy. It can be seen that at a depth of ≈7 cm, the crack cannot be seen in GPR-gram (Table 4-8). However, crack starts appearing at a depth of ≈10 cm which is actually the start of crack in the specimen (bottom of crack in the specimen). At a depth of ≈17 cm the crack intensity (hyperbola) is at its peak. However, at depth of ≈20 cm, the crack vanishes from GPR-gram which is actually the bottom of crack too.

Table 4-7. The bottom-up crack detection in "BB" (GRED-3D and ReflexW)

Data: LID100025
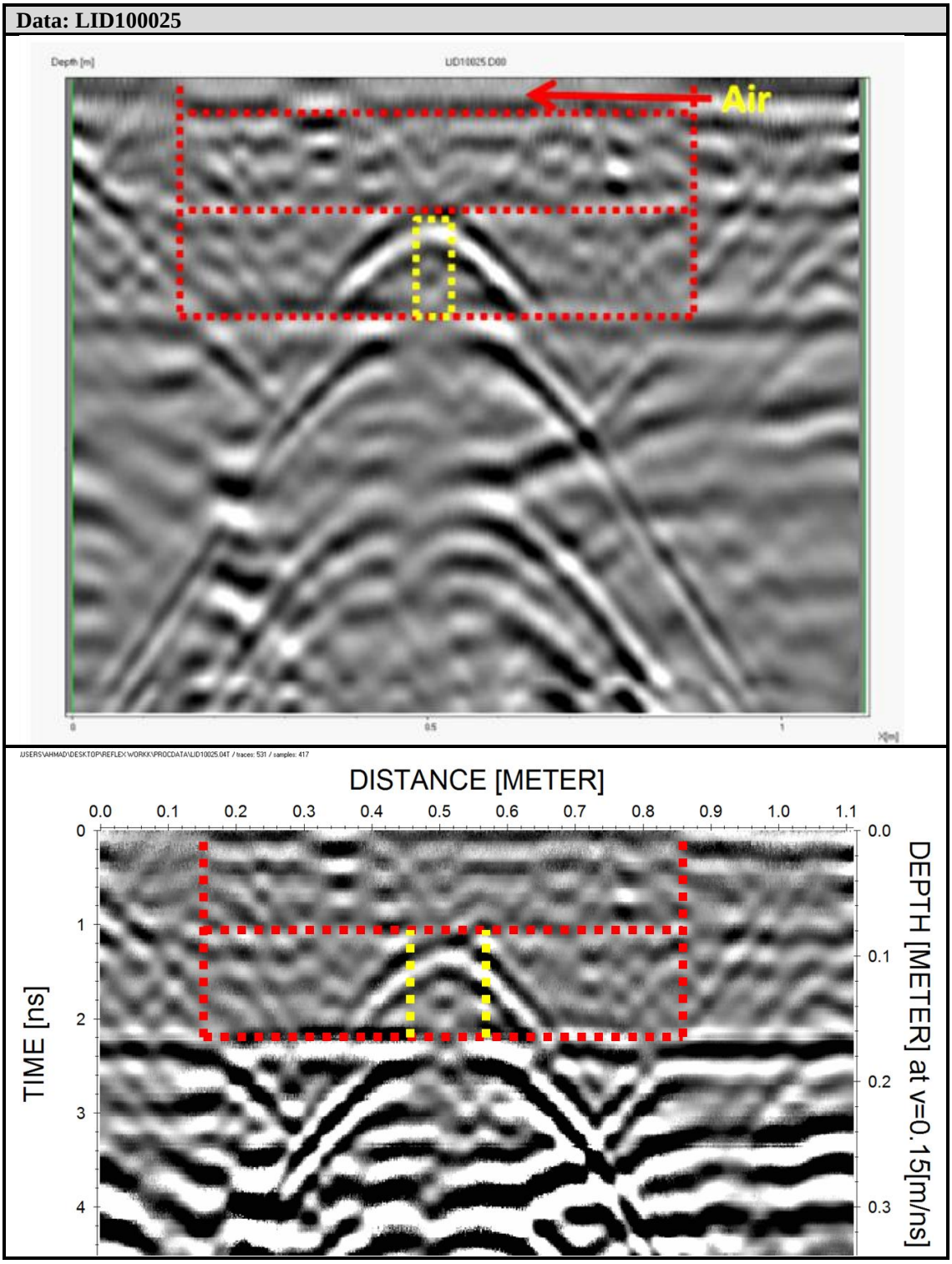

The specimens can be differentiated by their colours in the GPR-grams. At a depth of ≈10 cm, the specimen's colour is different from what is seen in at ≈7 cm depth. At 10 cm was actually the interface of jointed asphalt specimens in Specimen BB. The same difference in colours can be marked between GPR-grams at a depth of 15 cm (when EM waves are still in specimen) and 18 cm when sand layer starts. Thus the 3-D results were promising in

regard of bottom-up crack detection and its location investigation. The crack width measurement was however, not possible.

Table 4-8: Bottom-up crack detection in specimen BB by 3-D survey (Software: GRED-3D)

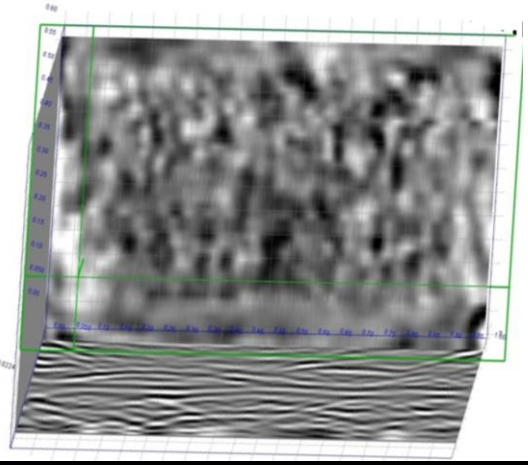	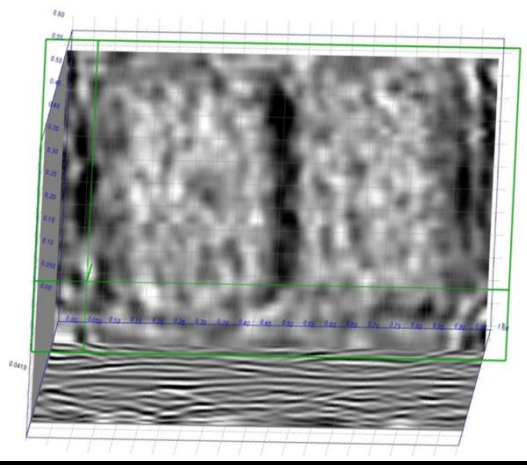
At 7 cm cross-sectional depth	At 10 cm cross-sectional depth
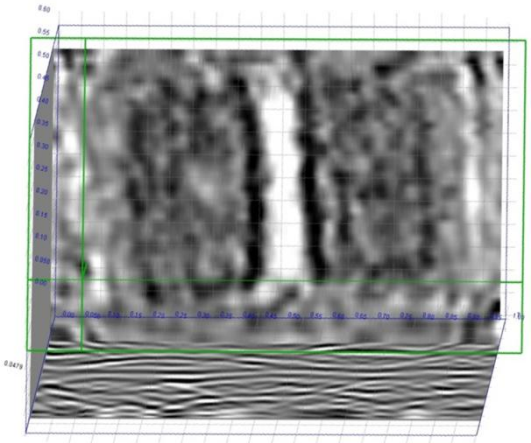	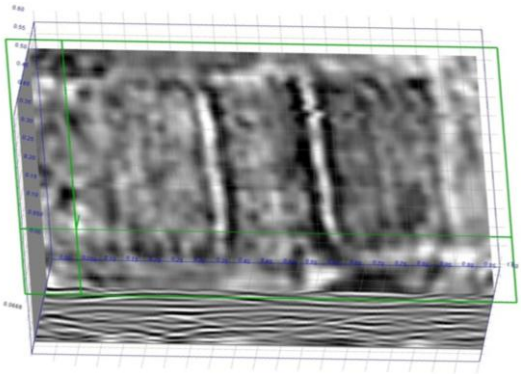
At 17 cm cross-sectional depth	At 20 cm cross-sectional depth

4.2.3 Effect of crack fill

To find out the effect of crack fill on GPR results, specimens "AH" and "BB" were considered. Initially, the specimen "AH" was tested with Groundvue 3 and finally specimen "BB" was investigated with Aladdin GPR system. For the comparison of tests, the data processing steps and their extent was kept constant in case of Aladdin GPR survey. The test setup for specimen AH is shown in Figure 4.9(a) whereas the outcomes are shown in Figure 4.9 (b and c). The specimen was place in open air on a wooden bench. At the first stage, the four cracks of Specimen AH were tested with air as crack fill medium. All four cracks are detected however; the 1 cm deep crack can hardly be seen in GPR-gram presented in Figure 4.9(b). Despite that, the cracks can be differentiated from one another in the GPR-grams, based on their respective hyperbolas strength.

To check the influence of crack fill on crack detection, a metal wire was placed in cracks. The properties of GPR equipment (antenna configuration) were kept the same as were in

case of air as crack fill medium (Figure 4.9(b)). The results of crack detection with wire are given in Figure 4.9(c). It can be seen in GPR-gram (Figure 4.9(c)) that the crack hyperbolas are clearer compared to the air filled cracks. The influence of metal compared to air as a crack fill medium resulted in stronger hyperbolas with large spans. The 1 cm deep crack is also clearer in these outcomes. Although the effect of crack fill material was justified for crack detection, it was decided to check outcomes by testing further materials as crack fill. As the cracks in specimen AH had limited width which was not suitable to be used for crack fill investigations, specimen BB was used for further testing.

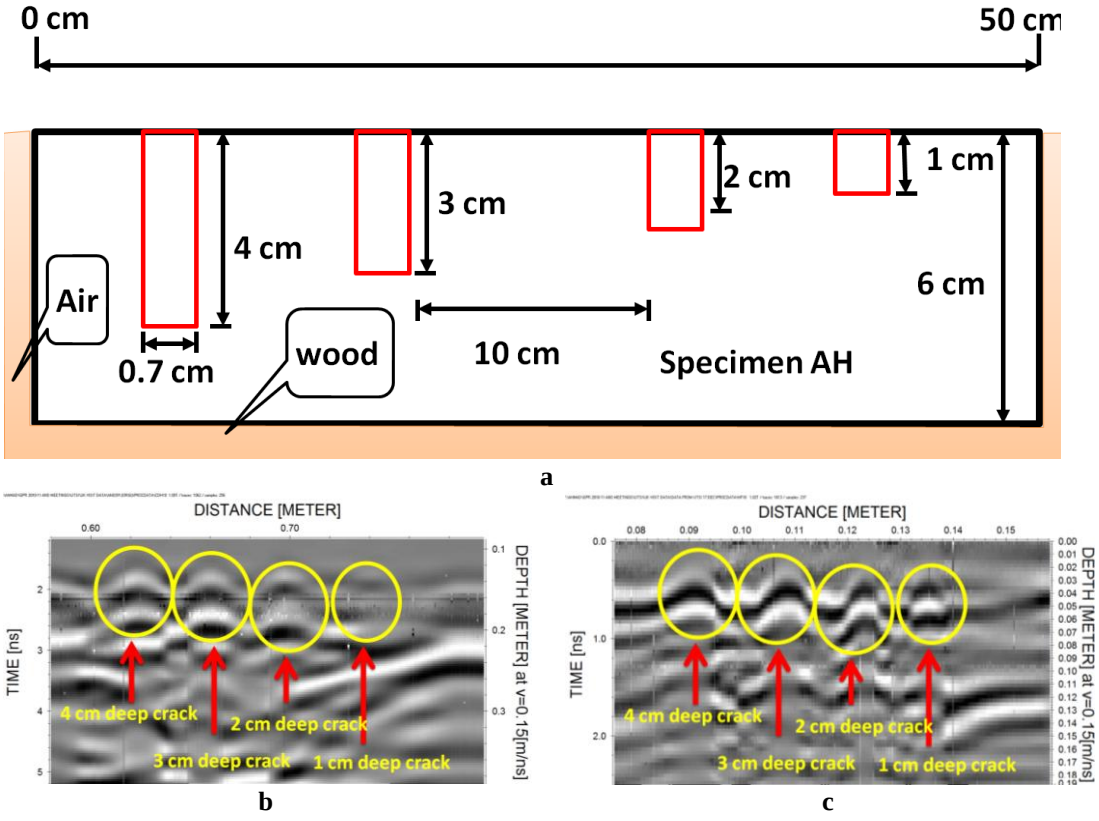

Figure 4.9. Crack detection in specimen AH (a) test setup, (b) air as crack fill medium and, (c) metal wire as crack fill medium (GPR-grams not to scale - System= Groundvue 3, Software = ReflexW)

The crack fills used in Specimen "BB" were air, sand and water. The reason to choose air, sand and water as crack fill was that these are the common crack fills found in nature on asphalt pavement. The 2-D and 3-D survey techniques with Aladdin GPR system were carried out on Specimen BB. The system configuration was 512 samples per scan, 0.02 meter scan distance and 8 ns travel time window. The data was standard processed by ReflexW software for 2-D survey and GRED-3D for 3-D survey. The test setup is shown in Figure 4.10.

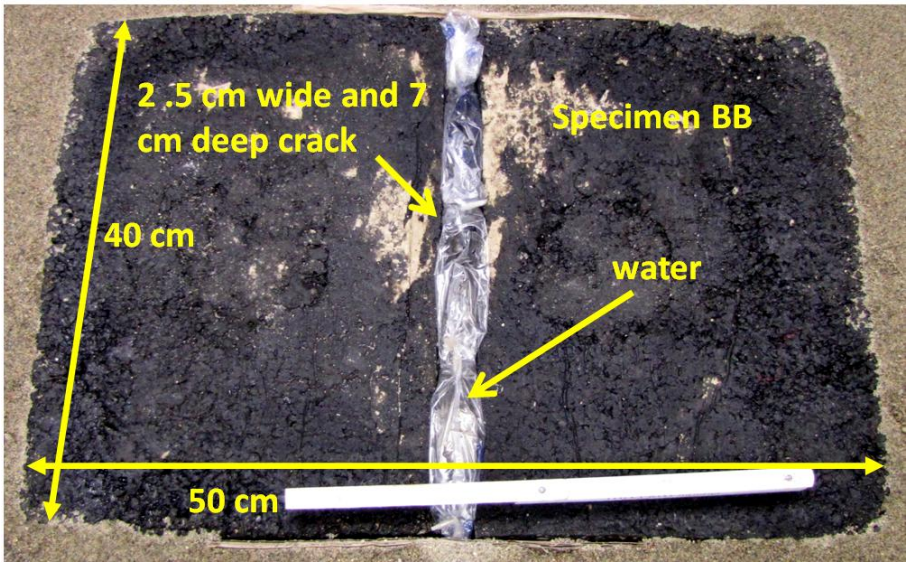

Figure 4.10. Test setup regarding crack fill investigations on Specimen BB

The 2-D results presented in Table 4-9 were promising. The crack was detected in all three cases of crack filling materials i.e. air, sand and water. The outcomes in case of air are shown in Table 4-9 (first row). The crack hyperbola is visible in GPR-gram and is encircled in yellow. Together with crack, the boundaries of the specimen and test setup base were also detected by the GPR. Moreover, the crack bottom could be clearly identified in case of air and water as crack filling mediums (Table 4-9) except in case of sand, where the crack is less clear and crack bottom could not be identified.

In case of sand, the hyperbola shown in second row of Table 4-9 is weaker than that of air. This is because the difference in dielectric constant values for asphalt and sand is smaller than that of air and asphalt (Table 2-1). Therefore, the crack bottom hyperbola cannot be seen whereas the specimen bottom is clear.

In the last stage, water was used as crack fill medium. The finding is presented in the third row of Table 4-9. This time not only the crack was detected but also the hyperbola intensity was higher together with spread wings (marked red), compared to previous results. However, the crack bottom could not be detected. The water influenced GPR results and reflections continued till the bottom of GPR-gram. The effect of water in GPR-gram is highlighted with red arrows.

Table 4-9: Crack filling medium effect on crack detection quality (specimen "BB")

Air	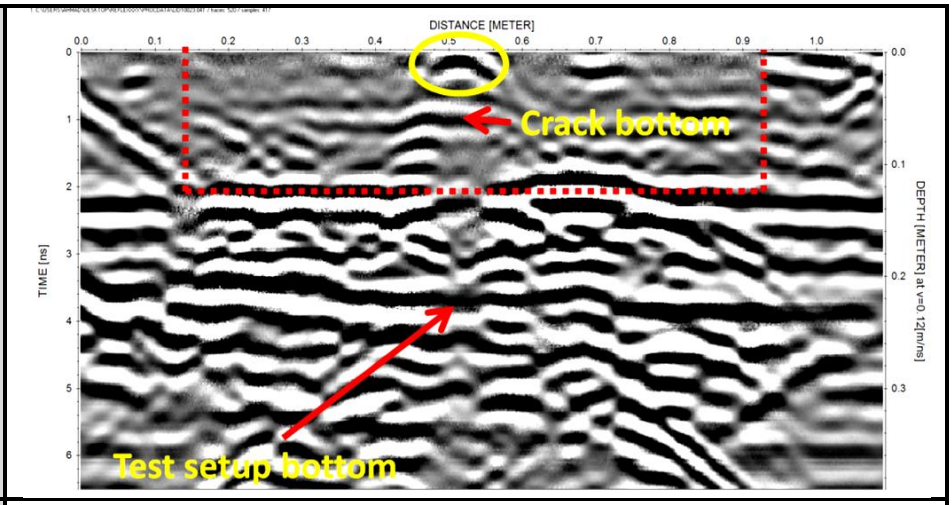
Sand	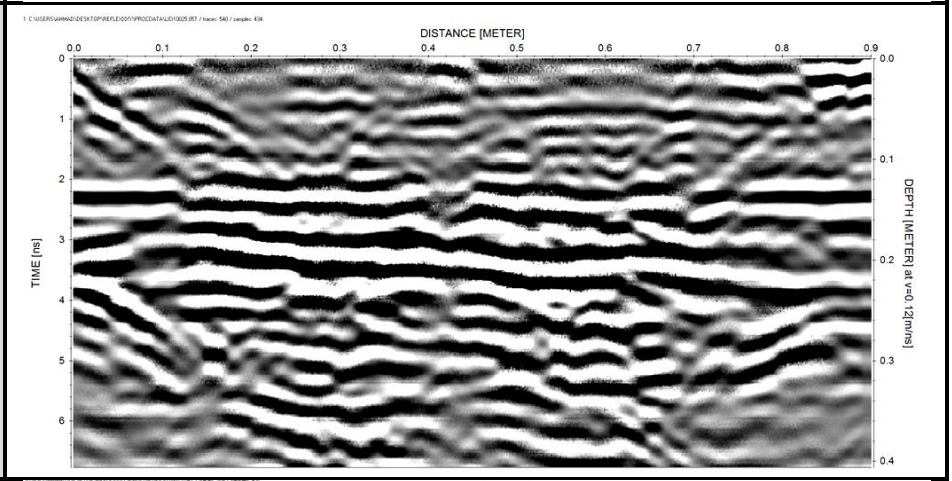
Water	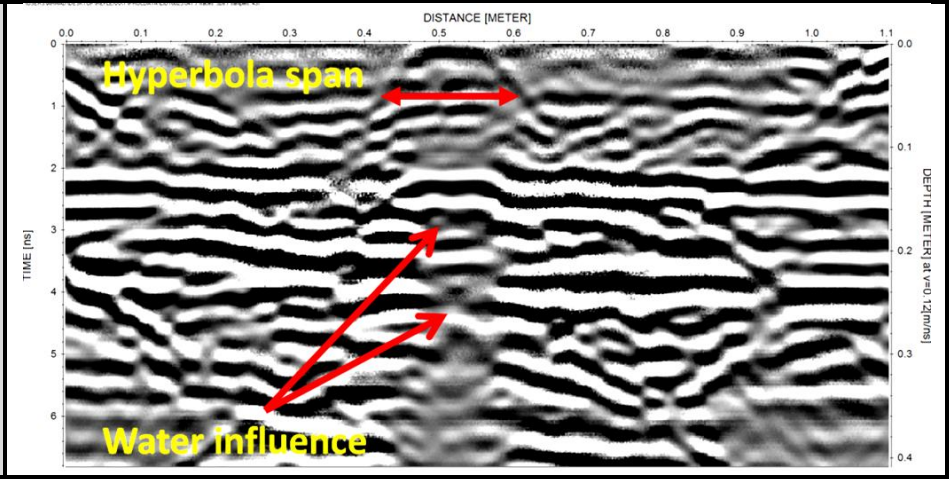

To validate the 2-D survey results (Table 4-9), 3-D survey was carried out. The test setup is shown in Figure 4.10 whereas the outcomes are provided in Table 4-10. In 3-D outcomes, not only the crack was detected but also its start and end location could be marked. The difference between air, sand and water as crack fill can easily be marked. Again the results of air as crack filling material were outstanding and sand the least. In Table 4-10, all three crack filling materials i.e. air, sand and water are compared on the same cross-sectional

depth. Due to higher dielectric constant of water, the EM wave's maximum energy was reflected at the top. Thus water influences greatly when compared to sand and water.

Table 4-10: The crack fill effect on crack detection (depth = 0.7, 3.5, 7.0 cm)

Cross-sectional depth	Air	Sand	Water
0.7 cm	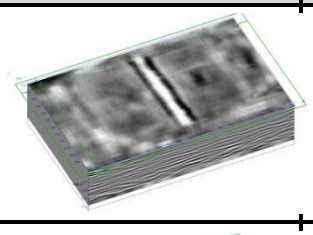	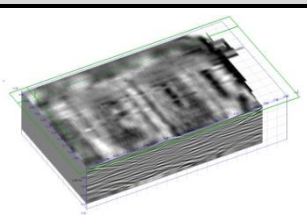	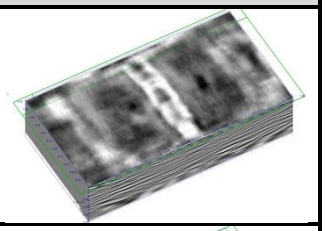
3.5 cm	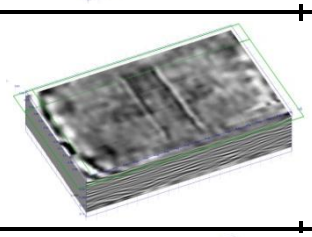	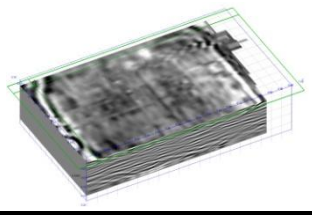	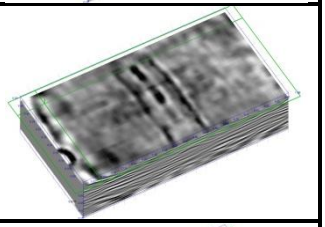
7 cm	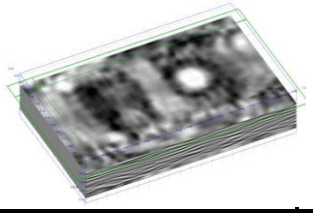	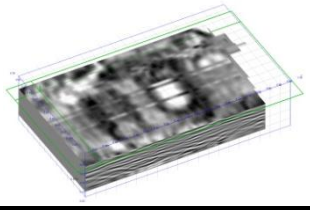	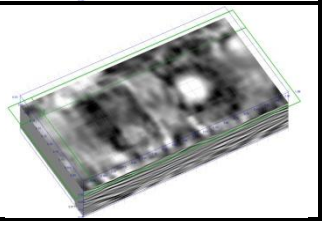

The results at a cross-sectional depth of 0.7 cm (Table 4-10(1st row)) shows crack top. In case of air as crack filing material, the crack is vivid in GPR-outcomes (Table 4-10(1st row-first column)). In case of sand, the crack is hardly seen, as was the case in 2-D surveys. In case of water, the crack is spread irregularly. At 3.5 cm cross-sectional depth, the crack geometry is close to reality in case of air whereas in case of sand, it is hardly seen and in case of water it is wider and irregular.

In case of air, at cross-sectional depth of 7 cm, the crack bottom is clear which is different in colour then that of 3.5 cm cross-sectional depth result. Also the circular void in top specimen is obvious, showing bottom of specimen and end of crack. However, in case of sand, the crack is darker and has narrow width compared to that of air (Table 4-10(third row-second column)). In case of water, though the crack is clear, it has a non-realistic width. Thus it is proved that air as crack filling material gives the best results, sand average whereas water the least. Also water influences a large area which can lead to misconceptions.

4.2.4 Effect of temperature

To investigate the influence of temperature on crack detection, tests were carried out over a year span. The cracks at 55 m location on Site C were monitored in four seasons. The widths of cracks were measured regularly to find out in which season the cracks have their

maximum width. This is because the positive influence of crack width was already investigated. The comparison of cracks in summer and winter is provided in Figure 4.11.

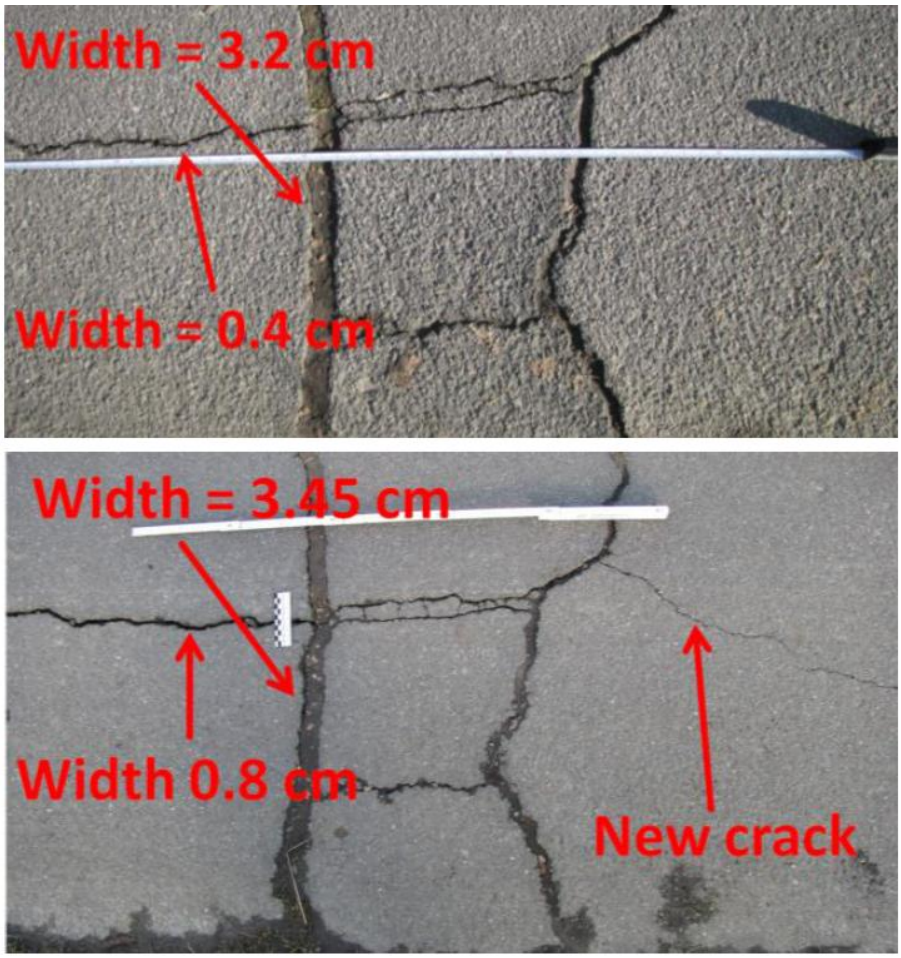

Figure 4.11. Crack width variation monitoring at Site "C" (top) cracks width on November 8th, 2011 (8° C) and, (bottom) cracks width on 26th January, 2012 (-12° C)

The regular crack monitoring on Site "C" revealed that the cracks have their maximum width in winter season. Not only the width of crack has increased at low temperature but also a new crack was observed on the locations. Based on monitoring outcomes, it was concluded that the optimum temperature for crack detection survey is the lowest possible temperature. The GPR investigations however, revealed opposite to this conclusion.

The tests were conducted on Site "C". On Site "C", cracks at location 36.95 m, 42.78 m and 46.01 m were selected for GPR testing. The pavement dielectric constant value was calculated as 2.14 in summer (16° C) and 3.0 in winter (-12° C). It was assumed that the dielectric value of crack fill also increases with decrease in temperature. The effect of temperature on the crack fill was however not verified due to limited amount of crack fill. The tests were carried out with Aladdin system.

The crack detection quality in GPR-grams is categorised based on assigning grades according to the quality of crack detection. The grades are from 0 to 5 where 0 means not at all detected (cannot be seen in GPR graphs) and 5 means clearly detected. For example, grades 2, 3 and 4 are shown in Figure 4.12. Three pavement cracks at 36.95, 42.78 and

46.10 m distance encircled in red were selected for reference. The crack assigned grade 4 in GPR diagram is visible and clearer than crack graded as 2 (Figure 4.12).

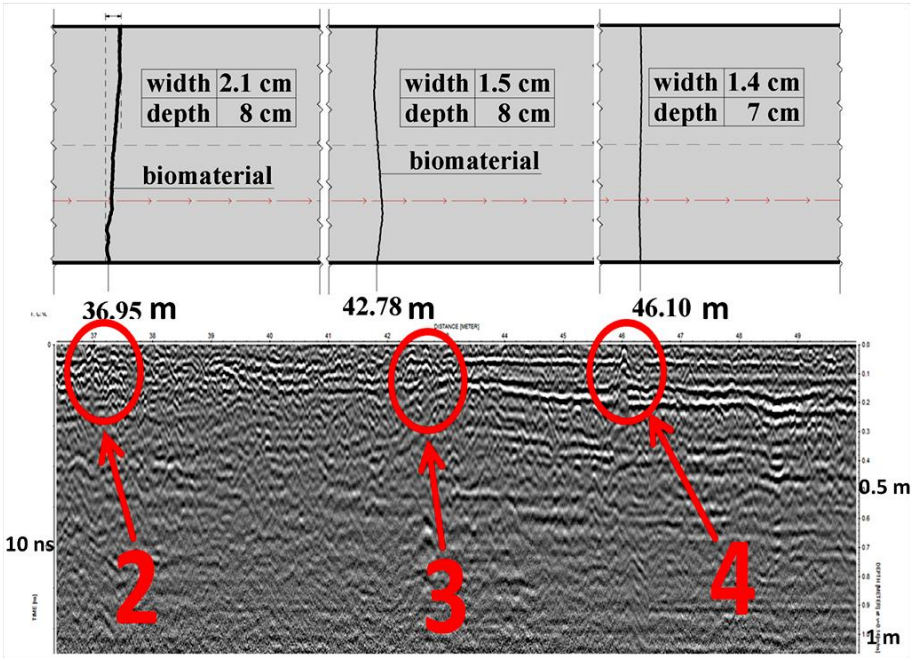

Figure 4.12. Grades assigned to crack detection quality on Site "C"

The GPR surveys were conducted at temperatures of 16° C, 4° C, -6° C and -12° C. The survey was carried out with 512 samples per scan, 4 mm EM pulse repetition distance between horizontal profiles and with 32 ns time travel.

The results of temperate effect are provided in Figure 4.13. It can be observed that the crack detection quality is increasing with increase in temperature. Most of the cracks on the tests section were detected while survey at 16° C. The 4° C survey results are also acceptable as compared to -6° C and -12° C survey results. Some cracks were even not detected during -12° C survey. Thus, cold weather, specially freezing temperatures are not recommended for crack detection survey with GPR. The laboratory tests regarding temperature influence on GPR outcomes were however, not conducted due to technical limitations.

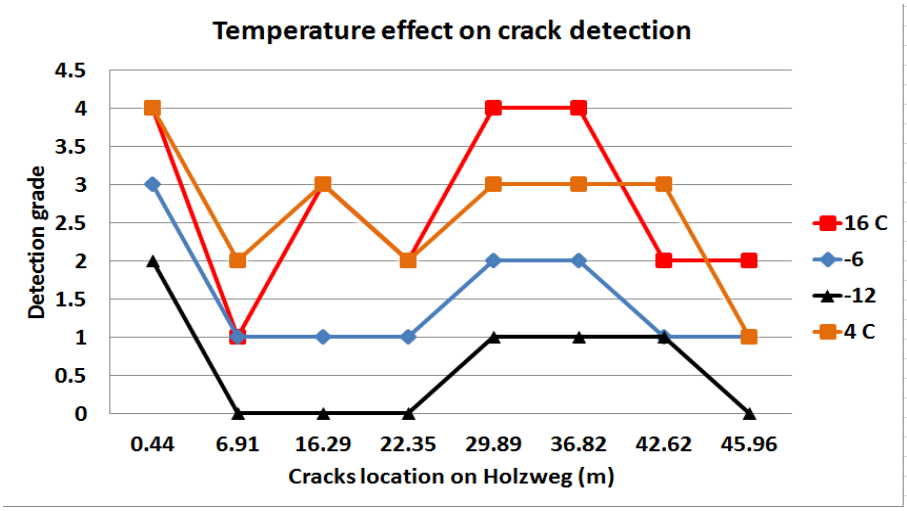

Figure 4.13. Effect of temperature on crack detection

4.3 Effect of GPR system

Due to different sophisticated techniques involved in GPR functioning, their effect on crack detection might be an issue. A 2 GHz central frequency antenna from one company may not be equal to the same frequency antenna from another company. Therefore, in this section, the influences of GPR system hardware characteristics including its antenna type, polarization, frequency and bandwidth on survey are investigated.

4.3.1 The influence of GPR transmission technique

For investigation of transmission technique, the crack at 46 meter location (Site C) was selected for investigation. The crack properties are provided in Table 3-14 and Figure 3.19. For the investigation of hardware influence on GPR outcomes, GeoScope and Aladdin GPR systems were selected. The reason for selecting these systems was based on their EM wave transmission techniques i.e. impulse and CW. The 3-D survey results were compared. The data from GeoScope was processed by its system integrated software whereas Aladdin data was processed by GPR-SLICE. The laboratory specimens could not be tested in regard of transmission technique due to bigger antenna size of in hand GeoScope (2.5 m) system.
The outcomes of tests results from GeoScope are shown in Figure 4.14. From analysed data, it was possible to locate start of the crack at pavement surface (0 m) by discontinuity in wearing course and a weak hyperbola. Also its vertical path inside pavement structure is obvious. Hence it was possible to evaluate crack from different depths. The GeoScope GPR-gram shown in Figure 4.14(top) is pavement cross-sectional view in the direction of travel. The crack path is marked in yellow whereas the pavement layers are also labelled. The red-line in GPR-gram shows pavement surface (0 m depth) whereas the blue line indicates point of measurements. It can also be seen that (Figure 4.14(top)) a layer with bright colours is recorded in GPR-grams. This was later discovered as an old asphalt layer from core samples.

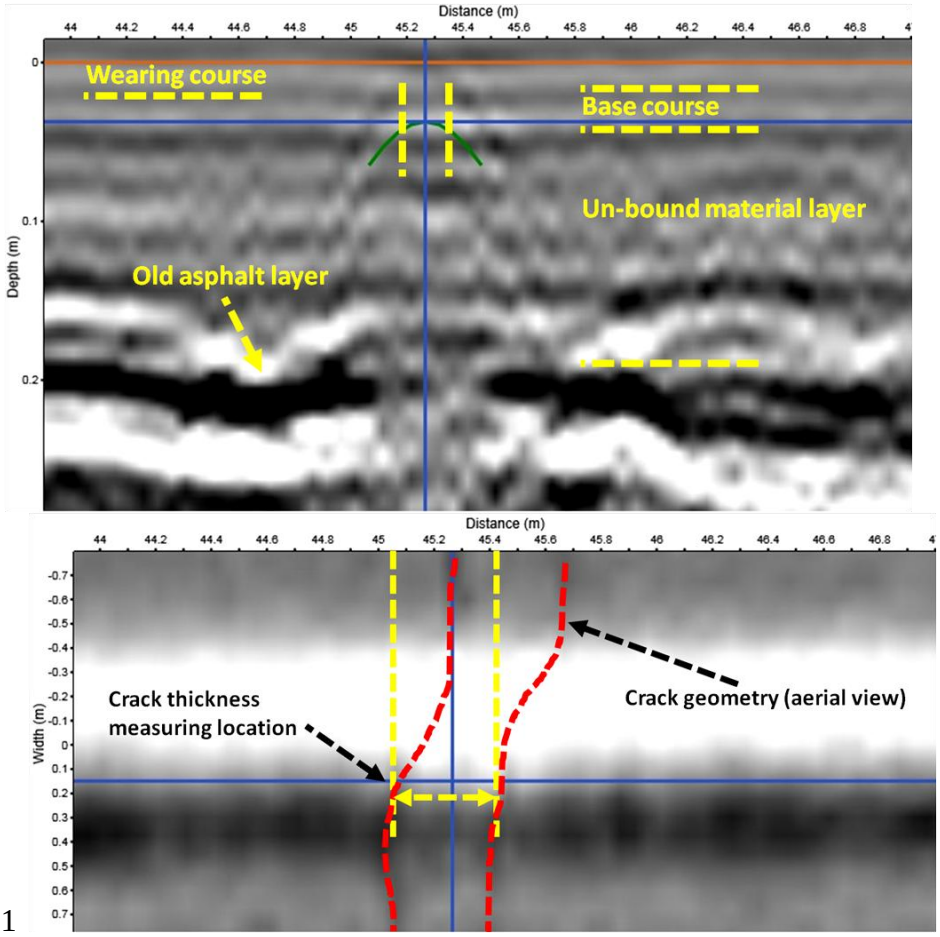

1

Figure 4.14. The investigation of crack at 46 m on Site C by GeoScope System, (top) crack depth in the pavement and, (bottom) the crack geometry at 4 cm depth (software: 3dr-Examiner)

As it was possible to follow the crack path in pavement structure, data was further analysed to find out crack's end and measure crack width at different depths. By moving the blue line (Figure 4.14(top)) it was possible to analyse crack at different depths. The crack measuring procedure is shown in Figure 4.14(bottom). The crack width is approximately measured at a depth of 4 cm from point where blue line meets crack perpendicularly. The irregular geometry of crack is also shown in red dashed line. With the same procedure, crack width at different depths in the pavement structure are measured and presented in Table 4-11.

It can be seen in Table 4-11 (2nd column) that the crack location (start and end) are changing along travel direction. This is due to irregular crack geometry at different depths. As the accuracy of axis in GPR-grams (x and y) could not be changed due to limited software use, approximate crack width values Table 4-11 (3rd column) are taken. Also due to technical limitations, it was hard to measure exact crack depth in pavement structure, although it was approximately measured by pavement coring in the end of survey. Despite approximated values, it can be seen that with the help of GPR, crack width can be measured (accuracy level compromised) in pavement structure. Due to crack irregular shape, its width do not have uniform trend. Its width is increasing from surface till 1.3 cm

depth but then decreasing at 2.9 cm depth. At a depth of 6.6 cm, the crack is vanishing and therefore, has maximum width of 42 cm. Although the crack width values measured by GeoScope system greatly differ from real crack width values, it has a uniform trend. Therefore, in future, a relation between GPR values and real values may help extracting desired crack dimensions with higher accuracy. The GeoScope outcomes were later validated by laboratory investigations provided in Section 4.2.1.

Table 4-11: The width of 45.4 m crack Site C at different depths (by GeoScope system)

Depth (m)	Crack location along survey direction (m)		Crack width measured (m) (Approx. values)	Crack width real (m) (Approx. values)
	Start	End		
0.013	45.09	45.42	0.33	0.016
0.029	45.09	45.40	0.31	0.018
0.040	45.08	45.43	0.35	0.02
0.050	45.08	45.42	0.34	0.022
0.066	45.06	45.48	0.42	0.03

The same crack on 45.4 m (≈46 m) on Site C was investigated by Aladdin system. The data was processed by GPR-Slice. This time only 1.2 meter section was investigated from where the crack had to be measured (Figure 4.14(bottom)). The results are presented in Figure 4.15. The crack was successfully detected by the Aladdin GPR system in 3D surveying. The crack at a depth of 1.57 cm is shown in Figure 4.15 (left). The 3-D surveying could differentiate among asphalt and crack as asphalt is in red whereas crack is in blue. The crack width measurement was not possible due to software limitations. The pavement surface i.e. crack starting point is shown in Figure 4.15(left). The bottom of asphalt layers are shown in Figure 4.15 (right) where the crack can be seen still propagating into pavement. The crack area in blue (in Figure 4.15(right)) is the same area marked as crack path in Figure 4.14. The crack width measurement was ≈10 cm which was more erroneous than measured by GeoScope.

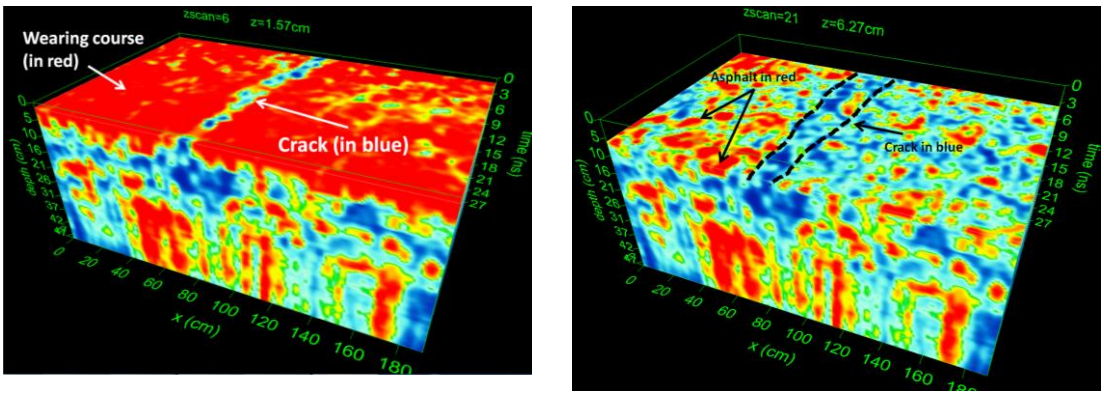

Figure 4.15. Investigation of crack at 46 m at Site C by Aladdin, (left) crack at 1.57 cm depth, (right) bottom of old asphalt layer and crack pattern at 6.27 cm depth

4.3.2 The influence of GPR central frequency

To investigate influence of GPR systems properties i.e. its central frequency on crack detection, laboratory specimens as well as field tests were conducted. The GPR systems included for the investigations were SIR-20, MALA HF and Aladdin. The SIR-20 and MALA HF systems were considered for considered for laboratory and field surveys whereas Aladdin was considered only for field tests. The properties of systems are provided in Table 3-1. For laboratory tests, specimens AB, AC, AI, AH, C and AJ respectively were laid in a series, as shown in Figure 4.16. The specimens were placed on metal plates.

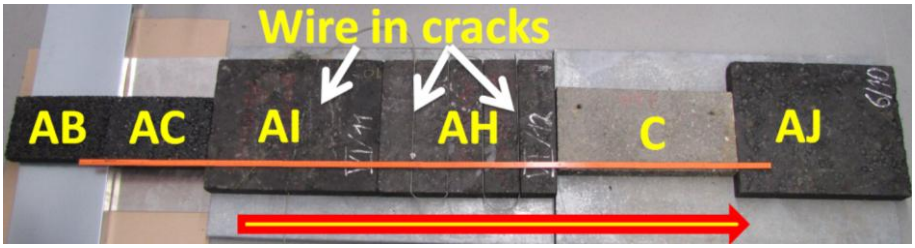

Figure 4.16. Test setup showing specimens sequence and direction of survey in red

In the first phase, SIR-20 and MALA HF with double antennas (two different frequencies, Table 3-1) were deployed. Air was used as crack filling material in the cracks of specimen AH and AI. ReflexW was used to standard process the raw data i.e. dewow, background-removal, static correction, and gain increase. The sequence and strength of processing techniques were kept same for outcomes of SIR-20 and MALA HF equipments used in this survey. The outcomes are presented in Figure 4.17.

The cracks (specimens AH and AI) were detected by 1500 MHz and 1600 MHz systems Figure 4.17(a & c). The 1cm deep crack in specimen AH was however not detected by 1600 MHz system (Figure 4.17(c)). Surprisingly, the crack detection quality was promising in case of 1500 MHz system compared to 1600 MHz (Figure 4.17(a & c)). Therefore, it can be concluded that not only central frequency but other GPR system characteristics must also be considered.

In addition to crack detection, the outcomes revealed that different asphalt mixtures can also be distinguished by the GPR. The specimens AI, AH and AJ having same asphalt mixture properties and therefore have identical curved shape bases in the GPR-grams. On the other hand the specimen C despite having same asphalt mixture properties i.e. aggregate and layer type has a flat base. This is probably because the properties of specimen C were changed during its use in asphalt pavement whereas specimens AI, AH and AJ were freshly constructed. Also specimen AC which is a dual-layered specimen has two bases i.e. two extra black line in the GPR-grams shown in Figure 4.17(a, b & d). Despite freshly constructed and well bonded layers (specimen AC); GPR could differentiate among two asphalt types in a specimen. The specimen AB which is a porous asphalt specimen is different from all other specimens. It is possible that due to difference in aggregate type (Diabase) and void ratio, its formation in the GPR-gram is unique.

Back to influence of GPR system frequency on crack detection, in case of 2600 MHz system, cracks in specimen AI and AH were detected but in case of 2300 MHz system, the cracks were hardly detected (Figure 4.17 (b & d)). Although it is logical that the data quality of 2600 MHz is higher than 2300 MHz, it was not expected that the 2300 MHz antennas will not detect crack at all. This is because the 1600 MHz antenna of same system (MALA HF) could detect the cracks which were not detected by 2300 MHz antenna. Also the crack detection quality of 1500 MHz antenna of same system is better than its 2600 MHz system (Figure 4.17 (a & c)). Therefore, question arises that are the lower frequency antennas optimal for crack detection as was in the outcomes of Diamanti et al., 2012. To answer it, further tests were carried out keeping the test setup same shown in Figure 4.16. It was expected that the crack dimensions i.e. 0.7 cm wide and 1-4 cm deep cracks may be difficult to detect and thus is hard to compare GPR systems on this base. Therefore, a metal wire was placed in the cracks of specimens AI and AH as shown in Figure 4.18. The raw data was again standard processed and processing intensity was kept constant. The outcomes are shown in Figure 4.18. This time due to wire in cracks, the crack hyperbolas are prominent in all GPR-grams.

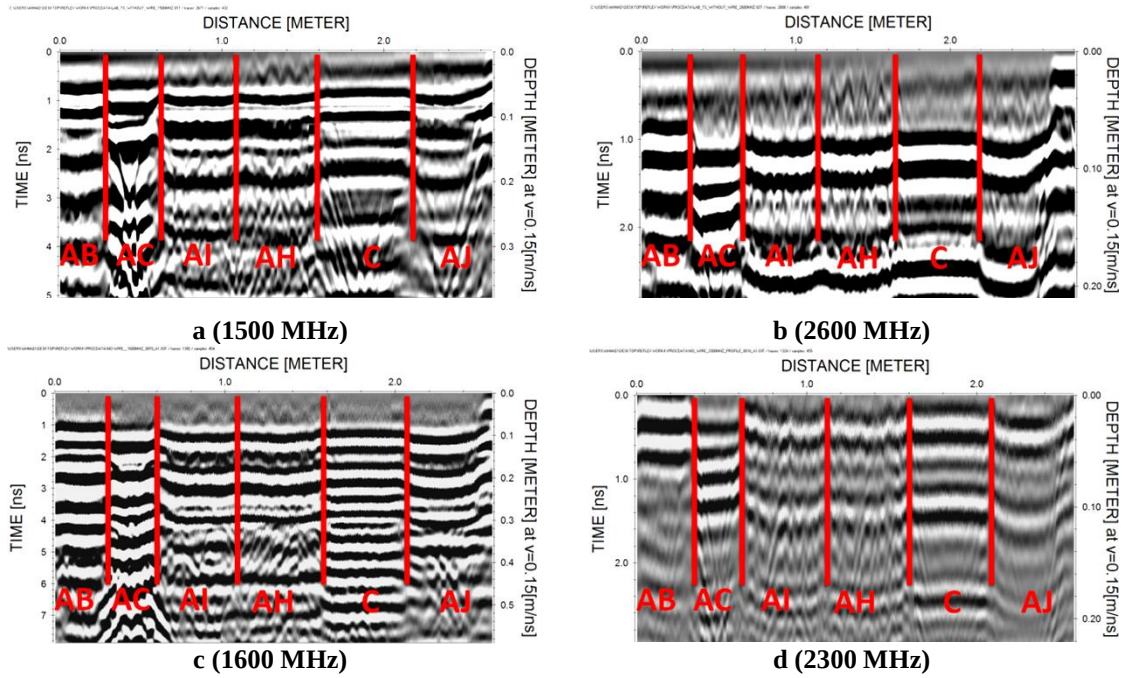

Figure 4.17. Results from GPR measurements on test track of specimens, (a, b) results from SIR-20 with 1500 and 2600 MHz antennas, (c, d) results from MALA HF with 1600 and 2300 MHz antennas

The 1500 MHz system results were again better than 1600 MHz which confirms previous outcomes in Figure 4.17(a & c). However, this time the results are clear and hyperbolas of cracks are visible due to wire in cracks (as crack filling material). The results in Figure 4.17(b & d) are less promising compared to results shown in Figure 4.17(a & c) especially regarding specimen AI. Thus outcomes verify past literature such as outcomes in Diamanti et al., 2012. Author personally discussed and confirmed outcomes with many scientists including N. Diamanti (Author of Diamanti et al., 2012) who stated that topic is under

investigation. It is therefore recommended to either wait for latest outcomes or carry out further investigations.

In Figure 4.17(a), the cracks in specimen AH are angular whereas crack in specimen AI is more circular. It could be because of diagonal crack which appeared in circular hyperbola compared to all straight cracks hyperbolas in specimen AH. One more surprising results was that the same depth crack in specimen AI and AH (1 cm deep) have similar hyperbolas. Also the deeper cracks in specimen AH have hyperbolas with maximum peaks which can be observed in all outcomes Figure 4.17(a-d). Thus it can be concluded that it is possible to differentiate among different depth cracks in GPR surveys.

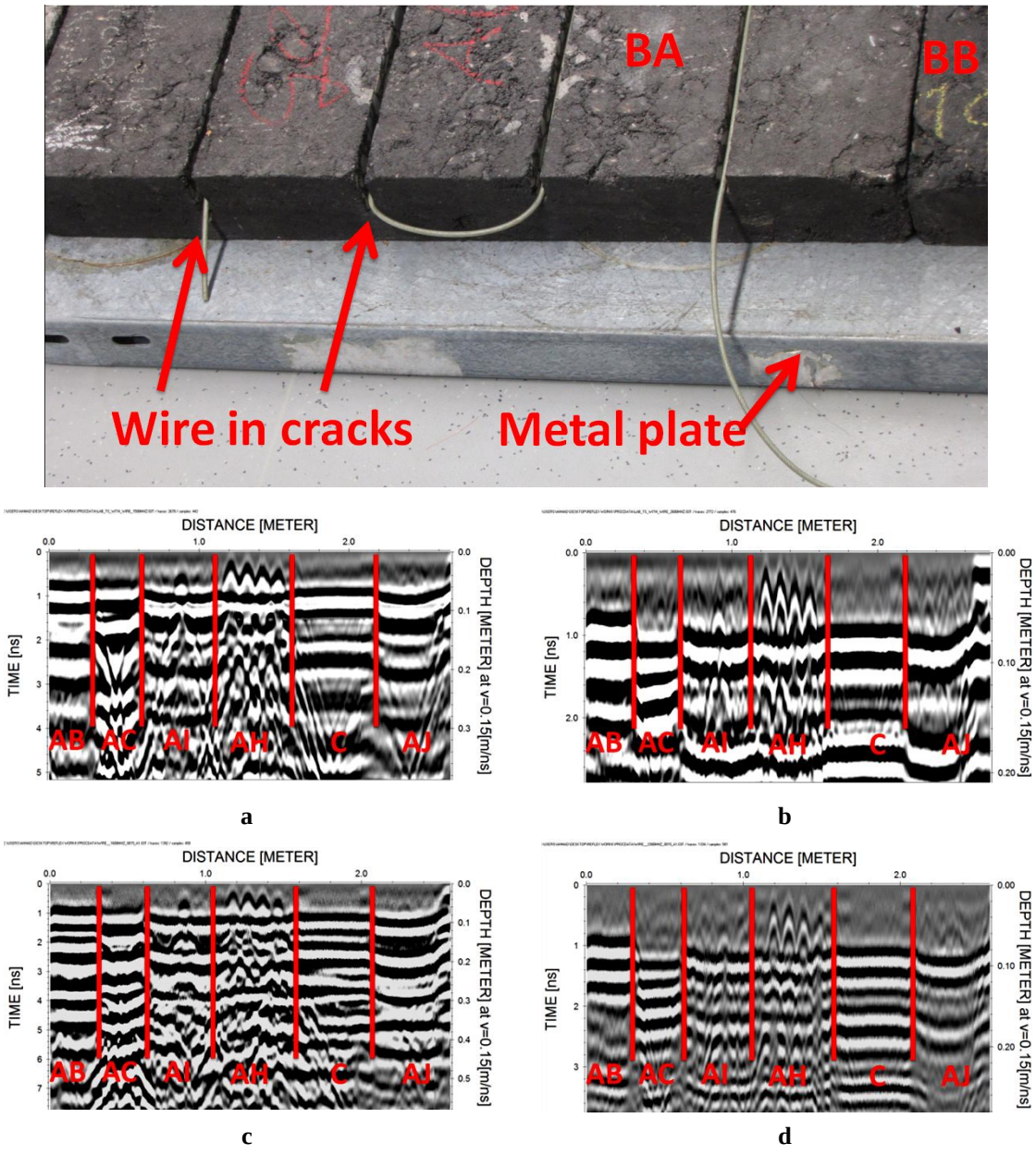

Figure 4.18. The GPR measurements on test track using wire as crack fill in cut specimens AH and AI, (top) wire in cracks, in cracks of specimen AH (a, b) results from SIR-20 with 1500 and 2600 MHz antenna respectively, (c, d) results from MALA HF with 1600 and 2300 MHz antennas

To investigate equipment central frequency effect on asphalt pavements crack detection, Site A was selected. On site A, the first crack (crack "α") was filled with mixture of organic material, clay and sand. The second crack (crack "β".) was a joint which was sealed off with bitumen. The site and cracks are shown in Figure 3.17. The tests were conducted with three systems namely Aladdin, SIR-20 and MALA HF. The results are standard processed and presented in Figure 4.19.

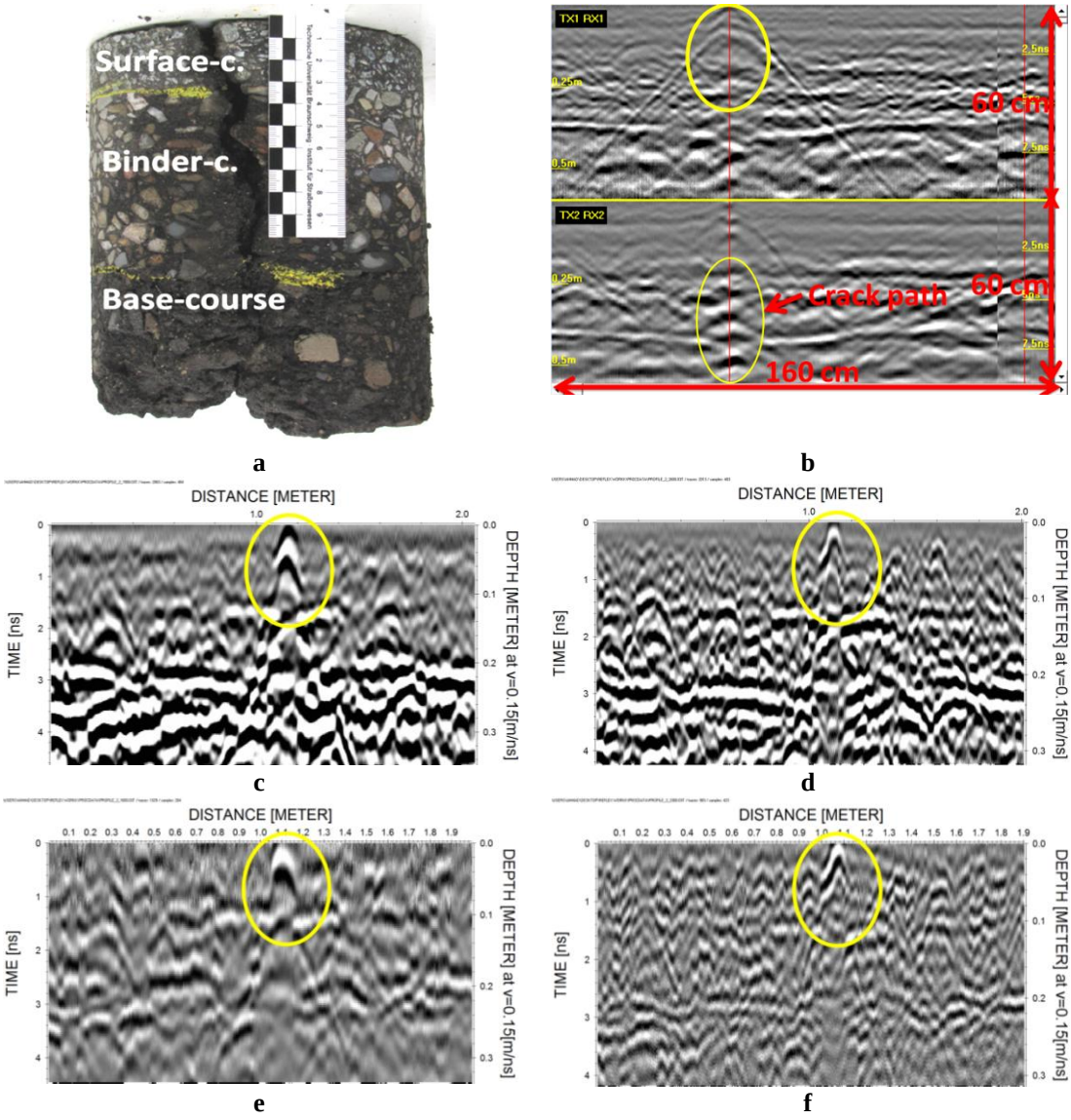

Figure 4.19. The outcomes of crack "α" (site A) analysis, (a) pavement core sample, (b) Aladdin 2000 MHz antenna, (c) SIR-20 1500 MHz, (d) SIR-20 2600 MHz, (e) MALA HF 1600 MHz, and (f) MALA HF 2300 MHz antennas

The crack "α" was detected by all three GPR equipments. The crack dimensions and asphalt layers thickness is shown in core sample which was taken at the end of survey (Figure 4.19(a)). It can be seen in core sample that crack do not have a perfect geometry, which is different from asphalt specimens. The crack also continued till end of asphalt layers i.e. 18 cm deep. As Aladdin can survey objects with multi-transmitters simultaneously, its GPR-gram is divided into two (Figure 4.19(b)). The upper half is

showing results of survey perpendicular to crack whereas lower part at 180°. By this means, crack width measurement is theoretically possible.

The Aladdin system detected crack successfully, marked in yellow in the GPR-gram shown in (Figure 4.19(b)). The second transmitter detected the crack path (marked in yellow) in the pavement structure which is not detected by any other system. This path may have foreign materials which intrude from crack into pavement structure. The results of SIR-20 were also promising. However, the results of 1500 MHz antenna were better than 2600 MHz regarding crack detection. The 1500 MHz antenna GPR-gram highlighted the crack (encircled in yellow) clearer than 2600 MHz (Figure 4.19(d)). The pavement asphalt layers are however, clearer in 2600 MHz GPR-gram (black lines at 12 and 22 cm). The MALA HF also detected crack successfully. The crack was detected by 1600 and 2300 MHz antennas (Figure 4.19(e & f)). The crack detection quality is however, inferior to SIR-20 outcomes. The pavement asphalt layers are also less clear in the outcomes. From crack "α" survey outcomes, once again lower frequency antennas proved themselves to be optimum for crack detection.

The same radar equipments were used for testing crack "β". The raw data was standard processed and the results are provided in Figure 4.20. The pavement core sample, taken at the end of survey is shown in Figure 4.20(a). It can be seen that the crack was sealed off with bitumen. The bonding between binder and base course was weak and therefore in GPR-grams there is a strong black line on the left of crack at a depth of 12 cm (Figure 4.20(b-f)).

As bitumen was used as crack fill material in crack "β", the contrast between crack and asphalt pavement was less. This contributed to crack detection with difficulty compare to crack "α" which was filled with organic materials. Therefore, Aladdin first antenna hardly detected the crack shown in Figure 4.20(b-top). The layer separation at 12 cm depth is however clear. The second antenna of Aladdin (Figure 4.20(b-bottom)) detected the crack path in pavement structure. The SIR-20 1500 MHz antenna detected crack as well as pavement layers including wearing course. The 2600 MHz antennas could highlight the layer separation with quality. The MALA HF system 1600 and 2300 MHz antennas results were not promising. Classical round shaped hyperbolas were missing in the GPR-grams. The GPR-gram was also disturbed by noise at crack (Figure 4.20(f)).

From outcomes of cracks "α" and "β", it can be concluded that lower frequency antennas (limit = 1500 MHz) are optimum for crack detection. The high frequency antennas (limit = 2600 MHz) can provide better resolution such as layers delamination, layers identification in asphalt pavement however, their crack detection quality is compromised. It can also be concluded that crack fill plays an important role in crack detection. Crack filling material with more contrast to asphalt (difference in dielectric constant) helps increase crack detection quality as was in case of crack "α" vs. crack "β" (organic + clay + sand vs. bitumen).

In addition to analysing GPR abilities for crack detection, its abilities to differentiate among different materials were also proved. Interestingly, each asphalt specimen in GPR

outcomes provided in Figure 4.17 and Figure 4.18 can be clearly recognised. This not only proves that GPR can differentiate among different materials but also proves the influence of material properties on GPR outcomes. Also specimen AI, AH and AJ looks same as they had same material properties. The asphalt pavement cut-section specimen C was dissimilar to other specimens and thus have straight base compared to AH, AI and AJ. Where these specimen have curved bases in the GPR-gram (Figure 4.17 and Figure 4.18. The multi-layered specimen AC has two bases in the GPR-grams. Although layers were freshly prepared and well bounded, SIR-20 and MALA HF equipments could successfully differentiate among layers.

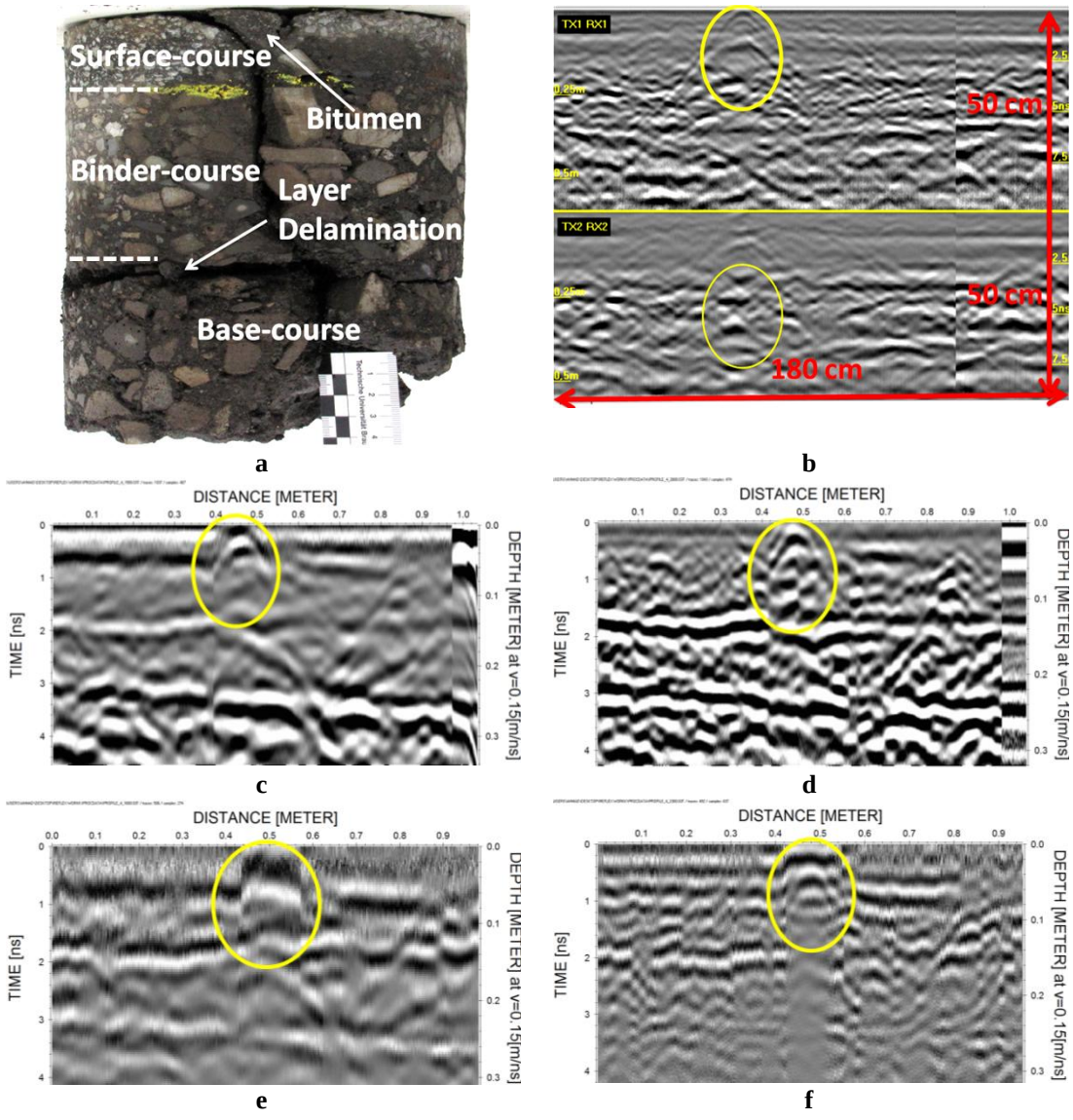

Figure 4.20. The GPR measurements on crack "β" (site A), (a) pavement core sample, (b) Aladdin 2000 MHz, (c) SIR-20 1500 MHz, (d) SIR-20 2600 MHz, (e) MALA HF 1600 MHz, (f) MALA HF 2300 MHz outcomes

As 1500 MHz antenna (SIR-20) results were promising compared to 1600 MHz antenna (MALA HF) it can be concluded that there are other parts of system which improves crack

detection quality. However, little information is provided by the manufacturer, regarding other components in the system.

4.4 Effect of surveying

The effect of surveying on GPR abilities for crack detection regarding number of scans per length and angle between crack and EM wave propagation was investigated. The numbers of samples per scan for a desired survey are mostly user defined as was case Aladdin system. On the other hand, the crack had random geometry and thus surveying from various angles may reveal different outcomes. In the following sections, therefore, the above two factors will be investigated.

4.4.1 The number of samples per scan

The samples per scan somehow increase the resolution of GPR-grams. To find out if increased samples per scan also clarify the cracks which are otherwise not clear, tests were conducted in laboratory and in field. The Aladdin GPR system was used for this purpose. For the comparison of results, single software (ReflexW) and standard processing with same sequence was applied. The description of tests and outcome is provided in the following section.

4.4.1.1 Laboratory tests

Two specimens "BA" each with two cracks were inverted on sand (bottom-up cracking) for the above mentioned parameter investigation. The cracks in the first specimen were each 2 cm wide with a depth of 3.5 and 2.5 cm respectively. The cracks in the second specimen were fixed in depth i.e. 1 cm whereas their width was 0.5 and 1 cm respectively. The cracks were of different geometry to bring forth the effect of samples per scan on GPR-grams quality. The test setup was the same as shown in Figure 4.5 except that this times it was top-down cracking with different geometry cracks. The survey outcomes are presented in Table 4-12.

It can be seen in Table 4-12 that the 512 samples per scan results are having a weak hyperbola for crack 1 and 2 (specimen 1). The cracks in specimen 2 are even not clear and without prior information regarding crack position, it could not be possible identify them in the GPR-gram. In 512 samples per scan results (Table 4-12), the cracks likely position with respect to test setup is encircled in yellow and specimen boundaries with sand layers are marked, which may help understand further outcomes regarding samples per scan results. The 1024 samples per scan results (Table 4-12) brought very little change compared to 512 samples per scan results. However, the 2048 samples per scan results are better than 512 and 1024 samples per scan results regarding crack 1 & 2 (specimen 1) and the joint of specimen. The fourth crack (specimen 2) with 1 cm depth and 1 cm width was however, clear in 4096 samples per scan results. The yellow marks are showing specimen start, cracks position, joint between specimens and the end of specimen 2. The first two cracks (specimen 1) and joint between specimens are also clear in 4096 samples per scan results.

Despite higher samples per scan, the crack 3 (specimen 2) was still do not appear in 8192 samples per scan result. Therefore, conduction of more tests was decided.

Table 4-12: Effect of samples per scan on crack detection quality

Samples per scan	Outcomes
512	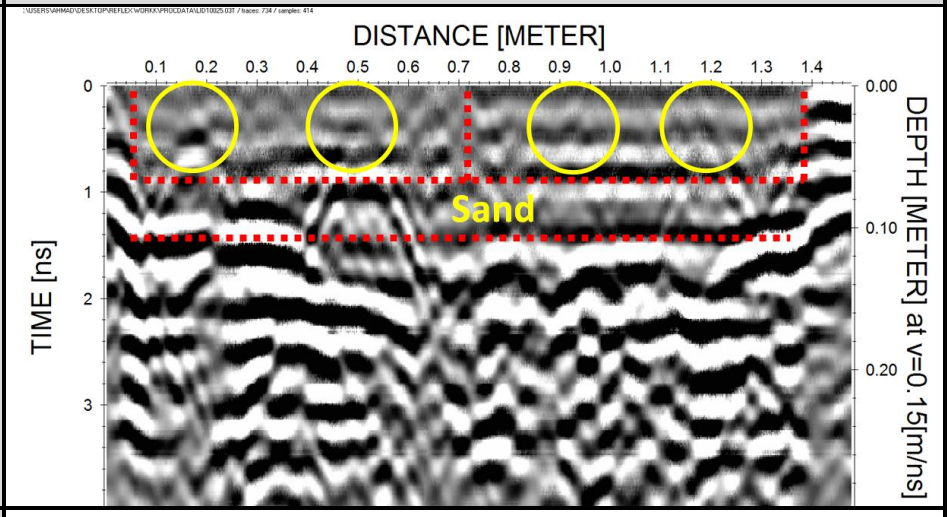
1024	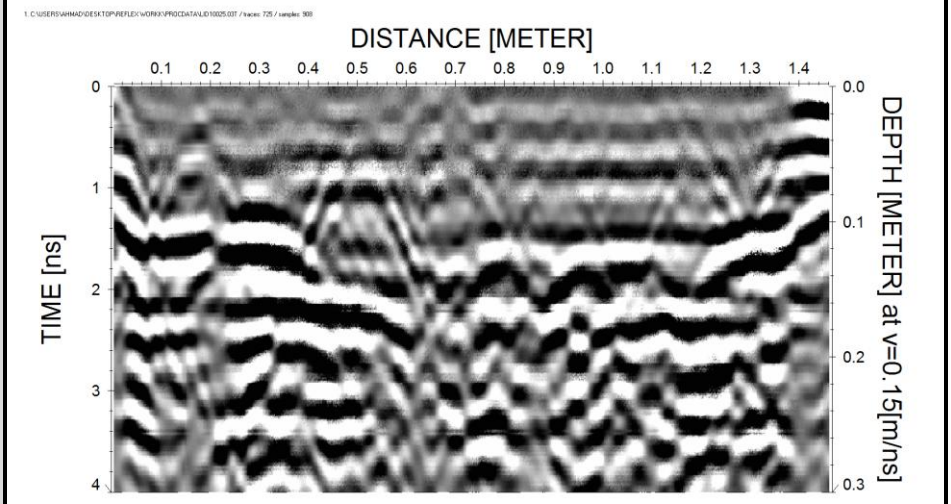
2048	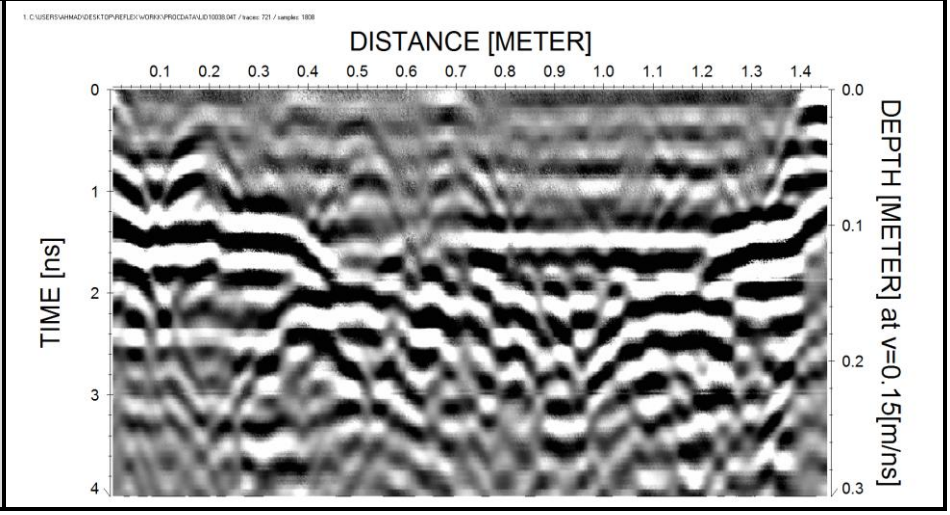

4096	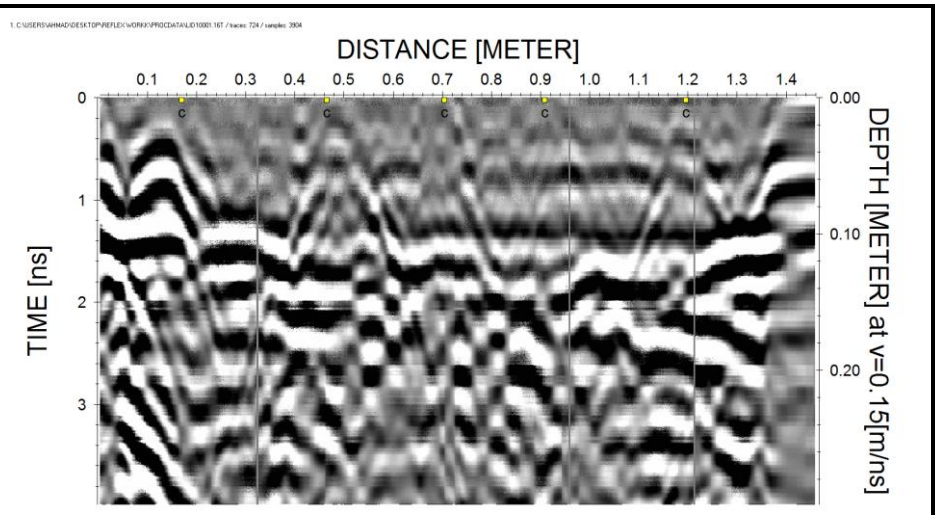
8192	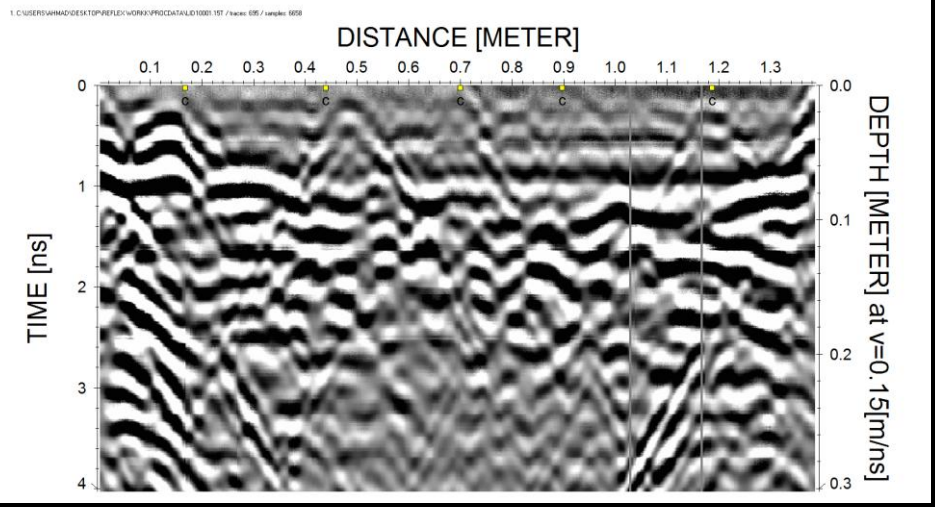

The specimen "BA" with two cracks of 2 cm x 3.5 cm and 1 cm x 2.5 cm (width x depth) was setup for the testing as shown in Figure 4.21. The cracks were sealed off with dry papers to prevent sand intrusion. The specimen was inverted on sand thereby depicting bottom-up cracking. The GPR system Aladdin was used and the data was processed by ReflexW software. The specimen cracks were investigated in the order given above i.e. 2 x 3.5 cm^2 crack was crack "1" and 1 x 2.5 cm^2 crack was crack "2" starting from 0.00 cm. Contrary to last time, the 512 samples per scan was not investigated. The outcomes are provided in Table 4-13.

This time due to the increased depth and width of crack, both cracks were detected. The specimen boundaries (in red) and cracks are encircled (in yellow) in the result shown in first row of Table 4-13. It can be seen that the crack "1" with increased volume has intense and clear hyperbola then crack "2". It proves that it is possible to differentiate among different cracks with varying depth or width.

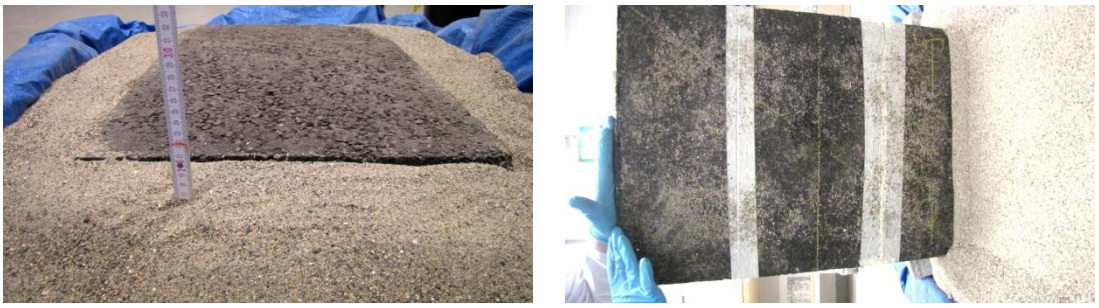

a b

Figure 4.21. The specimen "BA" tests setup, (a) the specimen surrounded in sand, (b) the specimen after test with sealed cracks

The 512 samples per scan results detected both cracks successfully. The boundary of specimen is also clear. Comparing 1024 samples per scan results with that of 512, it can be seen that there is not much difference in the cracks hyperbola. In the outcomes of 2048 samples per scan, the cracks according to their depth can be differentiated. The hyperbola of 3.5 cm deep crack (left) is higher (bottom-up cracking) then that of crack 2. The cracks however, cannot still be differentiated based on their width.

The 4096 samples per scan results shown in Table 4-13 (3rd row), made it possible to differentiate among cracks based on their depths as hyperbola are not on same depth. The 4096 samples per scan results are not much different than that of 2048. The 8192 samples per scan results were promising regarding clarity of data. Also the 8192 samples per scan GPR-gram needs less processing i.e. gain increase. Based on the outcomes it can be concluded that 512, 1024 and 2048 samples per scan do not have much difference. It was decided to conduct more tests to authenticate the outcomes before coming to any conclusion.

Table 4-13. The scan per resolution effect on crack detection (specimen "BA")

Samples per scan	Outcomes
1024	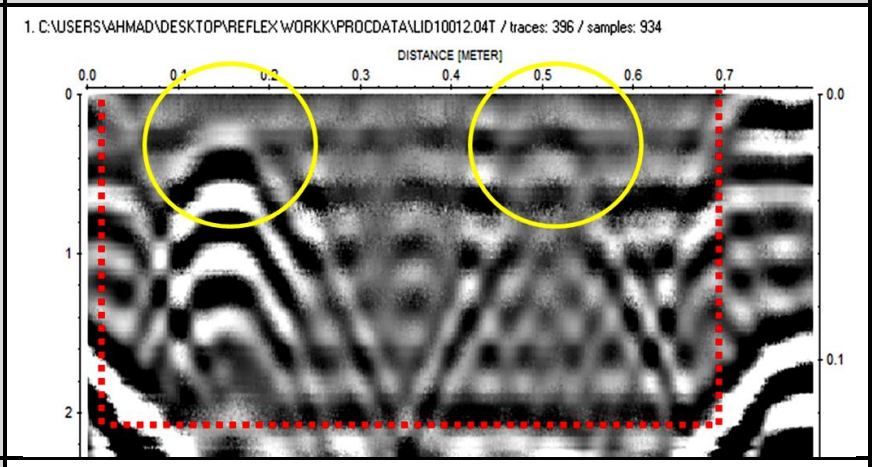
2048	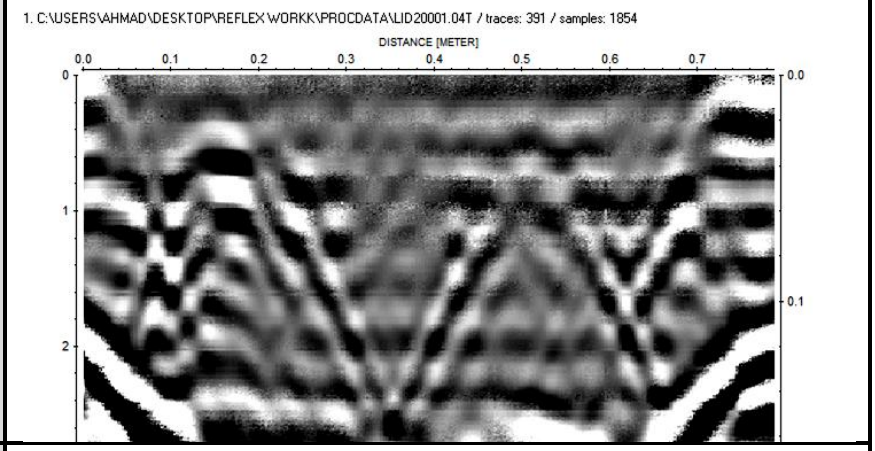
4096	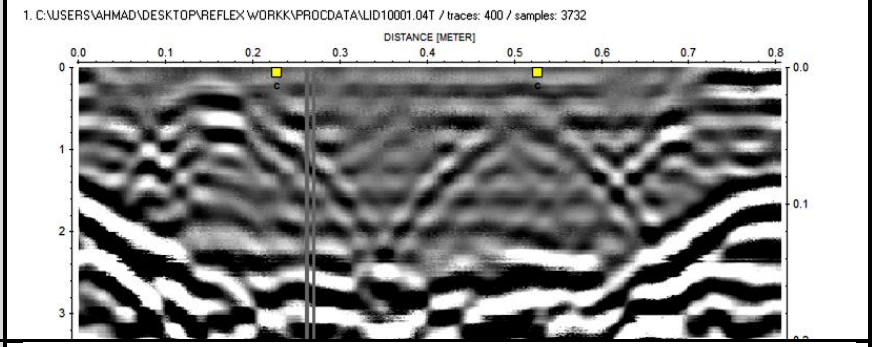
8192	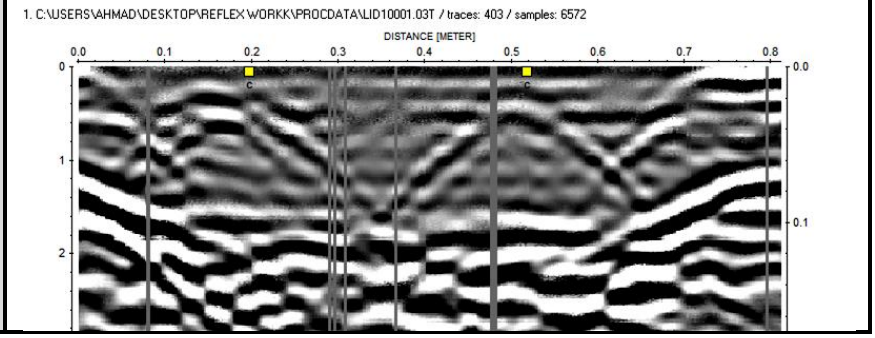

The next phase of investigation consists of a series of tests conducted on specimen BA with a single crack but with varying depth. The test setup was the same as shown in Figure 4.1. The data was collected by antenna configuration of 512, 1024 and 2048 samples per scan, 8 ns time window and 0.00202 m pulse transmission distance.

The specimen "BA" was first tested with 1 cm wide crack but the crack depth was increased gradually to 2 and 3 cm. This time 512, 1024 and 2048 samples per scan were considered to be investigated regarding crack detection. The result of 512 samples per scan is shown in Figure 4.22. The outcomes of 512 samples per scan easily highlighted the crack (encircled in yellow) with specimen's boundary (marked in red). What promising in these outcomes is that despite less crack depth and width compared to the cracks in previous tests (1 cm x 1 cm versus 1 cm wide and 2.5 cm deep crack), the crack's hyperbola is clearer. The reason can be less number of cracks per specimen which resulted in decreased noise and distortion. The further outcomes of are provided in Table 4-14.

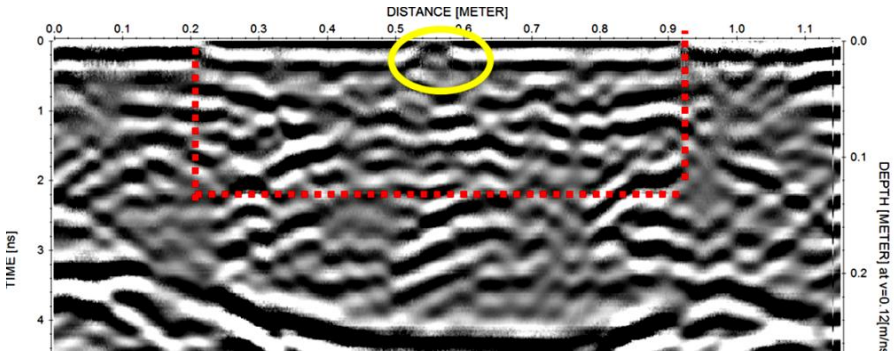

Figure 4.22. Detection of 1 cm wide and 1 cm deep crack (specimen BA) with 512 samples per scan

Table 4-14: The effect of samples per scan on detection of 1 x 1, 1 x 2 and 1 x 3 (width x depth) cm^2 cracks

SPS	1 cm wide and 1 cm deep crack	1 cm wide and 2 cm deep crack	1 cm wide and 3 cm deep crack
512		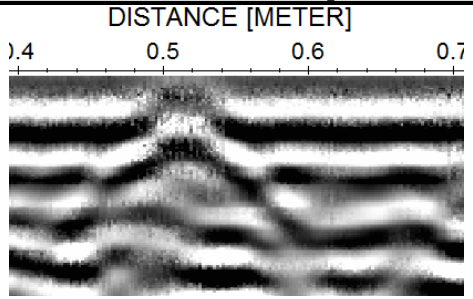	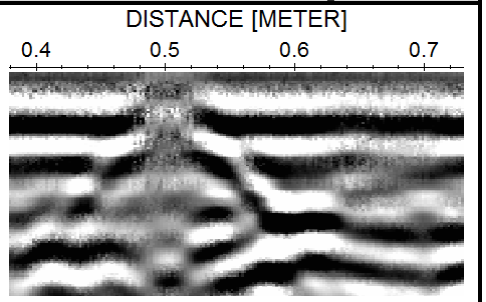
1024	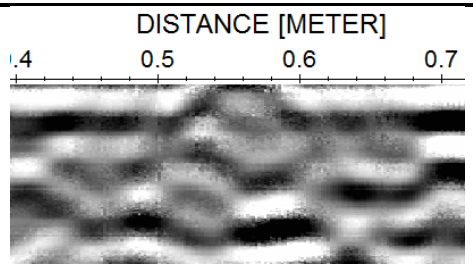	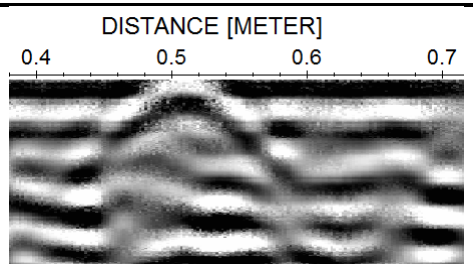	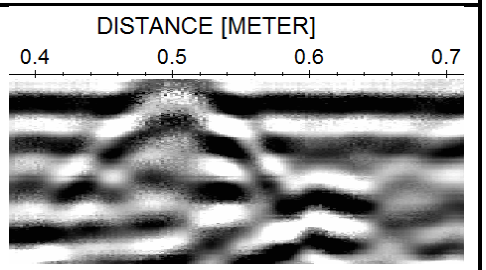
2048	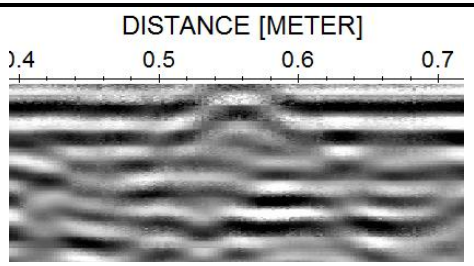	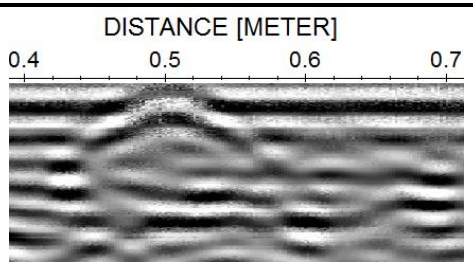	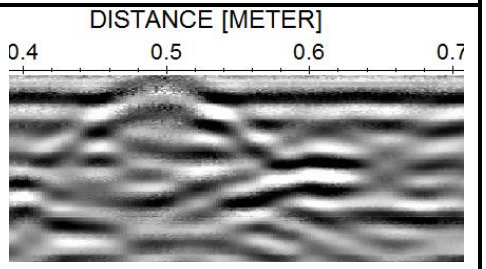

The results shown in Table 4-14 (1st column) are of 1 cm wide and 1 cm deep crack. It can be observed that by increasing samples per scan, the crack detection quality is decreasing. In case of 512 samples per scan, there is a cut in specimen surface lines whereas in 2048 samples per scan outcomes, this cut is decreased and unclear. Same is true for 2 and 3 cm deep crack which also can be hardly detected in 2048 samples per scan results. Thus it can be concluded that 512 samples per scan is optimal for crack detection and that crack detection quality may not increase by increasing samples per san. However, before any final conclusion, it was decided to check the effect of scan per resolution effect on crack detection quality in field (pavements).

4.4.1.2 Field testing

To find out the impact of samples per scan on crack detection, tests were carried out on Site C. The cracks from 0 m to 50 m were selected for GPR testing.

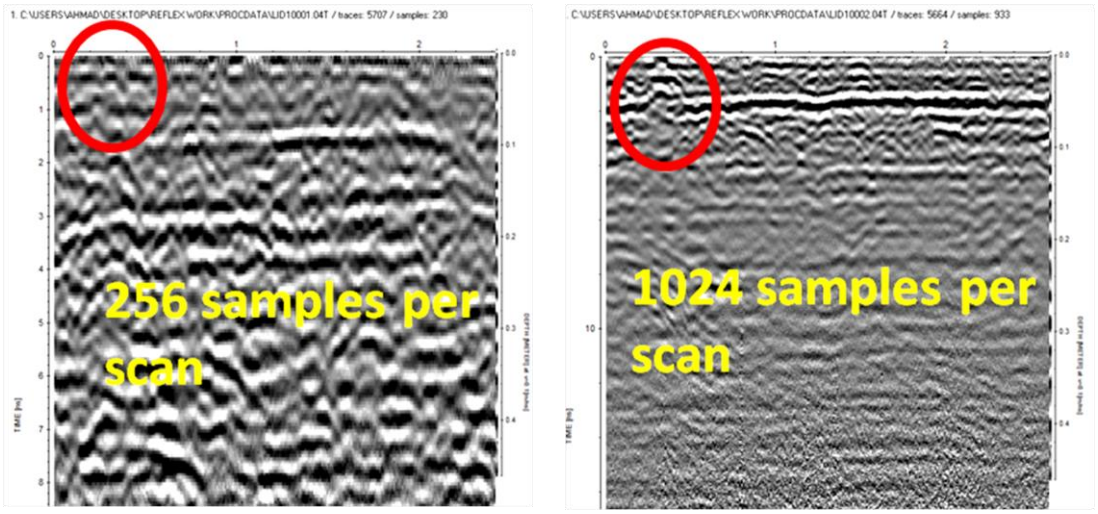

Figure 4.23. The effect of samples per scan on crack detection quality at Site C 0.44 m crack, (a) GPR-gram with 256 samples per san and, (b) GPR-gram with 1048 samples per san

Different GPR samples per scan were selected during surveys in order to find out the effect on crack detection. Samples per scan of 128, 256, 384, 512 and 1024 were verified for the crack detection. The GPR survey with higher samples per scan resolution such as, 1048 survey needed more time i.e. survey speed and data processing was slow. On the other hand, GPR survey with low samples per scan resolution such as 128 was fast.

In Figure 4.23(a), the crack 0.44 m on Site C is shown with red circle. The GPR-gram is with 256 samples per scan. Crack hyperbola can hardly be seen. Without prior information, the crack may not be marked in GPR-gram. On the other hand, the GPR-gram in Figure 4.23(b) is showing a clear hyperbola in GPR-gram. The difference is that the GPR-gram in Figure 4.23(b) is results of survey with 1048 samples per scan. Thus surveys with samples per scan from 128 to 1048 were selected to find out the effect of samples per scan.

In Figure 4.24 average of four GPR surveys with different samples per scan on Holzweg for crack detection is given. The crack width in Figure 4.24 is taken as average crack width

in winter (Table 3-14). It can be seen that the crack detection quality increases with increase in samples per scan, in Figure 4.24. Samples per scan of 1048 nearly detect all cracks with good quality. The samples per scan of 512 and 384 also detected all cracks with acceptable grades. The samples per scan resolution of 256 and 128 missed some cracks (of $\geq$ 0.5 cm width) and the quality of crack detection was also poor.

Comparing samples per scan of 1048 and 512, based on time factor, GPR surveys with 1048 samples per scan resolution were possible with 0.55 m/s speed (average) without missing the data and ultimately cracks. On the other hand, for GPR surveys with 512 samples per scan, a speed of 0.98 m/s (average) was required. The time taken by GPR surveys with 1048 GPR samples per scan resolution is almost double compared to 512 samples per scan GPR surveys. Therefore, based on results in Figure 4.24, a GPR survey of 512 samples per scan is recommended for crack detection

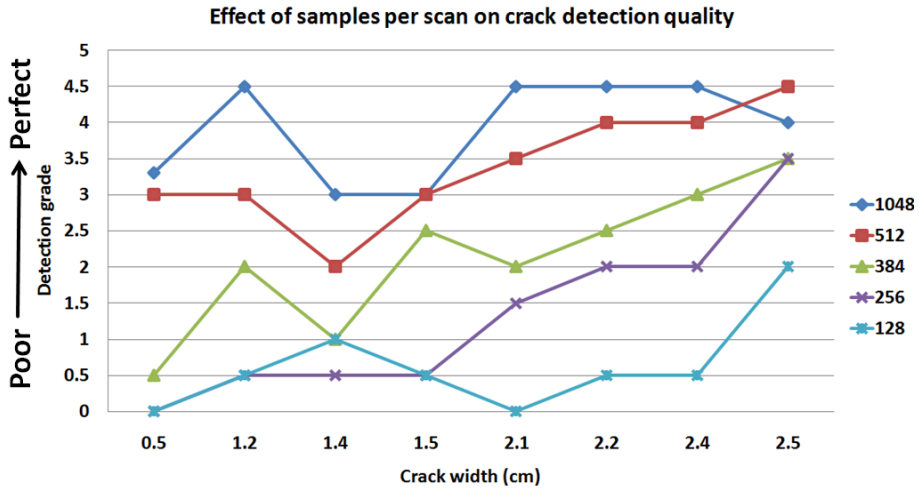

Figure 4.24. The effect of samples per scan on detection quality of cracks in asphalt pavements (GPR system: Aladdin)

4.4.2 Effect of survey angle

In asphalt pavements, straight and standard dimensions (rectangular, cubical, etc.) cracks are seldom. The pavement's crack direction inside the structure or along the pavement may differ from cracks investigated by GPR (laboratory and field) in the previous sections. On the other hand, most GPR surveys are carried out along the pavement and therefore, GPR has 90° to the cracks perpendicular to the pavement (transversal cracks). To find out what will be effect of crack angle if cracks are random or make 0° angle (longitudinal cracks) with GPR, investigations were carried on asphalt specimens in the laboratory and in field. The Aladdin GPR system was used in surveys. The Aladdin system was selected due to its capability of surveying with two transmitters at the same time thereby making it possible to survey a single crack from multi-directions. The location of transmitters and receivers in Aladdin system with respect to an arbitrary crack is shown in Figure 4.25.

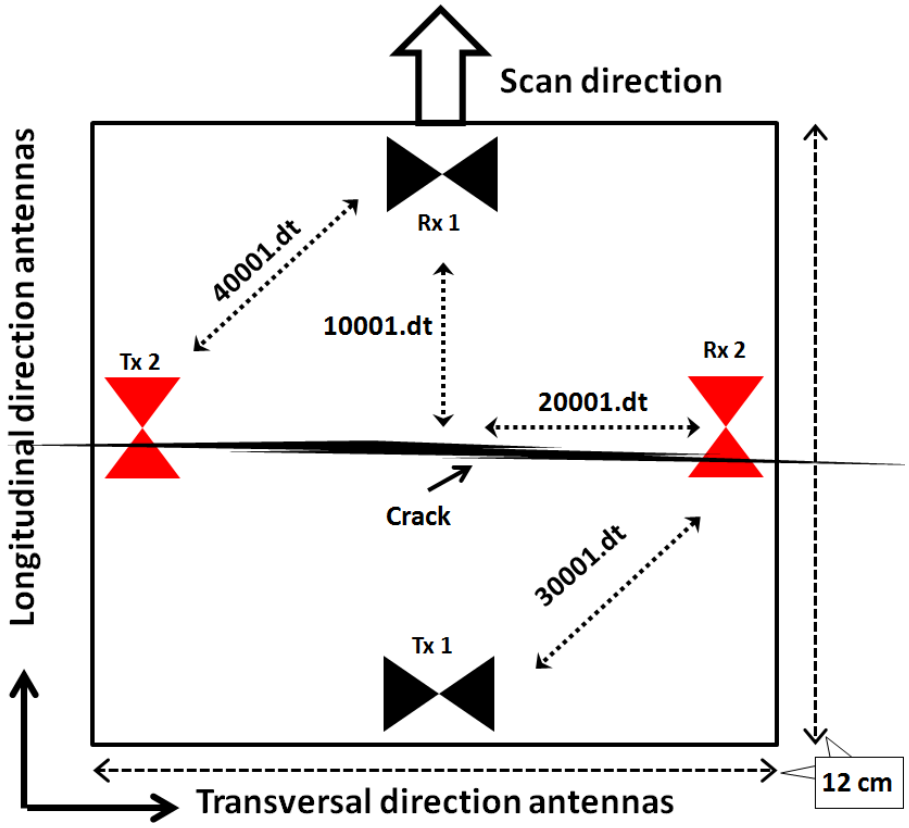

Figure 4.25. Dual polarized 2 GHz antenna of Aladdin GPR system

For the crack detection survey, the Aladdin antenna was configured to switch on both transmitters (Tx) and receivers (Rx) in the antenna. The transmitters and receivers could work simultaneously.

Table 4-15: Formation of 2-D survey scans by Aladdin antenna

Scan	Transmitter (Tx)	Receiver (Rx)	Data format
1	Tx 1	Rx 1	LID10001.dt
2	Tx 2	Rx 2	LID20001.dt
3	Tx 1	Rx 2	LID30001.dt
4	Tx 2	Rx 1	LID40001.dt

The configuration of transmitters and antennas is shown in Table 4-15 together with all possible data types. For investigations, the data was collected with different configuration. Configuration of GPR system includes samples per scan, time window and pulse transmission distance. With each survey the information will be provided accordingly. The data was standard and equally processed for a each survey.

4.4.2.1 Laboratory testing

For the laboratory testing, specimen "BA" was considered. The cracks were two in number, dividing the specimen in three equal parts. The crack 1 was 0.3 cm wide and 3 cm deep whereas crack 2 was 0.6 cm wide and 1 cm deep. The specimen was placed in a plastic box filled with sand. The test setup is shown in Figure 4.26.

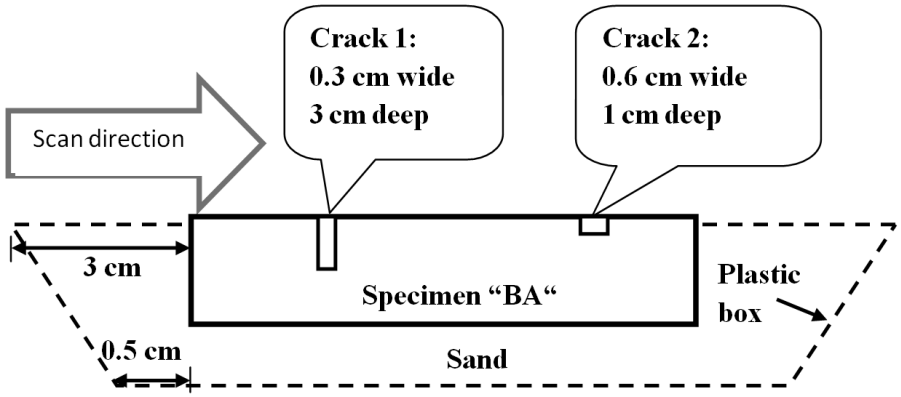

Figure 4.26. The test setup plan for crack-GPR angle effects investigations

The outcomes of survey regarding crack-GPR angle are provided in Table 4-16. The GPR survey was conducted with 512 samples per scan, 10 ns time window and 2mm scan distance. In all the GPR-grams, according to survey direction (Figure 4.26), crack 1 comes first (on x-axis) and then the crack 2 follows. The results provided in Table 4-16 shows that both the cracks were successfully detected. The scan 1, outcome of classical Tx1-Rx1 configuration (Table 4-15), is shown in Table 4-16 (1st row-1st column). The cracks are marked in yellow (also small yellow markers at the top of GPR-gram) and specimen boundary in dashed red lines. The crack 1 which is deeper than crack 2 has bold hyperbola. Also the crack 1 hyperbola is penetrating deep into the GPR-gram. According to GPR-crack angle (Figure 4.25), it was estimated that the scan 2 results will be outstanding. The outcomes were however, less promising then scan 1. Although both crack in specimen BA were detected, the detection quality declined. Also the deep penetrating hyperbola of crack 1 shortened. Despite poor quality of scan 2 than scan 1, difference in cracks due to their sizes was possible.

As scan 3 and 4 had the same crack-GPR angle, it was supposed that crack detection quality will be the same in both scans. The scan 3 and 4 proved the supposition. Both scan 3 and 4 are equal in crack detection quality i.e. cracks can be seen with almost equal strength hyperbolas. It was also expected, as also in case of scan 2, that the crack detection quality in scan 3 and 4 will be higher than 1 and lower then 2. The results however, were not as expected i.e. scan 1 results were superior in quality then all scans.

Table 4-16: The test outcomes regarding crack-GPR angle investigations

Scan 1 and 3	Scan 2 and 4
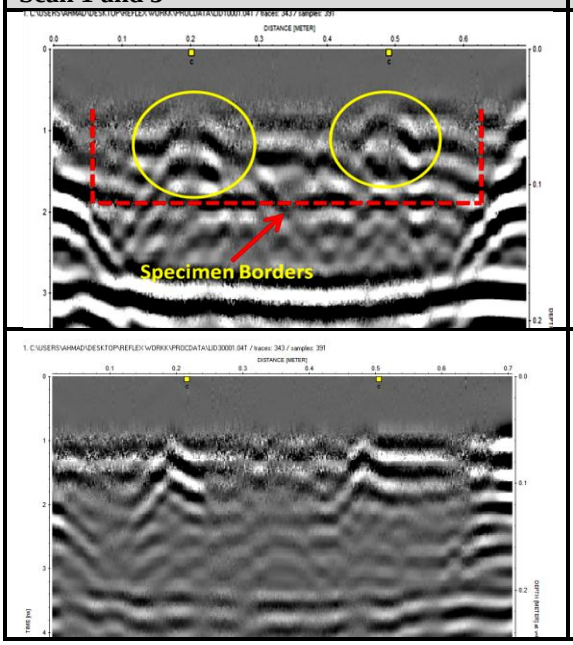	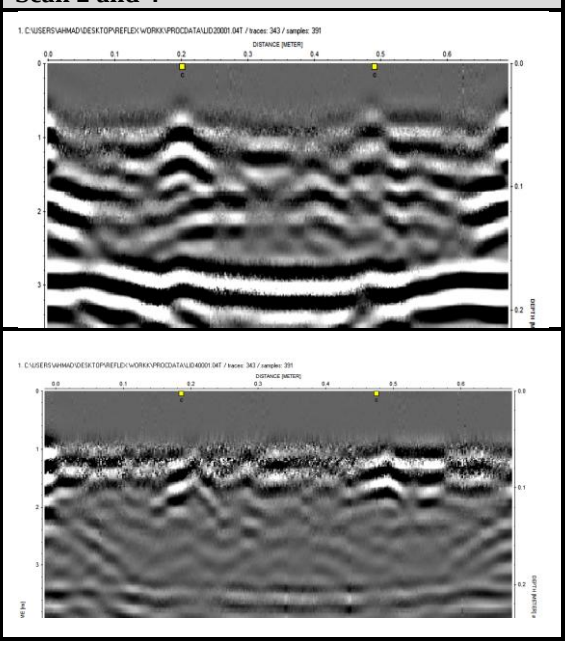

Following the results in Table 4-16, it was decided to survey the crack from 180° i.e. surveying along the crack to verify if scan 2 crack detection quality improves compared to scan 1. Asphalt specimen "BA" was with one crack was used for the investigations. The crack in the centre of specimen was 3 cm wide and 3 cm deep, filled with dry paper. The samples per scan of 512 with 2 mm pulse transmission distance were selected. The investigation outcomes are presented in

Table 4-17: The crack-GPR angle effect investigation by 180° surveying

Scan 1 and 3	Scan 2 and 4
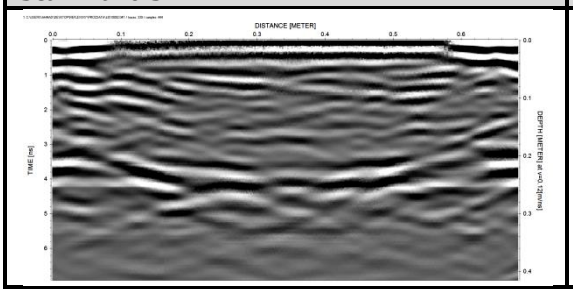	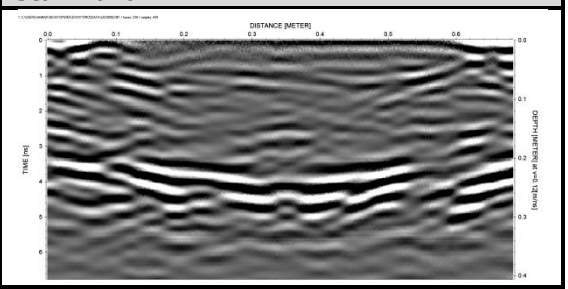
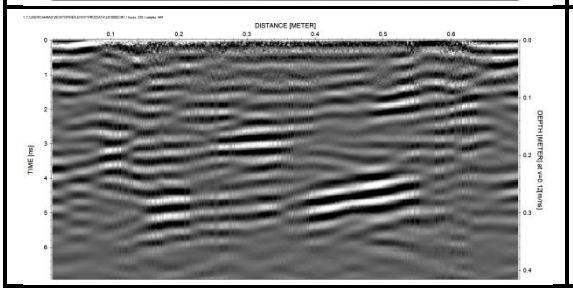	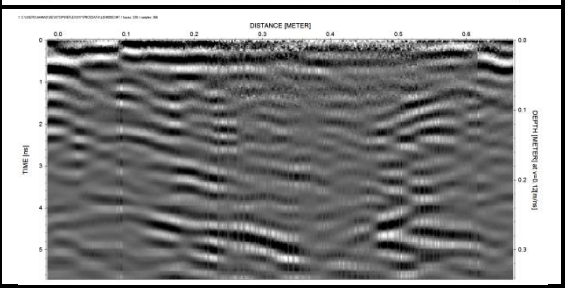

Despite greater size/volume of crack compared to the crack detection results in Table 4-16, the crack is not detected. Not only the crack but also the specimen boundaries are missing

in the GPR-grams. The scan 2 results are improved compared to scan 1 as specimen start and end can be marked. Also the base of sand-box is clearer in scan 2 compared to scan 1, 3 and 4. It is concluded that the crack-GPR angle is important in crack detection surveys. If the cracks are along the survey profile, it may be difficult to detect them.

4.4.2.2 Field testing

For the field testing, transversal crack on Site "D" (Gutswiese) was considered. The crack with a width of 10 mm was surveyed by moving along the road. Survey was conducted with 512 samples per scan, 10 ns time window and 2 mm pulse transmission distance. The results are provided in Table 4-18. The crack is encircled in yellow in scan 1 in Table 4-18.

Table 4-18: Outcomes of crack detection on Gutswiese from different angles

Scan 1 and 3	Scan 2 and 4
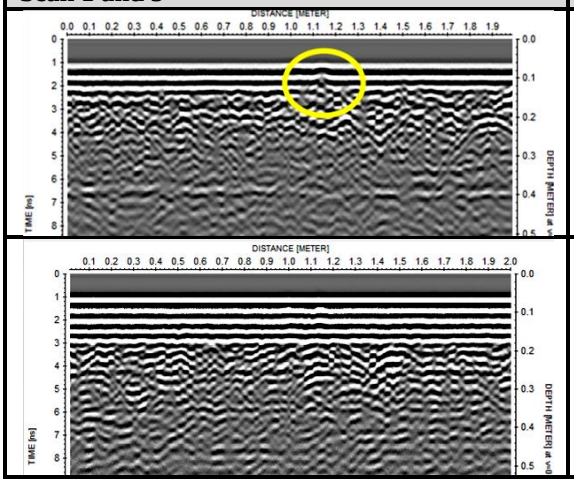	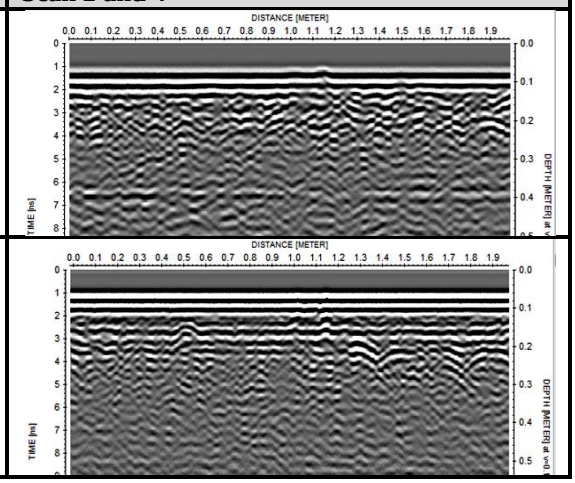

It can be seen in the results provided in Table 4-18 that the crack detection quality is not the same in all GPR-grams despite they were conducted on same crack (same geometry and crack fill). Note that the crack is located at 1.15 m in each GPR-gram. The scan 1 (Table 4-18) outcome is promising regarding crack detection. The crack in scan 2 is however less clear compared to scan 1. The scan 3 hardly detected the crack top but showed some distortion at a depth of ≈18 cm. It must be however noted that the depth may not depict real depth in pavement as air static correction (zero time correction) was not performed on raw data. The scan 4 equally detected crack's top and bottom. Although there are some disturbances in scan 4 and without prior information, it's hard to notice crack in the GPR-gram, the result were promising. As the quality of scans in these outcomes is, from highest to lowest 1, 4, 2 and 3 respectively compared to results in Table 4-16 where it was 1, 2, 3 and 4, a clear conclusion could not be made. Thus it was decided to conduct 3-D survey in order to further investigate GPR-crack angle.

For 3-D surveying, as the crack survey from different angles other than 90° were not promising, it was decided to survey only at 90°. The different 2-D scans (Table 4-15)

however, will be combined to form 3-D files. Thus total, 6 GPR-grams in 3-D can be generated as shown in Table 4-19.

Table 4-19: The 3-D survey from different 2-D file combinations

Scans	2-D file 1	2-D file 2	Crack scans angle (transverse crack)	Remarks
1 and 2	LID10001.dt	LID20001.dt	90° and 180°	Promising results
1 and 3	LID10001.dt	LID30001.dt	90° and 135°	Acceptable results
1 and 4	LID10001.dt	LID40001.dt	90° and 315°	Acceptable results
2 and 3	LID20001.dt	LID30001.dt	180° and 135°	Not recommended
2 and 4	LID20001.dt	LID40001.dt	180° and 315°	Not recommended
3 and 4	LID30001.dt	LID40001.dt	135° and 315°	Not recommended

The scan angle in 2-D files may not be useful alone but when combined with other 2-D scan, may be useful. For example the scan 2 has less crack detection quality compared to scan 1. However it is possible that its combination may results in promising 3-D files.
The crack at site “D” was selected for the 3-D surveys. The area 2 (Figure 3.22(a)) was selected for 3-D surveying. The antenna configuration was set to 512 samples per scan with 2 mm pulse repetition frequency. The results are provided in Table 4-20. It can be seen in the results that the classical method of 3-D files combination i.e. scan 1 and 2 give the best results. The crack in red colour at the top of 3-D data can be easily seen. The quality of crack detection decreases in 3-D file from scans 1-4, 1-3 and 2-3 respectively. The crack in red can hardly be seen these 3-D files. The 3-D file from scans 2-4 gave better results than results from 1-4, 1-3 and 2-3 scans. The 3-D file from 2-4 scans has large area of crack which is however in yellow compared to other 3-D results where it is in red. This is due to processing of data with different processing values. The least quality 3-D file was composed of scan 3 and 4. Thus it can be concluded that the classical method of 3-D survey comprising of scan 1-2, provides the best results.

Table 4-20: The 3-D survey of site "D" for crack-GPR angle investigation

Scans	3-D outcome
1 and 2	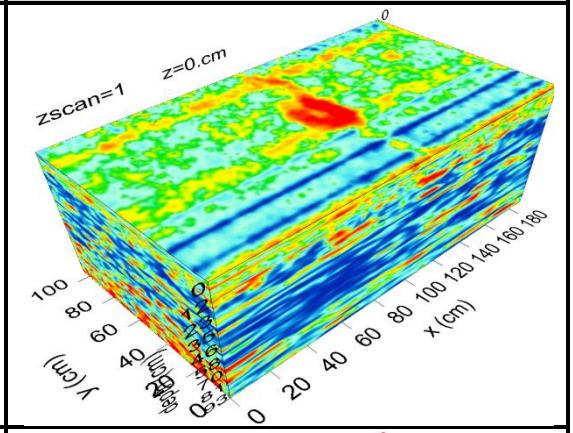
1 and 3	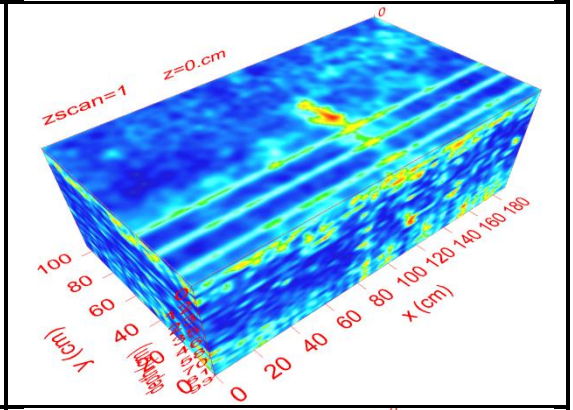
1 and 4	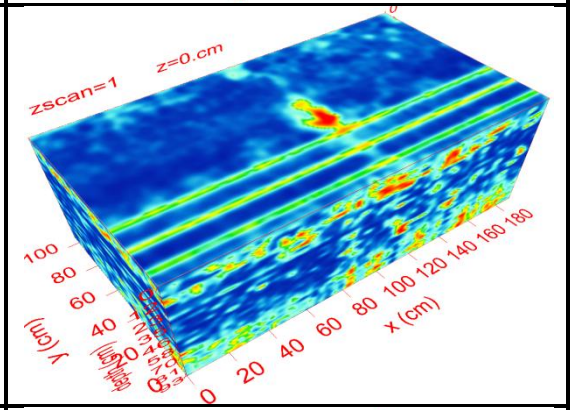
2 and 3	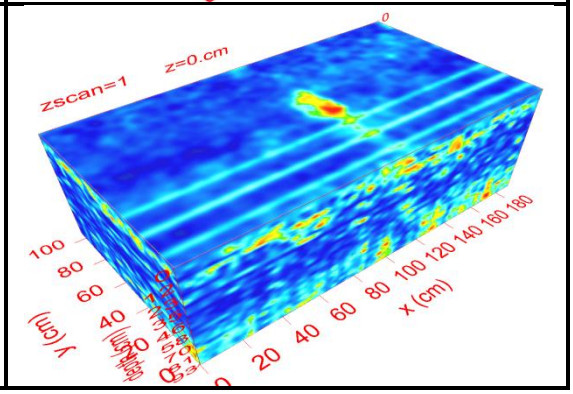

2 and 4	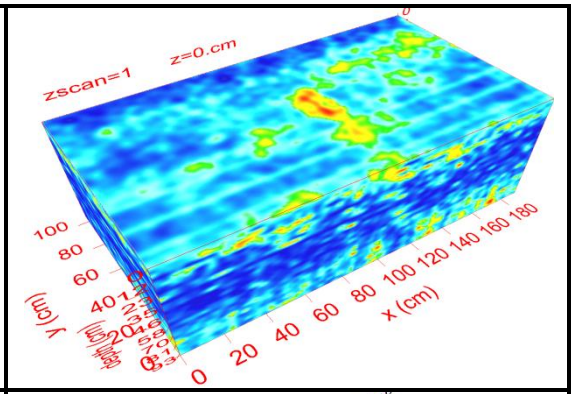
3 and 4	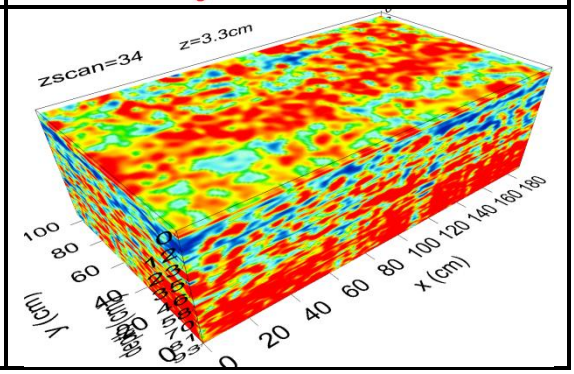

4.5 Effect of processing techniques

To investigate the effect of processing on the acquired data, f-k filtering and the EM wave travel time calculation was considered. The effect of these processing techniques was investigated by processing the raw data.

4.5.1 The f-k filtering

To investigate whether f-k filtering can enhance GPR capabilities of crack detection, data was processed with ReflexW software. The data collected from laboratory as well as from pavements surveying will be investigated to find out the effect of f-k filtering. For the validation of f-k filtering to reveal cracks in GPR-grams, the scan type 1 in Table 4-15 will be filtered for laboratory data whereas for field data, all scans type will be processed.

4.5.1.1 Laboratory testing

Specimen BA with a single crack (3 cm wide and 3 cm deep) shown in Figure 4.1 was surveyed with Aladdin GPR. The raw data obtained was processed by f-k filtering. The results shown in Table 4-21 are based on the investigation for optimum filter parameters. As the filter parameters depend upon many factors, the optimum velocity range (meter/nanoseconds) selection is a challenge. For the results provided in Table 4-21 (1st row-1st column), the velocity range (upper and lower) selected was 009 and 0.001 (positive and negative values) which covered the minimum raw data. By increasing the upper range from 0.009 to 0.03 and decreasing the lower velocity range from 0.1 to 0.09, the crack again did not appear in outcomes provided in Table 4-21 (1st row-2nd column). In the third trial, upper range was decreased to 0.003, whereas lower range was increased to -0.2 which resulted in crack appearance in the GPR-gram Table 4-21 (2nd row-1st column). In the

fourth trial therefore, the same trend was extended further i.e. upper range was decreased and lower range was increased. As can be seen in the outcomes provided in Table 4-21 (2nd row-2nd column), the crack is clearer with a prominent hyperbola. However, at the specimen surface there is noise and therefore, crack's hyperbola is less dominant. In the fifth trial, upper and lower filter ranges are reduced to 0.003 and 0.3. This time the results are promising as only the crack's hyperbola appeared without any noise in the GPR-gram. Although the range selection in f-k filtering is time consuming, the range values can be kept constant for the outcomes from similar setup. It must also be noted that time in f-k filtering is also saved by avoiding standard processing needed for the raw data.

Table 4-21: The f-k filtering applied to 3 cm wide and 3 cm deep crack in specimen "BA"

Velocity ranges (m/ns)	The outcomes	Velocity ranges (m/ns)	The outcomes
-0.009 -0.1 +0.009 +0.1	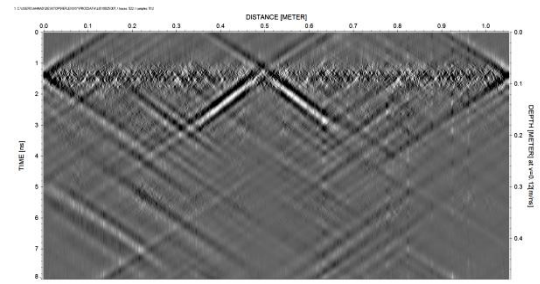	-0.03 -0.09 +0.03 +0.09	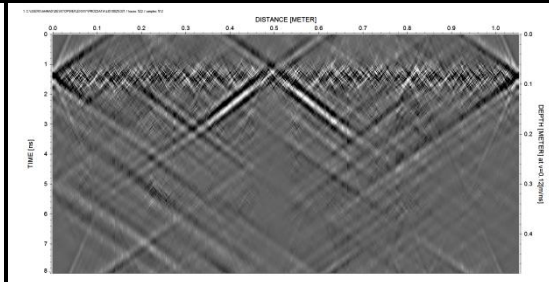
-0.003 -0.2 +0.003 +0.2	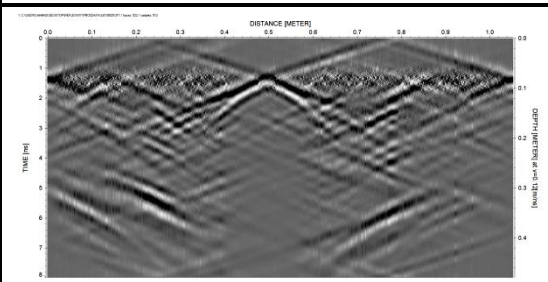	-0.009 -0.9 +0.009 +0.9	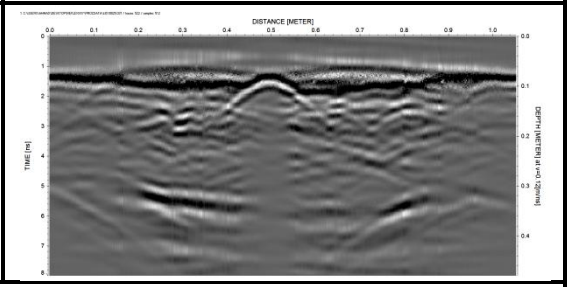
-0.003 -0.3 +0.003 +0.3	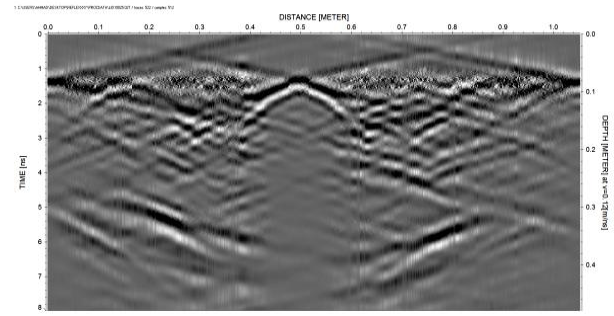		

After gaining confidence from promising f-k filtering results for 3 cm wide and 3 cm deep crack, the efficiency of f-k filtering was investigated on 2 cracks of 1 cm width but with a depth of 1 cm and 3 cm in specimen "BA". The idea was to investigate if f-k filtering can differentiate among the different geometry cracks. The outcomes are shown in Table 4-22. The results presented in Table 4-22 are filtered with the f-k range as was the last case in Table 4-21 (3rd row-2nd column).

Table 4-22: The f-k filtering applied on different geometry cracks of specimen "BA"

Crack	Filter ranges	The outcomes
1 cm wide 1 cm deep	-0.009 -0.3 +0.009 +0.3	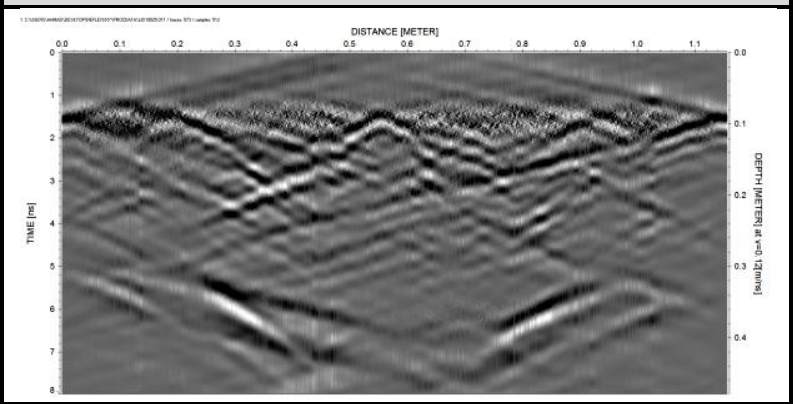
1 cm wide 3 cm deep	-0.009 -0.3 +0.009 +0.3	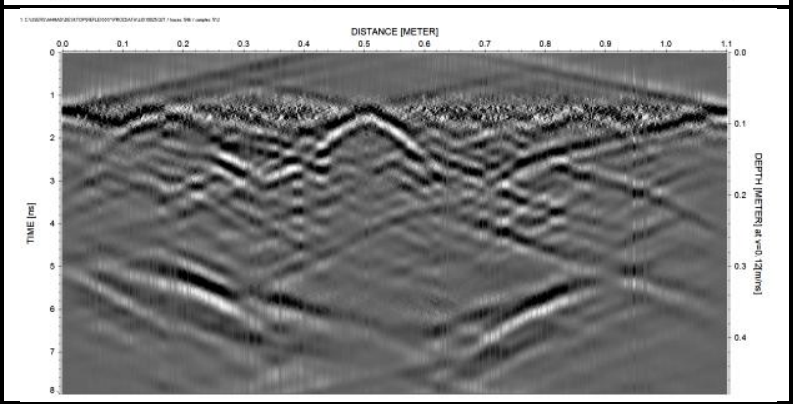
3 cm wide 3 cm deep (outcome from Table 4-21 (3rd row-2nd column)	-0.009 -0.3 +0.009 +0.3	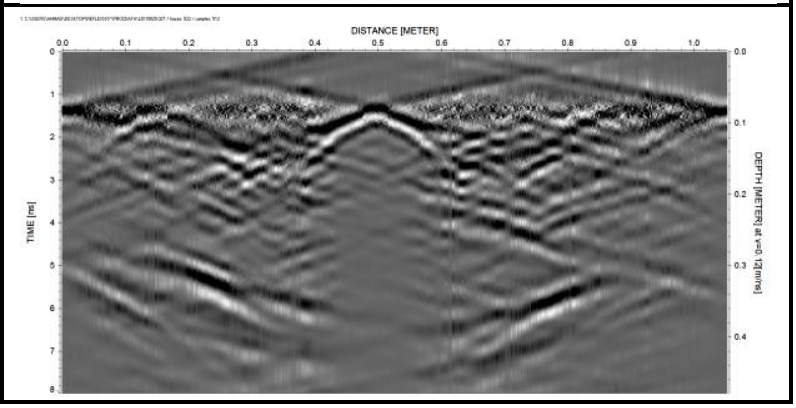

The crack was detected in each case provided in Table 4-22. The noise was removed successfully leaving behind the hyperbola of the crack. In the outcomes, the hyperbola wings are clearer in each case (1 cm and 3 cm deep) making it possible to differentiate among the different geometry cracks. It can be observed that the 1 cm deep crack's

hyperbola wings are not deeper in the GPR-gram compared to 3 cm deep crack. To investigate the effect of crack width, 3 cm wide and 3 cm deep crack outcomes from Table 4-21 (3rd row-2nd column) were compared. It can be seen that due to crack width, the hyperbola in Table 4-22 (3rd row-2nd column) has a flat portion at the top compared to 3 cm deep crack outcomes in Table 4-22 (2nd row-2nd column). It can therefore be concluded that with the help of f-k filtering not only outcomes quality is promising regarding crack detection but also fine details can be highlighted.

4.5.1.2 Field testing

For the field testing, Site D was selected. The crack in the centre of area 1 (Figure 3.22) was surveyed. The antenna configuration was set to 512 samples per scan, 2 mm pulse transmission distance. The crack was scanned from four different angles (Table 4-15). The aim was to investigate effectiveness of f-k filtering for different scans. The crack in GPR-grams is located at 1.1 m (x-axis). The results are shown in Table 4-23. It can be seen that the crack is becoming clearer in the scans 3 and 4. From standard processing of scans 3 and 4, crack was not detected whereas by f-k filtering and the use of colour palette instead of classical gray scale, the scan 4 gave promising results. In scan 1, noise and reflections from materials are masking the crack reflection. However, the scan 4 has least noise and clearer crack due to f-k filtering.

Table 4-23: Crack detection of crack in Area 1 (Site D) by f-k filtering

Scans 1 and 3	Scans 2 and 4
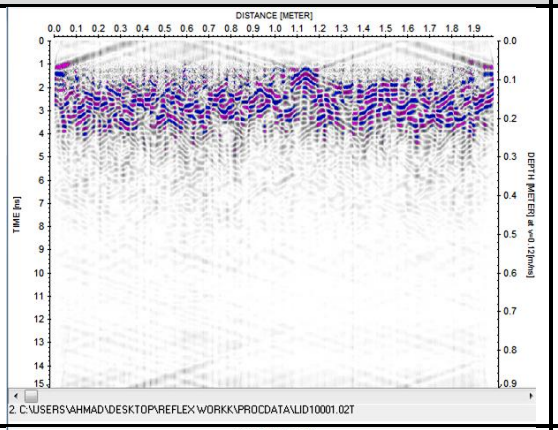	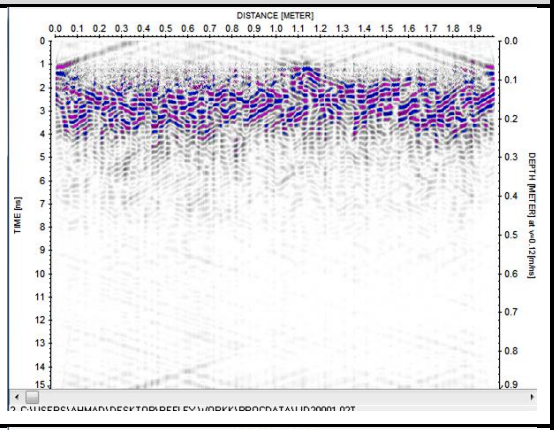
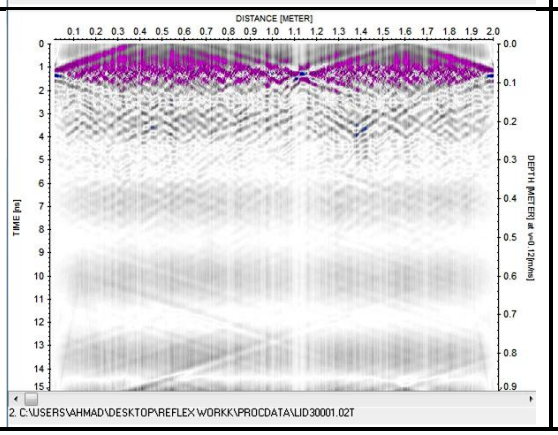	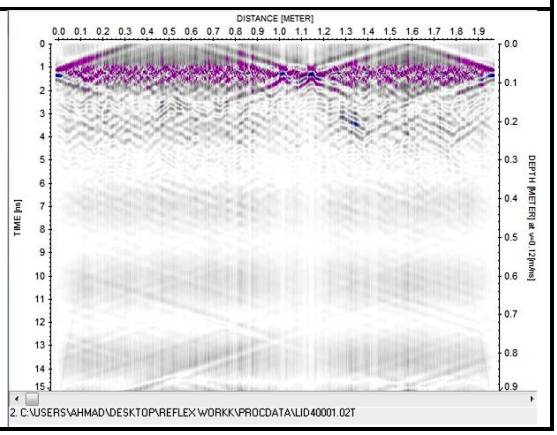

4.5.2 The reflected EM wave's travel time calculation

The construction of GPR-grams is based on collection of EM waves according to their arrival time. Any disruption due to object in EM path will cause delay in travel time of wave by offering longer path for EM wave propagation. This phenomenon is similar when EM wave has to pass through a crack. In case of surface crack, the direct EM waves (referring to earlier Figure 2.16) propagating closer to surface has to pass wider crack portion compared to EM waves propagating deep down in surface. Knowing the amount of delay in arrival of EM waves, crack width can also predicted, subjected to conditions. In this section, aim is to calculate and graphically plot delay in EM wave arrival time such that cracks can be easily and clearly identified.

For this purpose, asphalt specimen BA with a crack dimensions 3 cm x 3 cm was tested with Aladdin GPR. ReflexW software was used to calculate the time delay in arrival of early waves. The process of EM wave's identification is shown in Figure 4.27. The data shown in Figure 4.27 is not processed other than background removal. Four EM waves path are marked in colours whereas crack (3x3 cm^2) is also shown. The wave's paths and waves are named as 1 to 4 according to their position from top. The EM wave from each path is considered and its travel time calculated and matched with crack.

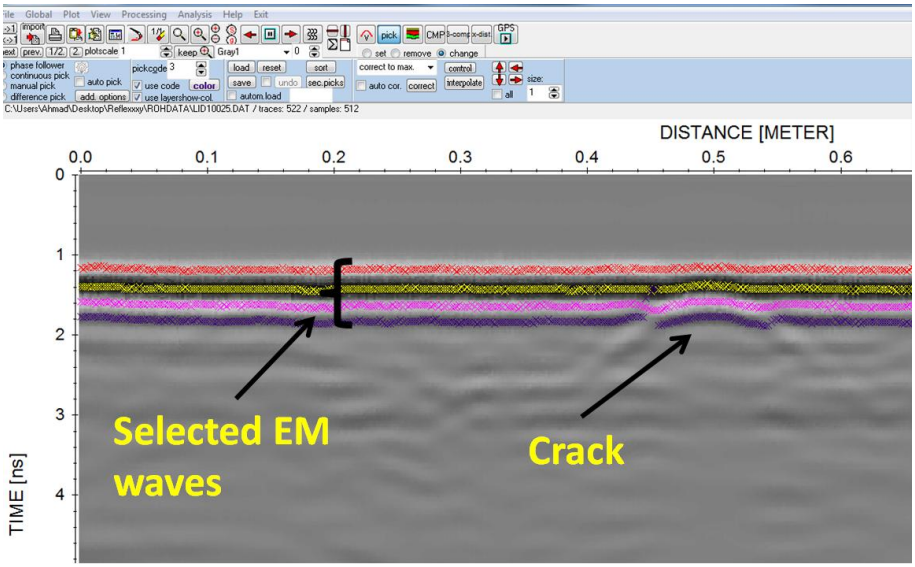

Figure 4.27. Layer picking for travel time calculation of EM waves (ReflexW)

In the ReflexW software, the any selected wave's travel time can be calculated and saved as ASCII file. These ASCII files can be plotted on top of the respective GPR-grams such as shown in Figure 4.28. The time delays and GPR-grams combination helps analyse effectiveness of this technique. For example the travel time calculation in Figure 4.28 shows that there are two different types of materials, other than crack i.e. sand and asphalt.

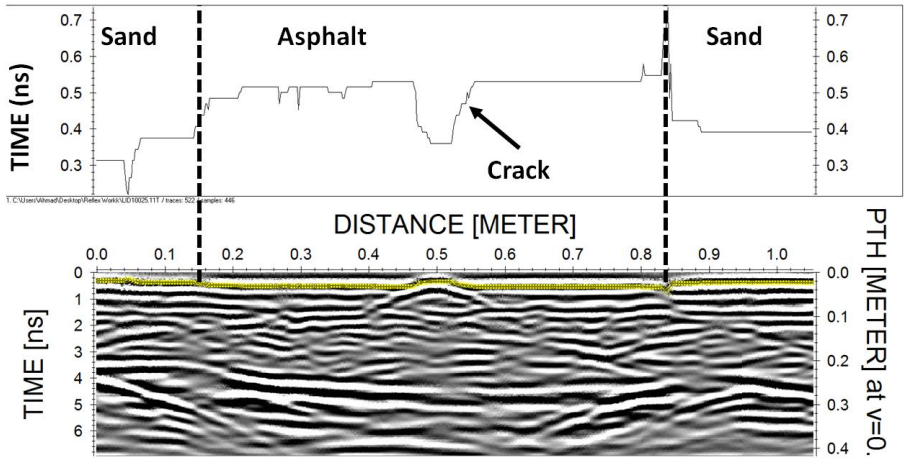

Figure 4.28. Travel time of EM wave on a 3 cm wide and 3 cm deep crack (v = 0.12 meter /nanosecond (m/ns))

The tests in laboratory were performed on specimen "BA". The four Aladdin scans (Table 4-15) collected on 3 x 3 (width x depth) cm^2 crack was selected for the travel time calculations. The propagation velocity of EM wave was selected for asphalt as 0.12 meter/nanosecond. The results are shown in Table 4-24.

Table 4-24: The wave travel time calculation for 3 x 3 (width x depth) cm^2 crack

Scan 1 and 3	Scan 2 and 4
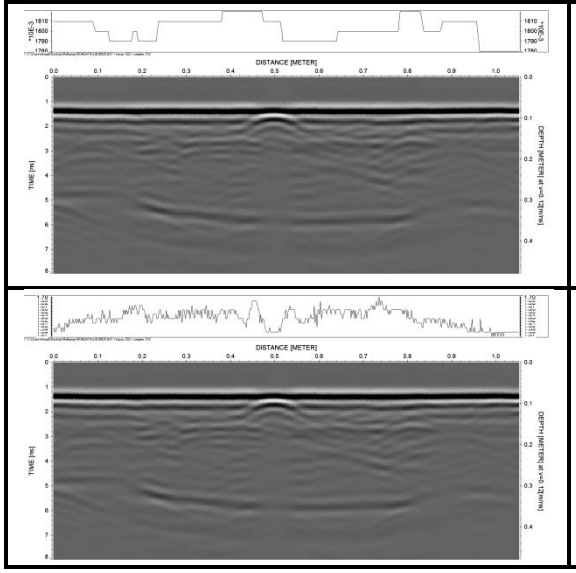	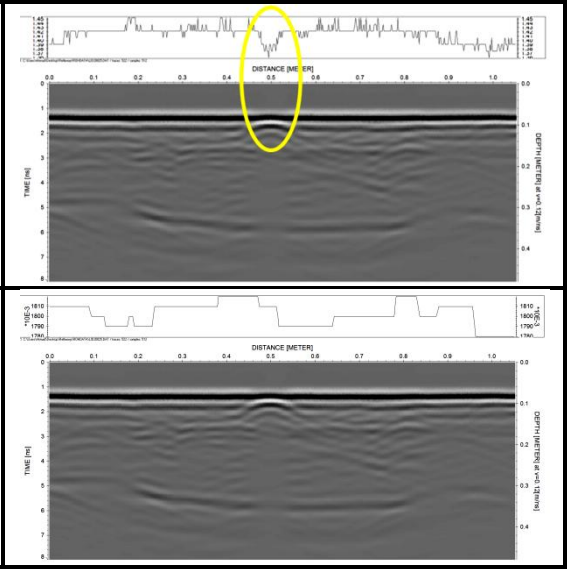

It can be seen that the scan 1 arrival time graph is not logical. There is no significance change in travel time at the crack. On the other hand, scan 2 is more promising. Scan 2 shows a sudden fall (decrease in travel time of EM wave) exactly at the location of crack. Scan 3 is similar to scan 2 however, the travel time of wave is not logical at the start and end of GPR-gram. Scan 4 results were similar to scan 1. To verify the outcomes, more tests were conducted which will follow in the upcoming sections.

To investigate different geometry crack, a 2 cm wide and 3 cm deep crack (specimen BA) was considered for the travel time calculation. The paths 1, 2, 3 and 4 in were considered.

The path 1 was least affected by crack thus is not plotted. The results of paths 2, 3 and 4 are shown in Table 4-25. It can be seen that travel time delay in path 2 is influenced on crack positions despite some side reflections influence at the start and end of GPR-gram. The path 3 has significance change in travel time (more than path 2) at the crack position. The path 4 travel time however, is highly influenced due to crack. Not only the change in EM wave travel time is significance but the noise due to side reflections is reduced.

Table 4-25: The EM wave travel time calculation on a 2 x 3 (width x depth) cm^2 crack

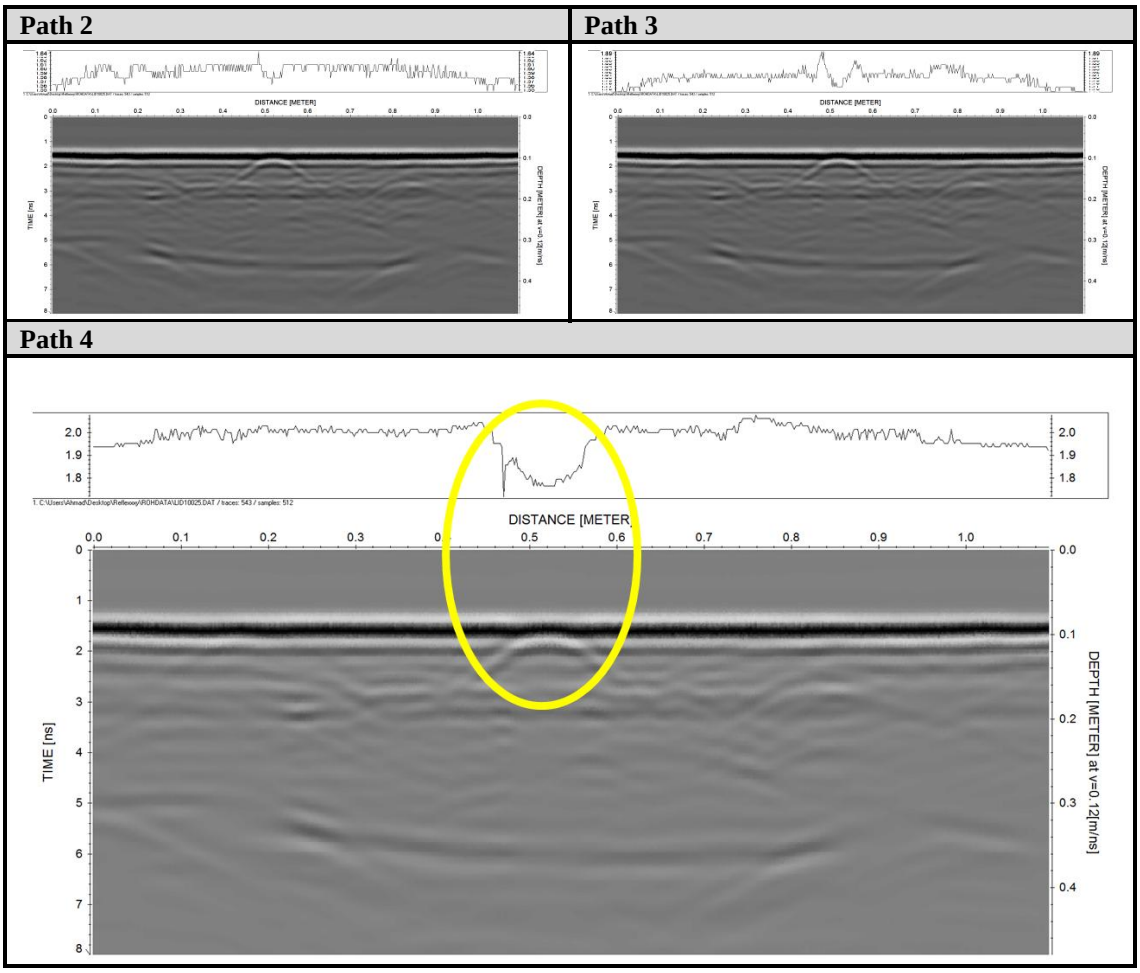

The calculated EM wave travel time data (Table 4-24 and Table 4-25) can also be analysed in other programmes such as Microsoft Excel. For this reason, the data must be saved in ASCII format. The EM wave travel time data on cracks 1 x 1, 1 x 2, 1 x 3, 2 x 3 and 3 x 3 (width x depth) cm^2 in specimen "BA" was calculated. The layer 4 in scan 1 was considered for all cracks. The plotted data is shown in Figure 4.29 where the crack is at ≈ 0.5 m distance.

The travel time (ns) values on y-axis (Figure 4.29) are not real as due to similar time values because of same medium (sand and asphalt) the graphs were overlapping. The aim in Figure 4.29 results is to show the travel time difference of EM wave due to crack and to analyse the impact of crack size on EM wave travel time delay.

It can be seen in the plotted data in Figure 4.29 that travel time of EM wave changes for all cracks except for 1 x 1 (width x depth) cm^2 crack. The change in EM wave travel time increases with increase in crack's volume i.e. either width or depth. The change in travel time due to crack increases for 1 x 2, 1 x 3, 2 x 3 and 3 x 3 (width x depth) cracks respectively.

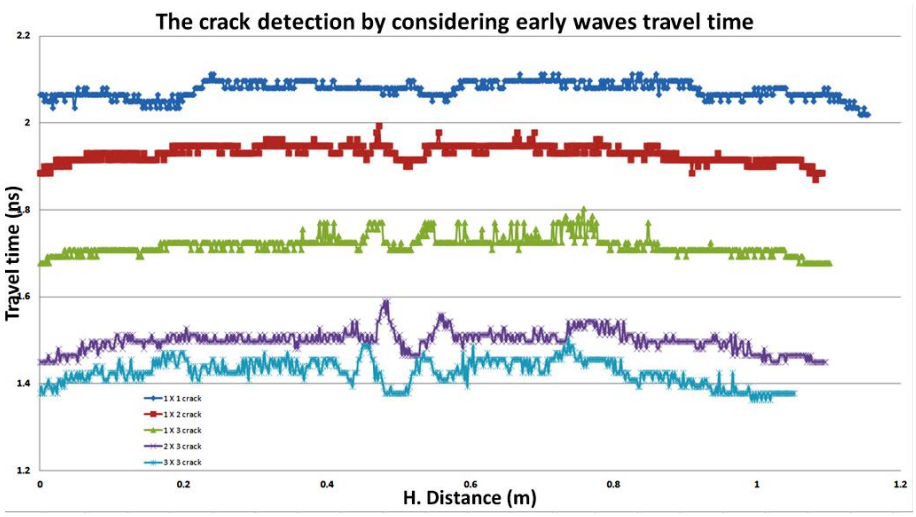

Figure 4.29. EM waves travel time calculated on different cracks (ReflexW)

The advantage of this technique is time saving as in this method raw data without standard processing is used. Despite promising results, this method however needs to be further investigated.

4.6 Summary

In this section GPR abilities for crack detection were investigated. Asphalt specimens of specific asphalt mix types were prepared. The asphalt specimens were cut to simulate cracks. GPR was used to study detection of crack, its width and its depth. The parameters influencing GPR ability for crack detection were studied in detail. The identified parameters were divided into three categories i.e. material, system hardware and data processing techniques. To find out material related influences on GPR outcomes, different geometries of cracks were investigated. The cracks were filled with different materials to study the crack filling material effect on survey outcomes. For the investigation of hardware related issues, different GPR systems were comparatively used. It was observed that cracks with increased volume have good chance to be detected by GPR. In addition the crack filling material with a dielectric constant value close to the asphalt dielectric value like bitumen or sand decreases crack detection chances. Hardware with increased bandwidth has high capabilities even for detection of fine cracks. The material and hardware related outcomes were finally validated on asphalt pavements. F-k filtering and time delay methods were applied to crack survey data. The outcomes were compared to that of standard processed data. It is concluded that the processing techniques such as f-k

filtering has abilities to minimise the noise in data and highlight fine details. Also the calculation of reflected EM wave time delay can be helpful to use GPR for crack detection.

5 Conclusions

5.1 General

This research work was aimed to investigate the abilities of GPR to be used as crack investigation tool in asphalt pavements. However, there were certain challenges identified to be overcome before GPR can be deployed. These challenges include the general question if GPR can detect a crack although it can detect foreign objects in mediums. And if yes, are there any parameters to be considered for crack detection. The past literature suggests that GPR outcomes are influenced by hardware characteristics, software attributes, material electromagnetic properties, crack characteristics and environmental factors. On the other hand, the GPR technique of functioning itself plays a vital role when it comes to GPR effectiveness for crack detection. However, past literature study reveals that documentation on these parameters affecting GPR abilities is missing. The parameters relating GPR abilities have been though individually studied but no any document contains their effect of these parameters on GPR abilities together. Also GPR abilities for cracking source investigation have never been explored. Therefore, this research work was carried out utilizing sophisticated GPR systems and software on pavements and laboratory specially to investigate the limitations hindering GPR use for crack detection in asphalt pavements. Moreover, GPR effectiveness for cracking sources evaluation is also investigated. In the following sections, the outcomes of this study are presented.

5.2 The crack geometry

From the laboratory and field investigations, it can be concluded that the crack depth and width have a great influence on GPR properties of crack detection. The increase in crack volume either by increase in depth or width enhanced chances of crack detection by the GPR. With the help of 2 GHz central frequency GPR system, 2 mm wide and 5 mm deep crack were detected. On the other hand, the crack geometry according to EM wave propagation direction had a great influence on GPR outcomes. The likelihood of crack detection was increased by scanning the crack from an angle so that the EM wave propagates more in the crack.

The GPR successfully differentiated among the different geometry cracks. The wider and deeper cracks had different hyperbolas in the GPR-grams which are easily readable. The increase in crack width resulted in solid hyperbolas with increased intensity. On the other hand, the increase in crack depth resulted in hyperbolas with deeper spans in GPR-grams. Although it was possible to distinguish among cracks of different geometries, the measurement of crack depth and width from GPR-grams resulted in inauspicious outcomes. The GPR abilities regarding crack depth and width measurement should be therefore further investigated.

5.3 The GPR system properties

To investigate the effect of GPR attributes on its abilities of crack detection, different hi-tech systems were deployed for testing. In this research, GPR systems from a frequency range of 250 MHz to 3000 MHz were tested. Based on the laboratory and tests on pavements, the following can be concluded:

1) Frequency antennas in the range of 1500 to 2000 MHz have more promising results in crack detection compared to 2300 to 2600 MHz frequency antennas. The resolution of outcomes was decreased however; crack was prominent in the GPR-grams. There are however, other characteristics of antenna such as its footprint, UWB, etc. which should be taken into consideration.
2) GPR crack detection abilities may not be judged only based on its central frequency. There are other properties of system for example data acquiring and saving techniques, etc. which may not necessary be accessible to the user.
3) The frequency higher than 2 GHz results in better resolution thus thereby making GPR-grams understandable. The higher resolution GPR-grams needs less processing which saves time and the risk of data damage by processing is decreased. However, for crack detection frequency range between 700 and 2000 MHz is recommended.
4) The increase in bandwidth increases the chances to detect fine as well as major cracks by GPR. The increased bandwidth of GPR provides better results in measuring crack geometry. Also the increased bandwidth helps to investigate cracks related to asphalt and un-bound layers.
5) Based on the outcomes, it is recommended to deploy 2 GHz central frequency antenna for 2 mm wide cracks on asphalt pavements.

5.4 The GPR surveying effects

The GPR survey type in regard of 2-D and 3-D influenced outcomes significantly. The 2D survey consuming less time could detect cracks with less accuracy. Also the GPR data needed multiple iterations of processing step till optimum outcomes. Moreover, the 2-D survey is highly dependent on crack formation and geometry. This is because in 2-D survey the EM pulse is induced after regular intervals. In this research, 2 mm wide cracks were successfully detected with a scan distance (EM pulse repetition) of 2 mm. However, when scan distance is larger than the crack width, chances are that crack may not appear in the GPR-gram. Therefore, it is recommended that for repeatability of outcomes and better chances of crack detection, the pulse repetition frequency must not be less than the crack width.

On the other hand the 3-D survey results were promising. In 3-D outcomes crack and its sources can be investigated by viewing GPR-gram from many angles and cross-sections. Also scan distance do not influence the outcomes. Therefore, 3-D survey facilitates the crack investigations by GPR. The time consumption in 3-D survey is relatively higher which can be reduced by deploying many antennas at the same time.

The increase in number of samples per scan does not increase the chances of crack detection in GPR outcomes. Moreover, the time consumption increases in case of surveying with increased number of scans. The outcomes of 512 samples per scan were found optimum for crack detection survey.
The effect of crack and EM wave propagation direction was substantial on GPR outcomes. The EM wave propagation direction in case of pavement is almost constant whereas the crack geometry can be varying. However with certain manoeuvres, crack can be scanned from optimum angle so that EM wave propagates for longer time in the cracks. In this research, dipole antennas proved to be better solution for this shortcoming.

5.5 The processing technique effects

The data processing techniques (other than standard) investigated were f-k filtering and time delay calculation techniques. Although the standard processing steps highlight the information in GPR data, these two aforementioned techniques were found promising for crack detection. The benefit of the two methods is that standard processing steps are not required and time is saved. The f-k filtering proved to be useful for removing the noise from GPR data and highlight the cracks profoundly. However, the f-k filtering is technical and section of optimum ranges for filtering is time consuming. Furthermore, the f-k filtering proved itself to be useful for small distances.
On the other hand calculating delay in reflected wave arrival called the time delay technique was found helpful in detecting fine cracks which may not be detected otherwise. The influence of EM wave scattering from pavement surface and other objects, masking crack in the GPR-grams; was also observed. Additionally, the time delay presentation in graphics together with GPR-grams helped in better understanding of outcomes. A combination of time delay technique with any automatic time picking software may result in automatic crack detection by GPR. The limitation of time delay method is that it is not recommended for bottom-up crack detection.

5.6 Material electromagnetic properties

The material properties either of asphalt or crack fill influences GPR outcomes. In this research, the crack filling material's die- electrical property with regard to asphalt was investigated in light of crack detection. The asphalt material electrical properties were varied by preparing specimens from different asphalt mixtures, having different physical compositions. The crack fill materials exclusively investigated in this research work were air, bitumen, sand and water. It was found that sand and bitumen as crack fill resulted to be least helpful for crack detection. On the other hand water and air proved to be the best suited crack fills for crack investigation with GPR. Therefore, bottom-up cracks due to air or water as crack fill have better chances of detection by GPR.
Investigations were carried out to find the temperature influence on GPR outcomes. It was revealed by testing on asphalt pavements that although cracks have their maximum width in winter, the surveys carried out in summer have the best results. The quality of crack

detection increased with increase in temperature. This conclusion is however restricted to sand-clay crack fill up to a temperature range of 12^{o} C to 16^{o} C.

5.7 The crack cause investigation

The investigations carried out on asphalt pavements proved GPR as a promising tool for crack source detection. The crack causes included support loss and layer anomaly were successfully analysed with the help of GPR. One pavement section had uneven wearing course as well as support loss from unbound layers. The GPR measured the anomaly in wearing course to ±1cm accuracy. The 3-D investigations proved to be best for support loss investigations. This is because support loss can be anywhere in the pavement.

5.8 Practical implications

The outcomes of this research work brought forward GPR abilities as a crack investigation tool which will surely broaden GPR use. This study not only investigated the above mentioned GPR ability but also it's influencing factors. If these parameters for example, GPR system properties, temperature, crack-filing material, etc. are considered properly, GPR survey accuracy could be improved. This will not only make possible real time authentic results but also a lot of money and time could be saved. The following outcomes of this research are worth to mention in this regard,

1. GPR can investigate cracks irrespective of asphalt mix and pavement thickness. During this study, GPR was used on Autobahn A-2 where decades old Asphalt layers comprised >50 cm thick pavement. However, cracks including top-down and bottom-up were successfully investigated.
2. Crack investigation with GPR might be useful on sections where traffic flow interruption is unavoidable, e.g. in tunnels and busy highways. In this research work, 6 motorway sections including a 400 meter long section were investigated within two hours.
3. The crack filling materials affects GPR outcomes and there are methods to overcome this issue.
4. Effect of temperature on crack investigation can be minimised if optimum temperature range is considered.
5. For fine details e.g. crack location and its geometry investigation, 3-D survey is recommended, although it takes more time compared to 2-D survey.
6. GPR configuration such as scans per horizontal length, samples per scan, etc. must be selected according to each new survey. Desirable and authentic results heavily depend on GPR system configuration.
7. The data processing time can be reduced by considering sophisticated processing techniques such as f-k filtering and time delay methods. However, these techniques are not user friendly.

6 References

Ahmad, N., Lorenzl, H. and Wistuba, M. 2011. Crack detection in Asphalt Pavements: How useful is the GPR? 6th International Workshop on Advanced Ground Penetrating Radar (IWAGPR) 22-24 June, 2011, Aachen, Germany. Publisher: The Institute of Electrical and Electronics Engineers (IEEE).

Ahmad, N., Wistuba, M. and Lorenzl, H. 2012. GPR as a crack detection tool for asphalt pavements, possibilities and limitations. The 14th International Conference on Ground Penetrating Radar, 4-8 June 2012, Shanghai, China. Publisher: The Institute of Electrical and Electronics Engineers (IEEE), 551 - 555.

AI-Qadi, I., Lahouar, S., Jiang, K., McGhee, K. K. and Mokarem, D. 2005a. Accuracy of Ground Penetrating Radar for Estimating Rigid and Flexible Pavement Layer Thicknesses, Transportation Research Record: Journal of the Transportation Research Board, No. 1940, Transportation Research Board of the National Academies, Washington, D.C., 2005b, 69-78.

Al-Qadi, I. L. and Lahouar, S. 2005b. Measuring layer thicknesses with GPR – Theory to practice. Construction and Building Materials, Volume 19, 763–772.

Al-Qadi, I., Buttler, W. G., Baek, J. and Kim, M. 2009. Cost Effectiveness and Performance of Overlay System in Illinois, Vol. 1: Effectiveness Assessment of HMA Overlay Interlayer System Used to Retard Reflective Cracking, Research Report: ICT-09-044, Illinois Center for Transportation, Illinois.

Al-Qadi, I., Leng, Z., Lahouar, S., and Baek, J. 2010. In-place Hot-Mix Asphalt Density Estimation Using Ground Penetrating Radar. Paper Number 10-1735, Transportation Research Board, 89th Annual Meeting, January 10-14, 2010, Washington, D.C.

Annan, A. P. 2004. GPR-Principles, Procedures & Applications. Sensors and Software, Mississauga, Canada.

Annan, A. P. 2009. Electromagnetic principles of GPR. In: Ground Penetrating Radar: Theory and Applications. 1st edition, Elsevier Science, Amsterdam.

Asphalt Institute. 1989. MS-4, The Asphalt Handbook, 1989, Lexington(Kentucky).

Asphalt-StB, Teil 33. 2010. Asphalt – Prüfung - TP Asphalt-StB – Teil 33: Herstellung von Asphaltprobeplatten, die Forschungsgesellschaft für Straßen- und Verkehrswesen (FGSV), Germany.

Balanis, C. A. 1997. Antenna theory - Design and Analysis. 2nd edition, John Wiley & Sons Inc. New York.

Boll, J., van Rijn, R. P. G., Weiler, K. W., and Ewen, J. A. (1996). Using ground-penetratingradar to detect layers in a sandy field soil. Geoderma, 70 (2-4):117–132.

Braun, E. 1991. Bitumen. 2., überarbeitete und erweiterte Auflage, Verlagsgesellschaft Rudolf Müller GmbH, Köln. ISBN: 3-481-00274-2.

Bristow, C. S. and Jol, H. M. 2003. Ground Penetrating Radar in Sediments. Special Publications, Geological Society, London.

Bristow, C. 2009. Ground Penetrating Radar in Aeolian Dune Sands. In: Ground Penetrating Radar: Theory and Applications. 1st edition, Elsevier Science, Amsterdam.

Cassidy, N. J. 2009a. Electrical and Magnetic Properties of Rocks, Soils and Fluids. In: Ground Penetrating Radar: Theory and Applications. 1st edition, Elsevier Science, Amsterdam.

Cassidy, N. J. 2009b. Ground Penetrating Radar Data Processing, Modelling and Analysis. In: Ground Penetrating Radar: Theory and Applications. 1st edition, Elsevier Science, Amsterdam.

Chang C. -M., Chen, J. -S. and Wu, T. -B. (2011). Dielectric Modeling of Asphalt Mixtures and Relationship with Density [Journal] // Journal of Transportation Engineering. - [s.l.] : ASCE, 2011. - 2 : Vol. 137. - 1943-5436.

Chen, D. H. and Won, M. 2007. Field Investigations of Cracking on Concrete Pavements. Journal of Performance of Constructed Facilities, Vol. 21, No. 6, December 1, 2007. DOI: 10.1061/(ASCE)0887-3828(2007)21:6(450).

Conyers, L. B. 2004. Ground-Penetrating Radar for Archaeology. Volume 1, AltaMira Press, Walnut Creek, California.

Daniels, D. J. 1996. Surface penetrating radar. Electronics & Communication Engineering journal August 1996, 165-182.

Daniels, D. J. 2004. Ground Penetrating Radar. 2nd ed. Published by: The Institution of Electrical Engineers, London, United Kingdom, 1-723

Daniels, D. J. 2007. Ground Penetrating Radar Fundamentals. 2nd edition, Institution of Engineering and Technology, London.

Daniels, D. J. 2009. Antennas. In: Ground Penetrating Radar: Theory and Applications. 1st edition, Elsevier Science, Amsterdam.

Davis, J. L. and Annan, A. P. 1989. Ground-Penetrating Radar for High-Resolution mapping of Soil and Rock Stratigraphy. Geophysical Prospecting, Volume 37, 531-551.

Diamanti, N. and Redman, D. 2012. Field observations and numerical models of GPR response from vertical pavement cracks. Journal of Applied Geophysics 81, 106-116. DOI:10.1016/j.jappgeo.2011.09.006.

Evans, R. D., Forest, M. W., Dixon, N. and Stonecliffe-Jones, M. 2008. The response of ground penetrating radar (GPR) to changes in temperature and moisture condition of pavement materials. IN: Proceedings of the 1st International Conference on Transportation Geotechnics, 25th -27th August 2008, Nottingham, UK.

Forest, R. and Utsi, V. 2004. Non destructive crack depth measurements with Ground Penetrating Radar. 10th International Conference on Ground Penetrating Radar, 21-24 June, 2004, Delft, the Netherland, 799-802.

Ghazanfari, E., Pamukcu, S., Yoon, S., Suleiman, M. T. and Cheng, L. 2012. Geotechnical sensing using electromagnetic attenuation between radio transceivers. Smart Materials and Structures, Volume 21, September 2012, 1-12. DOI:10.1088/0964-1726/21/12/125017

Harari, Z. 1996. Ground-penetrating radar (GPR) for imaging stratigraphic features and groundwater in sand dunes. Journal of Applied Geophysics. Volume 36, 43-52.

Hugenschmidt, J., Partl, M. N. and de Witte, H. 1998. GPR inspection of a mountain motorway in Switzerland. Journal of Applied Geophysics, Volume 40, 95-104.

Hugenschmidt, J. 2009. Zusammenhang zwischen dielektrischen Eigenschaften und Zustandsmerkmalen von bitumenhaltigen Fahrbahnbelägen (Pilotuntersuchung). Forschungsauftrag VSS 2005/701 auf Antrag des Schweizerischen Verbandes der Strassen- und Verkehrsfachleute (VSS) – 1265, 1-62.

Huisman, J. A., Hubbard, S.S., Redman, J. D. and Annan, A. P. 2003. Measuring Soil Water Content with Ground Penetrating Radar: A Review. Soil Science Society of America, Vadose Zone Journal, Volume 2, 476-491.

Jaselskis, E. J., Grigas, J. and Brilingas., A. 2003. Dielectric Properties of Asphalt Pavement. Journal of Materials in Civil Engineering, Vol. 15, No. 5, 427-434. DOI: 10.1061/(ASCE)0899-1561(2003)15:5(427).

Koppenjan, S. 2009. Ground Penetrating Radar Systems and Design. In: Ground Penetrating Radar: Theory and Applications. 1st edition, Elsevier Science, Amsterdam.

Lahouar, S. 2003. Development of Data Analysis Algorithms for Interpretation of Ground Penetrating Radar Data. Ph.D. Dissertation, Faculty of the Virginia Polytechnic Institute and State University, Blacksburg, Virginia.

Leckebusch, J. 2011. Comparison of a Stepped-Frequency ContinuousWave and a Pulsed GPR System. Archaeological Prospect, Volume 18, 15-25. DOI: 10.1002/arp.396.

Leng, Z., Al-Qadi, I. and Lahouar, S. 2011. Development and validation for in situ asphalt mixture density prediction models. NDT&E International, Volume 44, 369–375.

Liu, W. and Scullion, T. 2006. Integrating Deflection and Ground Penetrating radar Data for Pavement Evaluation. Project report - FHWA/TX-06/0-4495-1, Texas Transportation Institute, Texas.

Loizos, A. and Plati, C. 2007. Accuracy of pavement thicknesses estimation using different Ground Penetrating Radar analysis approaches. NDT & E International, Volume 40, 147-157

Loizos, A. and Plati, C. 2010. Ground penetrating radar as an engineering diagnostic tool for foamed asphalt treated pavement layers. International Journal of Pavement Engineering, Volume 8(2), 147-155. DOI: 10.1080/10298430601149528.

Manuel, C., Mejia, D., Ertem, S., Nazarian, S., Rao, C., Von Quintus, H., Shokouhi, P., 2010. Evaluation of NDT technologies to access presence and extent of delamination of HMA Airfield pavements. AAPTP research Project 06-04/Airfield Asphalt Pavement Technology Program. Federal Aviation Administration , Texas, 2010. PP 1-132.

Maser, K. R. 2003. Non-Destructive Measurement of Pavement Layer Thickness. Final Report FHWA/CA/OR-2003/03, California Department of Transportation, California.

Molinda, G. M., Monaghan, W. D., Mowrey, G. L. and Persetic, G. F. 1996. Using Ground Penetrating Radar for Roof Hazard Detection in Underground Mines. Report-9625, United States Department of Energy, Pittsburgh Research Center, the USA.

Morey, R. M. 1998. Synthesis of Highway Practice 255: Ground Penetrating Radar for Evaluating Subsurface Conditions for Transportation Facilities. National cooperative Highway Research Program, Washington, D. C. 20418.

MS-4 The Asphalt Handbook [Book]. - P.O. Box 14052, Lexington : Asphalt Institute, 1989. - 1989 : Vol. 4.

Olhoeft, G. R. 1999. Applications and frustrations in using Ground Penetrating Radar. Proceedings Ultra Wideband Conference, 20-22 September 1999 Washington, DC.

Orlando, L. and Slob, E. 2009. Using multicomponent GPR to monitor cracks in a historical building. Journal of Applied Geophysics, Volume 67, 327-334.

Papagiannakis, A. T., and Masad, E. A. 2008. Pavement Design and Materials. 1st edition, Wiley & Sons, Hoboken, New Jersey, USA.

Pearce, J. and Mittleman, D. 2002. Defining the Fresnel zone for broadband radiation. Journal of Physical Review, Volume 66. DOI: 10.1103/PhysRevE.66.056602.

Perez-Gracia, V., Gonzalez-Drigo, R. and Capua, D. D. 2008. Horizontal resolution in a non-destructive shallow GPR survey: An experimental evaluation. NDT&E International, Volume 41, 611-620. DOI:10.1016/j.ndteint.2008.06.002.

Ranalli, D., Scozzafava, M., Tallini, M. and Colagrande, S. 2007. GPR signal attenuation vs. depth on damaged flexible road pavements. Proceedings of the 4th International Workshop on Advanced Ground Penetrating Radar IWAGPR; 2007, Naples, Italy.

Saarenketo, T. 1998. Electrical properties of water in clay and silty soils. Journal of Applied Geophysics, Volume 40, 73-88.

Saarenketo, T. 2006. Electrical Properties of Road materials and Subgrade Soils and the Use of Ground Penetration Radar in Traffic Infrastructure Surveys. PhD thesis, Faculty of Science, Department of Geosciences, University of Oulu.

Saarenketo, T. 2009. NDT Transportation. In: Ground Penetrating Radar: Theory and Applications. 1st edition, Elsevier Science, Amsterdam.

Skolnik, M. I. 1981. Introduction to Radar Systems. 2nd edition, McGraw-Hill Book Company, Singapore

Toshioka, T., Tsuchida, T. and Sasahara, K. 1995. Application of GPR to detecting and mapping cracks in rock slopes. Journal of Applied Geophysics, Volume 33, 119-124.

Ulriksen, C. P. F. 1982. Application of Impulse radar to civil engineering. Doctoral thesis, Department of Engineering Geology, Lund University of Technology, Lund.

Utsi, E., Birtwisle, A. and Cook, J. 2008. Detection of Subsurface Reflective Cracking Using GPR. Proceedings of 12th International Conference on Structural Faults & Repair, 10-12 June, 2008, Edinburgh, 74-83.

Van Wijk, A. J., Harvey J. and Hartman A.M. 2007. Assessing Material Properties for Pavement Rehabilitation Design. Proceedings of the 9th Conference on Asphalt Pavements for Southern Africa, 2-5 September 2007, Gaborone, Botswana.

Wimsatt, A., Scullion, T., Ragsdale, J. and Servos, S. 1998. The Use of Ground Penetrating Radar in Pavement Rehabilitation Strategy Selection and Pavement Condition Assessment. Proceedings of Structural Materials Technology III: An NDT Conference, Volume 3400, March 31, 1998, San Antonio, Texas.

Yelf, R. and Yelf, D. 2006. Where is True Time Zero? Electromagnetic Phenomena, March.7, 2006, 158-163.

Appendix: Support loss investigation through GPR

I. Introduction

Variations in the thickness of pavement layers or sub-grade settlement or both are main source for cracking in asphalt pavements. As in this study cracked pavement sites were considered, GPR abilities were tested to find out the cracking causes at these sites. The sources of cracking were investigated for the pavement Sites "C" and "D", described in Section 3.5. GPR surveys were carried out in form of 2-D and 3-D investigate. The outcomes of the GPR tests were later confirmed by pavement coring.

II. Layer's thickness variation investigation

To investigate the variation in pavement's layers thickness, estimated dielectric values were used in data processing. The variations in layers thickness were studied by observing deflections in the layers profile in GPR-grams. Position of layer in the pavement structure was validation by core samples extracted from selected pavement locations. Details of investigations are provided in the following sections.

II.I. Site C (Holzweg)

At site C, a crack at 46 meter location was investigated to find out reason for its cracking. The crack had maximum width at pavement side A. The objectives of GPR surveying were to identify the reason for pavement cracking and the varying width of crack across pavement cross-section. The crack was first tested with Aladdin and later with GeoScope system. In the first phase, 2-D survey was carried out with Aladdin system. The survey was conducted in the direction of moving away from Cremlingen village i.e. station 0 towards station 50 meters. The survey was conducted in the centre of pavement and at the end of investigations; a core sample was taken from the pavement centre at 46 meter as is shown in Figure A. 1(a). With Aladdin system, the pavement up to a depth of 50 cm was investigated. The results are shown in Figure A. 1(b).

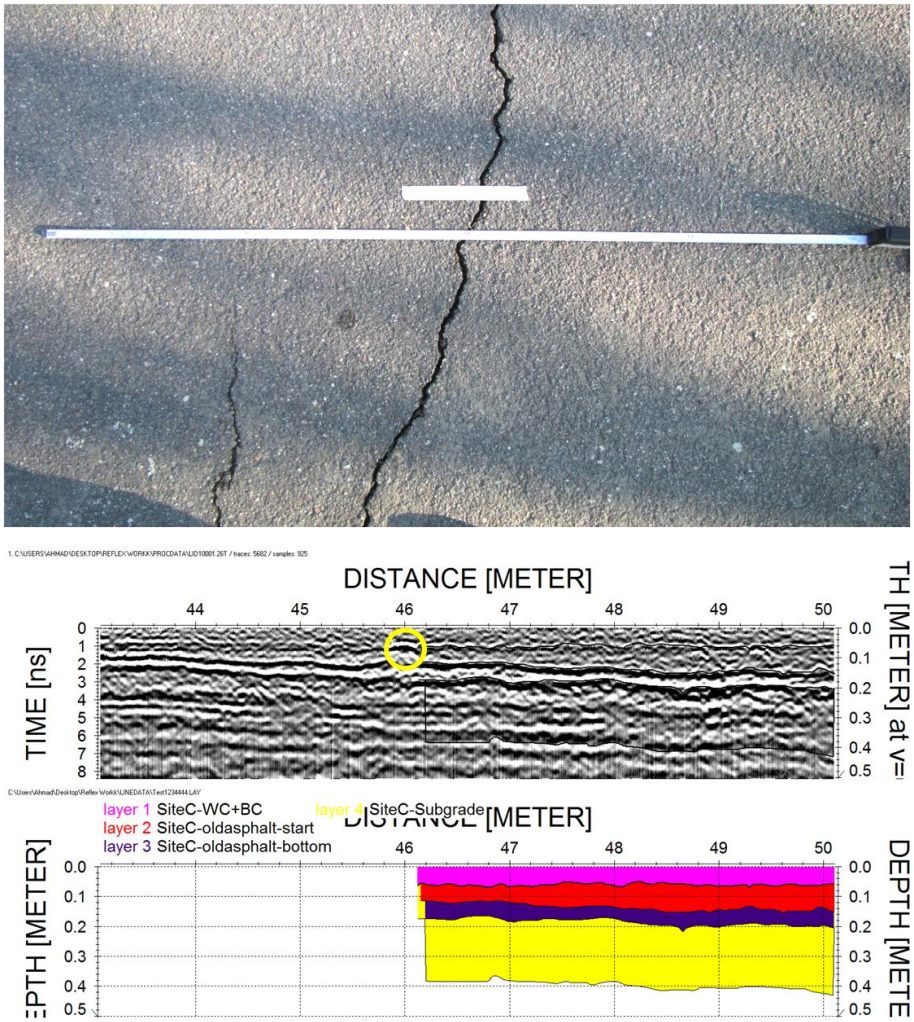

Figure A. 1. Pavement layers thickness anomaly analysis on Section C with Aladdin (EM wave velocity = 0.12 m/ns), (a) GPR-gram of crack at a position of 46 meter (ReflexW), (b) layer report (ReflexW)

The survey with Aladdin system was configured to 512 samples per scan with a scan distance of 4 mm. The results shown in Figure A. 1(b-top) are processed with ReflexW software. The processing techniques included standard background removal, static correction and vertical gain. The processing steps were standard except the vertical gain for which variable values were used. For the static correction, first negative wave peak was taken as layer's interface. As shown in GPR-gram of Figure A. 1(b-top), the layers at different depth in pavement can be well differentiated from one another. The crack bottom (encircled in yellow) in asphalt layers, could also be successfully detected. Although at this stage it was difficult to define layer type and material, it was confirmed that the layers have increased depth in the direction of travel. The first 10 cm asphalt layers i.e. wearing course and base course at the top have however, constant thickness. Also at a depth of 15-20 cm, there is a strong reflection which confirmed presence of different material than its surroundings i.e. a material with higher dielectric constant. At this investigation level, it was confirmed that the cracking in pavement was due to layers settlement in the direction of travel.

To have a better representation of layers shown in GPR-grams, a new method was developed with the help of ReflexW software developers. In this technique, layers in any GPR-gram could be picked and plotted graphically. The benefit of this technique was better understanding of layer by the users who have less understanding of GPR-grams. The layers in GPR-gram shown in Figure A. 1(b-top) are plotted in Figure A. 1(b-bottom). The depth of plotted layers (Figure A. 1 (b-bottom)) in pavement structure is approximated i.e. EM wave velocity = 0.12 m/ns. In the graphically represented layers (Figure A. 1 (b-bottom)), the change in pavement layers thickness is clearer due to horizontal scales compared to GPR-gram. Description of layer and their colours is provided in the legend. The layers settlement in the range of 15-20 cm depth is clearer in the graphically represented GPR-gram. Although it was certain that layers settlement contributed to pavement cracking, the reason for varying crack across pavement width was still not known. Thus further surveying was decided however, this time by 3-D surveying technique for which GeoScope system was selected.

The raw data from GeoScope system was processed with 3dr-Examinar software and a depth of 50 cm was analysed. By means of 3-D survey data, it was possible to differentiate among wearing course (2 cm) and the base course (4 cm). The outcomes of the surveying are presented in Figure A. 2. In Figure A. 2(a), the layers are marked with numbers. The number 1, 2, 3, 4 and 5 represent wearing course, base course, start of foreign material layer, end of foreign material layer and the sub-grade. The foreign material layer is clearer in the GPR-gram with a consolidation at 47 meter location. The results of outcomes thus confirmed previous outcomes shown in Figure A. 1.

To investigate the reason for varying crack depth across pavement width, a cross-section of pavement width was taken from the point where blue cursor is placed in Figure A. 2(a). The GPR-gram Figure A. 2(b) is across pavement width (transversal) with pavement crown right in the middle of GPR-gram. The position of pavement core, which was taken after surveying, is also shown. Furthermore, it can be seen in Figure A. 2(b) that there is layer delamination between wearing course and the asphalt base course at a depth of approximately 3 cm. Also there is void between asphalt base course and the underneath layer. Moreover, there is elevation difference between position of base course at side A and B which is marked in yellow. This means that asphalt base course lost its support on side A and consolidated which resulted in layer delamination between wearing course and the asphalt base course. Ultimately the pavement started cracking which was severe at side A.

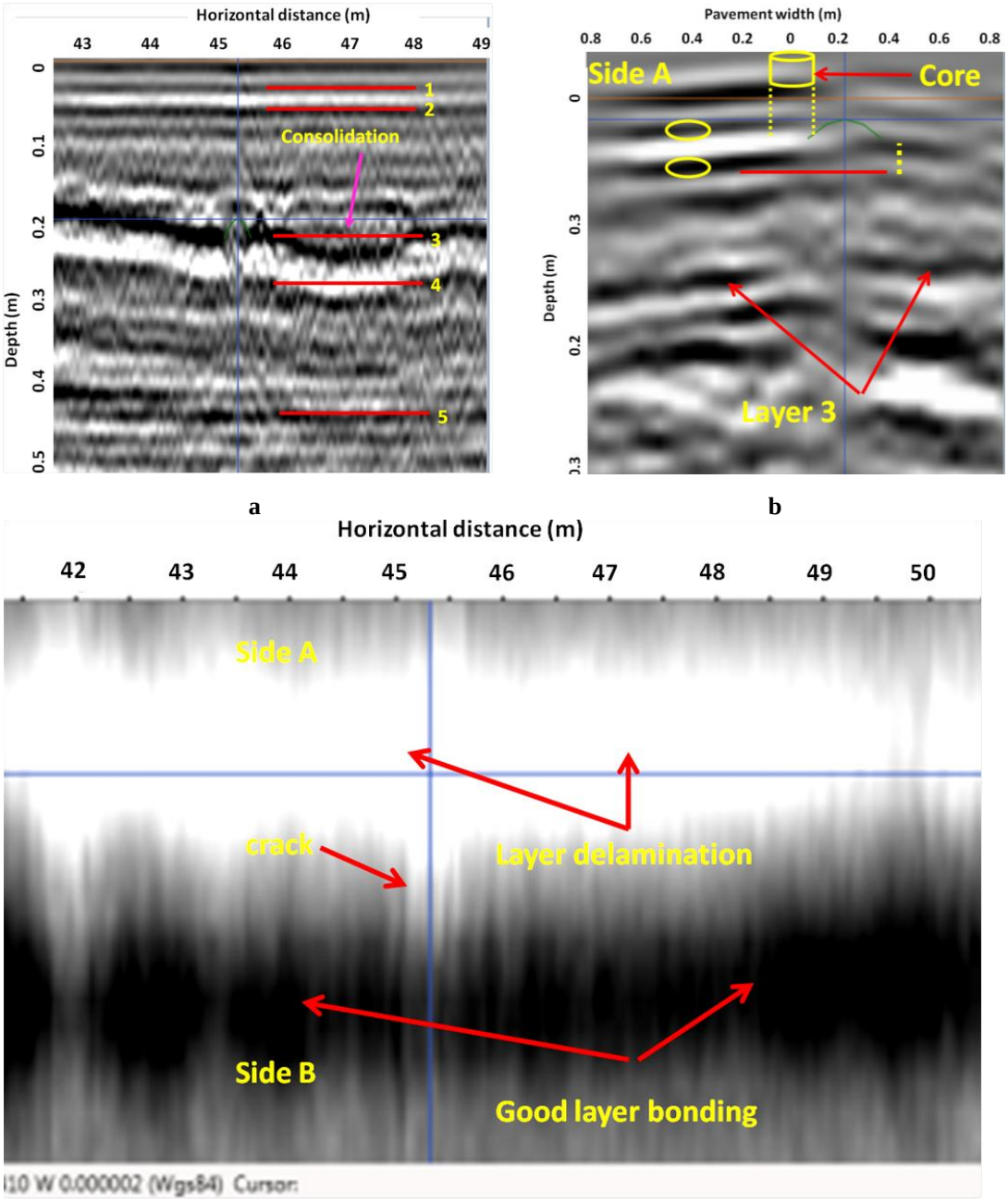

Figure A. 2. The radar-gram of GPR survey on Holzweg 46 m with 3D RADAR, (a) horizontal GPR-gram, (b) transversal GPR-gram and (c) horizontal slice at 2 cm depth

In addition, the position of layer 3, a foreign material layer is also depressed on side A. to confirm the outcomes, or at least the layer delamination between wearing course and the asphalt base course; pavement is viewed from top at a depth of approximately 3 cm. The horizontal slice is shown in Figure A. 2(c). In can be observed in the GPR-gram in Figure A. 2(c) that even on the same depth, the pavement has two different strong colours. The black colure showing uniform material i.e. asphalt whereas white colure is indicating the presence of any light material such as air. Hence the layer delamination was confirmed.

With the help of Aladdin and GeoScope systems, it was confirmed that the crack on 46 m location was because of consolidation of pavement layers in the direction of travel. Furthermore, it was confirmed that the layer delamination and support settlement at side A, was responsible for the increased crack width. To authenticate the outcomes, core sample was extracted from middle of the cracked pavement (Figure A. 1 (a)). The core sample is shown in Figure A. 3(a).

The core sampling confirmed presence of an asphalt layer at a depth of 15 to 20 cm in the pavement. Because of difference in dielectric constant of asphalt and the surrounding un-bound layers, the layers (layers 3 and 4 in Figure A. 2(a)) were clearer in the previous outcomes. With the help of core sample information, a layer profile of pavement up to a depth of 55 cm was constructed. The layer profile is shown in Figure A. 3(b). The layer profile shows the nature and position of layers in the pavement. Below the asphalt layer at ≈ 24 cm, about 1 cm gap was detected. However, due to disturbed core sampling, it was hard to measure exact gap thickness. The core sampling nonetheless confirmed outcomes presented in Figure A. 1 and Figure A. 2.

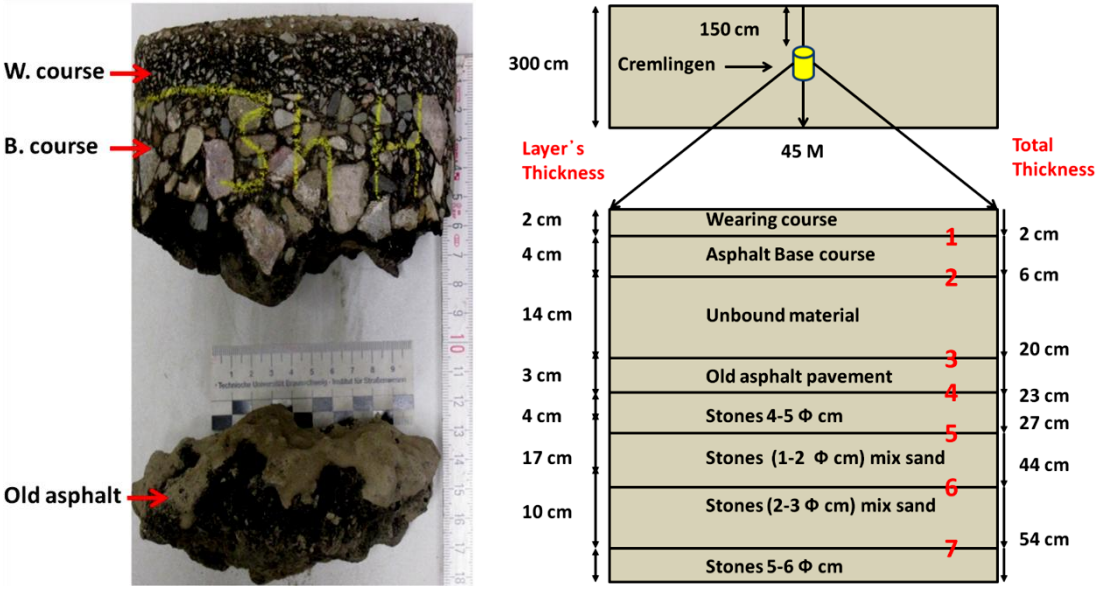

Figure A. 3. The core sample and layers profile of Holzweg 46, (a) pavement core including sub-grade and, (b) core-log of pavement at 45 m location

II.II. Site D (Gutswiese)

The site D was selected as there was only one crack in the whole section and this crack was also with varying depth. The crack was across pavement width starting from pavement extreme right side (Side D) to pavement left side (Side C). The crack width was maximum at right side and minimum at the left side. Therefore, it was decided to find out the reason for pavement cracking. The pavement was constructed on embankment and therefore due to possibility of sub-grade at extreme depth, lowest available frequency antenna was used i.e. Detector DUO GPR system with 700 and 250 MHz frequency. The 2-D survey was carried

out along pavement centre. The data was processed with GRED software. The survey outcomes are shown in Figure A. 4.

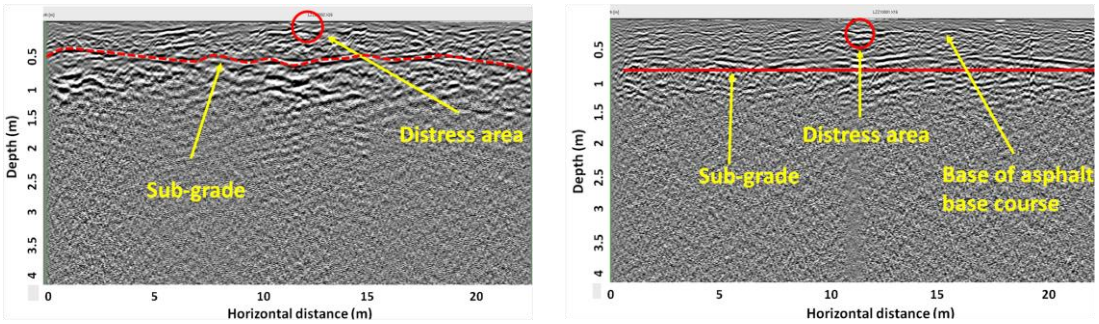

Figure A. 4. The 2D survey with Detector DUO GPR system on Site D, (a) 250 MHz antenna profile 1 (b) 700 MHz profile 2

In Figure A. 4(a), outcome from 250 MHz antenna is shown. The red line is indicating position of sub-grade whereas crack is encircled in red. The 250 MHz antenna detected some distress right underneath cracked section at a depth of ≈ 1 m. The asphalt layers were however, not clearly detected. It was assumed that the crack was caused due to settlement of sub-grade at cracked section. However, the sub-grade goes deeper at 25 m location where there is no crack. Thus 700 MHz antenna was used for further surveying.

With the help of 700 MHz antenna, the asphalt layers were successfully detected. The outcome is shown in Figure A. 4(b). The uneven formation of sub-grade was confirmed. Right beneath crack in pavement, the influence of water was detected starting from 1.5 to 4 meter. It was decided to thoroughly investigate pavement top layers till sub-grade. Therefore Aladdin with 2 GHz antenna was used for further investigations.

The survey with Aladdin GPR system was configured to 512 samples per scan with a scan distance of 4 mm. The survey was conducted on pavement centre. The data was processed with ReflexW software. The survey with Aladdin helped analyse the asphalt layers as well as depressions in the sub-grade. The outcomes are shown in Figure A. 5. The crack is encircled in yellow whereas asphalt layers and sub-grade is marked. The top dark line in GPR-gram (Figure A. 5 (a)) is representing the base of asphalt wearing course. It can be seen that the thickness of asphalt layer is minimum as the cracked section. Moreover, the thickness of wearing course is increased after cracked section in the direction of travel. This is the reason why despite depression in the sub-grade, no further cracking in pavement occurred. The 2 meter cracked section is considered to analyse it thoroughly. The outcome is provided in Figure A. 5(b) with crack at 0.9 meter.

The survey of two meter including cracked area helped figure out changes in the sub-grade of pavement. In Figure A. 5(b) the difference in sub-grade elevation at cracked section is highlighted with help of a red straight line. It can be seen that there is an abrupt depression at the cracked section. Hence it was certain that support settlement in form of sub-grade consolidation resulted in pavement cracking. However, it was still not clear that why the

crack has maximum width in pavement centre. For this reason, pavement asphalt layers thickness of side C, D and pavement centre were surveyed with Aladdin system.

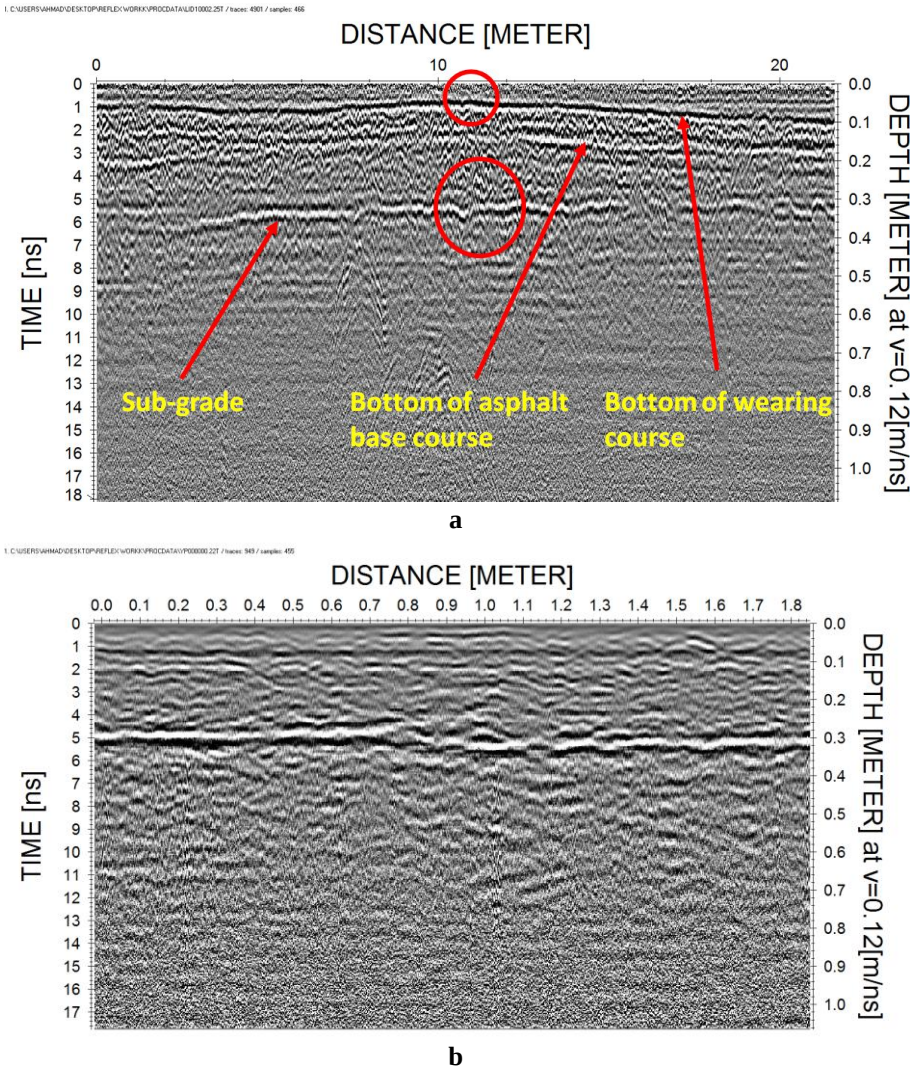

Figure A. 5. GPR survey on Site D with Aladdin system, (a) asphalt layers and sub-grade anomaly of 22 meter section with crack at 11 meter location, (b) 2 meter cracked section with crack at 0.9 meter

The 2-D survey with Aladdin was conducted with 512 samples per scan and a scan distance of 4 mm. The data was processed with ReflexW software. For this reason, survey was conducted along left, right and the pavement centre. The data was standard processed as for the previous survey. The asphalt layers were automatically picked in GPR-grams and values were saved as ASII files which were later converted Microsoft Excel data. The thickness of only asphalt wearing course was considered as asphalt base-course was sometimes hard to detect in the GPR-grams. The results are provided in Figure A. 6.

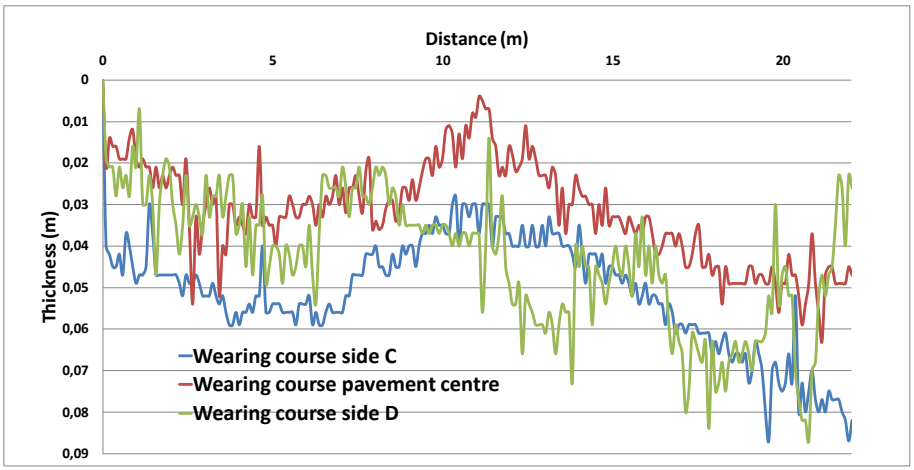

Figure A. 6. The variation in asphalt wearing course thickness on survey profiles 1, 2 and 3 (refer Figure 3.22)

It must be noted that the thickness of wearing course presented in Figure A. 6 are based on the approximate dielectric constant value of asphalt. However, objective was to analyse the mean layer thickness and its trend through 22 meter pavement section. It can be seen that the wearing course at side C, D and the pavement centre are near to design thickness i.e. 4 cm whereas at the cracked section, the thickness of wearing course in centre is greatly reduced. The anomaly in wearing course thicknesses at different sections on site C was later proved by core samples. The reason why pavement side D was not fully cracked was not known until investigations in Section III.II.

III. Sub-grade settlement investigation

III.I. Site C (Holzweg)

On site C at 55 meter location, there were two close cracks in form of English letter "U" connected by many fine cracks. The cracks were only at side A (left side) of the pavement. Therefore, objective of survey was to find out with help of GPR, the reason for pavement cracking focusing if support loss could be the reason. For this purpose 3-D surveys were carried out with GeoScope system. The data was standard processed with 3dr-Examinar software. The outcomes are provided in Figure A. 7.

The 3-D survey by GeoScope analysed the pavement layers and their position in pavement promisingly. An outcome at 0.4 m left side of pavement centre (moving away from Cremlingen) is shown in Figure A. 7(a). It can be observed that at ≈52.5 meter location, the sub-grade at ≈0.2 meter depth is missing. Both cracks at ≈54.5 and ≈55.4 meter location have no support. The sub-grade appears at ≈56 meter location but is elevated compared to sub-grade at ≈52.5 meter location. The difference in elevation of sub-grade at both locations is shown by red line at ≈0.2 meter depth. Because of the elevated sub-grade, the pavement surface at ≈56 meter location is also elevated. Thus support loss and uneven support are responsible for the cracking of pavement in this section. Later on, a core sample from pavement was taken to authenticate the outcomes.

To find out why pavement was cracked severely on the left side, cross-section of pavement across its width at 56 meter location was analysed. The cross-section is shown in Figure A. 7(b). It can be observed that the sub-grade is lifted at side B and so is the pavement surface. The bottom of asphalt base course is also darker on side B than side A. the reason could be layer delamination or presence of water. Nonetheless it was confirmed that the elevated sub-grade on side B or sub-grade settlement at side A resulted in severe cracking only at side A. The information regarding core sample taken from 56 meter location is provided in Figure A. 8.

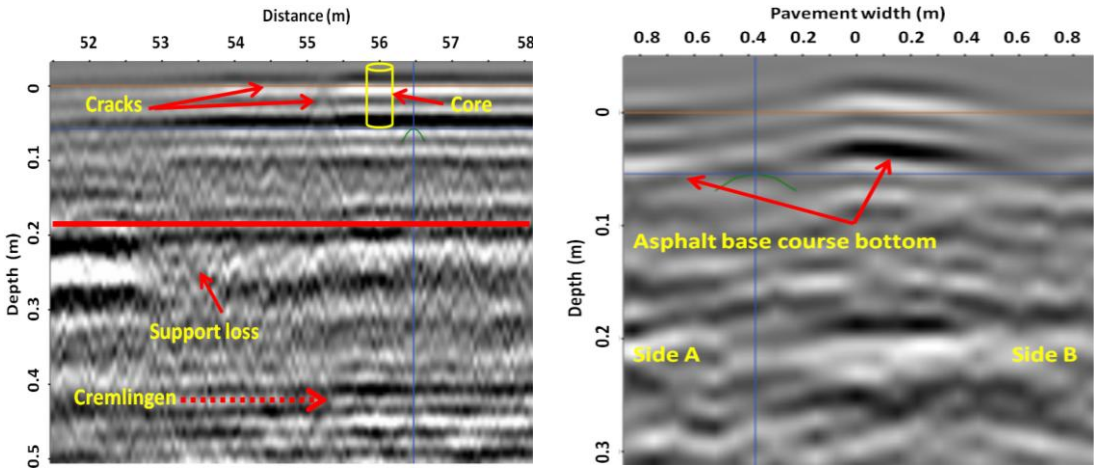

Figure A. 7. The GeoScope outcomes of survey on site C at a location of 55 m (a) longitudinal cross-section of pavement at 40 cm left from pavement centre in the direction of travel (b) cross-section of pavement width a transversal GPR-gram

To validate the survey outcomes, core sample was taken from location ≈56 meter. Based on the core samples to a depth of about 50 cm, layers information was gathered. The layers with material properties and layer thickness are provided in Figure A. 8(b).

The core sample is shown in Figure A. 8(a) whereas complete core-log is shown in Figure A. 8(b). The core sample confirmed presence of slag material in asphalt base course. This might be the reason why asphalt layers at 55 m location and onwards had a strong reflection in the GPR outcomes. Also if core sample of 56 meter location is compared to that of 45 meter location (Figure A. 3), the thickness of asphalt base has been doubled from 4 cm to 8cm. This can be also one reason why pavement was cracked at the junction of two different thickness asphalt base course layers.

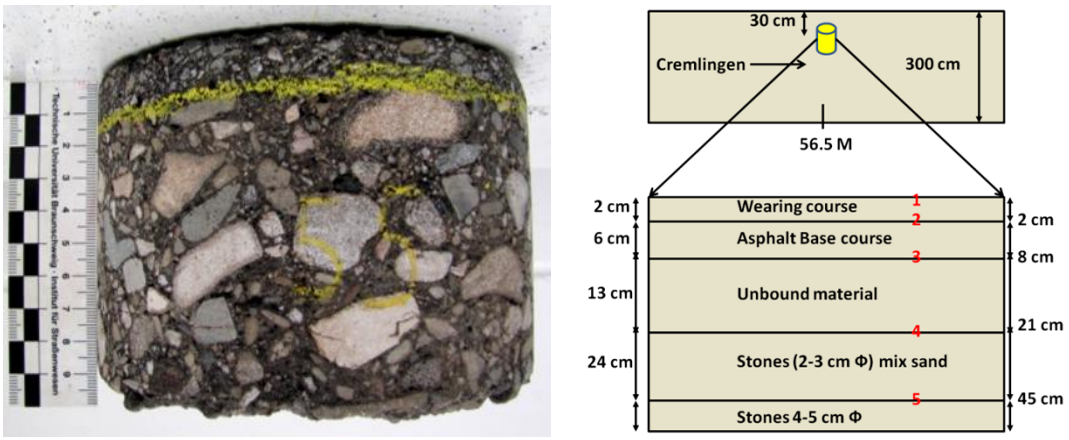

a **b**

Figure A. 8. Asphalt pavement construction information at site C on 56 metre location, (a) core sample and, (b) the pavement layers information based on core sample

III.II. Site D (Gutswiese)

A crack on Site was starting from right side of pavement (Side "D") with a maximum width at pavement centre and stopping ≈1.5 meter before left side of pavement (Side "D"). To find out what was the reason for pavement cracking at this section, 3-D survey was carried out. The Aladdin GPR system with 2 GHz frequency antenna was used for investigations whereas the data was processed by GPR-SLICE software. In 3-D survey, three 1 meter section with 2 meter length were surveyed. The three areas were selected from pavement side C, D and the centre. After survey, the data from these three sections were gathered and processed as single area. The results are shown in Figure A. 9.

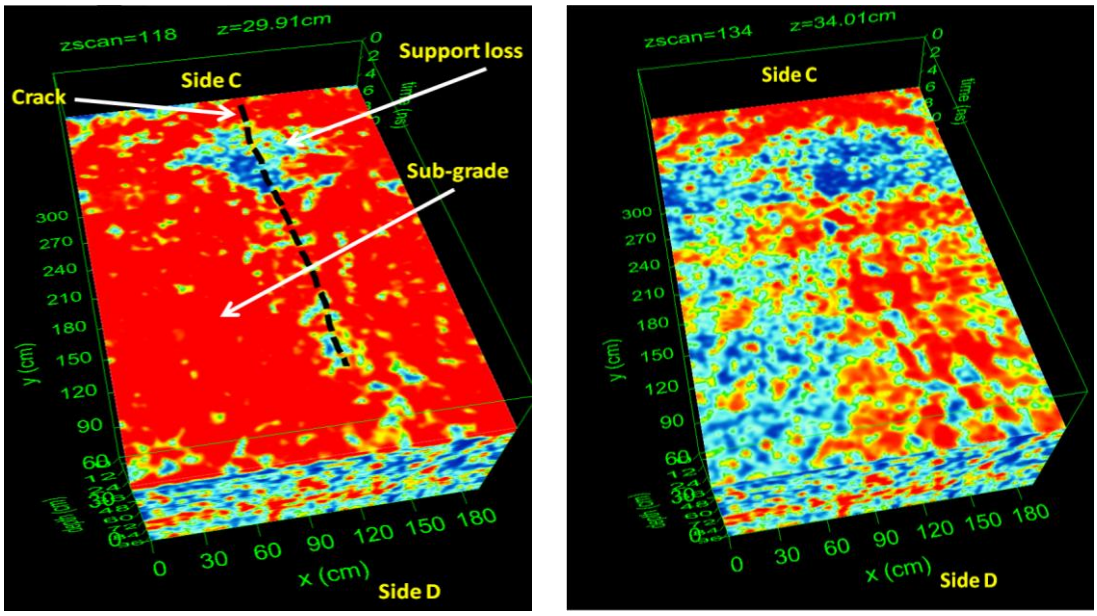

a **b**

Figure A. 9. The 3D survey results on site D crack, (a) sub-grade (red colour) at depth of 30 cm and, (b) sub-grade at a depth of 34 cm

In the outcome shown in Figure A. 9(a), red colour indicates sub-grade whereas blue colour means material beneath sub-grade. It can be seen that the sub-grade at a depth of 30 cm is missing at side C. On the other hand, in the outcome shown in Figure A. 9(b), the sub-grade is still present at a depth of 34 cm. It means that the thickness of sub-grade was more at side D compared to side D. Thus it was definite that crack started at side C due to support loss and stopped before pavement other end at side D due to thicker sub-grade. Also it is worth to mention that the thickness of asphalt layers t side D was also more than at side C which was confirmed in previous tests in Section II.II.II. To authenticate the survey outcomes, core samples were taken from three locations on Site D. The core samples and layers information are provided in Figure A. 10.

The sampling revealed that 4 cm thick sub-grade was of lean concrete (Figure A. 10 (a)). The difference of wearing course thickness on side C and D is marked on the core sample showed in Figure A. 10(b). The thickness of wearing course at side C and d was ≈2 cm. The difference of wearing course thickness together with pavement centre on cracked location is shown in Figure A. 10(c). It can be seen that the least thickness of wearing course is in case of pavement centre.

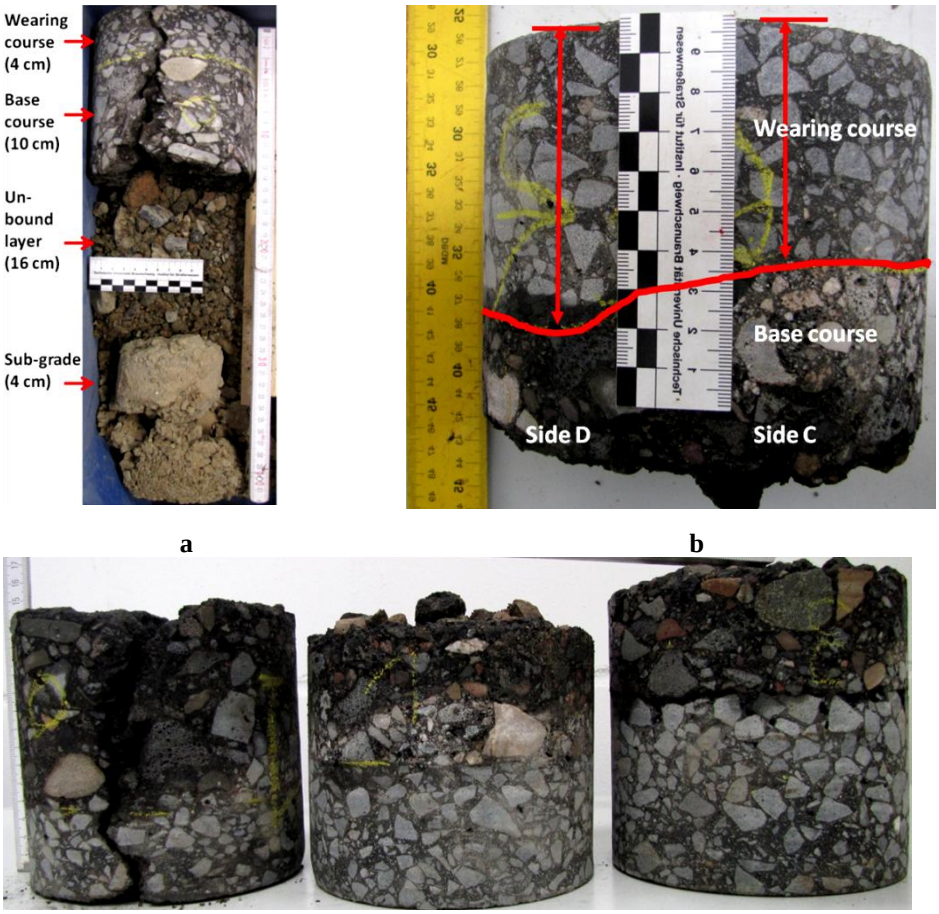

Figure A. 10. The pavement layers information on Site D, (a) 50 cm deep core extracted from cracked area in the pavement centre, (b) difference in wearing course thickness at side C and D, (c) comparison of wearing courses at pavement centre, side C and side D

IV. Miscellaneous crack causes investigation

On site B, there was a crack starting from pavement one side, running across its width and stopping in the pavement centre. The reason for pavement cracking was investigated in three phases. In the first phase Aladdin with 2 GHz antenna was used. Later, SIR-20 and MALA HF were used in second and third survey phases respectively. For the data processing in all three phases, ReflexW software was used. The outcomes are shown in Figure A. 11.

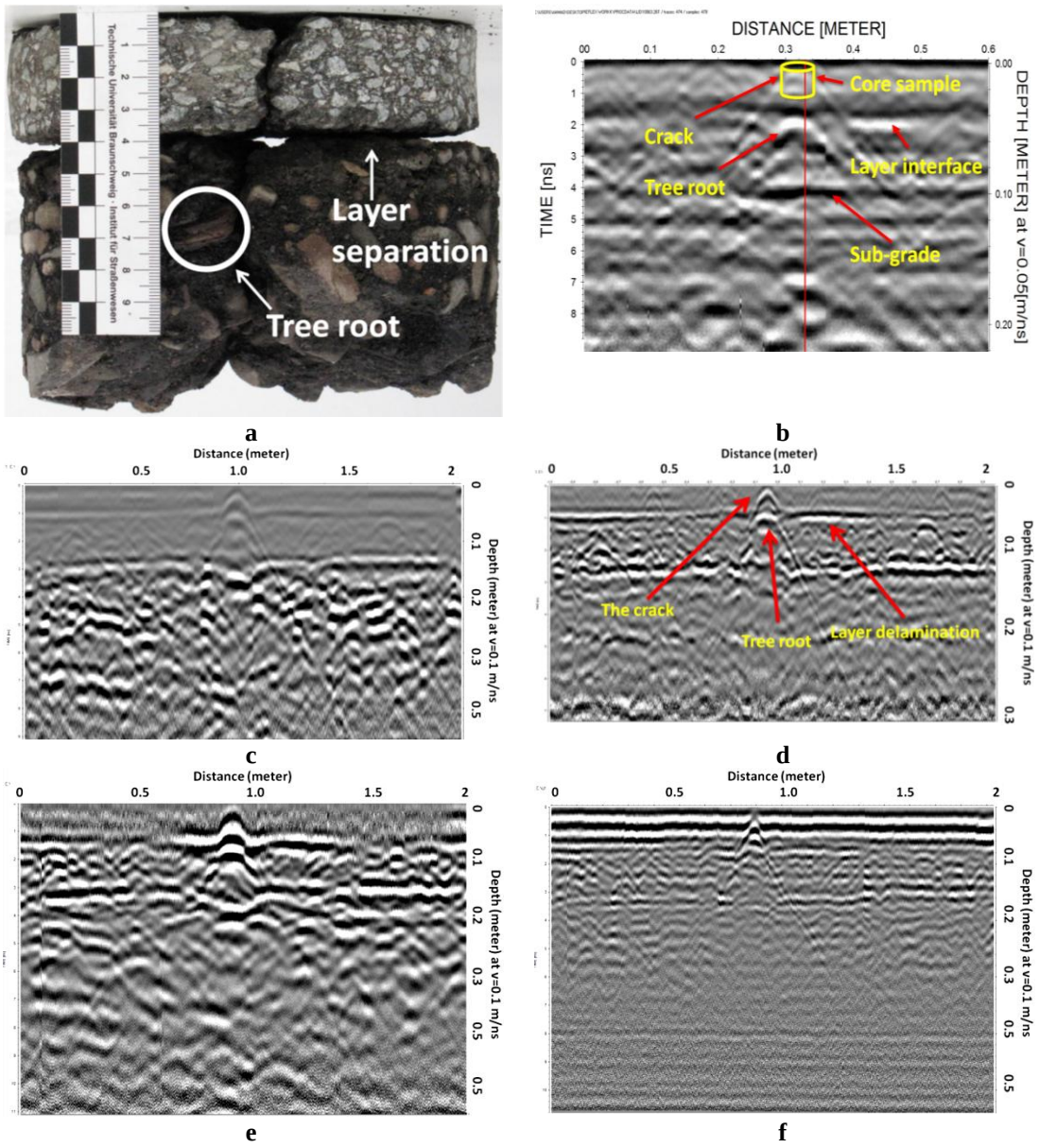

Figure A. 11. The GPR outcomes for the crack cause investigation of crack "λ" (site B), (a) core sample of asphalt pavement, (b) GPR-gram of Aladdin, (c, d) results from SIR-20 with 1500 and 2600 MHz antennas respectively and, (e, f) results from MALA HF with 1600 and 2300 MHz antennas.

In the outcomes of Aladdin system, not only the crack was successfully detected but also the layer boundary between wearing and base course at ≈10 cm depth was vivid in the GPR-gram shown in Figure A. 11(b). The bright boundary could be because of poor

bonding between asphalt layers. The crack detected in this survey was different from the past outcomes as its bottom was deep into base course. Therefore, crack was investigated with other GPR system with varying frequencies.
In the second phase, SIR-20 system with antennas of 1500 and 2600 MHz were used. Both antennas detected crack and the asphalt layers. The asphalt layers interface was clearer in 2600 MHz outcomes shown in Figure A. 11(d). The crack bottom was again detected to be in asphalt base course. Generally, the crack bottom is found at asphalt layers interface. The same outcomes were obtained in phase three tests with MALA HF 1600 and 2300 MHz antennas. The results are provided in Figure A. 11(e & f). The results in case of MALA HF 2300 MHz were however, not promising.
To validate the outcomes, core sample was taken at crack location. The core sample is shown in Figure A. 11(a). It was found that the asphalt layers were delimitated at this section. Due to presence of gap between wearing course and asphalt base course, the layer interface was brighter in the GPR-grams. Also a tree root was found just below the crack bottom inside the base course. As roots contains water (higher dielectric constant), it resulted into masking crack bottom and appeared itself as crack bottom inside the base course.

V. Summary

In this section causes for cracking in asphalt pavements was investigated with different type and frequency GPR systems. The objective was to investigate if GPR can be useful to avoid and cure pavement cracking. For this reason, different test sites with different types of cracks were selected. The pavements were investigated up to a depth of 60 cm. The GPR proved itself useful to investigate pavement layers anomalies and sub-grade depressions. GPR is also found useful investigating more than single crack sources at same location. The 3-D surveying was found more useful for the investigation of crack causes. Furthermore, with the use of different software techniques the layer thickness can be analysed more accurately than classical methods.